MATHEMATICAL MODELS OF MICROBIAL EVOLUTION

COOPERATIVE SYSTEMS

Submitted by
Bogna Julia Pawlowska
to the University of Exeter as a thesis for the degree of
Doctor of Philosophy in Biological Sciences
October, 2016

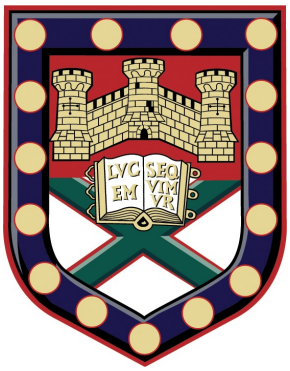

supervised by
Professor Ivana Gudelj
Professor Robert Beardmore

Publications

Richard J. Lindsay, Michael J. Kershaw, Bogna J. Pawlowska, Nicholas J. Talbot and Ivana Gudelj. ***"Harbouring low virulence cheats within a pathogen population increases both fitness and virulence"****. eLIFE, vol. 5, pp. 107-133, Dec. 2016*. This publication contains some of the results presented in Chapter 3.

Bogna J. Pawlowska and Ivana Gudelj. ***"Quantitatively Defined Spatial Structure Explains the Relationships between Population Density and Cooperation"****. in preparation*. This publication is based on the results presented in Chapter 4.

Abstract

Microbes usually live in large communities, where they interact with other organisms and species. These interactions include cooperation, when individuals facilitate each others growth and reproduction. Such cooperation has been for instance observed within pathogens in the process of infection. Therefore, given the number and the frequency of infectious diseases, understanding the nature and the dynamics of microbial cooperation may be a crucial step in modern medicine.

Microbes often secrete costly enzymes which extracellularly metabolise resources available in the environment. This external metabolism is a form of 'public good cooperation', in which individuals invest their energy in producing 'public goods', available to other organisms. To study this phenomenon we deploy mathematical models which are based on biologically relevant assumptions. Our models not only aim to capture the dynamics of studied microbial communities, but also to remove the natural complexity arising in the empirical studies and thus to provide a mechanistic understanding of their results.

We first recover and explain the recent empirical finding, about mixed strain infections, showing that an addition of a low virulent strain which does not produce public goods (termed 'cheat') may counter-intuitively enhance the total population virulence. What drives this result turns out to be an interaction of two different cooperative traits and the presence of spatial structure. Next we study the competition between the strains that do and do not produce public goods. Our results depend on environmental conditions, such as resource concentration and population density, but they are also determined by the degree of spatial structure - the ecological trait which so far has been treated only as a binary variable. Finally, we identify some environmental threats for the external metabolism feeding strategy, and we examine its competitiveness in comparison to 'internal metabolism', in which the costly enzymes are private.

Contents

List of Figures

List of Tables

Acknowledgements

I would like to thank my supervisor Ivana Gudelj for all of her guidance and patience, and for showing me how to turn mathematical tools into something incredibly useful. I also express my gratitude to my second supervisor, Robert Beardmore, for his numerous comments and help on mathematical modelling. Thanks to my colleagues - Lisa Butt for supervising me in the laboratory and showing the beauty of the experimental world. Thanks to Richard Lindsay for the fruitful collaboration: experimental data, insightful discussions, and for his patience to explain all the magic of the experimental side of our work.

I am grateful to the people from my team, for theoretical discussions and support, in particular to Carlos Reding-Roman, Michael Sieber, Peter Rashkov, and Mark Hewlett who has given me a lot of good advice and comments on my work. I would also like to thank Jessica Plucain and Fabio Gori for giving me a piece of home when I first arrived to Exeter, and for making my life here somewhat more cheerful. Jess, thanks for having said 'I have no doubts you will succeed with your PhD'. I used to recall that whenever I had any doubts myself.

A huge thanks to Cyrielle Tonneau, for being my most engaged proof reader, for her really helpful comments on the visual side of my work (and teaching me all the PowerPoint tricks...), but above all, for being a close friend, whom I could always consult with any problems. Thank you Cyrielle for bringing so much joy to the office and to my life.

Special thanks to Damian, for all of his love and support, and for being always, always, always on my side. The most special thanks to my parents: to my mother who has always been there for me, no matter what, and to my father, who has shown me what it means to be a good scientist. Dad, it is you who awoke my curiosity about the world, and who has been always asking me the right questions. Thank you for having always kept that spark of curiosity alive.

Chapter 1

General Introduction

Cooperation between single cells is the first step to the evolution of multicellularity [1], the process that led to appearance of complex organisms on Earth. Although this phenomenon is ubiquitous in nature, it is not yet fully understood, and the current studies keep bringing new insights into the field of microbial cooperation. In this Chapter we introduce the definition of different kinds of social interactions, in particular of cooperation. Then we briefly discuss some of the mechanisms known to promote cooperation in nature. Finally, we introduce the cooperative system studied in this thesis, namely the public good system of *Saccharomyces cerevisiae*.

1.1 Types of social interactions

Social behaviour can be defined as a behaviour which is exhibited by one individual (the actor), and which affects one or more other individuals (the recipients of that behaviour). Depending on the consequences of a social behaviour on its actors and recipients, it can be classified into four main types: mutual benefit, altruism, selfishness, and spite [2, 3], as shown in Fig. 1-1.

In particular, if an individual acts in order to decrease another's fitness, its behaviour may be termed either 'selfishness', if the actor of that behaviour increases its own fitness, or 'spite', if the behaviour implies some fitness costs for its actor. On the other hand, if an individual acts towards increasing another's fitness, its behaviour is termed 'mutual benefit' if it also increases its own fitness, or 'altruism' if it decreases its own fitness. Both of these cases are termed 'cooperation' [4].

Importantly, the consequence of a given behaviour for the fitness of its actor

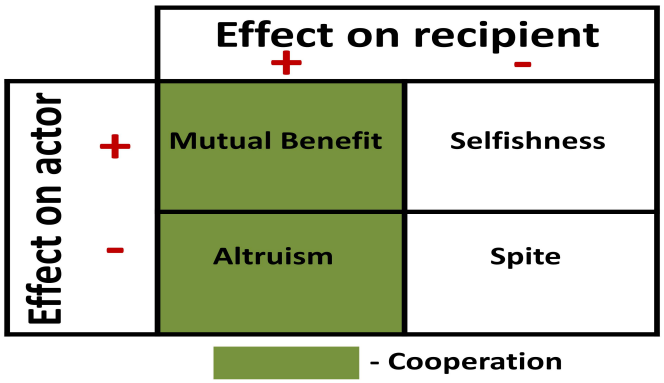

Figure 1-1: **Hamiltonian classification of social interactions between a pair of individuals.**

may depend on the 'reaction' of the recipient of that behaviour. An example of such a scenario is represented by the 'Prisoner's Dilemma', often described with the following scenario. Two prisoners have been accused for committing a crime. Since the police has not enough evidence to convict them, both prisoners are asked if the other one has committed the crime. Each of the prisoners can either choose to cooperate with the other by remaining silent, or to betray by admitting the other one did commit the crime. The sentence depends on the confessions of both prisoners and it is: punishment for both if both of them betray, a mild punishment for both if both remain silent, and if one of them betrays while the other remains silent, the one who betrays avoids the punishment, and the one who remains silent is severely punished. Thus both of the prisoners have an incentive to betray. This scenario shows that when one individual exhibits cooperative behaviour towards the other, it may either gain ('mutual benefit') or lose ('altruism') fitness, depending on the behaviour of the other individual.

In this thesis, by cooperation, we mean behaviour which brings some risk of a decrease in actor's fitness. Instead the cases of mutual benefit, which bring profits to the actors, regardless the effect on the recipients, have been proposed to be excluded from the definition of cooperation [5], and they are not considered in this thesis.

1.2 Mechanisms that promote cooperation in nature

According to the Darwinian theory of evolution, natural selection favours individuals with the highest reproductive success. Nonetheless, frequently in nature, individuals sacrifice a part of their own success in order to help the others.

Probably the most famous case of such behaviour is the example of honey bees brought by Darwin himself, who describes it as:

"... special difficulty, which at first appeared to me insuperable, and actually fatal to my whole theory. I allude to the neuters or sterile females in insect-communities: for these neuters often differ widely in instinct and in structure from both the males and fertile females, and yet, from being sterile, they cannot propagate their kind." **[6]**

The honey bees provide an extreme example of altruism: the majority of individuals in a population sacrifice their entire reproduction, in order to increase the reproductive success of just one individual, the queen bee.

Apart from insects, cooperative behaviour is widely observed within fishes, birds and mammals, as summarised in [7], and above all, in humans, who have developed the most complex cooperative structure on Earth : civilisation.

Why is cooperation so frequent in nature, if it clearly contradicts the classical Darwinian theory? Here we briefly describe a number of mechanisms that have been proposed to explain that phenomenon.

1.2.1 Kin Selection

The theory that successfully explained the cooperation in honey bees is the Kin Selection Theory [2]. It states that genes responsible for cooperative behaviour will be favoured by natural selection, if the actors and recipients of that behaviour are genetically related. Intuitively speaking, your kins are likely to share a big part of your genes, therefore by helping them, you increase the chances of your own genes to be promoted by natural selection. This effect is especially pronounced in haplodiploid honey bees, where the bee workers are more related to their full sisters (on average they share 75% of their genes), than they would be to their

potential offspring (on average they would share only 50% of their genes).

1.2.2 Direct and Indirect Reciprocity

How can cooperation be maintained between non-kins, for example within large human populations? If cooperation takes a form of a single act, there may be no good reason to risk your own fitness in order to increase the fitness of someone else. But what if you interact with the same person a number of times? If you help someone, that person may help you in future. This intuitive strategy is at the core of 'direct reciprocity', one of the mechanisms proposed to favour cooperation [8]. This concept has been tested in the scenario of iteratively played Prisoner's Dilemma, in which two players meet a number of times, and each time, they can decide to either cooperate or to defect. Various long-term strategies for such a game, have been proposed as 'optimal', for example 'tit for tat' [9], according to which a player repeats the previous decision of the other player, or 'generous tit for tat' [10], according to which a player adopts the 'tit for tat' strategy, but it may randomly choose to cooperate instead of defect. It turns out that in such a case, the cooperative acts can be observed in long term.

An extension of the concept of 'direct reciprocity', is the 'indirect reciprocity' [11], which explains why cooperation is maintained in large populations, in which the chances of interacting twice with the same individual are low, or in which the interactions are asymmetric. This is often the case within humans, where one individual may help someone, who is not in position for a direct reciprocation. The idea of indirect reciprocity is that those who often help have 'a good reputation' and are more likely to get help in the future from other individuals in the population [11].

1.2.3 Spatial Structure

There is yet another mechanism that may favour cooperation even in the lack of genetic relatedness and reciprocity. If you exhibit a cooperative behaviour towards a randomly met individual, there is a risk of not getting any help back. However, if the interactions take place only locally within predefined groups or networks of individuals which behave in a similar way, this risk is minimised. That idea has been studied within graph theory [12], group theory [13] and mathematical

modelling [14, 15], and it gives the same results regardless of the framework: as long as the cooperators are most likely to meet other cooperators, their behaviour may pay off and be maintained in nature.

1.3 Microbial Cooperation

Although cooperation is often discussed in the context of conscious decisions, as in case of humans, it is also widely observed in simpler organisms, in particular in microbes (see recent reviews: [16–18]). Studying microbial systems unravels that cooperation is a universal behaviour, and it may be driven by fundamental biological mechanisms, rather than the complexity of the human brain. The microbial world provides a unique opportunity to identify these mechanisms in simplified systems, which can be fully controlled in experimental setups. Not only can they be studied in entirely isolated laboratory cultures, but also, due to their short generation times, their evolution can be manipulated and observed in the timescale of laboratory experiments [19–22].

Apart from obtaining a better understanding of cooperation in general, studying microbial systems is also important in the light of modern medicine. In particular, cooperative behaviour is often observed within pathogens while infecting their hosts, for example within nutrient acquisition [23], quorum sensing [24, 25], or host cell lysis [26]. Therefore getting a deeper insight into the dynamics of cooperative systems within pathogens may significantly increase our chances to design successful antimicrobial therapies.

Although this thesis and other studies on microbial cooperation tend to use the terminology describing human interactions (for instance 'cooperator' or 'cheat') which may suggest that the studied organisms make conscious choices while interacting with others, we highlight that the 'choices' of microbial strategies are not conscious and they can be only understood in the sense of evolution, rather than on the individual level.

1.4 The public good system of *Saccharomyces cerevisiae*

Microbial public good systems are those in which individuals secrete some costly substances beneficial not only for themselves, but also for other organisms in their environment. This is a form of cooperation, because individuals invest their own energy in increasing the fitness of other organisms. Well studied examples of such systems include *Pseudomonas aeruginosa*, where individuals secrete extracellular iron-scavenging molecules, siderophores [27–29] or the system of *Vibrio cholerae* [26, 30, 31], in which the digestion of the primary food source, chitin, is mediated through costly extracellular enzymes.

In this thesis we study the public good system of *Saccharomyces cerevisiae* [1, 14, 32–34]. A schematic diagram representing this system is shown in Fig. 1-2. *S. cerevisiae* is a unicellular, eukaryotic organism commonly known as 'baker's yeast', which belongs to the Fungi kingdom. It is widely used in industry, especially in fermentation, where it plays the crucial role in converting sugars into ethanol.

The preferential carbon source of *S. cerevisiae* is glucose, however, when the available glucose is scarce, the yeast is also able to metabolise more complex facultative sugars, in particular: the abundant in nature disacharide, sucrose.

Although some *S. cerevisiae* strains are able to uptake sucrose directly, through the active $H+$ sucrose symport mediated by two possible pathways: an α-glucoside symport encoded by the gene $AGT1$, and maltose symport encoded by $MALxT$ [35], the main and most effective way of metabolising sucrose is its extracellular hydrolysis. This process is catalysed by an enzyme, invertase encoded by the gene $SUC2$.

The wild type strain of *S. cerevisiae* produces invertase and secretes it to the periplasm where the enzyme breaks down sucrose available in the environment into simple sugars, namely glucose and fructose. A part of these monosacharides is transported into the invertase producer cells, but the majority diffuses away, where it becomes available to all the other organisms in the environment [33].

Even though invertase production enhances the yeast's growth, it also imposes energetic costs to the organisms that secrete it. This is why the invertase

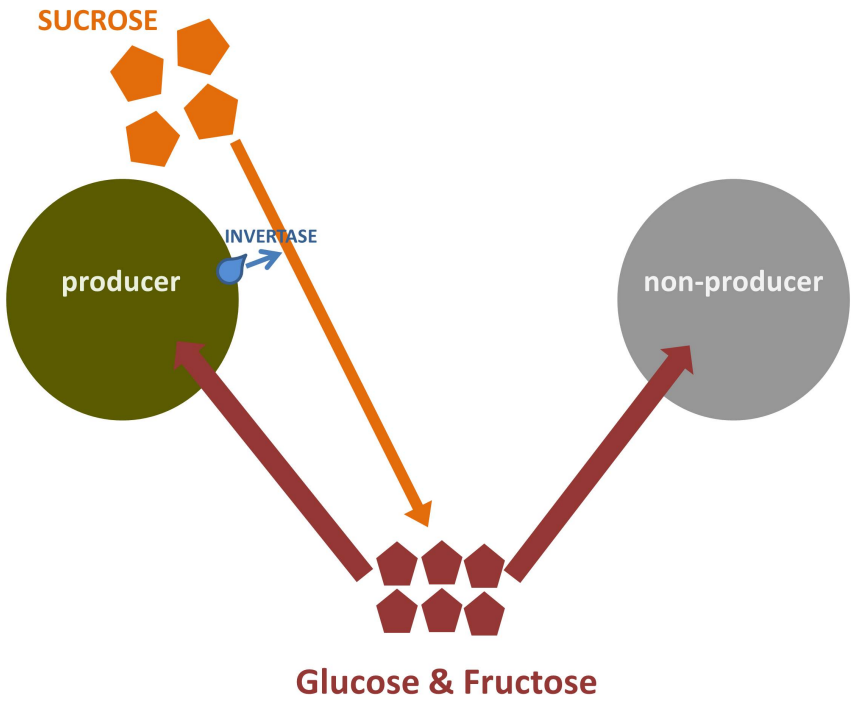

Figure 1-2: **A schematic representation of the public good system of *S. cerevisiae*.** Some individuals (termed 'producers') secrete an enzyme, invertase, which breaks down molecules of sucrose into simple sugars, namely glucose and fructose. Since that process takes place outside the invertase producer cells, it may benefit other organisms in the environment, in particular those who do not produce any invertase (termed 'non-producers').

and the simple sugars appearing in the environment thanks to its activity, are considered to be 'public goods' shared within all the population, but costly to produce.

Although the wild type strain of *S. cerevisiae* expresses the gene $SUC2$ and produces invertase, there are also strains that do not carry it [32]. Those strains, termed $\Delta suc2$ mutants, do not produce the costly invertase, but they are still able to uptake the simple sugars broken down in the environment [32].

Throughout the thesis, we term the individuals expressing the $SUC2$ gene, 'producers' or 'cooperators', and those not expressing $SUC2$ gene, 'non-producers' or 'cheats'. Moreover, the feeding strategy of producers will be termed 'external metabolism', because its first step, sucrose hydrolysis is performed extracellularly.

Although our study is motivated by the public good system of *S. cerevisiae*, we also apply our models to the system of a plant pathogen *Magnaporthe oryzae*. This system has been recently engineered in [36], and similarly as the system of *S. cerevisiae*, it is composed of invertase producers and of a strain that fails to produce invertase (termed $\Delta inv1$ mutant).

What happens if a fraction of cheats is introduced to the population of cooperators? How can a population of cooperators survive an invasion of cheats who do not pay any cost of invertase production, but reap the rewards? What are the advantages and disadvantages of external metabolism? Is this cooperative form of digestion competitive in comparison to the 'selfish metabolism' in which none of the steps of digestion is shared with the other cells? This thesis will attempt to answer these questions taking into account various environmental conditions facing microbes, for instance population density, spatial structure or resource abundance.

Despite many existing theoretical frameworks to study cooperation (such as kin selection [2] or game theory [12]), in this thesis we choose to deploy tools based on dynamical systems. To model the considered biological interactions, we use a bottom-up approach, building our models and results on a set of biologically relevant assumptions and parameters. In contrary to the game theory or kin selection models, here we do not presume any specific fitness effects of the studied evolutionary strategies. Instead, we let these effects arise from our basic assumptions. Notably, thanks to our dynamical approach, we can follow how these effects vary in time, and therefore we are in position to make quantitatively accurate predictions on the whole system dynamics. Moreover, because the fit-

ness effects arise from our models rather than being assumed *ad-hoc*, we are able to obtain mechanistic understanding of the processes observed in nature or in experimental studies. By varying the model assumptions, we can extrapolate the known experimental findings, and test *in silico* a number of different scenarios, possibly finding the key features which drive the observed results.

Structure of the Thesis

In Chapter 2 we describe the main assumptions of the mathematical models proposed in this thesis. We also describe the types of microbial cultures studied in this thesis, and we introduce the main tools used to analyse the dynamics of these cultures.

In Chapter 3 we explore the consequences for virulence of an introduction of 'cheats' to a public good system of a plant pathogen *Magnaporthe ryzae*. We verify our predictions in different environments.

In Chapter 4 we use a model of the public good system of *S. cerevisiae* to study the environmental factors under which public good producers can resist the invasion of cheats. In particular, we explore how the interplay between spatial structure and resource abundance affects the relationship between the population density and the relative fitness of public good producers to non-producers.

In Chapter 5 we study the performance of a cooperative population, in a continuous culture, and we identify the potential environmental threats for the populations performing external metabolism, which involves public goods secretion.

In Chapter 6 we study the competitiveness of the external metabolism feeding strategy in a wider microbial community. In particular, we study the long-term competition between "external metabolisers', which secrete invertase and 'internal metabolisers', which privitise their invertase production.

In Chapter 7 we keep studying the internal vs external metabolism. We propose a mutation-selection model to predict which of these two strategies can emerge in a long-term evolution process.

Each of the Chapters 3- 7 has an independent abstract, introduction and discussion sections, as well as its own supplementary material. The aim of this structure is to enable the reader to read each of the chapters as an independent piece of work. Since the complexity of the considered systems arises from Chapter 3 to Chapter 7, we recommend to read the chapters in the order they appear in the thesis, however this should not be necessary. The thesis concludes with a General Discussion (Chapter 8), which aims to link together the findings presented in Chapters 3-7, and to conclude our results.

Contributions

Chapter 3 is an extension of the study presented in the article: *Richard J. Lindsay, Michael J. Kershaw, Bogna J. Pawlowska, Nicholas J. Talbot and Ivana Gudelj.* ***"Harbouring low virulence cheats within a pathogen population increases both fitness and virulence"****. eLIFE, vol. 5, pp. 107-133, Dec. 2016*. The experimental data presented in the article has been collected by Richard J. Lindsay and Michael J. Kershaw. The mathematical model and its analysis has been performed by Bogna J. Pawlowska under the supervision of Ivana Gudelj.

Chapter 4 is based on the article: *Bogna J. Pawlowska and Ivana Gudelj.* ***"Quantitatively Defined Spatial Structure Explains the Relationships between Population Density and Cooperation"****. In preparation.* The design of the study and the mathematical model have been developed by Bogna J. Pawlowska and Ivana Gudelj. The numerical simulations have been conducted by Bogna Pawlowska.

The mathematical analysis in Chapter 5 has been conducted by Bogna Pawlowska under the supervision of Ivana Gudelj. The empirical data presented in Chapter 5 has been collected by Bogna J. Pawlowska under supervision of Lisa Butt. The improvements made to the chemostat design has been done by Bogna J. Pawlowska and Lisa Butt.

The mathematical analysis in Chapter 6 has been performed by Bogna J. Pawlowska, as a part of a collaborative project with Richard J. Lindsay who has collected the experimental data presented in: *Richard J. Lindsay.* ***"Polymorphic metabolism and the eco-evolutionary influence of social feeding strategies"****. PhD thesis, University of Exeter, April 2016*. The study design was performed collaboratively by Bogna J. Pawlowska, Richard Lindsay and Ivana Gudelj, and the obtained results are currently being prepared for publication.

The study in Chapter 7 has been conducted by Bogna Pawlowska under the supervision of Ivana Gudelj.

Chapter 2

Methods

2.1 Model assumptions

In order to describe the growth of microbial strains introduced in Chapter 1, in this thesis we will deploy mathematical models based on the model proposed in [14], which has proven ability to generate accurate quantitative predictions regarding cooperative production of invertase in yeast. Below we describe our basic assumptions.

Growth kinetics In our models the considered microbial strains take up resources R and use them to generate adenosine triphosphate (ATP) using a simple, unbranched pathway [37]. The rate of ATP production in the pathway is denoted by J^{ATP} and is given by

$$J^{ATP} = \eta^R_{ATP} J^R,$$

where J^R denotes the rate of the pathway which is a function of resource concentration R and is mathematically represented by $J^R(R)$. We assume the pathway rate $J^R(R)$ has a Michaelis-Menten form:

$$J^R = \frac{V^R_{max} R}{K^R_m + R},$$

and it represents the rate at which product is formed, which in this case is the same as the rate at which substrate is consumed. Therefore throughout this thesis we refer to V^R_{max} as the maximal rate of resource R uptake and K^R_m as the measure of affinity for resource R. The term η^R_{ATP} denotes the number of ATP

molecules produced in the pathway. We represent microbial growth as a linear function of the rate of ATP production [14, 37, 38] namely $r \cdot J^{ATP}$, where r is the constant amount of biomass formed per unit of ATP, and we define $\eta_e^R = r \cdot \eta_{ATP}^R$ as the efficiency of the metabolic pathway utilisng resource R, i.e. the amount of biomass created per unit resource.

Sucrose utilization. Some strains are able to take up sucrose (S) directly, through the $H+$ symport, and the rate of such sucrose pathway is defined by

$$J^S = \frac{V_{max}^S S}{K_m^S + S}$$

where V_{max}^S denotes the maximal rate of the pathway while K_m^S denotes the respective Michaelis-Menten constant. The efficiency of the pathway utilising sucrose is denoted by a constant η_e^S.

Invertase production. Invertase producers secrete invertase, an enzyme which catalyses the hydrolysis of sucrose (S) into glucose and fructose monosaccharides, which can be transported into yeast cells [39]. The rate of conversion of sucrose into glucose and fructose is a saturating function of sucrose concentration taking the following from:

$$Inv = r_{in} \frac{S}{k_{in} + S},$$

where r_{in} denotes invertase activity, while k_{in} denotes a saturation constant. Invertase is costly to produce, and its cost is denoted by a constant c.

Hexose utilisation. Instead of considering the glucose and fructose separately, we term both of the simple sugars 'hexose', and we introduce the hexose uptake rate J^H in the form:

$$J^H = \frac{V_{max}^H H}{K_m^H + H},$$

where V_{max}^H is the maximal rate of hexose pathway while K_m^H is the corresponding Michaelis-Menten constant.

Self-restraint through efficiency of resource utilisation. The efficiency of the pathway utilising simple sugars is denoted by η_e^{Hxt}. Yeast exposed to abundant hexose convert it inefficiently into growth compared with those exposed to lower hexose levels [40, 41]. We term this a rate-efficiency trade-off, where an increase in resource uptake rate leads to a decrease in the number of cells created per unit of resource. Therefore η_e^{Hxt} is a decreasing function of J^H, and hence we write $\eta_e^{Hxt}(J^H)$. Throughout this thesis, we will sometimes drop the rate efficiency trade-off assumption for the sake of simplicity, and in such case η_e^{Hxt} will be set to a constant.

Representation of space. For simplicity, the space we consider is assumed to be one dimensional and it is denoted by $\Omega = [0, l]$, where l is a positive constant. One dimensional space allows for very intuitive understanding and visualisation of the diffusive processes happening during microbial growth, and it simplifies the representation of spatially structured environments. Nevertheless, considering a number of two-dimensional distributions of microbes within the space they occupy could provide a new insight into our results, and it is one of possible directions to continue our study.

Whenever we study spatially heterogeneous systems, we model spatial interactions using a reaction-diffusion framework. It means that the movement of resources and cells across their spatial domain can be understood as the continuous version of a random walk.

The random walk can be explained as follows: the space in which the microbes grow and interact is divided into grid points and, at each timestep, each individual can choose to move on the grid one step to the right or one step to the left, with equal probabilities. In our model, both the timesteps, and the intervals on the grid are assumed o be infinitesimally small, and we track in time cell densities and concentrations of considered resources for each spatial location on the grid.

The resources and cells are not able to move outside the space boundaries (i.e the edges of an agar plate as in laboratory experiments), which is mathematically described by no-flux boundary conditions.

Diffusion coefficients. The resources diffuse in the environment and the rate of that diffusion is captured by the diffusion coefficients: D_S, for sucrose, and D_H

for hexose. Due to the molecule size we assume that the rate of movement of sucrose is twice as slow as that of glucose or fructose so that

$$D_S = D_H/2.$$

Although, yeast cells are non-motile, they spread into neighbouring spatial locations during proliferation; this expansion is approximated by a diffusion constant D_N which is significantly smaller than the D_H (i.e $D_N << D_H$).

2.2 Types of microbial cultures

The experimental protocols studying microbial populations include a number of different techniques of multiplying the microorganisms and allowing for population growth. These techniques differ in the way of feeding the microbes, and they may represent different natural conditions. Here we give a brief overview of the types of microbial cultures mathematically described and studied throughout this thesis: the continuous cultures (studied in Chapters 5 & 7), two types of batch cultures, namely: liquid (studied in Chapters 3 & 6) and spatially structured (studied in Chapters 3 & 4), as well as serial transfers (Chapter 6).

2.2.1 Continuous culture

In continuous culture microorganisms are grown in liquid medium and at steady state conditions. This allows them to grow at a constant rate and in a constant environment. In particular, in the continuous cultures, the carbon source and other resources necessary for microbial growth are supplied at a constant rate, so they do not get exhausted. One of the most standard continuous culture setups is the chemostat, i.e. a bioreactor, in which microbial cultures are grown under constant conditions. A schema representing the chemostat setting is presented in Fig. 2-1. The core feature of chemostats is a continuous inflow of resources from the reservoir to the chemostat vessels, and a continuous outflow of the content of the vessels (the media and the cells). The inflow and outflow happen at the same rate D, keeping the culture volume constant in the chemostat vessels. Another important feature of the standard chemostat setting is that the culture is well-mixed, and thus it is completely homogeneous in space.

Chemostat cultures can represent natural conditions characterised by a constant inflow of fresh resources and a constant outflow of the culture content [42]. For example in some human organs such as gut [43–46], mouth [47] or bladder [48] the nutrients are continuously flowing in, because of the food intake, and the waste products are continuously removed, as they transit through the digestive (or urinary) system.

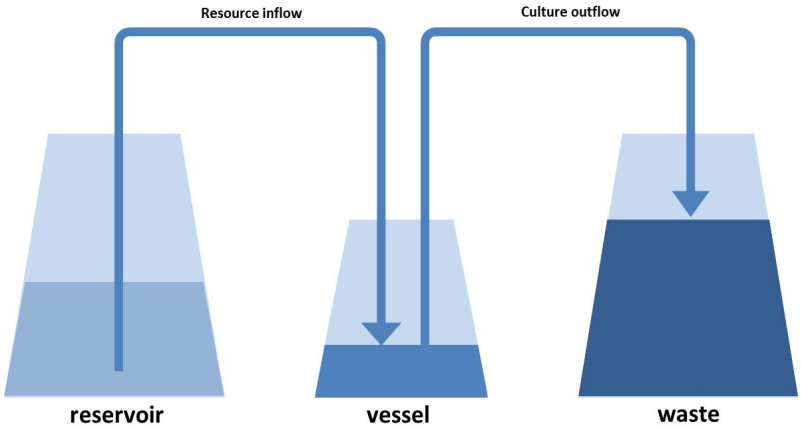

Figure 2-1: **A schema of the chemostat setting.**

In order to model the microbial growth in chemostat we deploy systems of Ordinary Differential Equations (ODEs), which describe the time trajectories of the resources and cells concentrations, as was done in the classical literature [49].

2.2.2 Batch culture

In contrary to the continuous cultures, the batch culture is a closed microbial system, once initiated with given conditions (such as population density or resource concentration) and not manipulated during the microbial growth. This means no resources are added for the duration of experiment, and no waste products are removed. Because of that the microbes can only grow for a limited amount of time, until the initially provided resources are exhausted, and they face conditions varying with time. The environment, initially abundant in resources, gradually changes into the one with little resources and numerous waste products created during the microbial growth.

This setup represents the natural variations in the ecological conditions. In particular the batch cultures can be either liquid, and thus creating a well mixed environment, with the conditions being the same for all the organisms, or they may be spatially structured, where microbes are grown on solid plates, and may face different environmental conditions depending on their spatial location within these plates. While the liquid batch cultures can represent aquatic environments, the spatially structured ones are better suited to represent microbial biofilms, where the individuals grow on spatially structured surfaces which limit their dispersal.

Whereas liquid batch cultures can be modelled with systems of ODEs, in the spatially structured ones the concentrations may vary in space and therefore one needs to track them in both: space and time. This can be done by systems of Partial Differential Equations (PDEs). For similar modelling approaches, see for example: [50–54].

2.2.3 Serial transfer

A special case of a batch culture is the serial transfer experiment. This is a typically used experimental evolution protocol, in which a studied population is iteratively grown in a liquid batch culture. The first batch culture is initiated with a fixed microbial population density N_0 and resource concentration S_0, and the microbes are grown for a fixed amount of time T. During that period (termed a 'season'), various phenotypes compete for resources and grow in the common environment, changing their frequencies depending on the selection pressures acting on the community. At the end of the season, a fraction of cells is taken from the culture and transfered into fresh media, at density N_0. Thus the new batch culture is initiated with the same initial resource concentration S_0 and population density N_0, but with different frequencies of studied phenotypes. This procedure is repeated for a number of times, until the frequencies of the studied phenotypes stabilise.

This protocol aims to represent the seasonality of environmental conditions, and can be modelled as a series of batch culture experiments.

2.3 Equilibria dynamics and bifurcation diagrams

Throughout this thesis we will be often interested in the steady state behaviour of the studied microbial communities. Here we briefly describe how we define and graphically represent such steady states.

Let us a consider a dynamical system described by variables $x = \{x_1, x_2, ..., x_N\}$, where N denotes a positive integer. The steady states (termed also 'equilibria') of that system, are the values of $x = \{x_1, x_2, ..., x_N\}$ at which the system is not changing in time, mathematically denoted as $\frac{dx}{dt} = 0$. We distinguish two types of equilibria: 'stable' (mathematically defined when all the eigenvalues of the Jacobian matrix of the ODE system have negative real parts) and 'unstable' (mathematically defined when some eigenvalues have positive real parts). If a steady state $x^* = \{x_1^*, x_2^*, ..., x_N^*\}$ is locally stable, then the culture started at initial conditions x^0 close to x^*, will converge (or 'be attracted') to this state and stay at this state in long-term. Otherwise, if the steady state x^* is unstable, a small perturbation from x^* may lead the system to move away from that equilibrium point. Therefore, in practice, what can be observed in nature are usually the stable steady states, because they are less vulnerable to random events and perturbations.

The steady states are usually plotted in 'bifurcation diagrams', which are a standard way of representing dynamical systems behaviour, and they show the system equilibria, depending on a chosen parameter. Here we explain how to read bifurcation diagrams, based on the example of logistic growth model [55]:

$$\frac{dN}{dt} = rN(1 - N/K), \tag{2.3.1}$$

where N denotes the population size, r its growth rate and K the carrying capacity of the environment. The equilibrium population size N^*, is such value of N which satisfies: $\frac{dN}{dt} = 0$, and it depends on the values of the model parameters, r and K. In Fig. 2-2 we show the system equilibria, depending on the carrying capacity parameter K. The bifurcation diagrams can be read in the following way. The x-axis represents values of a given parameter (in our case K), and on the y-axis we plot the values of one of the considered variables in steady state (in our case

N). Each value of the considered parameter is related to a number of steady states that can be reached at that parameter value. Hence, from a bifurcation diagram one can read the values and the number of steady states depending on the parameter value. In particular, from Fig. 2-2, it can be seen that for every value of the parameter $K > 0$, there are two steady states of N: one stable, when $N = K$, and one unstable, when $N = 0$ (Fig. 2-2).

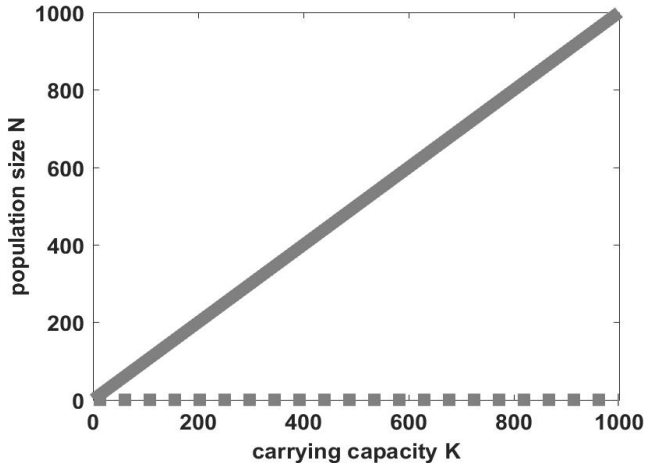

Figure 2-2: **Example of a bifurcation diagram.**
A bifurcation diagram showing the equilibrium population size N depending on the carrying capacity of the environment K, according to the logistic growth model (2.3.1). The stable equilibria are denoted by solid lines, while the unstable equilibria are denoted by dashed lines. Here, the growth rate parameter r is set to a positive constant $r > 0$.

2.4 Relative fitness

The evolutionary competition between two populations is often described by the 'relative fitness' of one population to another [19]. Throughout this thesis we will use this measure to quantify our results on competition between two microbial strains. Here we explain how to calculate and interpret the relative fitness.

We simulate competition between two considered strains: s_1 and s_2 for a given period of time T, termed a 'season'. The competition can be initiated with different ratios of the strain s_1 size to the total population size. This ratio is termed the 'frequency of the strain s_1'. Let $f_0 \in [0, 1]$ denote the initial frequency of the strain s_1 in the population and f_{end} denote its final frequency after the competition. By

$$Qf = f_{end}/f_0 \tag{2.4.1}$$

we denote the change in frequency of s_1 over one season.

Similarly, if N_0 and N_{end} denote the whole population size, at the beginning and at the end of competition, respectively, we define:

$$QN = N_{end}/N_0 > 0, \tag{2.4.2}$$

as the change in population size over one growth season. Subsequently, for a given initial frequency f_0 of the strain s_1, its relative fitness is given (as standard [19]) by:

$$W_{s_1}(f_0) = \frac{ln\Big(Qf \cdot QN\Big)}{ln\Big(\frac{1-f_0 \cdot Qf}{1-f_0} \cdot QN\Big)}. \tag{2.4.3}$$

Note, the relative fitness defined above is equal to:

$$W_{s_1}(f_0) = \frac{f_{end}N_{end}/f_0N_0}{(1-f_{end})N_{end}/(1-f_0)N_0}, \tag{2.4.4}$$

which may be understood as the ratio of growth rate of the strain s_1 to the growth rate of the strain s_2.

The definition (2.4.3) implies, that whenever $W_{s_1}(f_0) > 1$, the initial frequency f_0 of strain s_1 will increase over one season ($Qf > 1$). Otherwise if $W_{s_1}(f_0) < 1$, the frequency of s_1 will decrease over the season ($Qf < 1$). In particular, let us imagine the population competes for a series of seasons (as in the serial transfer experiment described in the subsection 2.2.3), changing their frequencies from season to season according to the relative fitness $W_{s_1}(f_0)$.

In such a case, if $W_{s_1}(f_0) > 1$ for all $f_0 \in (0,1)$, the strain s_1 will keep increasing in frequency until fixing in the environment, and thus, in the long-term it will outcompete the strain s_2. Otherwise, if $W_{s_1}(f_0) < 1$ for all $f_0 \in (0,1)$, the strain s_2 will eventually outcompete s_1. The coexistence occurs if there exists f_0^* such that $W_{s_1}(f_0^*) = 1$ which is equivalent to $Qf_0^* = 1$, meaning there is a frequency of strain s_1, that will remain unchanged after any number of seasons.

Moreover, if in the vicinity of f_0^* the relative fitness of strain s_1: $W_{s_1}(f)$ is a decreasing function of f (negative frequency dependence), as in the example shown in Fig. 2-3a, then that coexistence is locally stable. This is because in the culture started at high f_0 ($f_0 > f_0^*$) we have $W_{s_1}(f_0) < 1$, and the strain s_1 will decrease in frequency until $f_0 = f_0^*$ (grey arrows in Fig. 2-3a), and in cultures started at low

f_0 ($f_0 < f_0^*$) we have $W_{s_1}(f_0) > 1$, and the strain s_1 will increase in frequency until $f_0 = f_0^*$ (red arrows in Fig. 2-3a). Otherwise, if $W_{s_1}(f)$ is an increasing function of f (positive frequency dependence), as in the example shown in Fig. 2-3b, then the coexistence is unstable. Let us notice that in the culture started at $f_0 < f_0^*$, the strain s_1 will further decrease in frequency (grey arrows in Fig. 2-3b), and in cultures started at $f_0 > f_0^*$, the strain s_1 will further increase in frequency (red arrows in Fig. 2-3b). The frequencies of the two strains will keep changing until one of them fixes in the population ($f_0 = 0$ or $f_0 = 1$) or alternatively, until $W_{s_1}(f_0) = 1$.

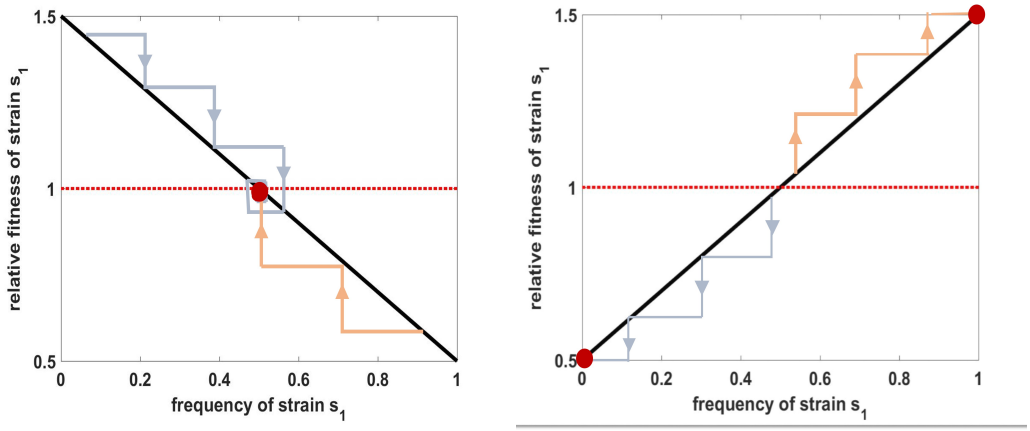

Figure 2-3: **Examples of relative fitness.**
2-3a: Decreasing (negative frequency dependent) relative fitness. The grey and red arrows show example trajectories of f_0, the frequency of s_1 over various seasons. The trajectories started at either low or high initial frequencies of the strain s_1 will both converge to the stable coexistence frequency f_0^* denoted by the red dot.
2-3b: Increasing (positive frequency dependent) relative fitness. The grey and red arrows show example trajectories of f_0, the frequency of s_1 over various seasons. The trajectories started at low initial frequencies of the strain s_1 will lead to extinction of the strain s_1 ($f_0 = 0$). On the contrary, the trajectories started at high frequencies of the strain s_1 will lead to its fixation in the environment ($f_0 = 1$). The stable frequencies $f_0 = 0$ and $f_0 = 1$ are denoted by red dots.

Chapter 3

Harbouring low virulence cheats within a pathogen population increases both fitness and virulence

Abstract

It is widely believed that reduction in virulence of selected individuals in a pathogen population leads to reduction of the overall virulence. Such a disease management strategy has been proposed in a number of previous studies [23–25, 27, 29, 56, 57]. However recent empirical data demonstrates that this strategy may fail, leading to the disease being more severe [36].

The empirical research studied a synthetic cooperative system of the rice blast fungus *Magnaporthe oryzae*. This fungus produces a public good, which facilitates the use of carbon sources available within the host plant, *Oryza sativa*. A synthetically created mutant strain, which fails to create the public good, was less able to sequester nutrients from the host, and therefore was less virulent than the wild type. Nonetheless, an introduction of such a low virulent mutant into the wild type population did not decrease the overall virulence. On the contrary, it led to an increase both in the total pathogen population size and virulence, thus rendering the disease more severe.

The rice blast fungus faces multiple cooperative acts while infecting the host. However, the previous studies were limited to considering single cooperative traits

only [23–25, 29]. Here we build a mathematical model, which shows that an interplay between multiple cooperative traits and spatial structure is sufficient to explain the counter-intuitive increase in population virulence under introduction of the low-virulent strain.

We control the strength of cooperative interactions and the spatial structure by varying: the competition time, resource uptake, and media viscosity. We predict that disabling some of the cooperative interactions or removing spatial structure will lead to the expected behaviour, that is to decreased virulence in the presence of the low virulent mutant. Our theoretical predictions are confirmed by experimental data shown in [36].

3.1 Introduction

An infection is frequently a cooperative process, in which a number of microbes help each other to invade the host [23–26]. A very common type of such cooperation between microbes is the public good cooperation, where individuals produce some extracellular factors (termed 'public goods') that benefit themselves but also other organisms in their neighbourhood. Examples of such behaviour can be found within nutrient acquisition [23, 32], quorum sensing [24, 25], antibiotic resistance [58], host cell lysis [26], or evasion of host immunity [59]. Existence of public goods in the environment often helps the microbial growth and therefore leads to a larger damage to their host [23, 25, 29]. Thus it is believed that the individuals failing to produce the public good will grow slower and therefore will exhibit lower virulence [60].

The public good producers are prone to exploitation by these individuals (termed 'cheats'), who do not invest energy in the public good production, but are still able to take advantage of goods produced by the others [32, 61–64]. These individuals are often not able to persist on their own, but in presence of the public good producers ('cooperators') they can grow and increase in frequency, potentially leading to extinction of public good producers and eventually to the collapse of the whole microbial population. This phenomenon is known as 'the tragedy of the commons' [65, 66], where organisms driven by their selfish interests lead to a decrease in the fitness of the whole group, and potentially to its extinction.

In the case of pathogen populations, forcing such a scenario seems to be a

promising antimicrobial strategy. Indeed, the use of low-virulent cheats that can invade wild type pathogen populations has been studied theoretically [67] and suggested as an effective disease management, termed 'Hamiltonian medicine' [68], which can potentially lead to a decrease in pathogen virulence. That disease management has been experimentally tested in mouse [24] and wax moth larva (*Galleria mellonella*) [23, 25], and until very recently it seemed to be very successful.

Nevertheless, the recent study on Hamiltonian medicine has shown that it may paradoxically render the desease more severe [36]. That study used a novel cooperative system of the rice blast fungus *Magnaporthe oryzae*: a pathogen that infects cultivated rice (*Oryza sativa*) leaves, and it causes significant losses in the worldwide economy. *M. oryzae* secretes an enzyme invertase which extracellularly breaks down sucrose (the most abundant carbon source within the plant host) into simpler sugars: glucose and fructose, which can be easily transported into the pathogen cells [69–73] and effectively metabolised. The mutant strain of *M. oryzae* created in the recent study [36] behaved as a classical cheat. It failed to produce invertase but was able to uptake the simple sugars available in the environment, thanks to the invertase activity of the other strains. As expected, the invertase mutant could not grow efficiently on its own on sucrose, and thus exhibited lower virulence than the wild type invertase producers. However, in a mixture with the wild type strain, it had a selective advantage over the invertase producers: it was able to persist and increase its frequency in the population [36].

Interestingly, contrary to the theoretical prediction that the virulence of a mixture of the two strains is lower than of a homogeneous wild type population [27, 56, 57, 67, 68], the rice leaf infection revealed that a mixture of cheats and public good producers may be in fact more virulent than the population of producers only [36].

What could explain that counter-intuitive result? We notice that previous studies take into account one isolated cooperative trait only. However, the rice blast fungus *M. oryzae* engages in more cooperative interactions while infecting a plant. In particular, apart from producing public goods, it is also subject to the social dilemma of self-restraint, where the individuals may either uptake resources slowly and efficiently (cooperative behaviour, beneficial to the group and harmful to the individual) or quickly and inefficiently (selfish behaviour, harmful to the

group and beneficial to the individual) as in the classical ecological scenario of the tragedy of the commons [65]. The pathogen *M. oryzae* faces a rate-efficiency trade-off [36], which is the core of the self-restraint social dilemma: cells can either uptake the resources quickly and inefficiently (resulting in large uptake rate, but low ATP yield from each molecule of substrate), or slowly and efficiently (resulting in a high ATP yield per molecule of substrate, but low uptake rate). Thus, once produced, public goods (simple sugars) can lead to the self-restraint dilemma and the resulting system is an interplay between the public good and self-restraint cooperative traits.

Here, we construct a mathematical model which takes into account the interplay of these two cooperative traits observed in rice blast infection. Our model is able to explain the novel result showing that a mixture of public good producers and cheats may be more virulent than a pure population of public good producers [36]. Moreover, it shows that when one of its key assumptions: the spatial structure or the rate-efficiency trade-off, is removed, the introduction of cheats into a cooperative population of producers leads to a decrease in the overall virulence. The experimental data obtained in [36] confirms our theoretical predictions: in the absence of spatial structure (liquid culture), the population size is maximised in the absence of cheats. Similarly, in the absence of rate-efficiency trade-off (small resource concentration), the pure producers culture maximises the population size.

Given that fungi secrete a wide range of extracellular enzymes that can become public goods, and that they may face a rate-efficiency trade-off, our results represent a scenario that is likely to happen in nature. Therefore we warn that the concept of Hamiltonian medicine may need to be revised in more complex settings before being applied to antibiotic therapies.

3.2 Mathematical model

3.2.1 Microbial growth

We investigate whether the spatial structure and the synergy between two social traits: public goods production and self-restraint are sufficient to explain why a mixture of public goods producers and non-producers enhances population fit-

ness. To this end, we develop a mathematical model based on a simplified version of the model developed in [14] which allows us to probe the effects of multi-trait interactions on population fitness. Next we briefly describe the basic assumptions of our model, which are described in more detail in Chapter 2: Methods. Although the model has been originally developed to describe the system of *S. cerevisiae*, we argue that its simplified version, which neglects many of the system specific details, can be applied to a wider class of microbial public good systems, and in particular to the cooperative system of *M. oryzae*, in which the costly invertase plays a role of the public good.

We consider two strains, an **invertase producer** (the wild-type, termed also 'cooperator') and a **non-producer** (the mutant strain, termed also 'cheat'). Both of the strains take up resources and use them to generate molecules of ATP, and eventually to convert into biomass. We represent the microbial growth as a linear function of ATP production, as explained in detail in Chapter 2: Methods.

Invertase producers secrete invertase which catalyses the hydrolysis of each molecule of sucrose (S) into two molecules of simple sugars, termed hexose (H). The rate of that hydrolysis is represented by Inv, a saturating function of sucrose concentration. The cost of invertase production is denoted by a constant c, estimated empirically in [14]. Since the ratio of population doublings of invertase producers to non-producers in competition on glucose was calculated as $(1-c)$, in our model we multiply the fitness of producers by $(1-c)$, as was done in [14, 33].

Both strains can take up sucrose (S) and the rate of sucrose pathway is defined by:

$$J^S = \frac{V^S_{max} S}{(K^S_m + S)}$$

where V^S_{max} denotes the maximal rate of the pathway while K^S_m denotes the respective Michaelis-Menten constant. The efficiency of the pathway utilising sucrose is denoted by a constant η^S_e.

Similarly, both strains can take up hexose (H) and the rate of hexose pathway is defined by:

$$J^H = \frac{(V^H_{max} H)}{(K^H_m + H)}$$

where V^H_{max} denotes the maximal rate of the pathway while K^H_m denotes the respective Michaelis-Menten constant. The efficiency of the pathway utilising hexose is denoted by η^{Hxt}_e and we assume that $J^H >> J^S$ (unless the resource concentra-

tions are very small), allowing for hexose to be the preferential carbon source (Fig. 3-1). We also assume that the biomass production related to sucrose uptake is independent of the biomass production related to the hexose uptake. This assumption, also made in [14], allows us to consider the microbial growth rate as the sum of the growth rates related to sucrose and to hexose uptake.

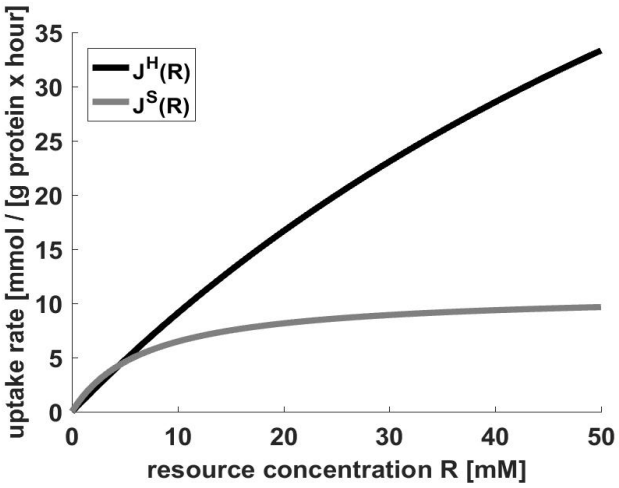

Figure 3-1: **Uptake rates of sucrose and hexose.**
Uptake rates of sucrose ($J^S(R)$) and hexose ($J^H(R)$) depending on the concentration (R) of sucrose and hexose respectively.

Individuals exposed to abundant hexose concentrations convert it inefficiently into growth compared with those exposed to lower hexose levels [40, 41]. We term this a rate-efficiency trade-off, where an increase in resource uptake rate leads to a decrease in the number of cells created per unit of resource, and therefore the efficiency of the metabolic pathway utilising hexose: η_e^{Hxt} is a decreasing function of J^H. Motivated by [54] we assume that:

$$\eta_e^{Hxt}(J^H) = a_1 + a_2/(1 + exp(a_3 + a_4 J^H)),$$

where a_i, $i = \{1, 2, 3, 4\}$ are constants listed in Supplementary Table 3.1. The shape of the function η_e^{Hxt} is shown in Supplementary Fig. 3-11.

3.2.2 Initial distribution of strains.

Consider a one-dimensional spatial domain $\Omega = [0, l]$, with l denoting a positive constant. We assume populations are initially distributed across a number of subpopulations each of which is normally distributed around a point in Ω. Mathematically, we define such initial population distribution (of both producers and

non-producers) as:

$$N_{all0}(x) = \frac{lN_0}{n} \sum_{i \in \mathbb{L}} g(x|x_i, \sigma), \quad x \in \Omega \tag{3.2.1}$$

where N_0 is a parameter describing the average initial population density per spatial location: $N_0 = \frac{1}{l} \int_0^l N_{all0}(x)dx$, and $g(x|x_i, \sigma)$ represents a normal distribution around $x_i \in \Omega$ with variance σ^2. Subsequently, $\mathbb{L} = \{1, ...n\}$ denotes a set of integers where n represents the number of local maxima in $N_{all0}(x)$. The representation in (3.2.1) is akin to an experimental setup where an initial environment contains n subpopulations (also termed patches) of the same size, each of which contains either producers or non-producers [14, 74]. The spatial locations of the local maxima, x_i, for $i \in \mathbb{L}$, denote centre-points of the respective 'patches' around which producers or non-producers are normally distributed.

The distribution $N_{all0}(x)$ is separated into distributions of producers $N_{p0}(x)$ and non-producers $N_{n0}(x)$ in the following way. We assume there are p producer patches located on one side of the plate and $q = n - p$ non-producer patches, located on the other side of the plate. Then we define the initial distribution of producers $N_{p0}(x)$ and non-producers $N_{n0}(x)$ as follows:

$$N_{p0}(x) = \frac{lN_0}{n} \sum_{i=1}^{p} g(x|x_i, \sigma), \tag{3.2.2}$$

$$N_{n0}(x) = \frac{lN_0}{n} \sum_{i=p+1}^{n} g(x|x_i, \sigma). \tag{3.2.3}$$

This is equivalent to an experimental setup where out of possible n 'patches', producers occupy p patches located around $x_i \in \Omega$ with $i \in \{1, 2, .., p\}$, on one side of the plate and non-producers occupy q patches located around $x_i \in \Omega$ with $i \in \{p + 1, , .., n\}$, on the other side of the plate. An example of the initial spatial distribution of producers and non-producers is shown in Fig. 3-2.

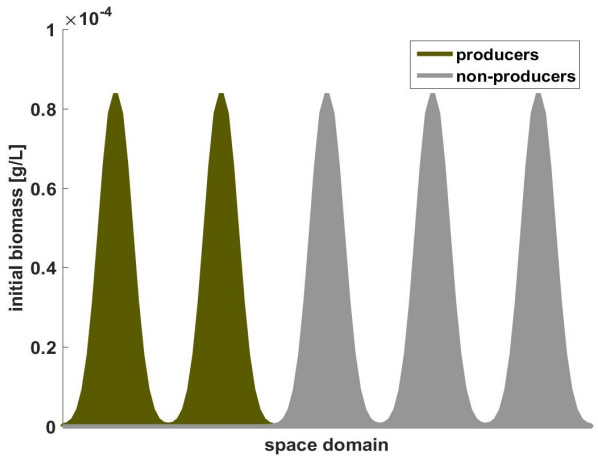

Figure 3-2: **An example of initial spatial distribution of producers and non-producers.**
Here the number of producer patches is $p = 2$ and the number of non-producer patches is $q = 3$.

3.2.3 The system dynamics

To predict the final size of the mixed strain population, we deploy a reaction-diffusion model enabling the explicit tracking of resource concentrations and population densities in both space and time. In particular let $N_p(x,t)$ and $N_n(x,t)$ denote the density of producers and non-producers, respectively, at time t and spatial location $x \in [0,l]$. Then the model takes the following form:

$$\frac{\partial S}{\partial t} = D_S \frac{\partial^2 S}{\partial x^2} - J^S(N_p + N_n) - InvN_p \tag{3.2.4}$$

$$\frac{\partial H}{\partial t} = D_H \frac{\partial^2 H}{\partial x^2} - J^H(N_p + N_n) + 2InvN_p \tag{3.2.5}$$

$$\frac{\partial N_p}{\partial t} = D_N \frac{\partial^2 N_p}{\partial x^2} + (1-c)(\eta_e^{Hxt}(J^H)J^H + \eta_e^S J^S)N_p \tag{3.2.6}$$

$$\frac{\partial N_n}{\partial t} = D_N \frac{\partial^2 N_n}{\partial x^2} + (\eta_e^{Hxt}(J^H)J^H + \eta_e^S J^S)N_n \tag{3.2.7}$$

where $\frac{\partial^2}{\partial x^2}$ is one-dimensional diffusion operator while D_* represent diffusion coefficients for sucrose (S), hexose (H) and cell density (N). Due to the molecular size we assume that the rate of movement of sucrose is twice as slow as that of hexose, while cells move at an even slower rate. Because the secreted invertase remains localised between the cell membrane and the cell wall [39], the enzyme itself does not diffuse. Moreover, invertase activity results in the hydrolysis of each molecule of sucrose into two molecules of hexose, which is represented by the fact that the rate of at which hexose is created: $2InvN_p$ is twice bigger than the rate at which sucrose disappears $InvN_p$. Note that the initial distribution of the two types described in the subsection 3.2.2, and sufficiently low diffusion coefficients D_S, D_H, D_N impose a spatial structured environment, meaning that the population is not homogeneously distributed in space. We impose no-flux boundary condi-

tions:

$$\frac{\partial S}{\partial x}(0,t) = \frac{\partial S}{\partial x}(l,t) = 0, \tag{3.2.8}$$

$$\frac{\partial H}{\partial x}(0,t) = \frac{\partial H}{\partial x}(l,t) = 0, \tag{3.2.9}$$

$$\frac{\partial N_p}{\partial x}(0,t) = \frac{\partial N_p}{\partial x}(l,t) = 0, \tag{3.2.10}$$

$$\frac{\partial N_n}{\partial x}(0,t) = \frac{\partial N_n}{\partial x}(l,t) = 0, \tag{3.2.11}$$

in addition to the following initial conditions: $S(x,0) = S_0$, where S_0 is a sucrose supply constant, $H(x,0) = 0$ with $N_p(x,0) = N_{p0}(x)$ and $N_n(x,0) = N_{n0}(x)$ representing an initial distribution of producers and non-producers, respectively.

3.3 Results

We study a population composed of invertase producers and non-producers, with a fixed average initial population density per spatial location:

$$N_0 = \frac{1}{l}\int_0^l (N_p(x,0) + N_n(x,0))dx, \tag{3.3.1}$$

and with various initial frequencies $f_0 = p/n$ of producers within the population. For each of the initial frequencies $f_0 \in [0, 0.2, 0.4, 0.6, 0.8, 1]$, we simulate the bath culture growth of producers and non-producers distributed on an agar plate, as described in the section 3.2. The growth is simulated for a sufficiently long time T, that is until the carbon sources are exhausted (representing the spatially structured batch culture, as described in the subsection 2.2.2 in Chapter 2: Methods), and for each case we record the final distributions of producers $N_{pend}(x)$ and non-producers $N_{nend}(x)$. Subsequently, we compute the final population density (i.e the final population size in a given volume of the microbial culture) as:

$$N_{end}(f_0) = \int_0^l (N_{pend}(x) + N_{nend}(x))dx. \tag{3.3.2}$$

In order to compare the final population sizes for different initial producers frequencies, we calculate the normalised population size as:

$$\overline{N_{end}(f_0)} = \frac{N_{end}(f_0)}{\max_{f\in[0,\,0.2,\,0.4,\,0.6,\,0.8,\,1]}\left(N_{end}(f)\right)}. \tag{3.3.3}$$

The normalised population size $\overline{N_{end}(f_0)}$, represents the ratio of the final size of two populations: the population started at the frequency f_0 of producers, and the population started at the 'optimal frequency' of producers, that is the frequency which maximises the final population size. For example, if $\overline{N_{end}(60\%)} = 1$ and $\overline{N_{end}(100\%)} = 0.9$, it means that the maximum population size is reached when the population is started with a mixture of 60% producers and 40% non-producers, and the population started with 100% of producers will only reach 90% of that size.

Because the model parameters have not been estimated elsewhere for the system of *M. oryzae*, we choose parameter values by fitting our model to the empirical results obtained in [36]. We restrict these values to be in a 'biologically realistic range', i.e. not differing more than one order of magnitude from the parameters measured for the system *S. cerevisiae*. We list such obtained values in Supplementary Table 3.1.

The normalised population size for various initial producer frequencies, calculated for the model (3.2.4)-(3.2.7) with the parameters from Supplementary Table 3.1 is presented in Fig. 3-3. It shows that the final population size is maximised when the initial population is composed of a mixture of producers and non-producers, similarly as in the recent empirical study [36].

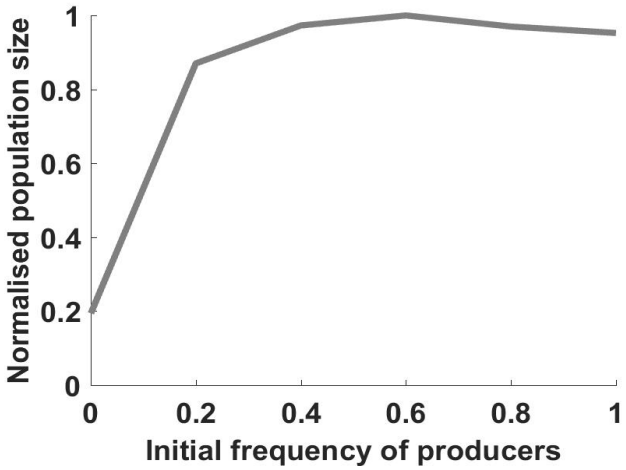

Figure 3-3: **Final population size after exhaustion of resources, in the spatially structured environment and in presence of rate-efficiency trade-off.**
Normalised population size after exhaustion of resources as a function of initial frequency of producers f_0.

3.3.1 The interplay of spatial structure and two cooperative traits

Having verified that our model is able to reproduce the experimental results, we study the key assumptions of that model, which drive these results. In order to study how the synergy between public goods production and self-restraint affects the results shown in Fig. 3-3, we eliminate the assumption of the rate-efficiency trade-off from the model. We set the efficiency of hexose uptake η_e^{Hxt} to a constant, equivalent to the hexose use efficiency at very low resource concentration (see Supplementary Fig. 3-11). Thus we leave only the public goods dilemma at play. In that case the model results return the classical finding that populations containing only producers lead to the maximal total population size (Fig. 3-4a).

This can be explained as follows: The abundance of producers results in excessive invertase production and a very quick decomposition of sucrose into simple sugars. This leads to large temporal spikes in hexose concentration (Fig. 3-5a), which, in the presence of rate-efficiency trade-off, cause rapid but inefficient population growth (Fig. 3-5c). Thus, although the culture grows very quickly, it burns resources inefficiently and is eventually not able to convert the resources into a large amount of biomass.

In contrast, if a fraction of non-producers is present in the population, the hexose generated around producers have a chance to diffuse away to the vicinity of non-producers, where no hexose is produced (Fig. 3-5b). Both producers and non-producers will benefit from such a scenario: the non-producers will receive additional resources and the producers will get a boost in efficiency (Fig. 3-5d). Thus the hexose spikes are smaller, and the culture uses its limited resources more efficiently and is able to convert it into more biomass than in absence of non-producers. The boost in the efficiency is especially visible at the border between producers and non-producers, where the population reaches the highest local densities (Fig. 3-5f), higher than those reached by a pure population of invertase producers (Fig. 3-5e).

When the system is not self-restrained, the introduction of non-producers does not bring any benefits to the population, as shown in Fig. 3-4a.

The positive effect of the introduction of non-producers into a culture is also removed when the population is spatially homogeneous (equivalent to liquid culture in the experimental set-up), as shown in Fig. 3-4b). In the model, this can be simply done by increasing the diffusion coefficients D_S, D_H, D_N. In such a scenario both strains (producers and non-producers) share the available resources equally, and the boost of efficiency, observed in spatial environments, at the boundary between the two strains, is not present here. Instead both strains are equally affected by the rate-efficiency trade-off. The final population sizes calculated for the model (3.2.4)-(3.2.7) in spatially homogeneous environments confirm the standard result that the total population size is maximised for a population composed only of producers (Fig. 3-4b).

Since removing either the rate-efficiency trade-off (Fig. 3-4a) or the spatial structure (Fig. 3-4b), recovers the classical result, in which the pure population of wild type producers is more virulent than a mixture of producers and non-producers, we conclude that what drives the result shown in Fig. 3-3, is the synergy between the spatial structure and two cooperative traits: public goods production and self-restraint.

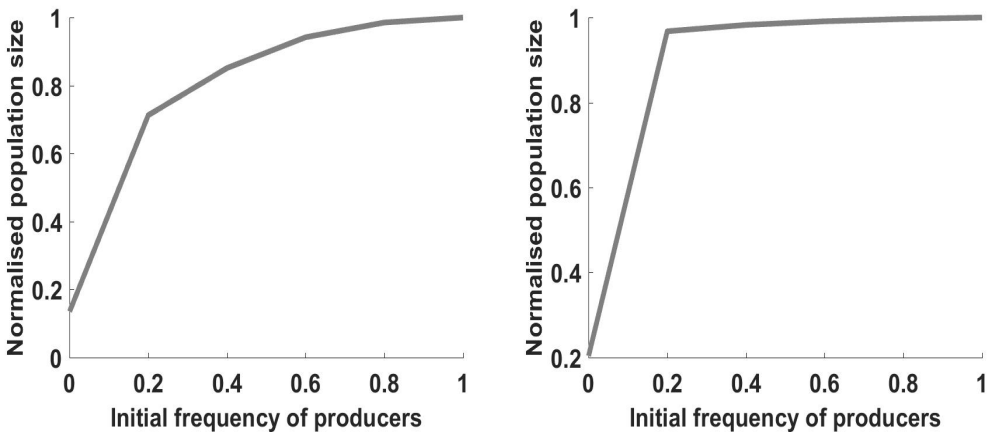

(a) *(b)*

Figure 3-4: **Final population size after exhaustion of resources, in the absence of rate-efficiency trade-off, or in homogeneous environment.**
Normalised population size after exhaustion of resources as a function of initial frequency of producers f_0, (3-4a): in the spatially structured environment and in the absence of rate efficiency trade-off (here $\eta_e^{Hxt} = 0.04$ [g/mmol]); (3-4b): in homogeneous environment and in the presence of rate-efficiency trade-off.

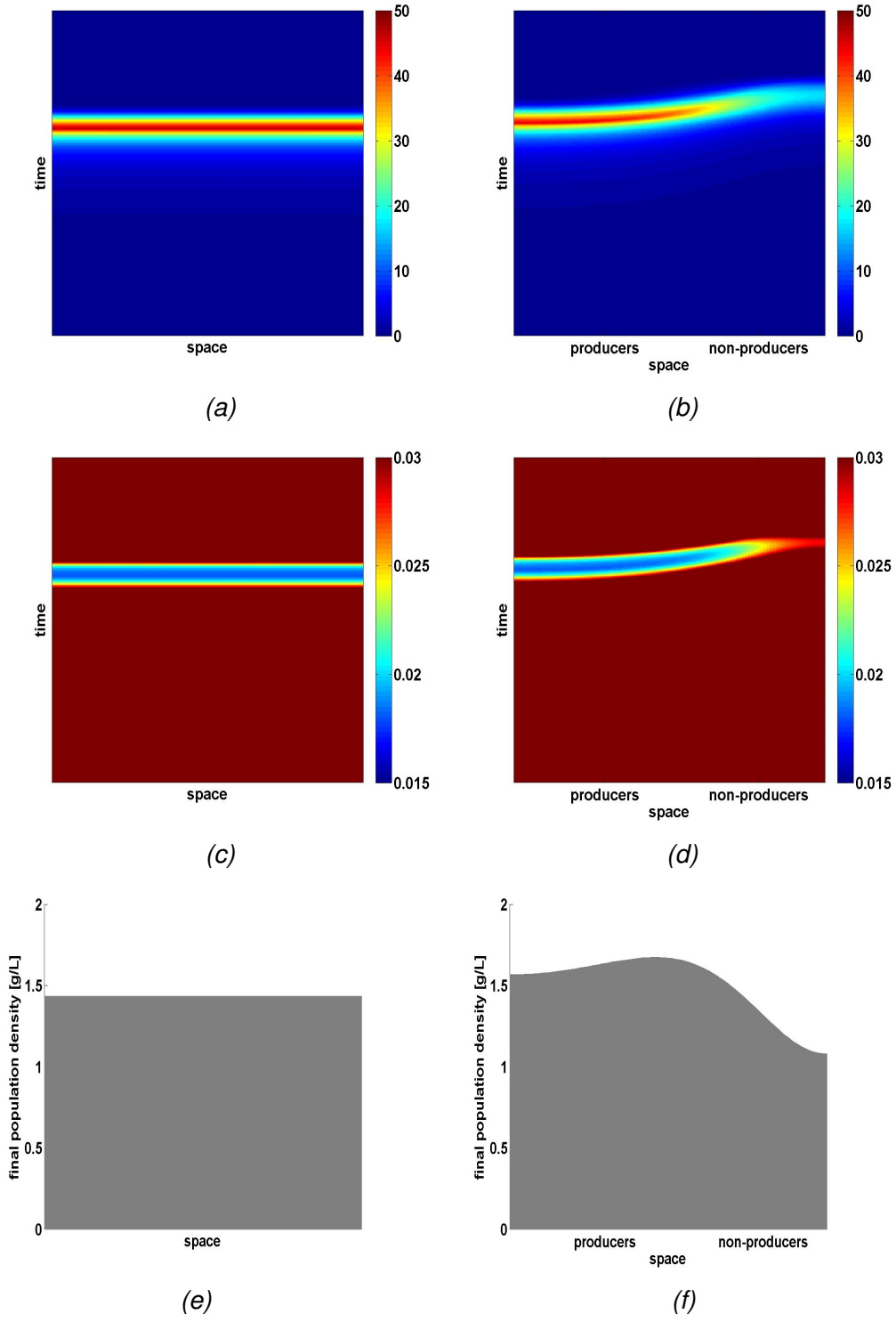

Figure 3-5: **Population growth in a mixture of producers and non-producers, and in a pure producer culture.**
(3-5a)-(3-5b): Hexose concentrations plotted in space and time, for the initial frequency of producers (3-5a): $f_0 = 1$; (3-5b):$f_0 = 0.6$.
(3-5c)-(3-5d): Hexose use efficiency η_e^{Hxt} plotted in space and time, for the initial frequency of producers (3-5c): $f_0 = 1$; (3-5d):$f_0 = 0.6$.
(3-5e)-(3-5f): Final population density plotted in space, for the initial frequency of producers (3-5e): $f_0 = 1$; (3-5f):$f_0 = 0.6$.
The results are calculated in the spatially structured environment and in the presence of rate efficiency trade-off.

3.3.2 Competition time

The experiment performed in [36] and the simulations performed in this study were run until the exhaustion of carbon sources. Here we investigate how the timespan of the experiment (termed here 'competition time') affects the obtained results. According to the model (3.2.4) - (3.2.7), we simulate the growth and competition for resources between invertase producers and non-producers for various times T, representing the timespan of the experiment. If the experiment is run for sufficiently long time, a mixture of producers and non-producers maximises the group benefit (Fig. 3-6a,3-6c). However, when it is run for a short time, its result may default to the expected: the pure invertase producers culture reaches higher population size than any mixture of producers and non-producers (Fig. 3-6a, 3-6b). This is due to the fact that the highest (and most harmful in terms of the hexose use efficiency) local hexose concentrations are observed only after some time from the beginning of the competition, i.e. when the population density is sufficiently high to break down sucrose sufficiently quickly (Fig. 3-7). Thus, apart from the spatial structure and metabolic rate-efficiency trade-off, it is also the competition time that matters for the outcome of the experiment presented in [36].

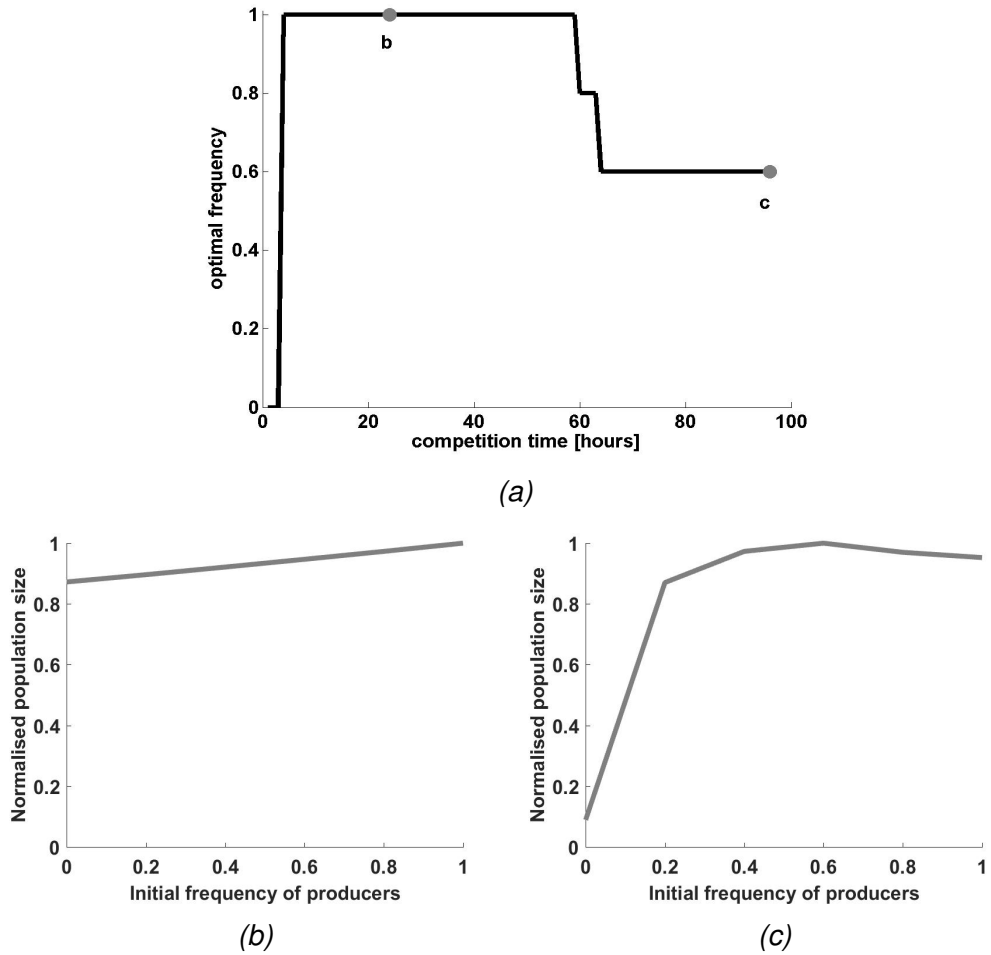

Figure 3-6: **The expected outcome of the experiment, depending on the competition time.**
(3-6a): The optimal producers frequency f_0 (the frequency $f_0 \in [0, 0.2, 0.4, 0.6, 0.8, 1]$ which maximises the final population size N_{end}) as a function of the competition time, in the presence of rate-efficiency trade-off and in spatially structured environment.
(3-6b)-(3-6c): Normalised population size in the end of the competition, as a function of initial producer frequency f_0. The results are simulated in the spatially structured environment and in presence of rate-efficiency trade-off. The competition time is (3-6b): 24 hours and (3-6c): 96 hours.

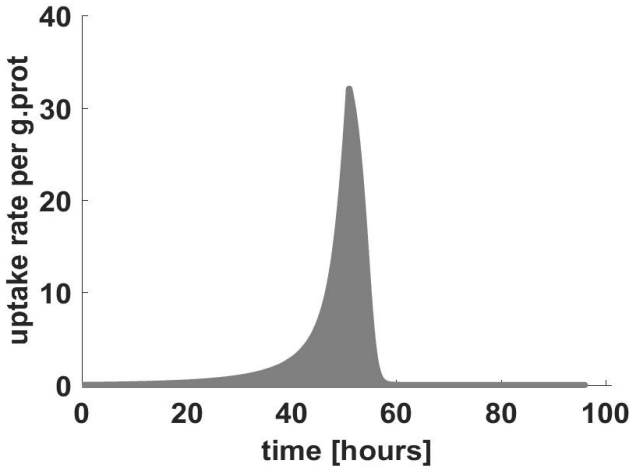

Figure 3-7: **Average hexose uptake rate (over all spatial locations), as a function of time.**
The uptake rate reaches its maximum around hour 50. This is calculated at initial frequency of producers $f_0 = 1$.

3.3.3 Viscosity

We also verify how the spatial structure affects the result observed empirically [36]. It turns out that this result can be obtained only at intermediate diffusion coefficients (Fig. 3-8). If we consider the two limiting cases: no diffusion ($D_S = D_H = D_N = 0\ [l^2/h]$) or homogeneous environment (sufficiently large D_S, D_H, D_N), in both cases the population of only producers will grow to higher densities than a mixture of producers and non-producers (Fig. 3-8, 3-9a, 3-9c). Since the producers and non-producers are initially distributed in separated patches, in the case of no diffusion they will not interact with each other throughout all the competition time. Because the non-producers can not grow efficiently without the help of producers, the final size of each patch of non-producers N_{Nend} will be smaller than the final size of each patch of producers N_{Pend}: $N_{Nend} < N_{Pend}$. Assuming no interaction between the patches the total final population size N_{end} will be simply the sum of the final size of each patch:

$$N_{end} = f_0 n \cdot N_{Pend} + (1 - f_0)n \cdot N_{Nend} \leq n \cdot N_{Pend} + 0 \cdot N_{Nend}, \tag{3.3.4}$$

where $f_0 n = p$ is the number of producer patches and $(1 - f_0)n = q$ is the number of non-producer patches. Thus, since $N_{Nend} < N_{Pend}$, the inequality (3.3.4) holds for all $f_0 \in [0, 1]$, and the group benefit is maximal if the population is composed of producers only (Fig. 3-9a).

In the case of entirely homogeneous environment, the presence of non-producers does not substantially boost the hexose use efficiency in any spatial region, because the simple sugars diffuse in space and form uniformly high concentrations which result in the costly rate-efficiency trade-off. Thus again the 100% of the producers maximises the group benefit (Fig. 3-8 & Fig. 3-9b). See the Discussion section for a more detailed explanation.

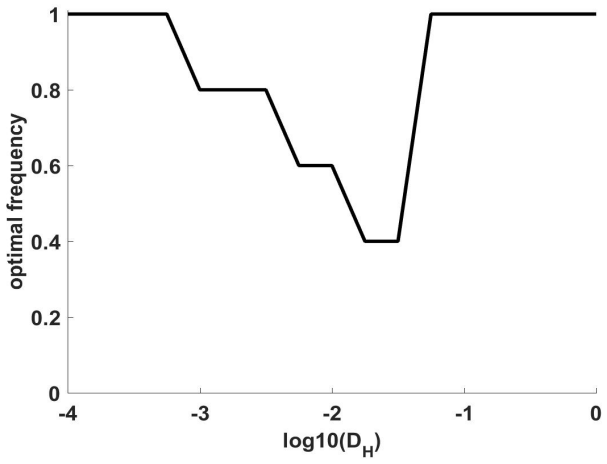

Figure 3-8: **Frequency of producers, which maximizes the final population size.** The optimal producers frequency f_0 as a function of media viscosity. The diffusion coefficients D_S and D_N change together with D_H, so that their ratios are kept constant to $D_S = D_H/2, D_N = D_H/50$.

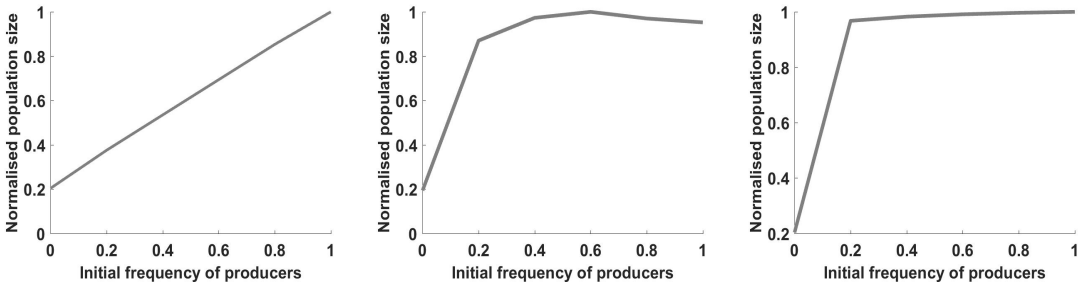

Figure 3-9: **Final population size after exhaustion of resources, depending on the media viscosity.**
Normalised population size, after exhaustion of resources, as a function of initial producer frequency f_0. The results are calculated in presence of rate-efficiency trade-off and in: (3-9a): spatially structured environment with no diffusion: $D_S = D_H = D_N = 0[l^2/h]$; (3-9b): spatially structured environment with diffusion: $D_H = 0.01[l^2/h], D_S = D_H/2, D_N = D_H/50$; (3-9c): homogeneous environment, that is $D_H = 10[l^2/h], D_S = D_H/2, D_N = D_H/50$.

3.3.4 Multiple nutrients uptake

Another important factor to explain our results is the direct sucrose uptake. In the case, in which the two strains are not able to uptake sucrose directly, and they rely only on simple sugars in the media, a mixture of producers and non-producers maximises the total population size not only in the presence of rate-efficiency trade-off and spatial structure (Fig. 3-10a), but also in their absence (Fig. 3-10b - 3-10c).

This is because, even when there is a small number of invertase producers in the culture, they will eventually break down all the sucrose available in the environment, and only a small number of individuals will pay the energetic cost of invertase production. Moreover, the lower the number of producers, the slower the hydrolysis of sucrose into hexose, resulting in a slower, and therefore more efficient hexose uptake. Thus the culture will use up all the available resources in the most efficient way, when the frequency of producers in the culture is minimal, even in the absence of spatial structure or metabolic rate-efficiency trade-off. That would not be the case in presence of direct sucrose uptake. In that case the direct sucrose uptake is less efficient than the hexose uptake (as shown in [14]). Therefore if the number of invertase producers is low, the sucrose will be uptaken inefficiently through the direct sucrose uptake, by the time it is hydrolysed to hexose. This is why the cultures unable to uptake sucrose directly are expected to reach higher population sizes than those that do uptake sucrose (Supplementary Fig. 3-12)

Let us notice that in the case of no sucrose uptake, the non-producers on their own would not only grow slower than producers, but they would not be able to survive. This is however not the case in the experimental system of *M. oryzae* [36].

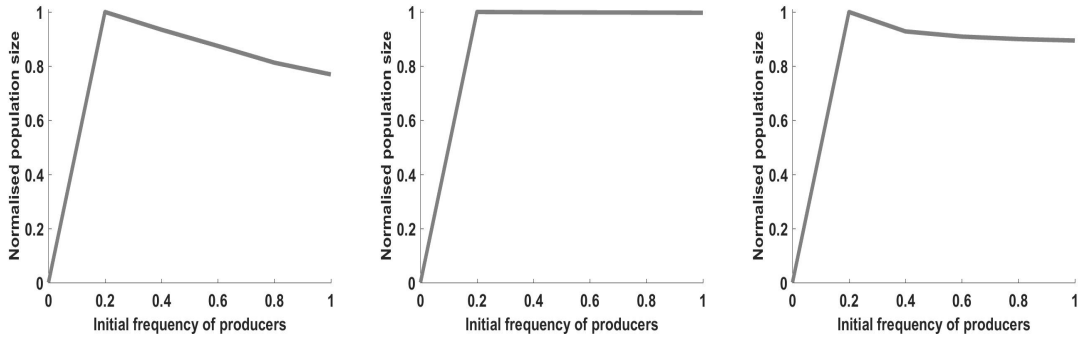

Figure 3-10: **Scenario with no sucrose uptake.**
Normalised population size after exhaustion of resources, as a function of initial producer frequency f_0, (3-10a): in the spatially structured environment and in the presence of rate-efficiency trade-off; (3-10b): in the spatially structured environment and in the absence of rate efficiency trade-off; (3-10c): in homogeneous environment and in the presence of rate-efficiency trade-off.

3.4 Discussion

Our mathematical model explains that the interplay between two social traits and the existence of spatial structure are sufficient to understand the puzzling empirical result [36], according to which a mixture of public good producers and non-producers may maximise the total size and therefore the virulence of a population. It also shows that removing one of these key assumptions leads to the classical results, in which an introduction of cheats into a cooperative population of producers causes a decrease in the overall virulence. In order to explain the obtained results, we propose a step-by-step analysis of the crucial components presented in the section 3.3.

First of all, let us consider our system with no direct sucrose uptake and no rate-efficiency trade-off. It means that the public simple sugars are the unique carbon source available for microbial growth, and are necessary for the survival of both types. In such a case, a small portion of producers is sufficient to make the population reach the maximal size. Although the simple sugars will be generated very slowly, they will eventually convert all the available nutrients into biomass and feed all of the population. At the same time the cost of invertase production will be paid only by a small portion of individuals (invertase producers). Such a scenario is beneficial for the population (Fig. 3-10b).

The extent to which the abundance of producers is harmful for the population changes depending on the existence of spatial structure and the rate-efficiency trade-off. In the presence of rate-efficiency trade-off, apart from paying the costs of producing invertase, the producers also pay a cost of the quick and inefficient hexose uptake. If the number of producers increases, more cells will pay the invertase cost, and the excess of produced invertase will lead to higher hexose concentration in the environment. This will increase the growth speed and, because of the rate-efficiency trade-off, the resources will be converted into biomass less efficiently, meaning that the limited sucrose amount S_0, supplied to the population will be converted into a smaller biomass N_{end}, than in the case of a population with a small fraction of producers. That is why the 'hump' in total population size becomes much more pronounced in the presence of rate-efficiency trade-off (Fig.

3-10a and Fig. 3-10c). In the homogeneous culture, the hexose produced will diffuse and all the individuals will be equally affected by the rate-efficiency trade-off (Fig. 3-10c). However, interestingly, in the spatially structured environment an introduction of non-producers not only decreases the overall hexose concentration (thus increasing the growth efficiency), but it also creates a spatial and temporal niche (at the boundary of the two strains) at which small concentrations of hexose that diffuse away from the producers can be metabolised with much higher efficiency (Fig. 3-5d and Fig. 3-5f). This is why, in this case, the presence of non-producers in the population is even more beneficial for the total population than in the other cases (Fig. 3-10a).

If the individuals are allowed to uptake sucrose (the non-preferred carbon source), abundance of invertase producers becomes more useful for all the population. This is because in the absence of invertase producers, the non-producers uptake sucrose, which is a less efficient metabolic pathway than uptaking simple sugars [14]. When there is only a small proportion of invertase producers in the population, by the time simple sugars diffuse to the non-producers, the non-producers will have uptaken some sucrose (instead of just 'waiting' for the simple sugars to arrive as in the case of no direct sucrose uptake). This means a waste of provided resource. Thus in the absence of rate-efficiency trade-off, the pure producers culture will maximise the population size, because it will use the provided resources in the most efficient way (Fig. 3-4a).

That efficiency however decreases when we also consider the metabolic rate-efficiency trade-off. In such a case, as explained before, an abundance of invertase producers leads to higher temporal concentrations of simple sugars, and therefore to the lower hexose use efficiencies. It is therefore clear that the gain of efficiency on the slow hexose uptake when there is little producers will be balanced with the loss of efficiency on the sucrose uptake. Thus an intermediate frequency of producers in the population may turn out to be optimal (Fig. 3-3).

Why does the result change depending on the existence of spatial structure? In the homogeneous culture a pure population of producers reaches a higher final size than any producer and non-producer mixture. However, when the space is structured, the population reaches its maximal size in presence of non-producers. Moreover that size is higher than the final population size of any homogeneous culture with direct sucrose uptake $V^S > 0$ (Supplementary Fig. 3-12). We argue

that in the spatially structured environment, there are spatial and temporal niches that allow for smoother peaks in hexose concentrations, and therefore for a more efficient metabolism. In particular, even if the average hexose concentration at a given time is sufficiently high to make the microbial population be substantially affected by the rate-efficiency trade-off (the case of a homogeneous culture), the local hexose concentrations around the border of producers and non-producers may be much lower and may lead to a significant increase in the hexose use efficiency (Fig. 3-5f).

3.5 Supplementary Material

In this section we provide additional details of our model and the results.

V_{max}^S	11 [mmol sucrose/ (g protein · hour)]
V_{max}^H	100 [mmol hexose/ (g protein · hour)]
K_m^S	7 [mM sucrose]
K_m^H	100 [mM hexose]
r_{in}	77 [mmol/ (g protein · hour)]
c	0.004
S_0	29.2 [mM]
N_0	$3 \cdot 10^{-5}$ [g protein/L]
D_H	0.01 [l^2/hour]
D_S	$D_H/2 = 0.005$ [l^2/hour]
D_N	$D_H/50 = 0.0002$ [l^2/hour]
η_e^S	0.01 [g protein/ mmol sucrose]
k_{in}	$5 \cdot 10^{-3}$ [mM sucrose]
a_1	0.0176
a_2	0.0318
a_3	-2.2649
a_4	0.205
σ	1/7
l	1

Supplementary Table 3.1: Parameters values for the mathematical model (3.2.4)-(3.2.7).

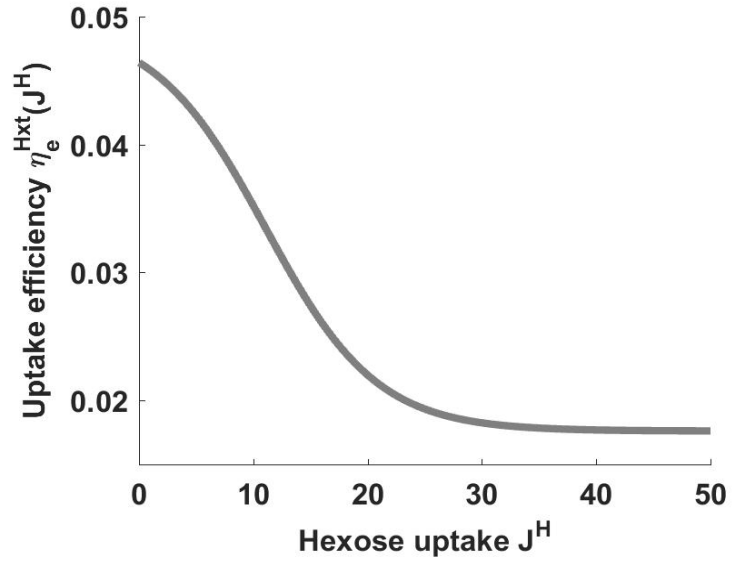

Supplementary Figure 3-11: **Efficiency of hexose utilisation as a function of hexose uptake.**
The hexose use efficiency $\eta_e^{Hxt}(J^H)$ as a function of the uptake rate J^H.

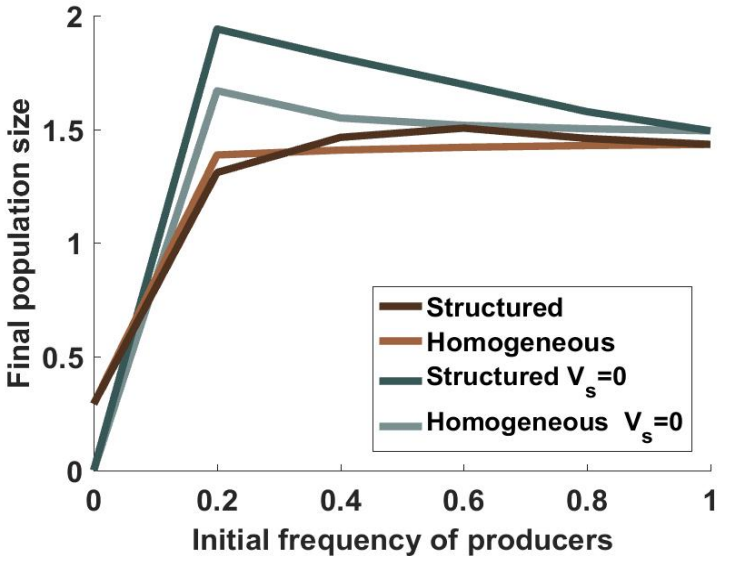

Supplementary Figure 3-12: **Final population size, after exhaustion of resources, in different scenarios.**
The total final population size (not normalised) after exhaustion of resources as a function of initial frequency of producers f_0. This figure compares the results in the spatially structured environment and homogeneous environments, assuming direct sucrose uptake ($V_{max}^S > 0$ [mmol/ (g · hour)]) or no sucrose uptake ($V_{max}^S = 0$ [mmol/ (g · hour)]).

Chapter 4

Quantitatively Defined Spatial Structure Explains the Relationships between Population Density and Cooperation

Abstract

Population density influences the selection for cooperation in microorganisms, with spatial structure and the type of social dilemma facing microbes shaping the outcome. However a consistent relationship between population density and cooperation is yet to emerge and we postulate this is due to the differences in the way spatial structure is represented and manipulated. To test this we define a quantitative measure of the degree of spatial structure within an environment and incorporate it into a dynamic model of microbial cooperation. By systematically manipulating spatial structure and resource concentration we uncovered a complex range of possible outcomes capable of reconciling different results from the literature. When environmental resources are at a very low or intermediate level, high population density favours cooperation in highly structured environments but favours cheats in environments with low spatial structure. When resources are at a low level, high population density favours cooperators regardless of the degree of spatial structure. Finally, when resources are plentiful, high population density promotes cheating in both high and low structured environments. We demonstrate that a systematic quantification of spatial structure and a consideration of

resource availability within an environment are essential for understanding the relationship between population density and cooperation.

4.1 Introduction

Population density is known to affect selection for cooperation in microorganisms [32, 34, 63, 75, 76]. However, whether high population density favours cooperation depends on the spatial structure of the environment [75, 76] and the type of social dilemma facing microbes [32, 63, 75, 76]. In particular, two types of social dilemmas are of relevance: public goods production and self-restraint. Public goods are extracellular factors used to perform a range of functions including nutrient acquisition, biofilm formation and quorum sensing [18]. They are costly to produce but benefit individuals in the locality, making them prone to exploitation by cheats who do not contribute to the production of public goods but still reap the rewards. The self-restraint social dilemma results from a metabolic trade-off that arises between growth rate and growth efficiency, whereby fast growth is necessarily less efficient than slow growth [37]. Efficient use of common resources conforms to the classical definition of a cooperative trait: it is beneficial to the group, because more biomass is produced per unit resource, but costly to individuals, because each divides at a slower rate [75].

A general relationship between population density and cooperation has not yet fully emerged. In spatially homogeneous environments the picture has so far been consistent. For public goods systems high population density favours cheats [34] while in self-restrained systems the opposite holds [75]. However, conflicting results have been found for spatially heterogeneous environments. In the case of self-restrained systems, while empirical studies found that high population density disfavours cooperation [75], theoretical studies indicate that this result may not universally hold [63]. In public goods systems, theory predicts that high cell density will favour cheats, because in dense populations cheats are 'physically closer' to cooperators and therefore can exploit them more efficiently [63]. However a more recent theoretical study suggests that high cell density can actually favour cooperators if cells diffuse slower than the public goods they produce [76]. While these theoretical results do not necessarily contradict each other, experiments with motile [63] and non-motile [32] cell populations producing diffusible public

goods both report the same outcome that high density populations favour cheats, even when cells diffuse slower that the public goods. These empirical results are consistent with the theoretical predictions in [63] but potentially conflict with the theoretical predictions in [76].

One explanation for the apparent lack of consensus could be that past theoretical and empirical studies on the relationship between population density and cooperation frequently consider both spatial structure and the type of cooperative trait to be binary quantities. For example, in such studies an environment is considered to be either spatially structured or unstructured and the cooperative trait is either public goods production or self-restraint. However, in reality cooperative traits do not appear in isolation and often interact with each other [77]. Moreover degrees of spatial structure can vary significantly between environments [78–80].

In general, theoretical studies do not necessarily consider spatial structure as a binary trait and instead often manipulate population viscosity to produce varying degrees of spatial structure [81–86]. However, this approach is rarely utilised in empirical studies with some notable exceptions [64, 87] where viscosity is varied by changing media composition in the experimental cultures. Some studies also vary mixing intensity of the experimental cultures to produce a non-binary spatial structuring of the environment [88].

However, more frequently empirical studies manipulate spatial structure through an initial distribution of organisms within an environment with many 'spatially heterogeneous' initial distributions all falling into the same category of 'structured' environments as we now discuss. For instance, microbial communities can be fragmented into subpopulations that are linked only through migration. Such metapopulation structure can be imposed experimentally by embedding populations into microlitre plates [74, 75, 89, 90] whereby the initial spatial distribution and the migration is controlled by the experimentalists. Another common way of manipulating spatial structure is to inoculate agar plates with a number of droplets containing microbial cultures, forming patches of interacting subpopulations [14, 63]. In this scenario the initial spatial distribution is controlled by the experimentalist but the subsequent interactions between subpopulations are not controlled. Finally homogeneous cultures can be inoculated onto plates [32, 61, 63, 85] or into unshaken flasks [91] allowing for the spatial structure to self-emerge. In that case both the initial spatial cell distribution and the subse-

quent interactions between the emergent subpopulations are not controlled.

Moreover, spatial structure can inadvertently be manipulated, giving rise to different degrees of structuring between biological replicates. For example, an environment containing 50% cooperators can have different spatial structure depending on the way subpopulations containing cooperators or cheats are distributed (Supplementary Fig. 4-6). This is of particular relevance for experimental methods in which the position of subpopulations, be it cheat or cooperator, is located randomly [14].

Could the apparent inconsistencies regarding the relationship between population density and cooperation be down to the fact that spatial structure can be represented and manipulated in many different ways? In this chapter we postulate that the answer is yes and we argue the importance of representing spatial heterogeneities in a way that systematically captures different degrees of structure.

To this end we develop a theoretical framework which introduces a quantitative measure of environmental structure and we apply it to a microbial cooperation system in which multiple social traits interact, namely public goods production and self-restraint. Therefore our framework provides a unique opportunity to bring together disparate results on the relationship between population density and cooperation into a unifying structure. Indeed, we can replicate the seemingly conflicting results and demonstrate that they are all part of a wide spectrum of possible outcomes.

4.2 Mathematical model

4.2.1 The Cooperative System

Given that the relationship between population density and cooperation depends on the type of cooperation, namely public goods production or self-restraint [63] here we consider a cooperative system where these two social traits interact. This allows us to systematically explore the relationship between cell density and cooperation not just for individual but also for interacting social traits. Moreover given the importance of spatial structure in determining the relationship between cell density and cooperation, we introduce a robust way of systematically varying

spatial structure.

In this section we first describe a spatial model of a cooperative system involving interacting social traits, before we discuss how to quantify a degree of spatial structure within an environment.

In order to secure nutrients microbes can cooperate by secreting enzymes that break down complex sugars into simple sugars that are easier to digest [39, 92]. Once simple sugars are available in the environment, microbes are then constrained by a rate-efficiency trade-off [37] which is at the core of the second social dilemma of self restraint: resources can be exploited slowly but efficiently or quickly but inefficiently. By varying resource concentration in the system, we can manipulate the strength of the rate-efficiency trade-off [14, 41]. When nutrients are scarce, the rate-efficiency trade-off is weak or non-existent [14, 41] and the nutrient acquisition through public goods production is expected to be the dominant constraint on microbial growth; however when nutrients are plentiful we expect that the rate-efficiency trade-off is the mechanism constraining growth.

An example of the system where both public goods production and self-restraint interact is an invertase production in *Saccharomyces cerevisiae* extensively used as a model system for studying cooperation [14, 32–34, 74, 75, 93]. Invertase is a costly extracellular enzyme used to break down sucrose into glucose and fructose, the preferred carbon sources, while *S. cerevisiae*'s growth on glucose and fructose is constrained by a rate-efficiency trade off [14].

As a basis of our theoretical model we use the well-established mathematical framework developed in [14] for invertase production in *S. cerevisiae*, which has proven capable of generating accurate quantitative predictions. In this framework the cooperative trait under consideration is the production of a public good: invertase. Although the two considered strains: invertase producer and non-producer, differ only in one gene, they are affected by two social dilemmas. The invertase producers and non-producers, in their localities, create different ecological environments (with the producers facing higher hexose concentrations), and thus they are also differently affected by the rate-efficiency trade-off, and utilise their resources with different efficiencies (the 'self-restraint' dilemma). This enables us to study the impact of self-restraint on the cooperative system of public good production.

Here we consider a simplification of the system-specific model in [14], which

is in line with other more general models of invertase production [33]. Moreover we also introduce one important component concerning the representation of spatially structured environments. In [14] the degree of spatial mixing was represented by a phenomenological parameter. In this chapter instead we model spatial interactions using a reaction-diffusion framework, this enables a better connection between the theory and experiments as we now explain.

Next we briefly describe the basic assumptions of the model with more detailed description presented in the Chapter 2: Methods. Consider two strains, a cooperator (also termed invertase producer) and a cheat (also termed a non-producer). In our model both strains take up resources R and use them to generate ATP using a simple, unbranched pathway [37]. We represent microbial growth as a linear function of the rate of ATP production, as described in more detail in the Chapter 2: Methods.

Both strains take up sucrose (S) and the rate of sucrose pathway is denoted by J^S, while it's efficiency is denoted by η_e^S. Invertase producers secrete invertase, that catalyses the extracellular hydrolysis of each molecule of sucrose into two molecules of monosaccharides, that is hexose (H). The rate of conversion of sucrose into hexose is represented by Inv, a saturating function of sucrose concentration. The cost of invertase production is denoted by a constant c, estimated empirically in [14]. Moreover, in [14] the fitness of invertase-producing cooperators was calculated as the ratio of population doublings during competition on glucose with non-producing cheats and it was found that producers suffer a fitness disadvantage. To reflect this in our model, we multiply the fitness of producers by $(1-c)$ as was done in [14, 33].

Simple sugars are transported into the cell by hexose transporters and the rate of the hexose pathway is denoted by J^H, where the efficiency of this pathway is denoted by η_e^{Hxt}. Yeast exposed to abundant hexose convert it inefficiently into growth compared with those exposed to lower hexose levels [40, 41]. We term this a rate-efficiency trade-off, where an increase in resource uptake rate leads to a decrease in the number of cells created per unit of resource, and therefore η_e^{Hxt} is a decreasing function of J^H. The parameterisation of all of the above terms can be found in the Supplementary Material 4.5.2, and the exact shape of the function $\eta_e^{Hxt}(J^H)$ is shown in Supplementary Fig. 4-7.

To predict the densities of the producer and non-producer strain in compe-

tition, we deploy a reaction-diffusion model enabling the explicit tracking of resource concentrations and population densities in both space and time. In particular let $N_p(x,t)$ and $N_n(x,t)$ denote the density of producers and non-producers, respectively, at time t and at spatial location x, $x \in \Omega$ where $\Omega = [0,l]$ is a one-dimensional domain with l denoting a positive constant. Similarly let $S(x,t)$ and $H(x,t)$ denote the concentration of sucrose and hexose, respectively, at time t and at spatial location x. Then the model takes the following form:

$$\frac{\partial S}{\partial t} = -J^S(N_p + N_n) - InvN_p + D_S\frac{\partial^2 S}{\partial x^2}, \tag{4.2.1}$$

$$\frac{\partial H}{\partial t} = -J^H(N_p + N_n) + 2InvN_p + D_H\frac{\partial^2 H}{\partial x^2}, \tag{4.2.2}$$

$$\frac{\partial N_p}{\partial t} = (1-c)[\eta_e^{Hxt}(J^H)J^H + \eta_e^S J^S]N_p + D_N\frac{\partial^2 N_p}{\partial x^2}, \tag{4.2.3}$$

$$\frac{\partial N_n}{\partial t} = [\eta_e^{Hxt}(J^H)J^H + \eta_e^S J^S]N_n + D_N\frac{\partial^2 N_n}{\partial x^2}. \tag{4.2.4}$$

where $\frac{\partial^2}{\partial x^2}$ is one-dimensional diffusion operator, while D_* represent diffusion coefficients for sucrose (S), hexose (H), and cell biomass (N). Due to their molecular size we assume that the rate of movement of sucrose is twice as slow as that of hexose, while cells move at an even slower rate. Note that secreted invertase remains localised between the cell membrane and the cell wall [39], and therefore the enzyme itself does not diffuse.

In order to link our model to laboratory experiments in which microbes are grown on agar plates, and neither the cells nor the resources can move outside the plate edges, we impose no-flux boundary conditions:

$$\frac{\partial S}{\partial x}(0,t) = \frac{\partial S}{\partial x}(l,t) = 0, \tag{4.2.5}$$

$$\frac{\partial H}{\partial x}(0,t) = \frac{\partial H}{\partial x}(l,t) = 0, \tag{4.2.6}$$

$$\frac{\partial N_p}{\partial x}(0,t) = \frac{\partial N_p}{\partial x}(l,t) = 0, \tag{4.2.7}$$

$$\frac{\partial N_n}{\partial x}(0,t) = \frac{\partial N_n}{\partial x}(l,t) = 0, \tag{4.2.8}$$

Such setting could also represent some natural environments, in which microbial cultures are kept within certain physical boundaries, such as fruit surface in case of *S. serevisiae* or rice leave edges in the case of *M. oryzae*. Additionally, we

assume the following initial conditions: $S(x,0) = S_0$, where S_0 is the initial sucrose supply constant while $H(x,0) = 0$. Moreover, $N_p(x,0) = N_{p0}(x)$ and $N_n(x,0) = N_{n0}(x)$ representing an initial distribution of producers and non-producers, respectively, with the average initial population density per spatial location denoted by $N_0 = \frac{1}{l}\int_{x\in\Omega}(N_{p0}(x) + N_{n0}(x))dx$. Thus we study the same model as the one proposed in the Chapter 3, with the parameters listed in Supplementary Table 4.1.

The model is simulated for different initial frequencies f_0 of producers within the population until all resources are exhausted (representing the spatially structured batch culture, as described in the subsection 2.2.2 in Chapter 2: Methods), and for each case we record the final population distribution of both producers denoted by $N_{pend}(x)$, and non-producers denoted by $N_{nend}(x)$. Subsequently, the long-term competition outcome is determined by calculating the relative fitness of invertase producers to non-producers $W_p(f_0)$, as described in the Chapter 2: Methods. If $W_p(f_0) > 1$ for all $f_0 \in (0,1)$, producers outcompete non-producers in the long-term while if $W_p(f_0) < 1$ for all $f_0 \in (0,1)$, we can conclude that non-producers outcompete producers. The coexistence occurs if there exists f_0^* such that $W_p(f_0^*) = 1$, meaning there is a value of producer frequency that remains unchanged in long term.

4.2.2 Quantifying a degree of spatial structure

Consider a one-dimensional spatial domain $\Omega = [0, l]$. We define an initial population distribution (of both producers and non-producers) as

$$N_{all0}(x) = \frac{lN_0}{n}\sum_{i\in\mathbb{L}} g(x|x_i,\sigma), \quad x \in \Omega \tag{4.2.9}$$

where $g(x|x_i,\sigma)$ represents a normal distribution around $x_i \in \Omega$ with variance σ^2, and $\mathbb{L} = \{1,...n\}$ is a set of integers where n represents the number of local maxima in $N_{all0}(x)$. The representation in (4.2.9) is akin to an experimental setup where an initial environment contains n subpopulations (also termed patches) of the same size, each of which contains either producers or non-producers [14, 74]. The spatial locations of the local maxima, x_i, $i \in \mathbb{L}$, denote centre-points of the respective 'patches' around which producers or non-producers are normally distributed. Even though we assume that microbial cells have low motility, the resources can

diffuse throughout the spatial domain which implicitly facilitates the interactions between cells in spatial locations both within and between different patches.

In order to separate $N_{all0}(x)$ into distributions of producers $N_{p0}(x)$ and non-producers $N_{n0}(x)$ we first introduce the following notation. Let $\mathbb{P}$ denote a subset of $\mathbb{L}$ with $p < n$ denoting the cardinality of $\mathbb{P}$ which also represents the number of local maxima in $N_{p0}(x)$. Similarly, let $\mathbb{Q} = \mathbb{L} \setminus \mathbb{P} := \{i \in \mathbb{L} : i \notin \mathbb{P}\}$ with $q = n - p$ denoting the cardinality of $\mathbb{Q}$ which also represents the number of local maxima in $N_{n0}(x)$. Then

$$N_{p0}(x) = \frac{lN_0}{n} \sum_{i \in \mathbb{P}} g(x|x_i, \sigma), \tag{4.2.10}$$

$$N_{n0}(x) = \frac{lN_0}{n} \sum_{i \in \mathbb{Q}} g(x|x_i, \sigma). \tag{4.2.11}$$

This is equivalent to an experimental setup where out of possible n 'patches', producers occupy p patches located around $x_i \in \Omega$ with $i \in \mathbb{P}$ while non-producers occupy q patches located around $x_i \in \Omega$ with $i \in \mathbb{Q}$.

The degree of spatial structuring in the environment can be manipulated through the number of patches occupied by producers (i.e p) as well as the position of such patches so we propose the following measure of the **D**egree of **S**patial **S**tructure (**DSS**):

$$DSS = \frac{1}{n} \sum_{i \in \mathbb{L}} Z_i, \tag{4.2.12}$$

where $0 \leq DSS < 1$,

$$Z_i = \frac{\mathbb{1}_{(i-1)\in\mathbb{Q} \wedge i\in\mathbb{Q}} + \mathbb{1}_{(i-1)\in\mathbb{P} \wedge i\in\mathbb{P}} + \mathbb{1}_{(i+1)\in\mathbb{Q} \wedge i\in\mathbb{Q}} + \mathbb{1}_{(i+1)\in\mathbb{P} \wedge i\in\mathbb{P}}}{\mathbb{1}_{(i-1)\in\mathbb{L}} + \mathbb{1}_{(i+1)\in\mathbb{L}}}, \tag{4.2.13}$$

and

$$\mathbb{1}_A = \begin{cases} 0, & \text{if A is true,} \\ 1, & \text{if A is false,} \end{cases} \tag{4.2.14}$$

with A denoting a proposition, meaning a statement which can be either true or false.

The numerator in (4.2.13) denotes the number of same-type patches in the nearest-neighbourhood of the patch i while the denominator in (4.2.13) denotes

the total number of patches in the nearest-neighbourhood of the patch i.

In other words, Z_i represents the fraction of the same type nearest-neighbour patches as the focal patch located at x_i, and DSS is the average fraction of the same type nearest-neighbour patches in the population. Therefore intuitively the DSS value is closer to its maximum (that is 1) when the producers and non-producers are well segregated. In that case a given focal patch is mainly surrounded by its own type and therefore its Z_i will be high, leading to high values of the DSS for the population. When the producers and non-producers are well mixed, a given focal patch will have lower Z_i than for the segregated spatial structure, giving rise to lower DSS values for the population.

As an illustration we next provide a detailed example of a one-dimensional DSS calculation but note that our definition of DSS can readily be applied to two-dimensional cases (for an example see Supplementary Material 4.5.3)

Example 1. *Fig. 4-1 provides an example of possible values DSS can take when $n = 3$ and $p = 1$. In this case the environment consists of 3 patches, one of which contains producers ($p = 1$) while the other two contain non-producers ($q = 2$). Since there are 3 locations where a patch of producers can be placed, there are three different $\mathbb{P}$ and the corresponding $\mathbb{Q}$ sets, namely:*

$$\mathbb{P}_a = \{1\} \text{ and } \mathbb{Q}_a = \mathbb{L} \setminus \mathbb{P}_a = \{2, 3\}, \tag{4.2.15}$$

$$\mathbb{P}_b = \{2\} \text{ and } \mathbb{Q}_b = \mathbb{L} \setminus \mathbb{P}_b = \{1, 3\}, \tag{4.2.16}$$

$$\mathbb{P}_c = \{3\} \text{ and } \mathbb{Q}_c = \mathbb{L} \setminus \mathbb{P}_c = \{1, 2\}. \tag{4.2.17}$$

Subsequently, combining (4.2.15-4.2.17) with (4.2.13) we first arrive at

$$\begin{aligned}
Z_{1a} &= \frac{\mathbb{1}_{0\in\mathbb{Q}_a \wedge 1\in\mathbb{Q}_a} + \mathbb{1}_{0\in\mathbb{P}_a \wedge 1\in\mathbb{P}_a} + \mathbb{1}_{2\in\mathbb{Q}_a \wedge 1\in\mathbb{Q}_a} + \mathbb{1}_{2\in\mathbb{P}_a \wedge 1\in\mathbb{P}_a}}{\mathbb{1}_{0\in\mathbb{L}} + \mathbb{1}_{2\in\mathbb{L}}} \\
&= \frac{0+0+0+0}{0+1} = 0, \\
Z_{2a} &= \frac{\mathbb{1}_{1\in\mathbb{Q}_a \wedge 2\in\mathbb{Q}_a} + \mathbb{1}_{1\in\mathbb{P}_a \wedge 2\in\mathbb{P}_a} + \mathbb{1}_{3\in\mathbb{Q}_a \wedge 2\in\mathbb{Q}_a} + \mathbb{1}_{3\in\mathbb{P}_a \wedge 2\in\mathbb{P}_a}}{\mathbb{1}_{1\in\mathbb{L}} + \mathbb{1}_{3\in\mathbb{L}}} \\
&= \frac{0+0+1+0}{1+1} = 0.5, \\
Z_{3a} &= \frac{\mathbb{1}_{2\in\mathbb{Q}_a \wedge 3\in\mathbb{Q}_a} + \mathbb{1}_{2\in\mathbb{P}_a \wedge 3\in\mathbb{P}_a} + \mathbb{1}_{4\in\mathbb{Q}_a \wedge 3\in\mathbb{Q}_a} + \mathbb{1}_{4\in\mathbb{P}_a \wedge 3\in\mathbb{P}_a}}{\mathbb{1}_{2\in\mathbb{L}} + \mathbb{1}_{4\in\mathbb{L}}} \\
&= \frac{1+0+0+0}{1+0} = 1.
\end{aligned}$$

Incorporating the above into (4.2.12) leads to:

$$DSS_a = \frac{0 + 0.5 + 1}{3} = 0.5.$$

Similarly we can also calculate

$$DSS_b = \frac{0 + 0 + 0}{3} = 0,$$
$$DSS_c = \frac{1 + 0.5 + 0}{3} = 0.5.$$

Therefore in a three-patch environment ($n = 3$) containing $f_0 = 1/3$ frequency of producers, our measure of spatial structure DSS can only take two values: $DSS = 0.5$, if producers are situated in either of the two outer patches (Fig. 4-1a&4-1c) and $DSS = 0$, if the producers are located in the middle patch (Fig. 4-1b).

In general, for an environment containing a finite number of patches, not all producer frequencies f_0 can be used to create a diverse range of spatial structures $0 < DSS < 1$.

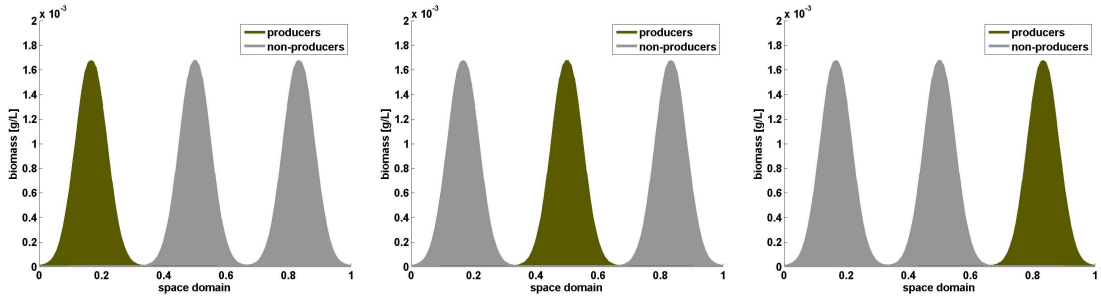

Figure 4-1: **An example of possible values DSS can take in a three patch environment where one patch contains invertase producers while the other two contain non-producers ($\mathbf{n = 3, p = 1, q = 2}$).**
(4-1a): $\mathbb{P}_a = \{1\}$ and $\mathbb{Q}_a = \mathbb{L} \setminus \mathbb{P}_a = \{2, 3\}$, resulting in $DSS = 0.5$;
(4-1b): $\mathbb{P}_b = \{2\}$ and $\mathbb{Q}_b = \mathbb{L} \setminus \mathbb{P}_b = \{1, 3\}$, resulting in $DSS = 0$;
(4-1c): $\mathbb{P}_c = \{3\}$ and $\mathbb{Q}_c = \mathbb{L} \setminus \mathbb{P}_c = \{1, 2\}$, resulting in $DSS = 0.5$.
The initial population density is $N_0 = 6 \cdot 10^{-4}$g. protein per L.

Our definition of the Degree of Spatial Structure (DSS) within an environment is simple and intuitive but also has some parallels with the existing measures of spatial relatedness proposed in cooperation literature [94–97]. The relatedness between nearest neighbours is often defined as the average local density of co-operators experienced by a cooperator and denoted by $q_{C|C}$. It can also be inter-

preted as the conditional probability that the recipient of a cooperative behaviour is a cooperator [84, 94, 96–98]. This definition is usually used in the network models [84, 94, 96–98],where the 'local density' experienced by an individual refers to the fraction of the occupied neighbouring sites.

In our system we can calculate the equivalent of q_{CIC} by considering the following simplifying assumptions: each microbial patch is treated an 'individual' and that pairwise interactions occur only between 'individuals' occupying the neighbouring sites (patches). In that case

$$q_{C|C} = \frac{1}{p} \sum_{i \in \mathbb{P}} Z_i, \tag{4.2.18}$$

that is the average fraction of cooperative neighbours for each cooperator.

According to [96] the spatial relatedness can only by expressed as q_{CIC} if the cooperative individuals are rare in a population. Otherwise a quantity,

$$\bar{r} = q_{C|C} - q_{C|D}, \tag{4.2.19}$$

is proposed [96], which had been previously defined as a measure of population viscosity [99]. Here, $q_{C|D}$ denotes the average local density of cooperators experienced by a cheat (defector).

Our measure of spatial structure DSS can also be related to $\bar{r}$ in the following way. Let $q_{D|D}$ denote the average local density of defectors experienced by a defector, which in our case similarly to (4.2.18) takes the form

$$q_{D|D} = \frac{1}{n-p} \sum_{i \in \mathbb{Q}} Z_i. \tag{4.2.20}$$

Moreover, by definition

$$q_{D|D} = 1 - q_{C|D}. \tag{4.2.21}$$

Then from (4.2.12) and using (4.2.20-4.2.21) we have

$$\begin{aligned} DSS &= \frac{1}{n}(\sum_{i\in\mathbb{P}} Z_i + \sum_{i\in\mathbb{Q}} Z_i) = \frac{1}{n}(pq_{C|C} + (n-p)q_{D|D}) \\ &= f_0 q_{C|C} + (1-f_0)q_{D|D} = f_0 q_{C|C} + (1-f_0)(1-q_{C|D}) \\ &= f_0 q_{C|C} - (1-f_0)q_{C|D} + (1-f_0), \end{aligned} \tag{4.2.22}$$

where $f_0 = p/n$ denotes the initial frequency of cooperators in the population.

In contrast to the definition of $\bar{r}$, our DSS in (4.2.19) weights the quantities $q_{C|C}$ and $q_{C|D}$ by the frequencies of cooperators and defectors, respectively. This impacts on how spatial structure of an environment is defined as illustrated in the Example 2 below.

Example 2. *Consider an environment where the initial population consist of* $n = 20$ *local maxima, so that* $\mathbb{L} = \{1, 2, ..., 20\}$. *Now consider the following two initial distributions*

Case 1: the initial frequency of producers is $f_0 = 10/20$ *with* $\mathbb{P} = \{1, 2, ..., 10\}$ *and* $p = 10$

Case 2: the initial frequency of producers is $f_0 = 1/20$ *with* $\mathbb{P} = \{1\}$ *and* $p = 1$.

We want to calculate DSS *and* $\bar{r}$ *for both Cases 1 and 2.*

Using (4.2.13-4.2.14) and (4.2.18) we arrive at

$$q_{C|C} = \begin{cases} 0.95, & \textit{for Case 1}, \\ 0, & \textit{for Case 2}, \end{cases} \tag{4.2.23}$$

and similarly using (4.2.13-4.2.14) and (4.2.20) we arrive at

$$q_{D|D} = \begin{cases} 0.95, & \textit{for Case 1}, \\ 0.974, & \textit{for Case 2}. \end{cases} \tag{4.2.24}$$

Subsequently from (4.2.19), (4.2.23-4.2.24) and remembering (4.2.21) we obtain

$$\bar{r} = \begin{cases} 0.9, & \textit{for Case 1}, \\ -0.026, & \textit{for Case 2}. \end{cases} \tag{4.2.25}$$

Similarly from (4.2.22-4.2.24) and remembering (4.2.21) and that $f_0 = 10/20$ *for*

the Case 1 while $f_0 = 1/20$ *for the Case 2, we obtain*

$$DSS = \begin{cases} 0.95, & \textit{for Case 1}, \\ 0.925, & \textit{for Case 2}, \end{cases} \tag{4.2.26}$$

Given that in both Case 1 and Case 2, producers and non-producers are well-segregated with only one producer patch bordering a non-producer patch, we would expect that both environments have similar spatial structures. While this indeed turns out to be the case for our definition of DSS *as shown in (4.2.26), the values of* $\bar{r}$ *significantly vary between the two cases (4.2.25). Therefore we argue that our definition of* DSS *is well suited for classifying spatial structure based on microbial experimental protocols used to manipulate the level of spatial segregation of different microbial strains [14, 74].*

4.3 Results

4.3.1 The impact of spatial structure on the outcome of competition

In spatially unstructured environments for a given initial frequency f_0, the producers will have a unique relative fitness $W_p(f_0)$ as defined in (2.4.3). However in spatially structured environments, where the initial population distribution $N_{all0}(x)$, defined in (4.2.9), has n local maxima, there are $\binom{n}{f_0 \cdot n}$ ways of representing the initial distribution of producers $N_{p0}(x)$, as defined in (4.2.10). Therefore there are $\binom{n}{f_0 \cdot n}$ possible initial distributions associated with a single producer frequency f_0, as illustrated in Fig. 4-1 for $n = 3$ and $f_0 = 1/3$.

Since our model (4.2.1-4.2.4) explicitly tracks resource concentrations and population densities in both space and time, we can follow how different initial population distributions give rise to different final population distributions, which in turn results in different final population sizes. Therefore, for a given number of local maxima n (or patches) and a given frequency of producers f_0 in an initial population, it follows from (2.4.3) that there are up to $\binom{n}{f_0 \cdot n}$ possible values of $W_p(f_0)$. In practice, some of the initial distribution are symmetric to each other (as for example the distributions shown in the Fig. 4-1a and 4-1c), and for each

pair of such symmetric distributions we expect to obtain the same relative fitness $W_p(f_0)$.

If for each f_0 the location of producer patches is allocated randomly as is often the case in experimental studies [14, 85], the relative fitness $W_p(f_0)$ could vary dramatically between biological replicates, as illustrated in Fig. 4-2a (grey dots) which plots all possible values of $W_p(f_0)$ calculated for all possible initial distributions, given a fixed n. This can lead to dramatically different competition outcomes ranging from coexistence (black line, Fig. 4-2a) to competitive exclusion (blue line, Fig. 4-2a) and including non-linear fitness functions (such as the one illustrated with the red line, Fig. 4-2a).

However, if for a given f_0, a measure of the degree of spatial structuring as defined in (4.2.12) is associated with each value of the relative fitness $W_p(f_0)$, a clear pattern emerges showing that as the degree of spatial structure (DSS) decreases, the relative fitness of producers tends to decrease (Fig. 4-2b & 4-2c). In addition, consistent with experimental findings [14, 64], our model confirms that the degree of spatial structure matters in maintaining cooperation as producers coexist with non-producers only for sufficiently high DSS (Fig. 4-2b).

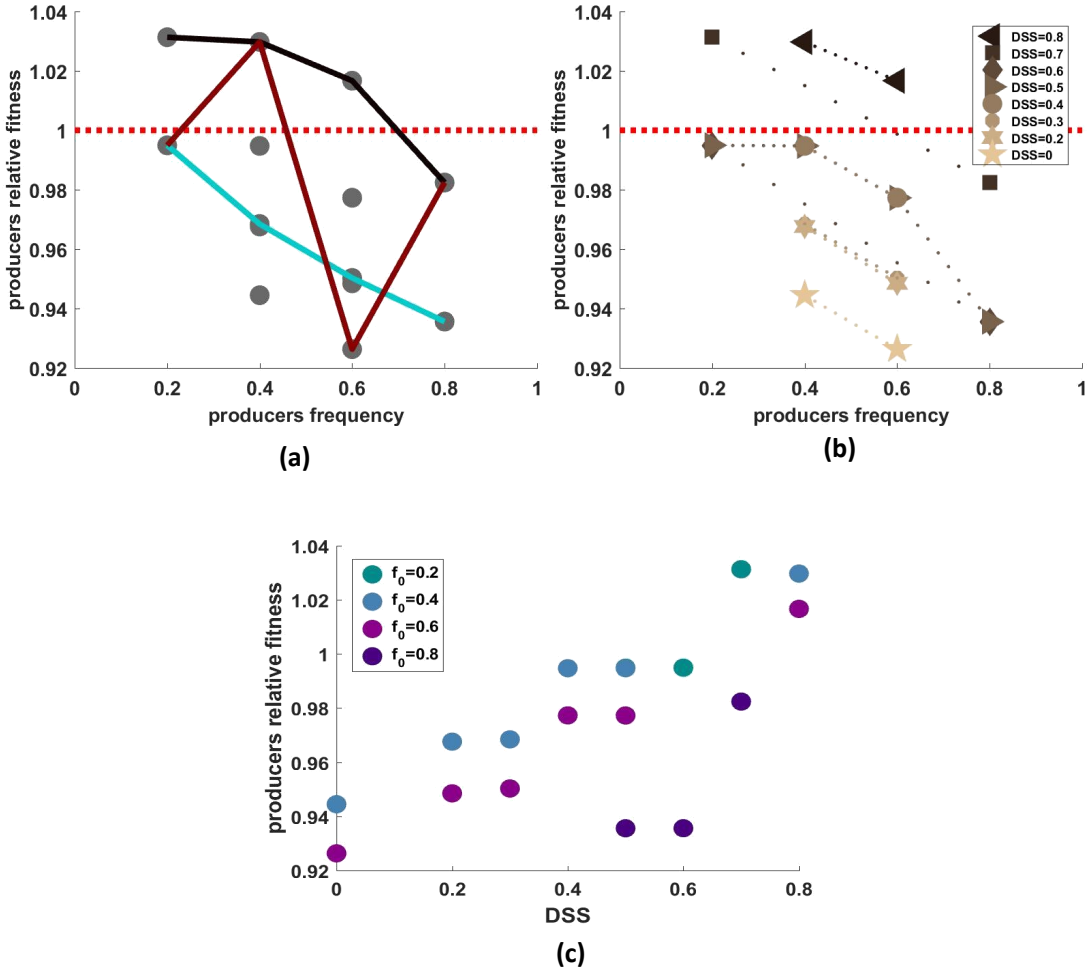

Figure 4-2: **The importance of adopting a quantitative approach to spatial structure:** (a): all possible values of the producers relative fitness $W_p(f_0)$, for various producers frequencies f_0 and $n = 5$. In total $W_p(f_0)$ takes two significantly different values for $f_0 = 0.2$ and $f_0 = 0.8$ each, and four significantly different values for $f_0 = 0.4$ and $f_0 = 0.6$ each, giving rise to $2 \times 4 \times 4 \times 2 = 64$ different curves for $W_p(f_0)$ as a function of f_0. The black, blue end red lines illustrate qualitatively different outcomes of the competition, depending on the random choice of the locations of producers patches. In particular the black line crosses the line of equal fitness where the relative producers fitness equals to one, and therefore a stable coexistence of producers and non-producers is predicted.The blue line lies entirely below the line of equal fitness, predicting exclusion of the producers. The red line indicates bistability: depending on initial frequency of producers, the system may converge to a stable coexistence of producers and non-producers, or to exclusion of producers. (b): all possible values of the producers relative fitness $W_p(f_0)$, associated with the initial degree of spatial structuring (DSS). (c): all possible values of the producers relative fitness $W_p(f_0)$, plotted against the value of DSS. For each initial frequency f_0 the relative fitness of producers tends to increase with increasing spatial structure measure DSS.

4.3.2 The effects of population density in the maintenance of cooperation

Whether high population density promotes cooperation depends on two factors: the resource concentration in the environment and the degree of spatial structure (Fig. 4-3a).

In particular, for highly structured environments (sufficiently high DSS), high population density promotes cooperation, when environmental resources are sufficiently low (Fig. 4-3a), with cooperators (producers) either outcompeting cheats (non-producers, e.g. Fig. 4-3b) or coexist with them (e.g Fig. 4-3c). However, when resource concentration is sufficiently high, the opposite result is observed with high population densities promoting cheats who in the long term outcompete cooperators.

We confirm the robustness of these results, by running the simulations based on the full model, containing more biological details of *S. cerevisiae*, and described in the Supplementary Material 4.5.4. The results of the complex model are consistent with our main findings. Namely, in highly structured environments high population density favours invertase producers for sufficiently low resource concentrations while high population density favours non-producers for sufficiently high resource concentrations (Supplementary Fig. 4-10). Moreover, this result is robust to further changes in parameter values.

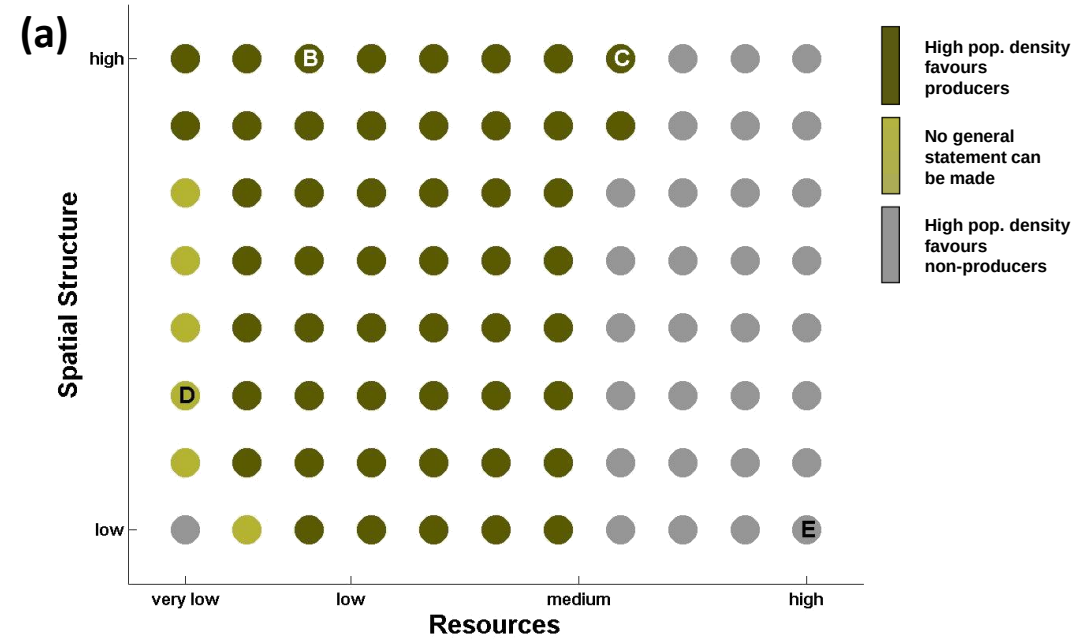
(a)
high
low
B
C
D
E
Spatial Structure
very low
low
medium
high
Resources
High pop. density favours producers
No general statement can be made
High pop. density favours non-producers

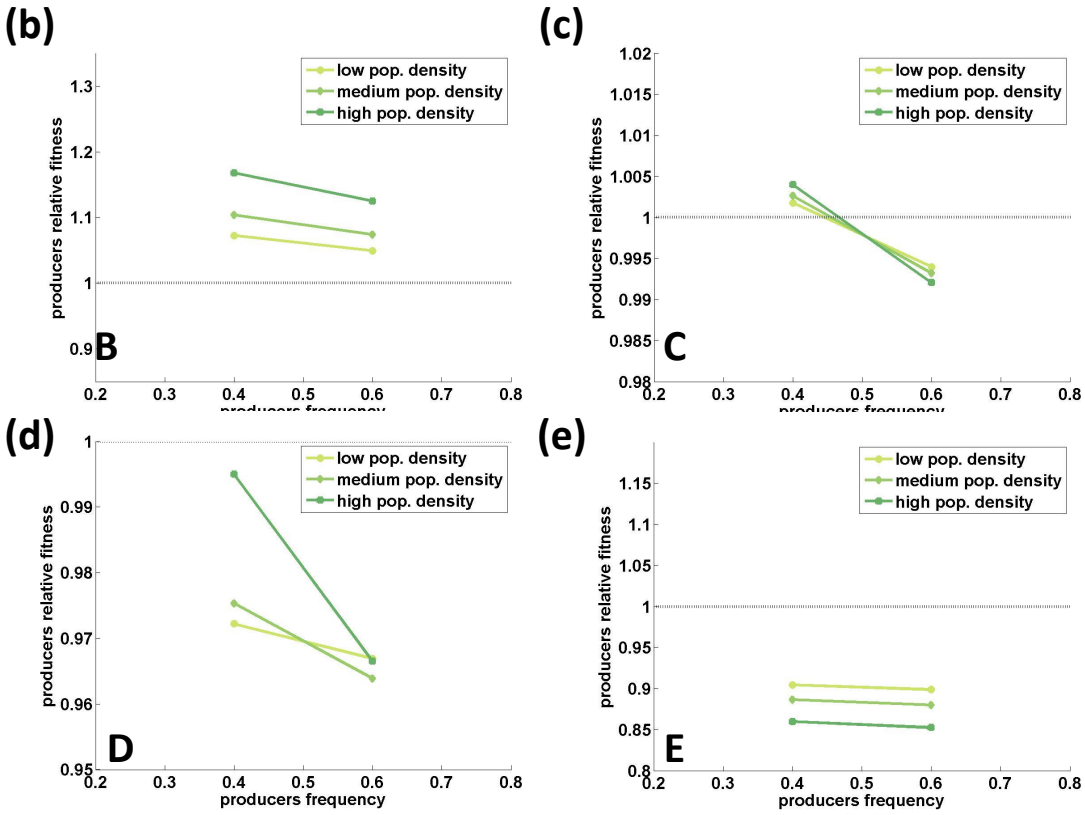
(b)
low pop. density
medium pop. density
high pop. density
producers relative fitness
B
(c)
C
(d)
D
producers frequency
(e)
E

Figure 4-3: **The effect of population density on cooperation as a function of the spatial structure and the resource concentration**
The effect of population density on cooperation as a function of the spatial structure and the resource concentration in the environment is shown in (a). We simulated 88 environmental conditions denoted by circles (8 different spatial structure level, 11 different resource concentrations) and the following initial population densities: low: $N_0 = 6 \cdot 10^{-6}$, medium: $N_0 = 6 \cdot 10^{-5}$, high: $N_0 = 6 \cdot 10^{-4}$ [g protein /L]. *Dark green circles:* high population density favours invertase producers (cooperators); *Grey circles:* high population density favours the non-producers (cheats); *Light green circles:* population density may favour producers or non-producers, depending on the details of the system. The outcome of numerical simulations were assessed in the following way. Let $W_p^l(f_0)$, $W_p^m(f_0)$ and $W_p^h(f_0)$ denote the relative fitness of producers for low, medium and high initial population densities, respectively. If the statement S_a: $W_p^l(f_0) < W_p^m(f_0) < W_p^h(f_0)$ is true (with accuracy 10^{-3}) for all f_0, then high population density favours producers (dark green circles) while if the statement S_b: $W_p^l(f_0) > W_p^m(f_0) > W_p^h(f_0)$ is true (with accuracy 10^{-3}) for all f_0 then high population density favours non-producers (grey circles). However if S_a and S_b are not true we first define $f_0^* \in (0,1)$ as the initial producer frequency for which $W_p(f_0^*)$=1. If $W_p(f_0^*) > 1$ for all $f_0 \in (0,1)$ we set $f_0^* = 1$ while if $W_p(f_0^*) < 1$ for all $f_0 \in (0,1)$ we set $f_0^* = 0$. Subsequently we use f_0^{l*}, f_0^{m*} and f_0^{h*} to denote f_0^* for low, medium and high population densities, respectively. If $f_0^{l*} < f_0^{m*} < f_0^{h*}$ we conclude that high population density favours producers (dark green circles). However, if $f_0^{l*} > f_0^{m*} > f_0^{h*}$ then high population density favours non-producers (grey circles). Otherwise no general statement can be made regarding the relationship between population density and cooperation (light green circles). Examples of the relative fitness of producers for a range of environmental conditions B-E marked in (a) are given in (b-e). In particular (b): $DSS = 0.8$ and the initial resource concentration is $S_0 = 2.33[mM]$; (c): $DSS = 0.8$ and $S_0 = 73.65[mM]$; (d) $DSS = 0.3$ and $S_0 = 0.585[mM]$; (e) $DSS = 0$ and $S_0 = 585[mM]$; Throughout (b-e), $n = 5$ and the relative fitness of producers as a function of producer frequency is calculated for low, medium and high initial population densities as described in (a). Note, in our framework as seen in (e), small DSS values can be obtained only at intermediate producer frequencies, because small or large frequencies do not allow for sufficient mixing required to generate low spatial heterogeneity.

Why can high population densities favour cooperation (as in Fig 4-3b)? We reason that the higher the density of cooperators, the quicker they will consume acquired resources (Fig. 4-4). Moreover, since the acquired resources in our highly structured environment are sufficiently scarce, they will be consumed by cooperators before they can become accessible to cheats, as also highlighted in [1, 76]. This effect is illustrated in Fig. 4-4 which shows that, in a well structured environment with sufficiently low resources, the resource uptake rate of cooperators is substantially higher than that of cheats when population density is high (Fig. 4-4b) compared to when the population density is low (Fig. 4-4a).

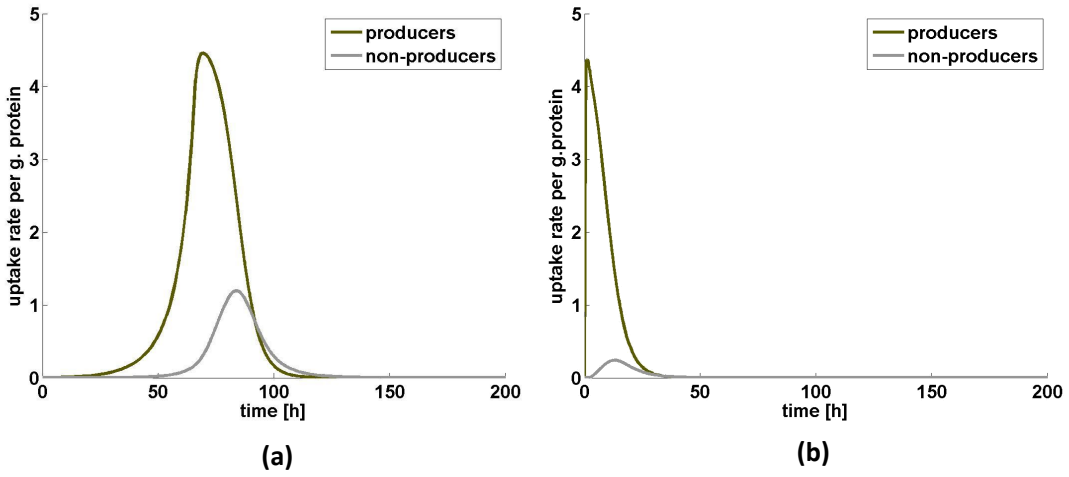

Figure 4-4: **Average hexose uptake rates (over all spatial locations) of producers and non-producers.**
This is calculated at (a) sufficiently low ($N_0 = 6 \cdot 10^{-6}[g\ protein/L]$) and (b) sufficiently high ($N_0 = 6 \cdot 10^{-2}[g\ protein/L]$) population densities. Throughout, $DSS = 0.7$, $n = 5$, $p = 1$, resources concentration: $S_0 = 5.85[mM\ sucrose]$.

For the environments with sufficiently low spatial structure (sufficiently low DSS), high population density promotes cheats at much wider range of resource concentrations than in the case of highly structured environments (Fig. 4-3a).

Apart from the parameter zones that result in high population density promoting cooperators and those resulting in high density promoting cheats, there are also regions (light green circles in Fig. 4-3a), for which no general statement can be made regarding the relationship between population density and cooperation. For example, for sufficiently high cooperator frequency an initial small increase in population density could favour cheats, while a further density increase could favour cooperators; however, for sufficiently low cooperator frequencies this non-

monotone relationship can be lost (Fig. 4-3d).

Our model also predicts that frequency dependence will not be observed in the environments where spatial structure is sufficiently low but the resource concentration is sufficiently high (e.g Fig. 4-3e). This is consistent with observations in [62], where it was empirically shown that the frequency dependence between the cooperative public goods producers and the cheating non-producers disappears when the population is not structured enough and the public good production does not benefit the population growth. In our case, in environments containing high resource concentration the public good production stops being beneficial for the populations, because of the rate-efficiency trade-off [14, 75].

Finally, we observe a non-monotone relationship between the relative fitness of cooperators and resource concentration in the environment. This relationship is shown in the Fig. 4-5a for a fixed initial frequency of producers. The fitness of cooperators is maximised for an intermediate resource concentrations, the value of which does not vary significantly with the population density or spatial structure (Fig. 4-5a). This result is also recovered with the full model, where the relative fitness of producers is maximised at some intermediate resource concentration (Supplementary Fig. 4-11).

This result could be linked to the Allee effect [100], a known feature of the *S. cerevisiae* cooperative system [74, 93], whereby the cooperative population reaches its maximal growth rate at an intermediate population density.

We can gain a further insight into the mechanism driving the result in (Fig. 4-5a) by tracking how much of the public good (hexose) produced by cooperators is taken up by the cells at each spatial location (Fig. 4-5b-d). In particular, in environments with sufficiently low initial resource concentration, population densities will be low which in turn will give rise to low hexose concentration in the vicinity of producers. Since the hexose uptake rate is a function of hexose concentration (see the form of J^R in Chapter 2: Methods) the resulting low hexose uptake rate by producers leads to this public good becoming accessible to non-producers through diffusion (Fig. 4-5b). In this case producers will not have a large advantage over non-producers, which is reflected in (Fig. 4-5a) by observing that the relative fitness of producers is smaller at low resource concentrations than intermediate resource concentration.

On the other hand, having sufficiently high resource concentrations in the envi-

ronment leads to the creation of large hexose spikes around producers, resulting in high hexose uptake rate for the producers. However, since the hexose uptake rate is a saturating function of hexose concentration, the excess hexose not taken up by producers will become accessible to neighbouring non-producers (Fig. 4-5d). In addition, producers are affected by the rate-efficiency trade-off whereby high rates of hexose uptake are associated with low growth efficiency further disadvantaging the producers. This is reflected in Fig. 4-5a by observing that the relative fitness of producers is less than one for sufficiently high resource concentrations.

At intermediate resource concentrations the hexose uptake by producers is sufficiently fast to capture the majority of available glucose (Fig. 4-5c) and the concentration of available hexose is sufficiently low so that producers are not affected by the rate-efficiency trade-off in hexose consumption. This gives producers an advantage over non-producers reflected in the fact that the relative fitness of producers is greater than one for low/medium resource concentrations (Fig. 4-5a).

The non-monotone relationship between the relative fitness of cooperators and resource concentration in the environment is also present in the absence of the rate-efficiency trade-off in hexose consumption (Supplementary Fig. 4-12). However in that case the hump-shaped distribution is less pronounced than in the presence of rate-efficiency trade-off (Fig. 4-5a) and the resrouce concentration that maximises the relative fitness of producers depends on the measure of spatial structure DSS. In the absence of rate-efficiency trade-off producers have an advantage over non-producers even in high resource environments (Supplementary Fig. 4-12), because the high hexose uptake rate experienced by producers in high resource environments does not incur a penalty in terms of a reduced growth efficiency. However this advantage of producers over non-producers at high resource concentrations is still smaller than the advantage producers have at intermediate resource concentrations (Supplementary Fig. 4-12). This is due to the fact that hexose uptake rate is a saturating function of hexose concentrations. Moreover, the lower the DSS the higher concentration of resources is needed for producers to sequester sufficiently high concentration of hexose in order to have an advantage over non-producers (Supplementary Fig. 4-12).

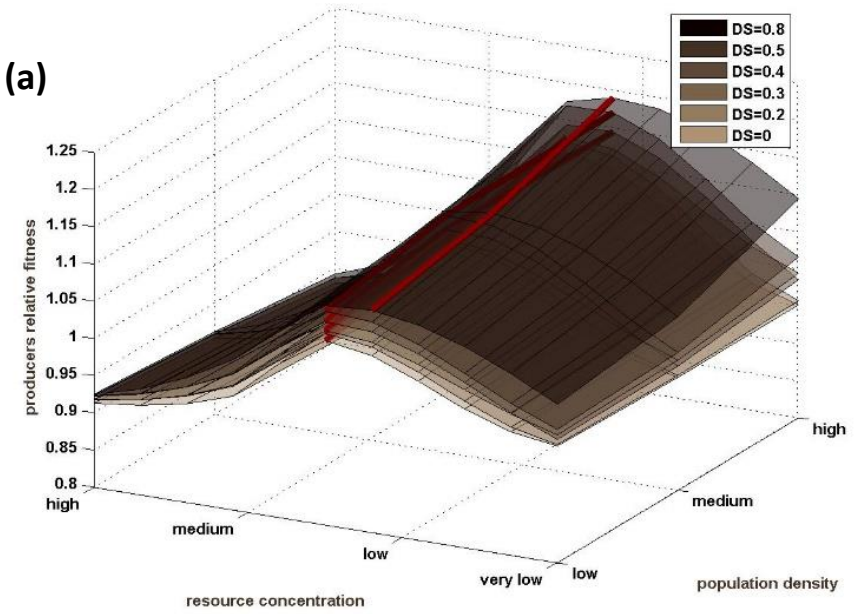
(a)
DS=0.8
DS=0.5
DS=0.4
DS=0.3
DS=0.2
DS=0
producers relative fitness
1.25
1.2
1.15
1.1
1.05
1
0.95
0.9
0.85
0.8
high
medium
low
very low
resource concentration
low
medium
high
population density

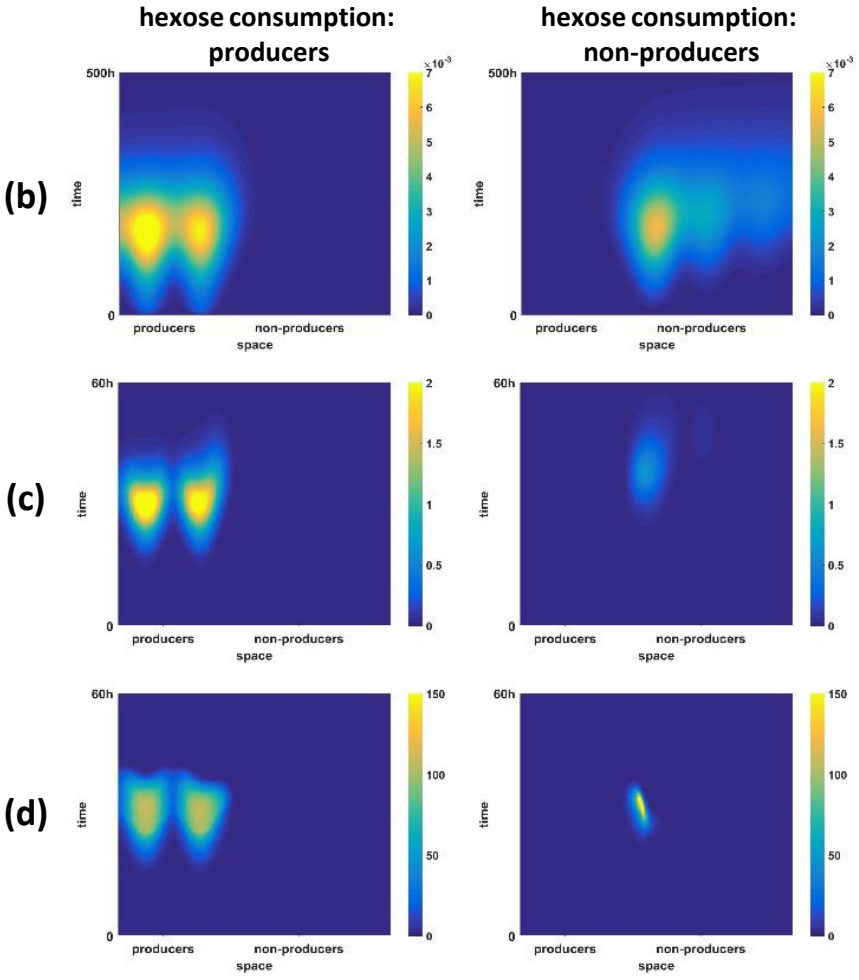
hexose consumption: producers
hexose consumption: non-producers
(b)
(c)
(d)
500h
60h
0
time
producers
non-producers
space
×10⁻³

Figure 4-5: **Relative fitness of producers as a function of resource concentration.**
(4-5a) Different surfaces denote the outcomes for various various population densities, resource concentrations and spatial structures for a fixed initial producer frequency $f_0 = 0.4$. The colour of surfaces changes depending on the level of the spatial structure (DSS). The red lines denote the resource concentration which maximise the producers relative fitness, at a given level of spatial structure DSS.
(4-5b)-(4-5d): Hexose uptake [mM/hour] by producers and non-producers in different spatial locations calculated for $n = 5, p = 2, DSS = 0.8, N_0 = 6 \cdot 10^{-4}$ [g/L] and
(4-5b) very low resource concentration $S_0 = 0.585[mMsucrose]$; (4-5c) low resource concentration $S_0 = 9.2716[mMsucrose]$ and (4-5d) high resource concentration $S_0 = 585[mMsucrose]$.

Note that the results presented in this section do not qualitatively change if we consider a system-specific mathematical model tailored to *S. cerevisiae* system (see Supplementary Material 4.5.4, for details).

4.4 Discussion

In this chapter we put forward a theoretical framework capable of reconciling seemingly conflicting results in the literature regarding the relationship between population density and cooperation in microorganisms. In general, the framework has two distinct features: first, the two social dilemmas facing microbes namely public goods production and self restraint interact and the strength of this interaction can be varied; second, the degree of spatial structure of an environment is defined in such a way that its value can be systematically varied.

In particular we quantify a degree of spatial structure (DSS) within an environment in a simple and intuitive way. In an experimental environment containing n patches, the degree of spatial structure is defined as $DSS = \frac{1}{n}\sum_{i=1}^{n} Z_i$ where Z_i represents the fraction of the same type nearest-neighbour patches as the focal patch i. While our simple measure is sufficient to explain the inconsistencies in the literature, it serves only as an example of spatial structure quantification and more sophisticated measures could easily be incorporated into our framework.

Past theoretical studies have explored the relationship between population density and cooperation in spatially structured environments [96, 98, 101]. The findings of these studies were interpreted through the use of the inclusive fitness theory [2] which involved extending the Hamilton's concept of relatedness to account for spatially structured environments. While the outcomes provided useful understanding of the effect of spatial structure on cooperative behaviour, such theoretical predictions are rarely challenged by microbial data.

The reason for this lack of empirical verification could be due to the fact that the past studies used island models [101] or infinite network models [96, 98] to represent spatial structure. While the island models assume that individuals are distributed into groups and can migrate between them, network models consider space as a regular infinite network in which each individual is connected to and therefore can interact with n other neighbours. However, it is not clear how these

frameworks could apply to microbial populations where individual cells often exhibit low-motility [102] and where the neighbourhood interactions with a focal individual are determined by the biophysical and biochemical properties of the cooperative trait rather than by a predetermined network. For example in the case of public goods cooperation, the number of neighbours interacting with the focal individual is determined by the diffusive properties of the public good in a given environment [1, 14, 31, 33, 64, 76, 103]. This also impacts the ability to calculate the spatially-extended relatedness coefficient [96] which requires recognition of the interacting pairs of individual cells.

Our theoretical framework deploys a system of partial differential equations widely used to elucidate the effects of spatial variation on populations [104]. In particular it enables us to explicitly track resource concentrations and population densities in both space and time. To mimic experimental protocols where an initial environment contains a number of microbial patches of the same size [14, 74] our initial population distributions (4.2.10-4.2.11) contain a number of local maxima. The spatial locations of the local maxima represent the centre-points of different patches in the environment, around which microbial cells are normally distributed. While we assume that cells have low motility (as is often the case with microorganisms [102]), resources diffuse throughout the spatial domain thus implicitly facilitating the interaction between cells at different spatial locations both within and between the patches.

The degree of impact of public-goods production and self restraint on microbial growth is varied through the initial resource concentration. In low-resource environments the growth rate is relatively low and the rate-efficiency trade-off is weak or non-existent [14], making public goods production the dominant constraint on microbial growth. Contrary to this, when resources are high, the growth rate is relatively high leading to the inefficient resource use [75].

By varying a degree of spatial structure and resource concentration in an environment, a more consistent picture of the relationship between the population density and cooperation emerged (Fig. 4-3a). When resources are plentiful, high population density promotes cheats in both high and low structured environments (Fig. 4-3a). Our results could be explained by the fact that when resources are high, public goods producing cooperators acquire large amount of nutrients and are therefore affected by the rate-efficiency trade-off. The higher the population

density of producers, the larger the spatial and temporal spike of hexose, which are harmful for the cells in their vicinity (that is producers), because they result in low hexose use efficiency. Moreover, as public goods non-producing cheats acquire lower concentrations of nutrients than the producers, they do not suffer the same efficiency constraints and will therefore be more efficient than producers.

For sufficiently low or intermediate resources, high population density promotes cooperation in highly structured environments (this result is also confirmed in some of the scenarios considered in [96, 98]), while in the environments with low spatial structure high population density promotes cheats. Our results are consistent with the recent theoretical predictions in [76] and importantly could explain why the empirical evidence for these predictions is seemingly lacking. Namely, [76] predicts that high population densities can promote either cooperation or cheating depending on whether cells diffuse faster or slower than the public goods they produce. However, empirical studies using motile [63] and non-motile [32] cell populations producing diffusible public goods, both find that high population density favours cheats; this is consistent with a different theoretical study predicting that high population densities will always favour cheats in public goods systems [63].

Instead of considering diffusibility of cells in comparison to the diffusibility of public goods as was the case in [76], our study predicts that it is the different degrees of spatial structure within the environment that influence whether high population densities will favour cooperators or cheats. In this context the empirical results in [32, 63] are consistent with our predictions since both empirical studies were conducted in environments with relatively low spatial structure. In particular, the experiments in [32, 63] were initiated by inoculating a mixture of cooperators and cheats onto an agar plate, allowing the spatial structure to self-emerge; however the self-emergence of spatial structure is known to be negligible when population densities are high [105].

In addition, our predicted dependence of the relationship between population density and cooperation on environmental structure has some empirical support [64] whereby high population density was found to favour cheats in environments with low spatial structure but not in the environments with high spatial structure.

In general we note that since, high population densities impede the self-segregation of cells [105], the experimental protocols relying on self-emergence of spatial

structure, as in [32, 61, 63, 74, 85, 90], will give rise to different levels of spatial structure across different population densities. Since an increase in population density inadvertently results in a decrease in the degree of spatial structure, and given that the absence of spatial structure can favour cheats [12, 34], it is imperative that the studies regarding the relationship between population density and cooperation also consider the role different spatial structure plays in shaping this relationship.

4.5 Supplementary Material

4.5.1 Supplementary figures

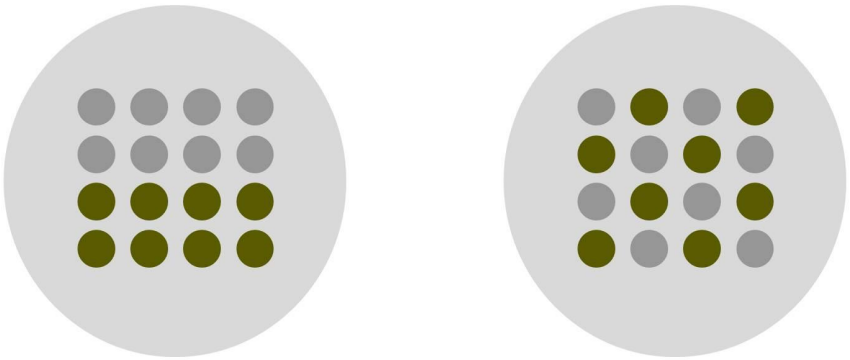

Supplementary Figure 4-6: **Various ways of distributing two subpopulations.** An example of two different spatial distributions of cooperator (green) and cheat (grey) subpopulations, where both distributions have the same cooperator frequency of 0.5.

4.5.2 Parameter values

The hexose diffusion coefficient D_H (and therefore $D_S = D_H/2$) was chosen arbitrarily to describe a sufficiently structured environment within the context of the partial-differential model (4.2.1)-(4.2.4) of the main text. The other parameter values were based on the ones estimated in [14] and are summarised in Supplementary Table 4.1. The list of parameters varying in the main text is listed in Supplementary Table 4.2.

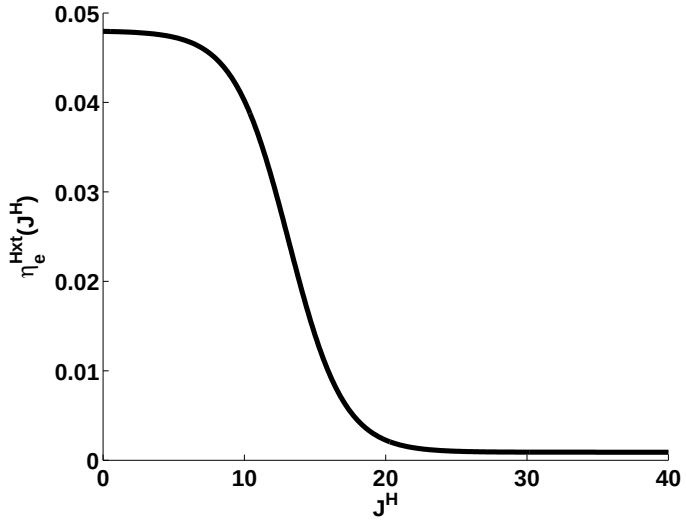

Supplementary Figure 4-7: **Efficiency of hexose utilisation as a function of hexose uptake rate,**
taking the form: $\eta_e^{Hxt}(J^H) = 0.0009 + 0.0471/(1 + \exp(-6.7598 + 0.5142 \cdot J^H))$.

Supplementary Table 4.1: Parameters values for the mathematical model (4.2.1)-(4.2.4).

V_{max}^S	11 [mmol sucrose / (g protein · hour)]
K_m^S	7 [mM sucrose]
V_{max}^H	50 [mmol hexose / (g protein · hour)]
K_m^H	100 mM hexose
η_e^S	0.02 [g protein/mmol sucrose]
r_{in}	77 [mmol/ (g protein · hour)]
c	0.04
k_{in}	$5 \cdot 10^{-3}$ [mM sucrose]
D_H	0.0005 [l^2/ hour]
D_N	0.00001 [l^2/ hour]

Supplementary Table 4.2: Varying Parameters values for the mathematical model (4.2.1)-(4.2.4).

S_0	{5.85, 1.17, 2.33, 4.65, 9.27, 18.5, 36.91, 73.65, 146.95, 293.19, 585} [mM]
N_0	$\{6 \cdot 10^{-6}, 6 \cdot 10^{-5}, 6 \cdot 10^{-4}\}$ [g/L]
f_0	{0.2, 0.4, 0.6, 0.8}
DSS	{0, 0.2, 0.3, 0.4, 0.5, 0.6, 0.7, 0.8}

4.5.3 Spatial Structure Measure DSS in 2D

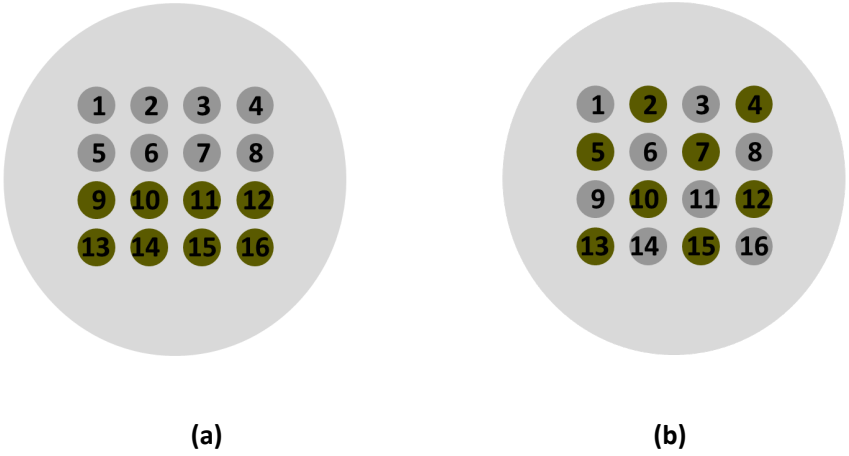

Supplementary Figure 4-8: **Two different ways of distributing two subpopulations.**

Supplementary Fig. 4-8 represents two possible distributions of 8 producer and 8 non-producer patches into an array of patches on a plate, and it labels all the patches. In order to quantify the measure of spatial structure in both settings, we can use the general definition of DSS: the average frequency of same type nearest-neighbour patches. Let us then compute DSS for the setting represented in Supplementary Fig. 4-8a ($DSS(a)$) and Supplementary Fig. 4-8b ($DSS(b)$).

In both cases we notice that each of the patches: $1, 4, 13, 16$ has three nearest neighbours, each of the patches $2, 3, 5, 8, 9, 12, 14, 15$ has five nearest neighbours, and each of the patches $6, 7, 10, 11$ has eight nearest neighbours. Now for every patch $i \in \{1, 2, ..., 16\}$, we can calculate the frequency of same type nearest neighbours: $Z_i(a)$ and $Z_i(b)$, for the settings represented in Fig.4-8a and Fig.4-8b respectively.

For the patches that are surrounded by its own type, we have:

$Z_1(a) = Z_2(a) = Z_3(a) = Z_4(a) = Z_{13}(a) = Z_{14}(a) = Z_{15}(a) = Z_{16}(a) = 1.$

Moreover $Z_5(a) = Z_8(a) = Z_9(a) = Z_{12}(a) = 3/5$ and

$Z_6(a) = Z_7(a) = Z_{10}(a) = Z_{11}(a) = 5/8.$

All together we have: $DSS(a) = \frac{1}{16}\sum_{i=1}^{16} Z_i(a) = \frac{12.9}{16} \approx 0.8$

The distribution represented in Fig.4-8b is more mixed, and therefore we expect the measure of spatial structure $DSS(b)$ to be smaller than in the previous case, that is $DSS(b) < DSS(a)$. We have:

$Z_1(b) = Z_4(b) = Z_{13}(b) = Z_{16}(b) = 1/3$. Additionally

$Z_2(b) = Z_3(b) = Z_5(b) = Z_8(b) = Z_9(b) = Z_{12}(b) = Z_{14}(b) = Z_{15}(b) = 2/5$.

The patches in the middle have the following fractions of same type neighbours:

$Z_6(b) = Z_7(b) = Z_{10}(b) = Z_{11}(b) = 4/8$.

All together we have $DSS(b) = \frac{1}{16}\sum_{i=1}^{16} Z_i(b) = \frac{6+8/15}{16} \approx 0.4$.

4.5.4 The full model

The mathematical model (4.2.1)-(4.2.4) in the main text shows that the observed results regarding the effect of population density on cooperation are guided by two key properties of the model: the existence of a rate-efficiency trade-off with respect to the utilisation of the secondary resource created through public goods production and the existence of spatial structure in the environment. In this section we demonstrate that these results also hold for the full model of the invertase production system in *Saccharomyces cerevisae* [14].

Our simplifying assumptions, used in the main model, are similar to [33], where only one simple carbon source is considered, the cost of public good production is assumed to be constant, and the growth benefits are denoted as a nonlinear function of producers frequency. Nevertheless, the model of the cooperative system *S. cerevisiae*, proposed in [14], takes into account more biological details.

Therefore we study the complex model of *S. cerevisiae*, by adding the following assumptions:

1. We do distinguish between glucose and fructose concentrations in the environment, and we consider separate uptake rates J^G and J^F for these two carbon sources. Glucose and fructose are transported into the cell by hexose transporters and, for simplicity, we assume that there are two specific carrier types: one for glucose only, and one for fructose only [106]. The rate of the hexose pathway when glucose is transported is defined by

$$J^G = \frac{V^G_{max} G}{K^G_m + G}, \tag{S4.5.1}$$

while, the rate of fructose transport is defined by

$$J^F = \frac{V^F_{max} F}{K^F_m + F}. \tag{S4.5.2}$$

In (S4.5.1) and (S4.5.2), $V^G_{max}(V^F_{max})$ denotes the maximal rate of the pathway for glucose (fructose), with K^G_m and K^F_m denoting the respective Michaelis-Menten constants. Similarly, the efficiency of uptake of both simple sugars

is now a function of both glucose and fructose uptake rates, and hence we write $\eta_e^{Hxt}(J^G + J^F)$. The form of this function is shown in Supplementary Fig. 4-9a.

2. The invertase activity r_{in} is a function of glucose consumption rate, as demonstrated in [107], hence we write $r_{in}(J^G)$. The form for invertase activity function used here has been estimated in [14] and is shown in Supplementary Fig. 4-9b;

3. The cost of invertase production c is a function of invertase activity r_{in}, and therefore we write $c(r_{in})$. It has been estimated empirically in [14] and shown in Supplementary Fig. 4-9c. It assumes that as invertase activity increases, the production per unit invertase becomes more costly as every invertase molecule made means one molecule of some other important protein is not made [108, 109].

4. Finally, the efficiency of sucrose metabolism which is denoted by η_e^S, is affected by the rate-efficiency trade-off [14]. Therefore we assume η_e^S is a decreasing function of J^S, which can be written as $\eta_e^S(J^S)$ and whose form has been estimated in [14] and shown in Supplementary Fig. 4-9 (d);

The resulting complex version of the model (4.2.1)-(4.2.4) from the main text, has the following form:

$$\frac{\partial S}{\partial t} = -J^S \cdot (N_p + N_n) - Inv \cdot N_p + D_S \frac{\partial^2 S}{\partial x^2}, \tag{S4.5.3}$$

$$\frac{\partial G}{\partial t} = -J^G \cdot (N_p + N_n) + Inv \cdot N_p + D_H \frac{\partial^2 G}{\partial x^2}, \tag{S4.5.4}$$

$$\frac{\partial F}{\partial t} = -J^F \cdot (N_p + N_n) + Inv \cdot N_p + D_H \frac{\partial^2 F}{\partial x^2}, \tag{S4.5.5}$$

$$\frac{\partial N_p}{\partial t} = (1 - c(r_{in}))[\eta_e^{Hxt}(J^G + J^F)(J^G + J^F) + \eta_e^S(J^S) \cdot J^S)]N_p + D_N \frac{\partial^2 N_p}{\partial x^2}, \tag{S4.5.6}$$

$$\frac{\partial N_n}{\partial t} = [\eta_e^{Hxt}(J^G + J^F) \cdot (J^G + J^F) + \eta_e^S(J^S) \cdot J^S]N_n + D_N \frac{\partial^2 N_n}{\partial x^2}, \tag{S4.5.7}$$

with the parameter values taken from [14] and shown in Supplementay Table 4.3.

Our simulations show that the principal outcome for the simple model shown in Fig. 4-3a of the main text is consistent with the more complex model (Supple-

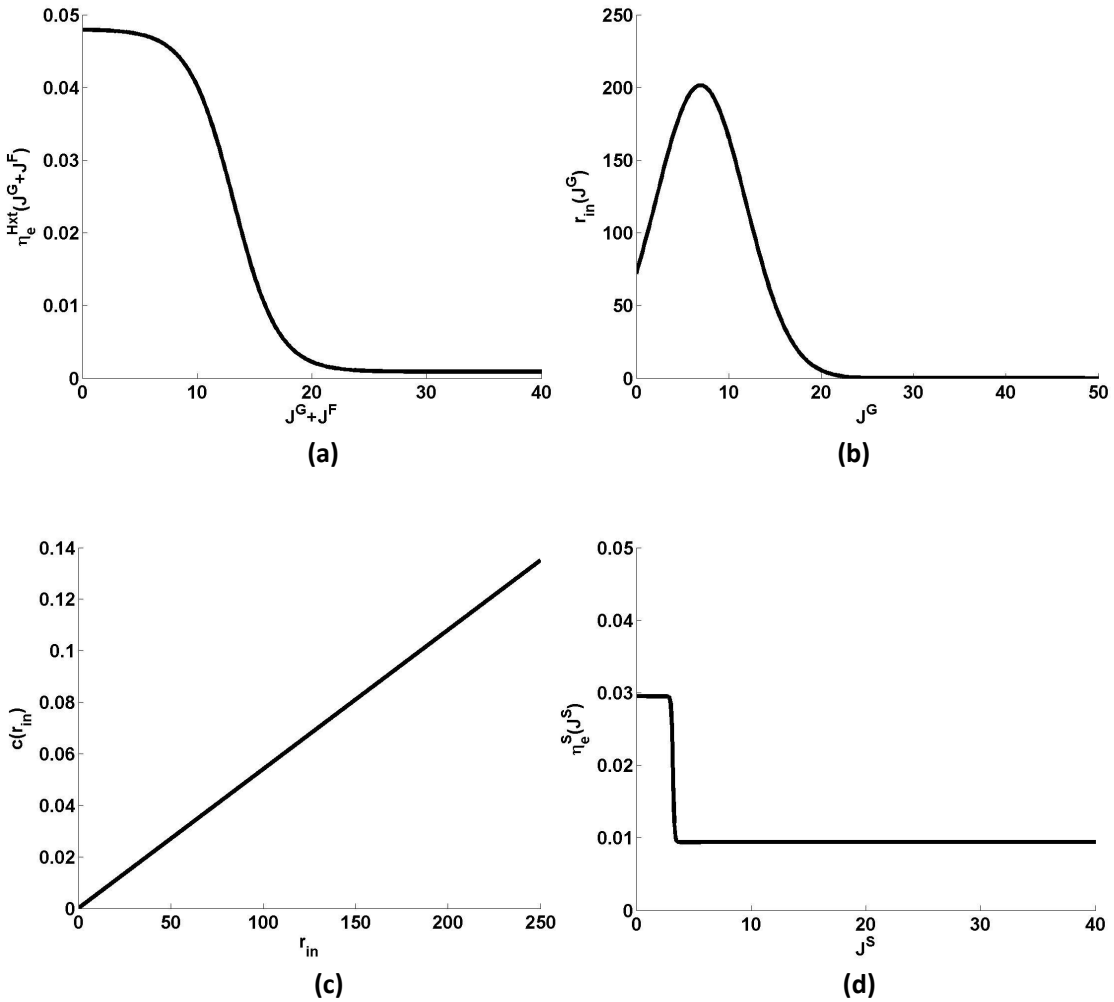

Supplementary Figure 4-9: **Shapes of the functions considered in the Full model.**
(a) Efficiency of hexose utilisation as a function of hexose uptake rate, taking the form $\eta_e^{Hxt}(J^G + J^F) = 0.0009 + 0.0471/(1 + \exp(-6.7598 + 0.5142 \cdot (J^G + J^F)))$.
(b) Invertase activity as a function of glucose uptake rate, taking the form $r_{in}(J^G) = 2447.3 \cdot f_G(J^G; \mu; \sigma)$. Here $f_G(J^G; \mu; \sigma)$ represents a normal distribution with mean $\mu = 6.952$ and standard deviation $\sigma = 4.8473$, evaluated at J^G.;
(c) cost of invertase activity, taking the form $c(r_{in}) = r_{in} \cdot 0.00054 \cdot \exp(0.000001 \cdot r_{in})$;
(d) efficiency of sucrose utilisation as a function of sucrose uptake rate, taking the form $\eta_e^S(J^S) = 0.0094 + 0.0201/(1 + \exp(-50 + 15.7232 \cdot J^S))$;
The form of each function in (a-d) has been estimated in [14] and here, for simplicity, we use a smooth interpolation of the estimates.

Supplementary Table 4.3: Aditional parameters values for the full mathematical model (S4.5.3)-(S4.5.7).

V_{max}^{G}	40 [mmol glucose / (g protein · hour)]
K_{m}^{G}	76 [mM glucose],
V_{max}^{F}	54.93 [mmol fructose / (g protein · hour)]
K_{m}^{F}	125 [mM fructose]

mentary Fig. 4-10) whereby in spatially structured environments high population density favours invertase producers for sufficiently low resource concentrations while high population density favours non-producers for sufficiently high resource concentrations. We find that this result is robust to further changes in parameter values. Similarly, the result in Fig. 4-3a indicating that in environments where spatial structure and resource concentration are sufficiently low, high population density favours non-producers, is also captured by the full model. This result, however, is dependent on the interplay between sucrose and hexose uptake and can be lost if the sucrose use efficiency is sufficiently low.

With our full model we also recover the result shown in Fig. 4-5 in the main text, where the relative fitness of producers is maximised at some intermediate resource concentration. This result is obtained with the full model (S4.5.3)-(S4.5.7), and it is shown in Supplementary Fig. 4-11.

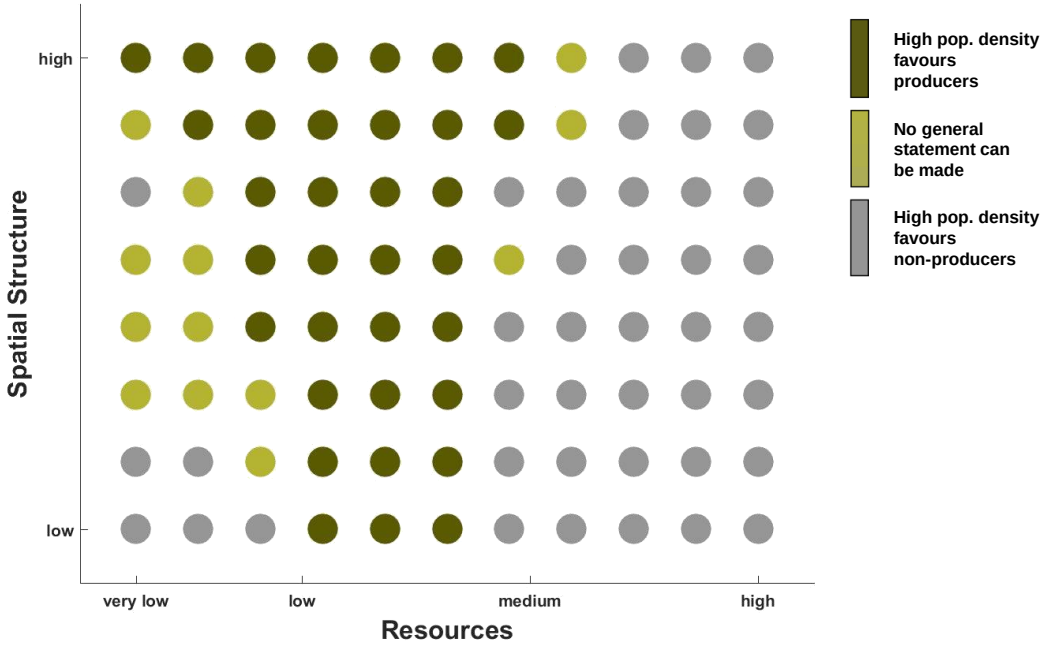

Supplementary Figure 4-10: **Full model. The effect of population density on cooperation as a function of the spatial structure and the resource concentration.**
The effect of population density on cooperation as a function of the spatial structure and the resource concentration in the environment. We simulated 88 environmental conditions denoted by circles (8 different spatial structure level, 11 different resource concentrations) and the following initial population densities: low: $N_0 = 6 \cdot 10^{-6}$, medium: $N_0 = 6 \cdot 10^{-5}$, high: $N_0 = 6 \cdot 10^{-4}$ [g protein /L]. *Dark green circles:* high population density favours invertase producers (cooperators); *Grey circles:* high population density favours the non-producers (cheats); *Light green circles:* population density may favour producers or non-producers, depending on the details of the system. The outcome of numerical simulations were assessed in the following way. Let $W_p^l(f_0)$, $W_p^m(f_0)$ and $W_p^h(f_0)$ denote the relative fitness of producers for low, medium and high initial population densities, respectively. If the statement S_a: $W_p^l(f_0) < W_p^m(f_0) < W_p^h(f_0)$ is true (with accuracy 10^{-3}) for all f_0, then high population density favours producers (dark green circles) while if the statement S_b: $W_p^l(f_0) > W_p^m(f_0) > W_p^h(f_0)$ is true (with accuracy 10^{-3}) for all f_0 then high population density favours non-producers (grey circles). However if S_a and S_b are not true we first define $f_0^* \in (0,1)$ as the initial producer frequency for which $W_p(f_0^*)$=1. If $W_p(f_0^*) > 1$ for all $f_0 \in (0,1)$ we set $f_0^* = 1$ while if $W_p(f_0^*) < 1$ for all $f_0 \in (0,1)$ we set $f_0^* = 0$. Subsequently we use f_0^{l*}, f_0^{m*} and f_0^{h*} to denote f_0^* for low, medium and high population densities, respectively. If $f_0^{l*} < f_0^{m*} < f_0^{h*}$ we conclude that high population density favours producers (dark green circles). However, if $f_0^{l*} > f_0^{m*} > f_0^{h*}$ then high population density favours non-producers (grey circles). Otherwise no general statement can be made regarding the relationship between population density and cooperation (light green circles).

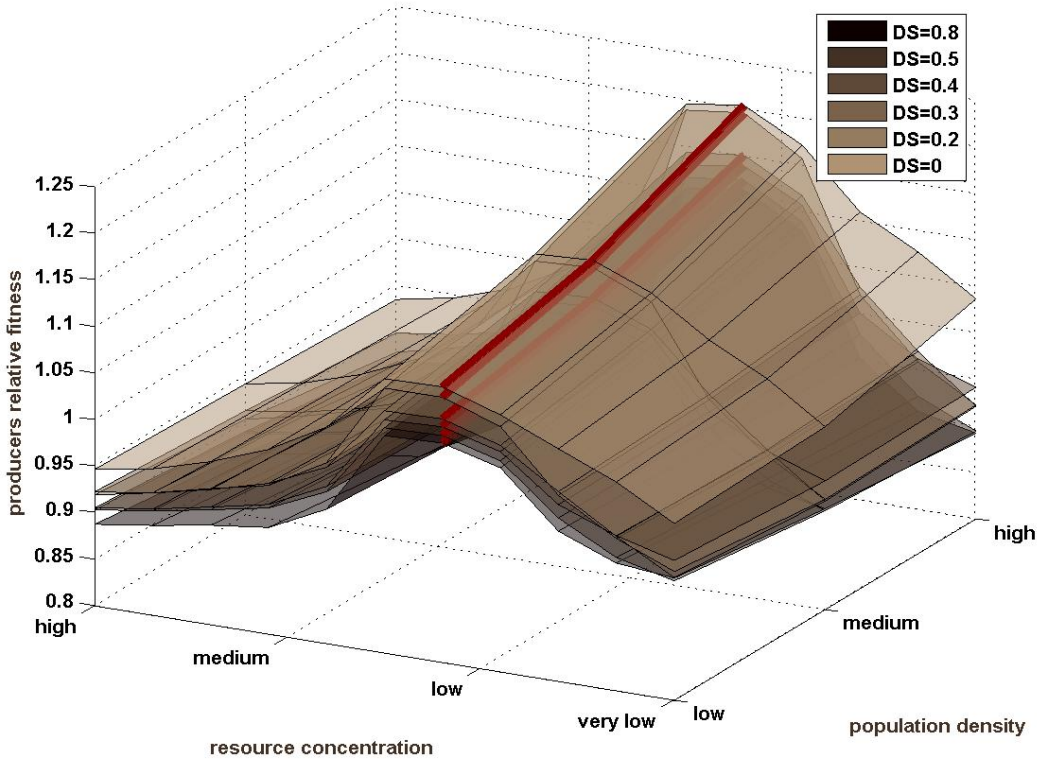

Supplementary Figure 4-11: **Full model. The relative fitness of producers as a function of resource concentration.**
Different surfaces denote the outcomes for various various population densities, resource concentrations and spatial structures for a fixed initial producer frequency $f_0 = 0.4$. The colour of surfaces changes depending on the level of the spatial structure (DSS). The red lines denote the resource concentration which maximise the producers relative fitness, at a given level of spatial structure DSS.

4.5.5 Main model, with no metabolic rate-efficiency trade-off

In order to understand the shape of Fig. 4-5 in the main text, we calculate the results of the main model (4.2.1)-(4.2.4), assuming there is no metabolic rate-efficiency trade-off, that is the hexose use efficiency is constant $\eta_e^{Hxt} = 0.048$. It turns out that, similarly as in the main model (4.2.1)-(4.2.4), it is the intermediate resource concentrations that maximise the producers relative fitness. Interestingly, in this case, that resource concentration depends on the considered level of spatial structure (Supplementary Fig. 4-12). This is because, the less spatial structured the environment, the bigger resource concentration (and therefore population density) is needed to privatise sufficient amount of public goods to have an advantage over non-producers. On the other hand, if the resource concentration is very large, the difference between producers and non-producers uptake rates is getting smaller, because the uptake rates are saturating functions of resource concentration.

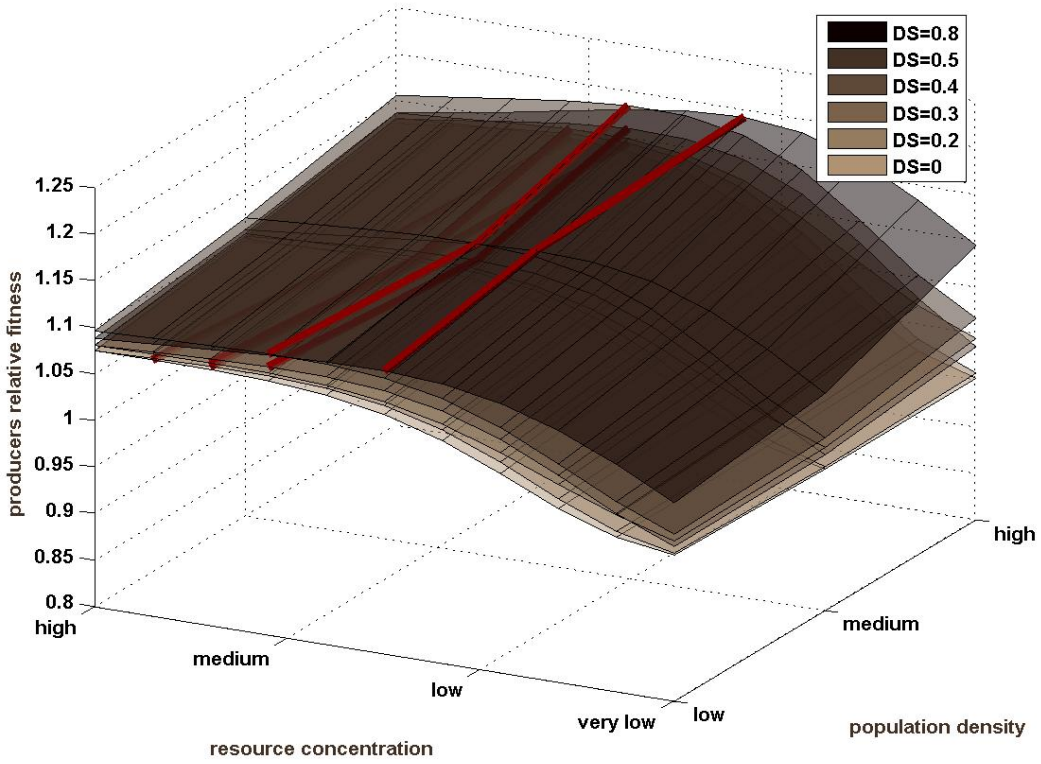

Supplementary Figure 4-12: **Main model with no trade-off. The relative fitness of producers as a function of resource concentration.**
Different surfaces denote the outcomes for various various population densities, resource concentrations and spatial structures for a fixed initial producer frequency $f_0 = 0.4$. The colour of surfaces changes depending on the level of the spatial structure (DSS). The red lines denote the resource concentration which maximise the producers relative fitness, at a given level of spatial structure DSS.

Chapter 5

Bistability in a Chemostat

Abstract

Classical chemostat theory states that a population grown at a given chemostat setting will converge to a unique globally steady state. Here we demonstrate that this may be not the case. We study a chemostat system of *Saccharomyces cerevisiae* and we find that, depending on the initial population density, the system may reach different steady states, varying from extinction (at low initial population density) to survival (at high initial population density). Thus we identify low population density as a potential threat for the survival of cooperative systems, such as the system of *S. cerevisiae*. Further, we show how the obtained multiple steady states depend on the metabolic pathway of the studied organisms.

5.1 Introduction

Chemostat culture is a laboratory setup known to represent the ecological conditions, in which microorganisms face a constant inflow of fresh resources and a constant outflow of the waste products and cells [42]. It may be used as an approximation of certain *in vivo* systems, for instance gut [43–46], mouth [47] or bladder [48]. In these human organs nutrients are continuously flowing in, because of the food intake, and the waste products are continuously removed, as they transit through the digestive (or urinary) system. Chemostats are also used in science and industry in order to study microbiological cultures in a growth phase [40, 110–112]. Due to such an extensive usage of the chemostat systems, they have been widely studied, resulting in a well-established chemostat theory [49].

The classical chemostat theory predicts that a chemostat culture containing multiple species grown on a single limiting nutrient, will converge to a unique globally stable state, at which only one species can be maintained at a specific growth rate [49]. This phenomenon is a special case of the *competitive exclusion principle* [113, 114], which is at the core of ecological discussions about species diversity, and it states that if a number of populations occupy the same ecological niche, one of them will outcompete all the others.

Similarly, a single species grown on multiple nutrients is believed to converge to a unique stable steady state, at which the nutrient in shortest supply controls the growth [115–117]. This is a consequence of the Liebig's law of the minimum [115, 118, 119], which states that the organism's growth is controlled by the scarcest resource in the environment.

Despite the theoretical predictions of the unique globally attractive steady state, oscillations have been observed in the experimental chemostat systems containing only one species [120, 121]. Moreover, it has been reported that depending on the way the chemostat system is initiated, it may converge to different (oscillatory or steady) states [122]. Furthermore, coexistence of various species has been reported in single nutrient chemostat cultures [123].

A number of extensions of the classical models have been proposed to explain the complex behaviour observed in the empirical systems. The coexistence of multiple species on a single carbon source can be explained by various heterogeneities in the culture. This can be either spatial heterogeneity that arises in unstired chemostats, as proposed in [124], or various forms of temporal heterogeneities, for example due to oscillations in the dilution rate [125, 126]. Also the product inhibition, which often is a consequence of accumulation of metabolic byproducts, has been proposed to be responsible for increased complexity in continuous cultures: for the coexistence of two species on one resource [127–130], as well as for the oscillatory states of a single species on a single resource [131–134]. Besides, variations in the resource yield have been proposed as a mechanism which drives oscillations observed in experimental cultures composed of a single species and a single resource [135].

All of these results suggest that complex ecological systems can only emerge in complex environments: meaning a complex nutrient composition, or existence of different spatial or temporal ecological niches. This however may not be the

case. Here we present a biological system whose behaviour cannot be captured by the classical chemostat theory, even though it faces the simplest possible environment: homogeneous in space and time, and supplied continuously with a single limiting nutrient. We find that the genetically homogeneous population of *Saccharomyces cerevisiae*, grown on a single limiting nutrient (sucrose) exhibits bistability and thus contradicts the standard chemostat theory. Depending on the initial conditions, the population of *S. cerevisiae* can either go extinct or survive at a fixed population density. In other words, there is no unique globally stable steady state for each chemostat setting, as expected. Instead, the trajectories may be attracted to two alternative steady states: survival or extinction.

Our system does not need to fulfill any of the assumptions previously proposed to explain multistability. The growth yield and the dilution rate are constant over time, and there is no product inhibition. Instead, what drives the bistability is the extracellular mode of digestion. In order to digest large molecules of sucrose, *S. cerevisiae* secrete an enzyme (invertase), which hydrolyses sucrose into simple sugars: glucose and fructose. Since that process happens outside the cell membrane, the simple sugars emerge in the environment and affect the microbial growth.

Bistability in the system of *S. cerevisiae* has been reported in a culture with temporal variations [93]. Here we show that, even if all the temporal heterogeneities are removed, the bistability can still be observed. This demonstrates that the observed complexities of ecological systems are not necessarily a consequence of the complex environment, as it tends to be believed. Instead, they may arise from the intrinsic characteristics of the biological systems.

Our results may also apply to industrial processes. The yeast *S. cerevisiae* is used worldwide in ethanol production, where it is grown in continuous cultures. Although the carbon source most commonly used in industry to grow *S. cerevisiae* is sucrose [136, 137], there is very little data available on the growth of *S. cerevisiae* in sucrose-limited chemostat cultures [137]. Moreover, the existing studies suggest that the continuous growth on sucrose does not phenomenologically differ from the growth on glucose [138, 139]. We show here this is not the case: while the chemostat culture of *S. cerevisiae* provided with glucose does not depend on the initial conditions, the growth of *S. cerevisiae* on sucrose may either cease or stabilise at a constant level, depending on the initial population density.

5.2 Mathematical model

We model the microbial growth in a chemostat i.e. a bioreactor, in which microbiological cultures are grown under constant conditions. The details of the chemostat systems are described in the subsection 2.2.1 and its schema is shown in Fig. 2-1.

5.2.1 Microbial growth

We consider the wild type strain of *Saccharomyces cerevisiae*, which is known to exhibit cooperative behaviour [32]. Namely it produces an enzyme, invertase, which is secreted outside the cell membrane [140], where it hydrolyses the sucrose present in the environment. Since this process happens outside the cells, its products (glucose and fructose) become available to all of the organisms in the environment.

Such a behaviour is termed 'public good cooperation', because individuals invest in the production of invertase, which results in presence of publicly available goods: simple sugars. Although such a system is vulnerable to exploitation by potential 'cheats' who do not invest their energy in the public good production, this will not be discussed in this chapter. Here we focus on the homogeneous population of cooperative cells.

We built a mathematical model of such a population, in order to study its behaviour in a chemostat. Our model is based on assumptions described in more detail in Chapter 2: Methods, and it tracks in time the concentrations of sucrose (S), simple sugars, such as glucose and fructose, both termed hexose (H), and the biomass of *S. cerevisiae* (N). Our cooperative cells take up resources and use them to generate molecules of ATP, and eventually to convert into biomass. We represent the microbial growth as a linear function of ATP production, as explained in detail in Chapter 2: Methods.

The cells secrete invertase which catalyses the hydrolysis of each molecule of sucrose (S) into two molecules of simple sugars, termed hexose (H). The rate of that hydrolysis is represented by Inv, a saturating function of sucrose concentration, introduced in Chapter 2: Methods. The cost of invertase production is denoted by a constant c, estimated empirically in [14]. Since the ratio of population

doublings of invertase producers to non-producers in competition was calculated as $(1-c)$, in our model we multiply the fitness of producers by $(1-c)$, as was done in [14, 33].

The individuals can take up both sucrose (S) and hexose (H), and the rates of these patways are denoted by J^S and J^H, respecitively, while their efficiencies are denoted by η_e^{Hxt} and η_e^S, which are for simplicity assumed to be constant.

5.2.2 The system dynamics

Based on the assumptions described in the previous subsection, we arrive at the following Ordinary Differential Equation (ODE) model, which tracks in time the concentrations of sucrose (S) and hexose (H), and the population density (N) in the chemostat culture:

$$\frac{dS}{dt} = -InvN - J^S N - D(S - S^0) \tag{5.2.1}$$

$$\frac{dH}{dt} = (2Inv - J^H)N - DH \tag{5.2.2}$$

$$\frac{dN}{dt} = (1-c)(\eta_e^{Hxt} J^H + \eta_e^S J^S)N - DN, \tag{5.2.3}$$

where D is the chemostat dilution rate and S^0 is the sucrose concentration in the chemostat reservoir. The parameter values used in our model are listed in Supplementary Table 5.1. The model (5.2.1)-(5.2.3) is a simplified and spatially homogeneous version of the model proposed in Chapters 3 and 4. Contrary to the previous model, here we consider only one strain of *S. cerevisiae* and no intraspecific competition. We assume the uptake efficiencies η_e^S and η_e^{Hxt} are constant, meaning there is no metabolic rate-efficiency trade-off. Most importantly, here we assume that all the reactions are global, and there is no spatial heterogeneity in any of the considered concentrations nor densities.

5.3 Results

We are interested in the steady states (termed also 'equilibria') of the system described in (5.2.1)-(5.2.3). This means we analyse the states (S^*, H^*, N^*) such that

$$\frac{dS}{dt}(S^*, H^*, N^*) = \frac{dH}{dt}(S^*, H^*, N^*) = \frac{dN}{dt}(S^*, H^*, N^*) = 0.$$

If such a state is reached, the population density, and concentrations of sucrose and hexose are constant: they will not change in time, unless there is a change in the system parameters D or S^0.

While the steady states at which there is no biomass ($N^* = 0$) are termed 'extinction' or 'trivial' steady states, the steady states with positive population density ($N^* > 0$) are termed 'survival' or 'nontrivial'.

In particular, we are interested in the system equilibria depending on the dilution rate D, which can be varied directly in chemostat experiments. Because the chemostat culture is continuously washed out at a rate D, the population needs to grow at the same rate, in order to survive and maintain constant population density. This feature is often used in the experimental studies. Constant growth rate G, can be forced by setting a chemostat dilution rate to $D = G$.

Apart from calculating the steady states and their stabilities, we also study how the population density N changes in time, depending on the initial population density N_0 inoculated to the chemostat. In that case we study the system (5.2.1)-(5.2.3), together with the following initial conditions $S(0) = S_0$, $H(0) = 0$, $N(0) = N_0$. In other words, we study the culture which is initiated and continuously provided with a single carbon source: sucrose.

Here we calculate all possible non-negative steady states of the system described by the model (5.2.1)-(5.2.3), and we verify if our system has a unique globally stable steady state, as predicted for the classical chemostat systems.

5.3.1 Bistability

To make our model even simpler, we first assume that there is no direct sucrose uptake, i.e. $V^S_{max} = 0$ [mmol/(g·hour)]. We calculate the steady states of the system

(5.2.1)-(5.2.3) and we present them in 'bifurcation diagrams', which are a standard way of representing dynamical systems behaviour, and are described in more detail in Chapter 2: Methods.

Each value of the dilution rate D set on the chemostat is related to a number of steady states (S^*, H^*, N^*) that can be reached at that rate. Thus when the chemostat is set to a specific dilution rate D (a point on the x-axis), the population density may stabilise at one of the values of N^* plotted for that value of D. For example in Fig. 5-1a, at the dilution rate $D = 0.75$ [1/hour], there are three steady states: two are stable (denoted by the solid lines) and one is unstable (denoted by the dashed line). However for a larger dilution rate $D = 1.5$ [1/hour], there is only one steady state, at which $N^* = 0$ [g/L]. It means that the population is not able to grow sufficiently quickly to balance out such a large wash out rate D, and its only possible behaviour is to go extinct. It can be seen from the equation (5.2.3) that the population will decrease and be eventually washed out, if its growth rate $G = (1 - c)(\eta_e^{Hxt} J^H + \eta_e^S J^S)$ is lower than the dilution rate D.

Contrary to the classical predictions, there are two branches of stable equilibria (the brown and the grey solid lines in the bifurcation digram in Fig. 5-1a), meaning that a culture started at different initial conditions, may converge to two significantly different equilibria: survival or extinction (Fig. 5-1b).

The reason of such different trajectories, converging to different stable steady states, is that larger communities break down sucrose quicker, and thus they face larger amounts of hexose. That amount of hexose in the environment is sufficiently high to sustain the population growth (brown line in Fig. 5-1c). On the contrary, the hexose concentration produced by small populations is not high enough to allow for a sufficient growth rate $G = D$, which can only be attained at the hexose concentration denoted by the brown dashed line in Fig. 5-1c. The phenomenon, in which small populations grow at slower rate than large populations, is termed the 'Allee effect', and it is known to affect *S. cerevisiae* cultured on sucrose [36, 93].

To confirm that what drives the complex behaviour shown in Fig. 5-1a is specifically the mode of sucrose digestion, we compute the steady states for the *S. cerevisiae* system, supplemented with hexose rather than sucrose. Such a sys-

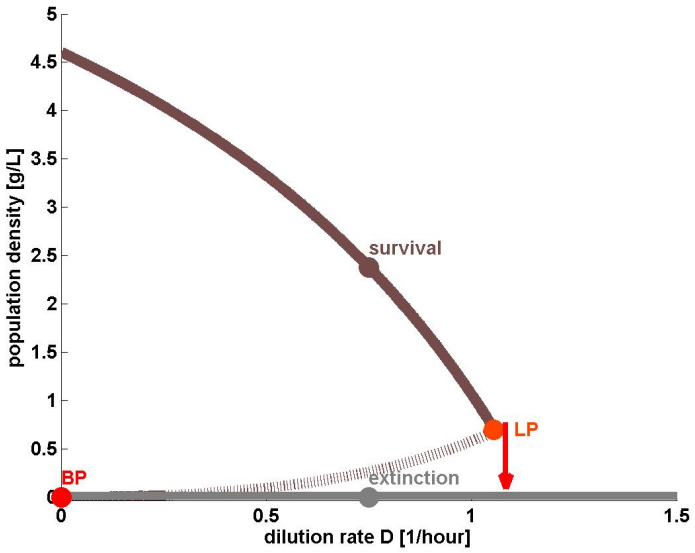

(a)

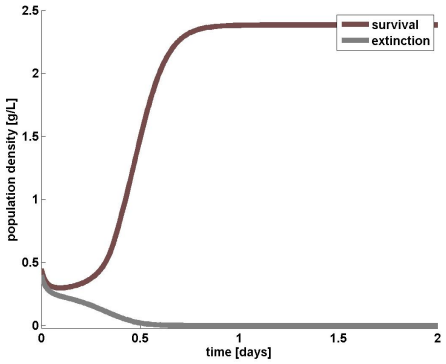

(b)

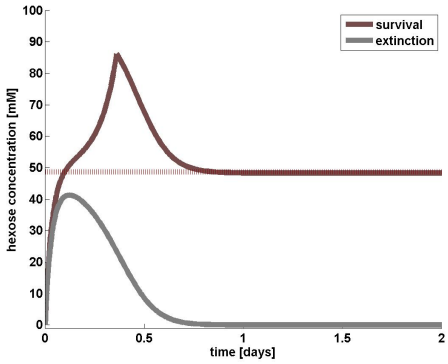

(c)

Figure 5-1: **The bistability in *S. cerevisiae* grown on sucrose in a chemostat.** (5-1a): Bifurcation diagram showing the population density at steady states. The stable steady states are denoted by solid lines, while the unstable steady states are denoted by dashed lines. The trivial steady states (extinction of the population) are plotted in grey, while the nontrivial steady states (survival of the population) are plotted in brown. At a fixed dilution rate D, either the survival or extinction stable steady states may be observed (as denoted by brown and grey dots). The branch point, at which a new branch of equilibria appears is denoted by 'BP', and the limit point, at which the stable and unstable survival branches meet and annihilate is denoted by 'LP'. The red vertical arrow shows the 'collapse scenario', in which a population at stable population density, affected by a perturbation in the dilution rate, may be driven to the parameter region where the only steady state is the extinction. Here: $V^S_{max} = 0$ [mmol/(g·hour)], and the values of other parameters are listed in Supplementary Table 5.1. As long as $V^S_{max} = 0$ [mmol/(g·hour)], this bifurcation diagram does not change qualitatively for different parameter values.
(5-1b)-(5-1c): Two trajectories of (5-1b): population density, and (5-1c): hexose concentration, in the chemostat culture. The trajectories plotted in brown converge to the stable survival equilibrium, and the ones plotted in grey converge to the stable extinction equilibrium. Both trajectories are started with similar initial conditions: $D = 0.75$ [1/hour], $S_0 = S^0$ [mM], $H_0 = 0$ [mM] and $N_0 = 0.45$ [g/L] or $N_0 = 0.4$ [g/L] for the brown and grey trajectories respectively. The brown dashed line in Fig. 5-1c indicates the minimal hexose concentration at which the growth rate $G = \eta^{Hxt}_e J^H$ can outbalance the dilution rate $D = 0.75$ [1/hour].

tem can be described with the following model:

$$\frac{dH}{dt} = -J^H N - D(H - H^0) \tag{5.3.1}$$

$$\frac{dN}{dt} = (1-c)\eta_e^{Hxt} J^H N - DN, \tag{5.3.2}$$

where H^0 is the hexose concentration in the chemostat reservoir.

In this case, the system behaviour obeys the classical theory: for every dilution rate D, there is just one globally stable steady state (the solid line in the bifurcation diagram in Fig. 5-2). For small dilution rates, the only stable steady state is the survival equilibrium (the brown solid line in Fig. 5-2), whereas for large dilution rates, there is no survival state, and all the trajectories are attracted to the globally stable extinction equilibrium (the grey solid line in Fig. 5-2). Importantly, the unique globally stable steady state is a continuous function of the dilution rate D, meaning that a small change in the dilution rate results in accordingly small change in the stable population density in the culture (Fig. 5-2).

A special point in this system is the 'branch point' (mathematically also termed a 'transcritical bifurcation') marked as 'BP' in Fig. 5-2. At that point, the trivial equilibria branch (grey line in Fig. 5-2), joins a nontrivial branch (brown line in Fig. 5-2), and the branches exchange stabilities. In other words, whereas for $D < BP$ the survival branch is stable and the extinction branch is unstable, for $D > BP$, the extinction branch becomes stable. It means that for $D > BP$ the population will go extinct and for $D < BP$ it will survive, regardless of its initial density. This behaviour conforms to the classical theory.

This is however not the case in the system (5.2.1)-(5.2.3) supplied with sucrose. In that case the branch point is at zero dilution rate $BP = 0$, meaning that the entire extinction branch $(S^0, 0, 0)$ is stable (grey line in Fig. 5-1a). It implies that a culture initiated at population density N_0 close to 0 will converge towards the extinction equilibrium. This may happen even at very low dilution rates D. Another specific trait of that system is existence of a 'tipping point': a point in the parameter values, at which two branches of equilibria meet and annihilate. In mathematical terms this point is called a 'fold bifurcation' and it is marked as 'LP' (that is 'limit point', in more general terms) in Fig. 5-1a. An increase of dilution rate D beyond that point leads to an abrupt change in the stable steady state: from survival to extinction. Such a scenario is indicated by the red vertical arrow

in Fig. 5-1a and presented in Fig. 5-3, where a population at a stable population density is affected by a small perturbation in the dilution rate and it goes extinct. It is worth to notice that in the natural systems, which can be represented by a chemostat culture, the dilution rate may commonly be perturbed. For example in gut, an episode of diarrhea could be understood as a sudden increase in the dilution rate. Similarly the dilution rate in bladder may be temporarily increased by a higher fluid intake.

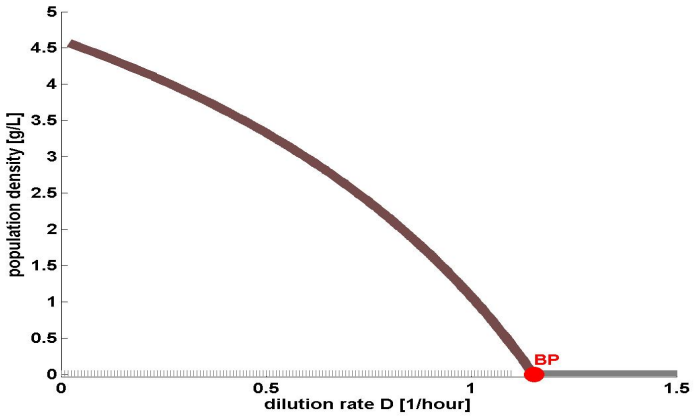

Figure 5-2: **Steady states in *S. cerevisiae* grown in a chemostat supplied with hexose only.**
Bifurcation diagram showing the population density at steady states. The stable steady states are denoted by solid lines, while the unstable steady states are denoted by dashed lines. The trivial steady states (extinction of the population) are plotted in grey, while the nontrivial steady states (survival of the population) are plotted in brown. The branch point, at which a new branch of equilibria appears is denoted by 'BP'. Here, the molar concentration $H^0 = 2S^0$, which is equivalent in terms of the mass and calorific value (because one molecule of sucrose is equivalent to two molecules of hexose).

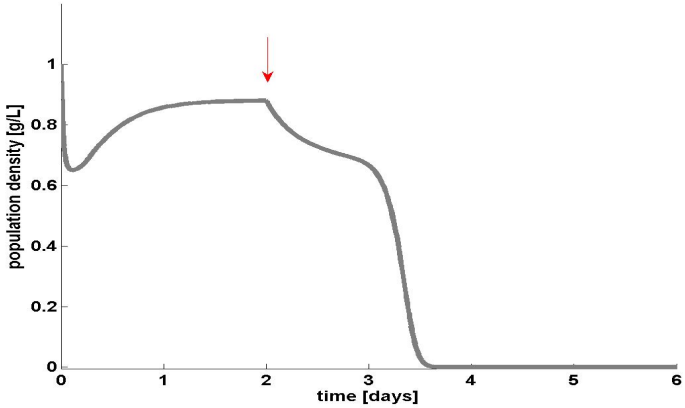

Figure 5-3: **Critical shift after a perturbation in the dilution rate.**
The population density in time. After it stabilises at $D = 1.03$ [1/hour], the dilution rate D is increased to $D = 1.06$ [1/hour], which drives the population to extinction. The perturbation in the dilution rate is indicated with the red vertical arrow.

5.3.2 The range of bistability depending on metabolic parameters

We verify how the parameters of the studied microbial culture influence the system behaviour. In particular, we study the resource supply S^0 and the metabolic parameters of *S. cerevisiae* that are expected to change in the course of evolution, namely the maximal hexose uptake rate V^H_{max} and the invertase activity r_{in} [141].

Changes in the studied parameters do not change qualitatively the bifurcation diagram (Fig. 5-4). In particular, regardless of the values of S^0, V^H_{max}, r_{in}, the dilution rate D equals to zero at the branch point, at which survival equilibria branch appears (red lines in Fig. 5-4). This means that regardless of the sucrose supply, hexose uptake rate, and the invertase activity, the entire extinction equilibria branch ($D > BP = 0$) is locally stable. Thus there is a risk of extinction, regardless of the speed of metabolism.

Although the branch point 'BP' is not affected by the metabolic parameters V^H_{max}, r_{in} and S^0, the limit point 'LP', which is the maximal dilution rate at which the population is able to survive, increases when the metabolism is enhanced (either by higher resource concentration S^0 (orange line in Fig. 5-4a), higher maximal hexose uptake rate V^H_{max} (orange line in Fig. 5-4b) or higher invertase activity r_{in} (orange line in Fig. 5-4c)). This confirms that, as expected, the strains with enhanced metabolism can survive at higher dilution rates. Additionally, at dilution rates $D < LP$, there are two stable equilibria: survival and extinction.

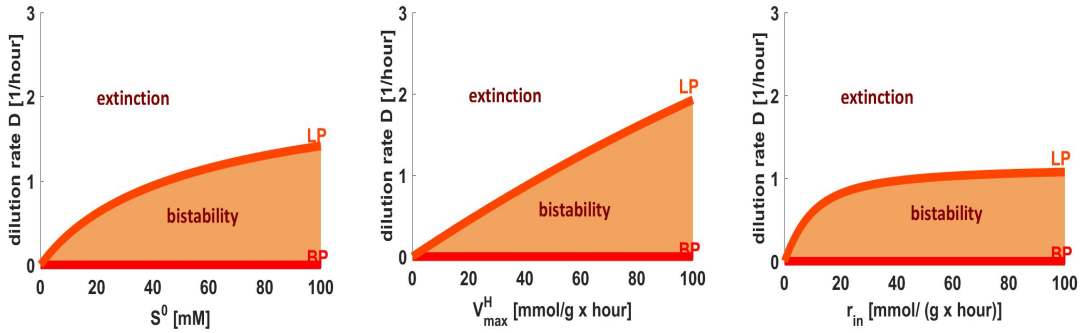

Figure 5-4: **Two parameter diagrams showing the range of dilution rates D resulting in bistability.**
The bistability is observed in the shaded area, i.e. at the dilution rates between the branch ('BP') and the limit ('LP') points (as observed in Fig. 5-1a). The branch points are denoted by the red lines, while the limit points are denoted by orange lines. The branch and the limit points depend on the metabolic parameters, that is:
(5-4a): concentration of sucrose in the reservoir S^0;
(5-4b): maximal uptake rate of hexose V^H_{max};
(5-4c): invertase activity r_{in}.

5.3.3 Direct sucrose uptake

Some of the studied strains of *S. cerevisiae* have been reported to be able to uptake sucrose directly [14]. Here we study if such a trait can change qualitatively the behaviour of the system, and we calculate the steady states of the system in which the maximal sucrose uptake $V^S_{max} > 0$ [mmol/(g·hour)] .

We observe that the direct sucrose uptake makes the system more robust to extinction, because it shifts the branch point 'BP' towards higher dilution rates (Fig. 5-5a & 5-5b). As explained previously, at the point 'BP', the extinction and survival branches exchange stabilities, and thus the extinction steady states become unstable for dilution rates $D \in (0, BP)$ (Fig. 5-5a). At these dilution rates, even the cultures initiated at very low population density will converge to the survival equilibrium and, will avoid the risk of extinction. Moreover, the quicker the sucrose uptake, the higher the BP and the bigger the range of dilution rates $D \in (0, BP)$ in which the population avoids the risk of extinction (Fig. 5-5b).

This result can be explained as follows. The dilution rate $D = BP$, at which the survival equilibria branch joins the trivial equilibria branch and changes its stability can be calculated analytically and be expressed as $BP = (\frac{\eta^S_e (1-c) S^0}{K^S_m + S^0}) V^S_{max}$ (see the Supplementary Material 5.6.2 for the calculations). From this formula it is clear that whenever there is no direct sucrose uptake ($V^S_{max} = 0$ [mmol/(g·hour)]), we have $BP = 0$. In that case, at all positive dilution rates ($D > BP = 0$), the extinction equilibria are locally stable. However, when there is a direct sucrose uptake ($V^S_{max} > 0$ [mmol/(g·hour)]), we have $BP > 0$ and there are some positive dilution rates $D < BP$, at which there is no risk of extinction.

Moreover, the presence of direct sucrose uptake in addition to the hexose uptake results in quicker growth, and therefore it allows the population to survive at higher dilution rates. This can be seen in Fig. 5-5b, which shows that the limit point 'LP' increases with increasing speed of sucrose uptake. Interestingly, although both: the branch and the limit points increase together with the increasing parameter V^S_{max}, the range of dilution rates, which result in bistability $D \in (BP, LP)$, becomes smaller at larger sucrose uptake rates (Fig. 5-5b).

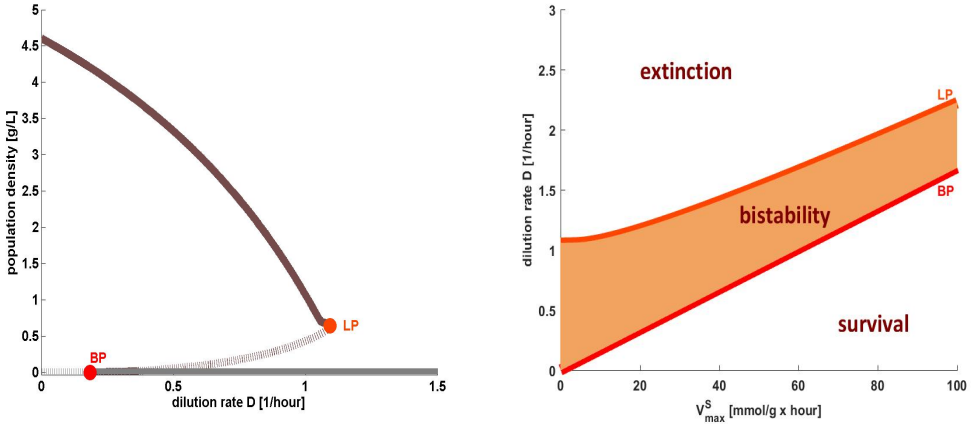

(a) *(b)*

Figure 5-5: **Behaviour of the system in the presence of direct sucrose uptake.**
(5-5a): Bifurcation diagram showing the population density at steady states. The stable steady states are denoted by solid lines, while the unstable steady states are denoted by dashed lines. The trivial steady states (extinction of the population) are plotted in grey, while the nontrivial steady states (survival of the population) are plotted in brown. The branch point, at which a new branch of equilibria appears is denoted by 'BP', and the limit point, at which the stable and unstable survival branches meet and annihilate is denoted by 'LP'. Here we assume $V^S_{max} = 11$ [mmol/(g·hour)].
(5-5b): The range of dilution rates resulting in bistability, depending on the maximal uptake rate of sucrose V^S_{max}. The bistability is observed in the shaded area, that is at the dilution rates between the branch ('BP') and the limit ('LP') points (as observed in Fig. 5-5a). The branch points are denoted by the red line, while the limit points are denoted by orange line.

5.3.4 Model with rate-efficiency trade-off

In order to verify the generality of our results on the system multistability, we study a more complex model of *S. cerevisiae* described in Chapter 2: Methods, and parametrised in [14]. In particular, here we take into account the metabolic rate-efficiency trade-off by assuming that the hexose use efficiency η_e^{Hxt} is a decreasing function of the hexose uptake rate, which can be written as $\eta_e^{Hxt}(J^H)$. This means the individuals may uptake the simple sugars either slowly and efficiently (low J^H and high η_e^{Hxt}) or quickly and inefficiently (high J^H and low η_e^{Hxt}), depending on the hexose concentration in the culture. Although, here we assume a constant inflow of resource, outflow of the culture, and no spatial heterogeneity, the description of the metabolic processes corresponds to the one proposed in Chapters 3 and 4.

Finally we arrive at the following model:

$$\frac{dS}{dt} = -InvN - J^S N - D(S - S^0) \tag{5.3.3}$$

$$\frac{dH}{dt} = (2Inv - J^H)N - DH \tag{5.3.4}$$

$$\frac{dN}{dt} = (1-c)(\eta_e^{Hxt}(J^H)J^H + \eta_e^S J^S)N - DN \tag{5.3.5}$$

The parameters of this model are the same as of the model (5.2.1)-(5.2.3), with the exception of the hexose use efficiency η_e^{Hxt}, which now is a function of hexose uptake and its shape is shown in Supplementary Fig. 5-12. We also allow for a direct sucrose uptake ($V_{max}^S > 0$ [mmol/(g·hour)]).

Similarly as in the main model (5.2.1)-(5.2.3), we observe multistability (Fig. 5-6). However an addition of the rate-efficiency trade-off assumption increases the complexity of the bifurcation diagram. In particular, another stable steady state appears, resulting in three possible stable equilibria: extinction, high population density (the brown branch in Fig. 5-6a) and the low population density (the pink branch in Fig. 5-6a, shown also in Fig. 5-6b). Therefore the trajectories of the system may converge to three different steady states, depending on the initial population density N_0 (Fig. 5-7).

The presence of the third stable steady state is due to the rate-efficiency trade-off. We confirm that observation by calculating the steady states in the simplified

version of the model (5.3.3)-(5.3.5), in which there is no direct sucrose uptake $V^S_{max} = 0$ [mmol/(g·hour)] (Supplementary Fig. 5-13). In that case all of the three stable equilibria branches can be recovered. The high population density equilibrium is linked to slow but efficient hexose uptake at low hexose concentration (brown line in Fig. 5-7b), and therefore it can be found only at low dilution rates (brown branch in Fig. 5-6a). At high dilution rates, at which the population needs to grow quickly in order not to be washed out from the culture, the equilibria are linked to a quick and inefficient uptake at large hexose concentration (pink line in Fig. 5-7b), resulting in small population density (pink branch in Fig. 5-6a & Fig. 5-6b).

Although, the bottom (pink) branch of equilibria exists for higher dilution rates than the top (brown) branch, it does not prevent extinction when a population at the top branch faces an increase in the dilution rate. Namely, an increase of the dilution rate around the tipping point 'LP' on the top branch leads the population to converge to extinction, rather than to the low population density state (Fig. 5-8). This is because, in order to stay at the bottom equilibria branch, there must be a high concentration of hexose in the culture (as shown in Fig. 5-7b). However, when a population at high density and low hexose concentration (top branch) is exposed to high dilution rate, it is not able to compensate for the lack of hexose and therefore it goes extinct.

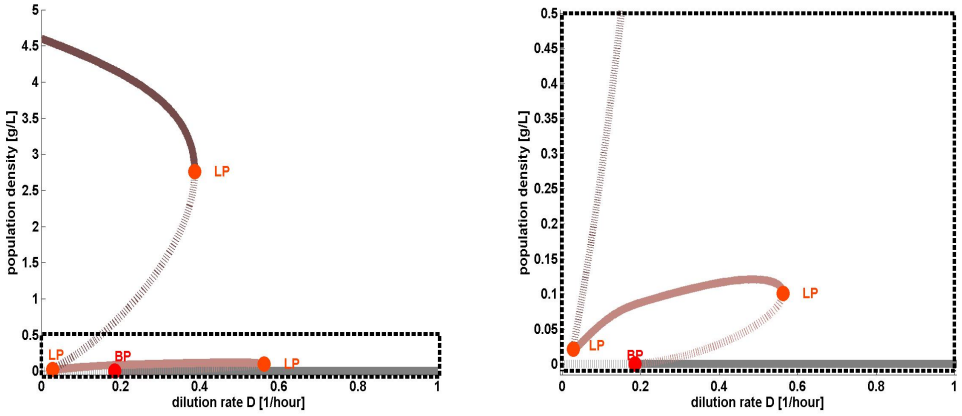

(a) *(b)*

Figure 5-6: **Behaviour of the system with the rate-efficiency trade-off assumption.**
(5-6a): Bifurcation diagram showing the population density at steady states. The stable steady states are denoted by solid lines, while the unstable steady states are denoted by dashed lines. The trivial steady states (extinction of the population) are plotted in grey, while the nontrivial steady states (survival of the population) are plotted in brown and pink. At a fixed dilution rate D, three different stable steady states may be observed. The branch point, at which survival equilibria appear is denoted by 'BP', and the limit points, at which the stable and unstable survival branches meet and annihilate are denoted by 'LP'.
(5-6b): Zoom into the bottom part of Fig. 5-6a, denoted by a dashed box.

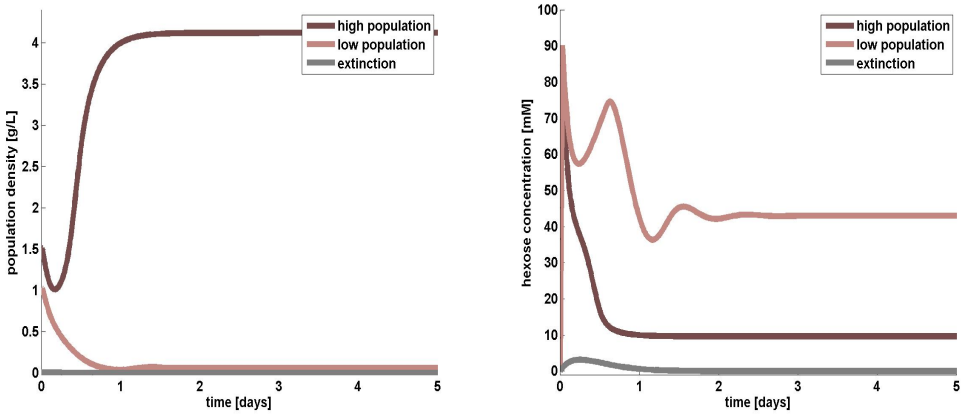

(a) *(b)*

Figure 5-7: **Trajectories converging to various stable equilibria.**
(5-7a)-(5-7b) Three trajectories: the brown converging to the stable high population density equilibrium, the pink converging to the stable low population density equilibrium, and the grey converging to the stable extinction equilibrium. Fig. 5-7a shows population density in time, while Fig. 5-7b shows hexose concentration in time. Here, $S_0 = S^0$, $H_0 = 0$ [mM] and $D = 0.2$ [1/hour].

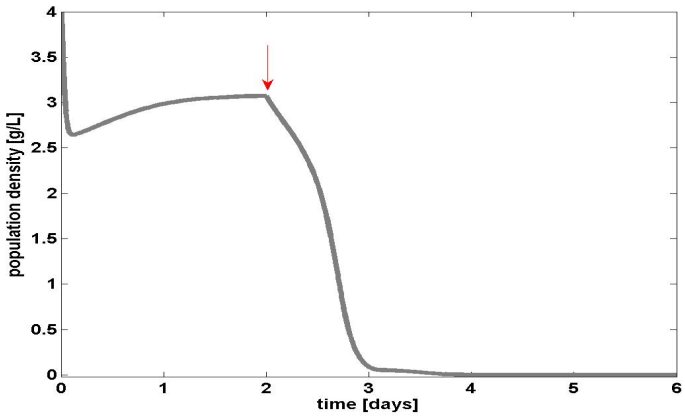

Figure 5-8: **Critical shift after an increase in the dilution rate.**
The population density in time. After it stabilises at high population density, at $D = 0.38$ [1/hour], the dilution rate D is increased to $D = 0.41$ [1/hour], which drives the population to extinction. The perturbation in the dilution rate is indicated with the red vertical arrow.

5.4 Experimental verification

We are currently performing laboratory experiments to confirm our theoretical results. We use a 'home-made' chemostat, in which we culture *S. cerevisiae* until they reach a steady state (that is until the population density does not change significantly for 24 hours). To the chemostat we continuously provide fresh media containing 25mM sucrose.

Our chemostat contains 6 vessels, which allow to study two different initial conditions in parallel (having 3 biological replicates for each condition). We inoculate different population densities N_0, with a fixed sucrose concentration ($S_0 = S^0$), and without hexose ($H_0 = 0$) to the chemostat vessels. We aim to obtain two significantly different steady states for cultures initiated at low and at high population densities. The size of inoculum N_0 is measured in optical density and then calibrated into the number of cells per mL of media.

5.4.1 Optical density to number of colonies calibration

Materials and Methods

We used the *S. cerevisiae* strain $DBY1034$ [142], cultured on supplemented minimal media (termed SMM) with 25mM sucrose (5 g/L ammonium sulfate, 1.7 g/L yeast nitrogen base w/o amino acids or ammonium sulfate, 50 mg/L uracil, 50 mg/L L-lysine and 20 mg/L L-histidine, and 8.56g/L sucrose). The media containing ammonium sulfate and yeast nitrogen base was autoclaved for 30 minutes at $121°C$ prior to addition of the filter sterilised stock of sucrose and amino-acids.

In order to perform the OD calibration measurement, 10mL of SMM media was seeded from a glycerol stock of *S. cerevisiae*, stored at $-80°C$. Cells were cultured for 48 hours at $30°C$ with continuous shaking at 150rpm. After 48 hours, 1mL of the culture was transfered into a 1mL sterile tube (Eppendorf) and was serially diluted by a series of transfers of 0.75mL of a culture into 0.25mL of fresh media. After each transfer, the new culture was vortexed for approximately 3 seconds, in order to obtain a homogeneous mixture of the cells and the media. In order to take the OD measurements, 150 μL of each culture was transferred into the

96-well microplate (Greiner): one culture per well. Optical density measurements were taken using a microplate reader, at 620 nm.

The same overnight culture was diluted four times, 10-fold. 25 μL of that culture was placed on an agar plate (SMM with 1.5% of agar). The plates were incubated for 72 hours at 30 $^{\circ}C$. Afterwards the number of colonies (m) was counted on each plate ($n = 3$ replicates), and the cell density N in the overnight culture was determined as the mean of $10^4 \cdot m \cdot 40$ cells/mL. The cells density of the $i-th$ dilution was then calculated as $N_i = (0.75)^i N$.

Optical density calibration

A range of population densities was prepared by 12 serial dilution steps, as described in Materials and Methods. The measured blank corrected optical density ('OD') for each cell density is shown in Fig. 5-9a. A function of population density was fitted to the optical density data (Fig. 5-9b), according to the method proposed in [93]. Although the optical density seems to be a linear function of population density up to $\approx 3 \cdot 10^7$ cells/mL, it eventually starts saturating to some maximal value. Therefore we fit to our data the saturating function proposed in [93]:

$$OD(N) = OD_{max}(1 - exp(-OD_{real}/OD_{max})) \tag{5.4.1}$$

where OD_{real} is a linear function of population density N, that is $OD_{real} = a \cdot N$, and a and OD_{max} are the parameters fitted to the data.

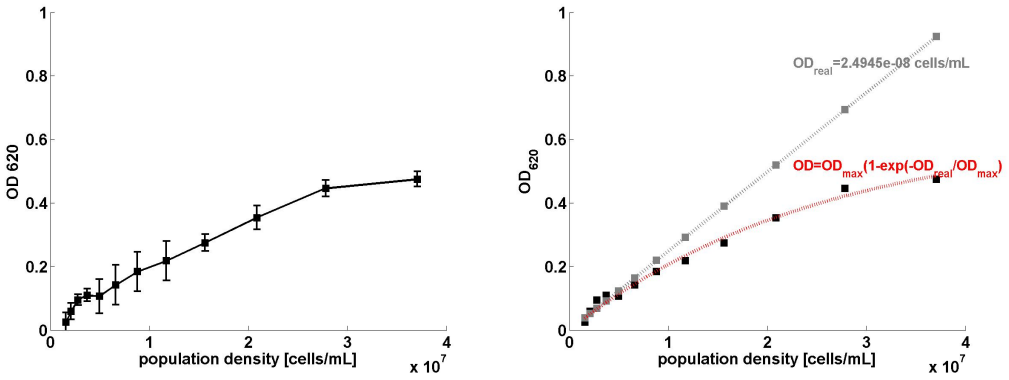

(a) *(b)*

Figure 5-9: **Calibration of optical density measurement.**
(5-9a): The optical density of *S. cerevisiae* cultures at various population densities. The error bars represent the standard deviation, and the number of replicates is $n = 3$.
(5-9b): Function $OD(N)$ fitted to the optical density data. The black squares represent the mean, blank corrected OD, the grey squares represent the OD calibrated to a form $OD_{real} = aN$, where N is the population density. The red curve represents the fitted function $OD(N)$. In our calibration $OD_{max} = 0.6323, a = 2.4945 \cdot 10^{-8}$.

5.4.2 Chemostat design

Our sterile chemostat (Fig. 5-10) is composed of six vessels of working volume 30mL, in which *S. cerevisiae* is cultured. The vessels are placed in a water bath which keeps them at constant temperature. All of them are connected to both: a 5L reservoir flask and to a 3L waste flask. The media is pumped from the reservoir into the chemostat vessels by a peristaltic pump. The rate at which the media is pumped can be set on the pump. The chemostat culture, containing a mixture of the media and the cells, is pumped out at the same rate from the vessels to the waste flask, by a vacuum pump.

The resource inflow tubes reach down to the bottom of chemostat vessels, and therefore the fresh supplied media is immediately mixed with the culture. The outflow tubes inside the vessels reach the top of the liquid volume of 30mL, and therefore the excess of the mixed culture becomes removed by the outflow tubes (see Fig. 5-11 for a schematic design of each of the vessels).

In order to prevent the vessels from drying out and to ensure the microbial cultures will not sink to the bottom of vessels, we improved the chemostat design by supplying the vessels with air. To do so, we puncture needles through the vessels sealing. The needles are covered with syringe filters, which filter the inflowing air, and thus keep the content of the chemostat vessels sterile (Fig. 5-11). The constant air and liquid flow keep the culture homogeneous and therefore we do not apply any additional form or shaking or stirring to the chemostat.

In practice, the stability of all the system depends on the subtle interplay between the pump pressure and the air flow. Namely, if the vacuum pump is too strong, and decreases significantly the pressure in the vessels, the air flowing in may be not sufficient to compensate for the change in pressure, and in consequence, the rate of inflow of the resources from the reservoir may be increased. This results in dilution rates being difficult to control.

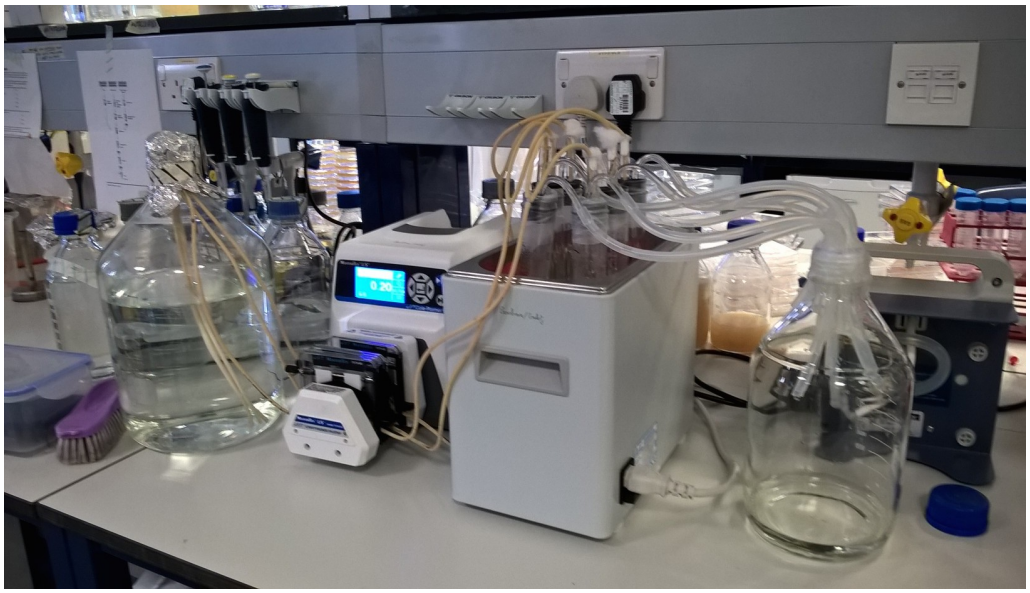

Figure 5-10: **Picture of our chemostat.**

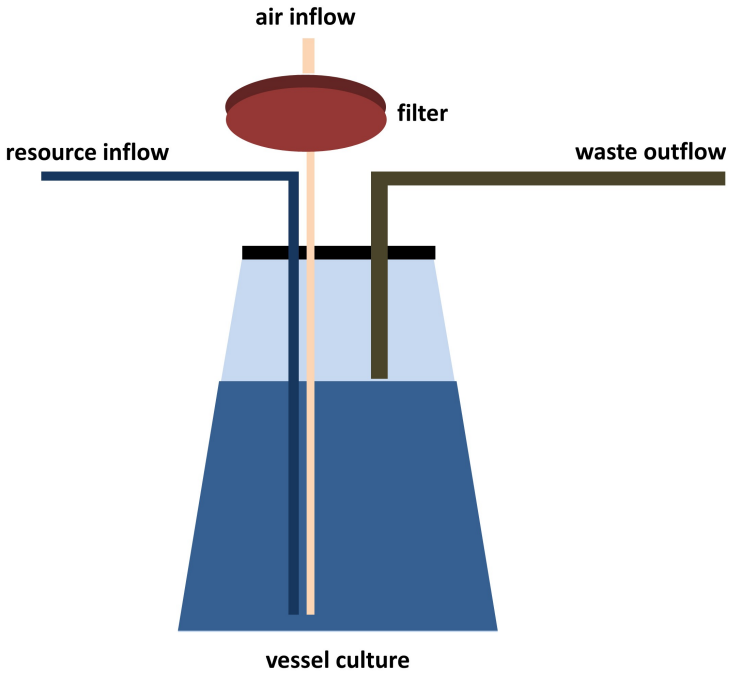

Figure 5-11: **Schema of the chemostat vessel.**

5.4.3 Future experimental protocol

The protocol described in this subsection has been designed in order to determine the steady states of the cultures in the chemostat. The experiment is still ongoing, with continuous improvements made to the chemostat design. So far we have taken several attempts to run the full chemostat culture. The chemostat design is however very sensitive to any changes in the pump pressure and so far we have not been able to keep the dilution rate constant for long enough (that is for more than 4 days).

The stable steady states of the cultures grown in our chemostat are determined as follows. The overnight culture is grown for 48 hours, on SMM, at $30°C$ and in shaking conditions. The density of the culture is determined by the OD measurement and calibration into the number of cells per mL (according to the inverse of the function presented in Fig. 5-9b.)

The chemostat reservoir and the chemostat vessels are filled with sterile media (SMM). Three of the six chemostat vessels (termed 'L') are filled with 10^3 cells from the overnight culture ('low initial density'), and the three remaining vessels (termed 'H') are filled with 10^6 cells from the overnight culture ('high initial density'). The peristaltic pump is set to the rate D=0.25ml/min, equivalent to 0.5 [1/hour], and the temperature of the vessels is kept at $30°C$. The level of the liquid in the reservoir and in the waste flask is verified every 24 hours to make sure that the dilution rate D is equal to the expected.

A sample from each of the vessels is taken every 24 hours, until the population density stops changing significantly for 24 consecutive hours. Each of the samples is serially diluted 10-fold, four times. 25μL of the original culture and the diluted culture are plated onto agar plates. This gives a total of 12 agar plates: 2 different dilutions per each of the 6 samples per day. The agar plates are incubated at $30°C$ for 72 hours, and then the number of formed colonies are counted to determine the population density of the original chemostat culture. The original samples are supplemented with 15% of glycerol and stored at $-20°C$.

When the population density in each vessel stop changing by more than 12% per 24 hours (that is 1% per volume change as in [139]), it is assumed to be at the stable steady state N^*.

The experiment may need to be repeated with various initial densities, in order to observe different resulting steady states. We also plan to repeat the experiment in a chemostat supplemented with glucose, rather than sucrose, in order to confirm that the mechanism responsible for the appearance of multiple stable steady states is the mode of sucrose metabolism.

5.5 Discussion

We study a homogeneous culture of *S. cerevisiae*, provided with a single limiting carbon source and grown in a chemostat. Although such a system is expected to obey the classical theory [49], in which only one globally stable steady state can be observed, we discover more complex dynamics.

We report that depending on the initial population size inoculated into the chemostat, the population may reach two different equilibria: survival or extinction (Fig. 5-1a). Apart from the locally stable trivial equilibria branch (extinction), we discover two nontrivial (survival) branches, connected with a fold bifurcation. This implies existence of the so-called 'tipping point', beyond which both nontrivial equilibria branches disappear and the system is necessarily driven to a collapse (Fig. 5-3).

Apart from the existence of a tipping point, the important feature of this system, which has not been reported before is that the whole trivial branch is locally stable. This means that even at a very low dilution rate, the population may fall at risk of extinction. This feature is absent in the classical chemostat systems [49], and it points out towards a potential threat to microbial cooperative systems: namely, low population density.

We also observe that the direct sucrose uptake may increase the culture robustness to extinction (Fig. 5-5). An ability to uptake sucrose before it is hydrolysed into simple sugars leads to destabilisation of a part of the extinction branch (for $D < BP$), which means that, at dilution rates $D < BP$, regardless of the initial population density, the culture will converge to the survival steady state. This is because, the growth rate resulting from the direct sucrose uptake $G = \eta_e^S J^S$ is sufficient to balance out a small wash out rate ($G > D$). We reason that, even if direct sucrose uptake is inefficient as argued in [14], it may give an important advantage to a population of *S. cerevisiae*: namely, it may protect low density colonies from extinction.

Although bistability in *S. cerevisiae* has been reported and studied [93], it was previously observed in a culture allowing for temporal variations in its components. Thus it did not contradict any classical predictions. The results obtained

in [93] are described with a phenomenological mathematical model. However, phenomenological models do not lend themselves to provide a mechanistic understanding of the underlying processes. In contrast, our model explicitly tracks in time the concentrations of the key components of the studied culture: sucrose, hexose and the biomass. It highlights that these three components, and in particular, the mode of sucrose metabolism, are sufficient to explain the observed bistability.

We show that the speed of hydrolysis is responsible for the system's survival or extinction. As can be deduced from the equation (5.2.2), the rate at which hexose appears in the culture $InvN$ is proportional to the population density. Dense cultures produce more invertase, and therefore break down sucrose into hexose much quicker than the cultures at small population density. Since the dense populations are exposed to higher concentrations of hexose in the environment, they have a higher growth rate and therefore are more likely to balance out the chemostat wash-out rate. Instead, if the chemostat is inoculated with a small population, the individuals may get washed out before they can produce enough hexose to sustain the growth (Fig. 5-1c).

This effect cannot be seen when the chemostat culture is supplied with hexose rather than sucrose (Fig. 5-2). In such case, the system dynamics defaults to the classical findings: at large dilution rates, the biomass is washed out from the culture, while at low dilution rates it converges to some stable density which does not depend on the initial conditions. The trivial branch is unstable for small dilution rates ($D < BP$), meaning that even the cultures started at very low population density should not go extinct, contrary to the case of chemostat run on sucrose.

This confirms our explanation that the observed complexity of the studied chemostat system is a result of the external metabolism when *S. cerevisiae* is grown on sucrose. It also highlights that the continuous growth of *S. cerevisiae* on sucrose differs significantly from the growth on glucose, contrary to what is believed in industry [138, 139]. Therefore, there is a clear need to obtain more experimental data on *S. cerevisiae* grown continuously on limiting sucrose, which is currently lacking in the literature [137].

How does our system relate to the complexity of the environment? Even if the population of *S. cerevisiae* is cultured in very simple conditions, the complex metabolism leads to changes in the environment, and to appearance of the

simple sugars. However, in our case it is not the environment that controls the dynamics of the population growth, but the population growth controls the environment. In particular, small and large communities turn out to create different environments and thus fall into different system equilibria. This is because the speed of extracellular metabolism depends on the population density.

Finally, we discover that adding more assumptions to the studied metabolic pathway, such as the rate-efficiency trade-off, leads to appearance of even more possible stable equlibria (Fig. 5-6). This confirms our argument that the biological complexity may not only originate because of the complex environments as believed in standard ecological theories [49, 115–118]. Instead complex ecological systems, with multiple stable steady states may arise because of some intrinsic traits of the studied organisms.

5.6 Supplementary Material

5.6.1 Parameter values

Supplementary Table 5.1: Parameters values for the mathematical model (5.2.1)-(5.2.3).

V_{max}^S	11 [mmol sucrose / (g protein · hour) unless stated otherwise]
K_m^S	7 [mM sucrose]
V_{max}^H	50 [mmol hexose / (g protein · hour)]
K_m^H	100 mM hexose
η_e^S	0.02 [g protein/mmol sucrose]
η_e^{Hxt}	0.048 [g protein/mmol hexose]
r_{in}	77 [mmol/ (g protein · hour)]
c	0.04
k_{in}	$5 \cdot 10^{-3}$ [mM sucrose]
S^0	50 [mM scurose]

5.6.2 Analytical calculation of the branch point 'BP'

We are interested in the dilution rate at which a branch of nontrivial equilibria appears. Therefore we study the eigenvalues of the system (5.2.1)-(5.2.3) at the trivial equilibrium $(S^*, H^*, N^*) = (S^0, 0, 0)$. First of all let us notice, that the point $(S^0, 0, 0)$ indeed is an equilibrium point for any dilution rate D. We have

$$\frac{dS}{dt} = -Inv(S^0)0 - J^S(S^0)0 - D(S^0 - S^0) = 0 \tag{S1}$$

$$\frac{dH}{dt} = (2Inv(S^0) - J^H(0))0 - D0 = 0 \tag{S2}$$

$$\frac{dN}{dt} = (1-c)(\eta_e^{Hxt} J^H(0) + \eta_e^S J^S(S^0))0 - D0 = 0. \tag{S3}$$

Let us denote

$$f_S(S,H,N) = \frac{dS}{dt} = -InvN - J^S N - D(S - S^0) \tag{S4}$$

$$f_H(S,H,N) = \frac{dH}{dt} = (2Inv - J^H)N - DH \tag{S5}$$

$$f_N(S,H,N) = \frac{dN}{dt} = (1-c)(\eta_e^{Hxt} J^H + \eta_e^S J^S)N - DN \tag{S6}$$

We then calculate the Jacobian of the system (5.2.1)-(5.3.5)

$$\begin{bmatrix} \frac{\partial f_S(S^*,H^*,N^*)}{\partial S} & \frac{\partial f_S(S^*,H^*,N^*)}{\partial H} & \frac{\partial f_S(S^*,H^*,N^*)}{\partial N} \\ \frac{\partial f_H(S^*,H^*,N^*)}{\partial S} & \frac{\partial f_H(S^*,H^*,N^*)}{\partial H} & \frac{\partial f_H(S^*,H^*,N^*)}{\partial N} \\ \frac{\partial f_N(S^*,H^*,N^*)}{\partial S} & \frac{\partial f_N(S^*,H^*,N^*)}{\partial H} & \frac{\partial f_N(S^*,H^*,N^*)}{\partial N} \end{bmatrix}$$

at the trivial equilibrium $(S^*, H^*, N^*) = (S^0, 0, 0)$, and we obtain

$$\begin{bmatrix} -D & 0 & (-Inv(S^0) - J^S(S^0)) \\ 0 & -D & 2Inv(S^0) \\ 0 & 0 & (1-c)(\eta_e^S J^S(S^0)) - D \end{bmatrix}$$

The eigenvalues of the above matrix are: $\lambda_1 = -D, \lambda_2 = -D, \lambda_3 = (1-c)(\eta_e^S J^S(S^0)) - D$. The bifurcation points are observed at values of D, at which one or more eigenvalues are equal to zero, that is: $D = 0$ and $D = (1-c)(\eta_e^S J^S(S^0)) = \frac{(1-c)\eta_e^S V_{max}^S}{K_m^S + S^0}$.

5.6.3 Supplementary figures

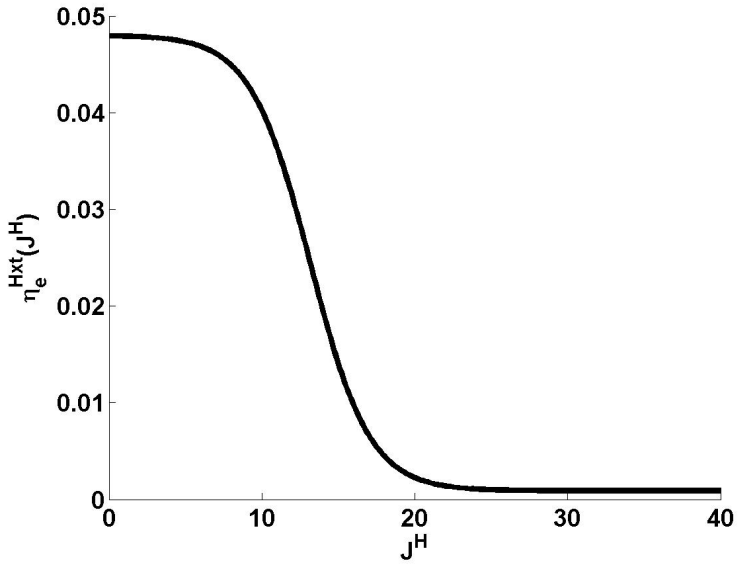

Supplementary Figure 5-12: **Shape of the metabolic rate-efficiency trade-off in the model with rate efficiency trade-off** (5.3.3)**-**(5.3.5)**.**
The efficiency of hexose utilisation as a function of hexose uptake rate, taking the form $\eta_e^{Hxt}(J^H) = 0.0009 + 0.0471/(1 + \exp(-6.7598 + 0.5142 \cdot J^H))$.

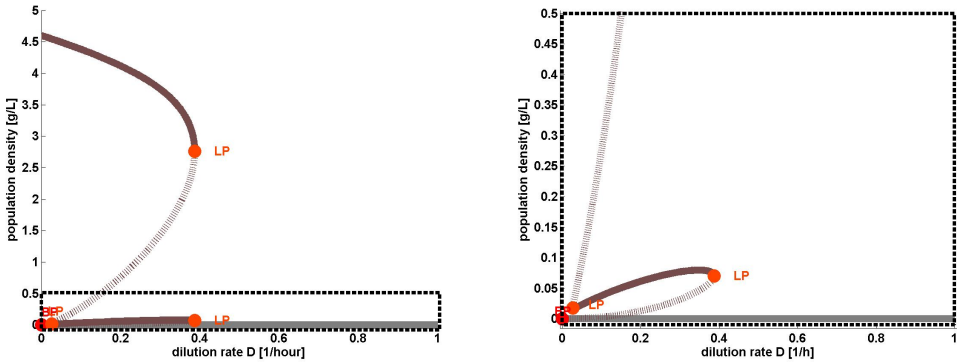

(a) *(b)*

Supplementary Figure 5-13: **Behaviour of the system with rate-efficiency trade-off and no sucrose uptake.**
(5-13a): Bifurcation diagram showing the population density at steady states. The stable steady states are denoted by solid lines, while the unstable steady states are denoted by dashed lines. The trivial steady states (extinction of the population) are plotted in grey, while the nontrivial steady states (survival of the population) are plotted in brown and pink. At the same dilution rate D, depending on the initial conditions, three different stable steady states may be observed. The branch point, at which a new branch of equilibria appears is denoted by 'BP', and the limit points, at which the stable and unstable survival branches meet and annihilate are denoted by 'LP'.
(5-13b): Zoom into the bottom part of Fig. 5-13a, denoted by a dashed box.

Chapter 6

Cooperation in larger microbial communities

Abstract

In nature, microbes live in large microbial communities, often composed of organisms representing a number of different strains and species. Yet, so far in this thesis we have only studied the system of public good producers and non-producers in isolation. Here we consider a larger community, composed of strains representing three different feeding strategies: external metabolism involving the secretion of public goods, internal metabolism which allows for keeping the goods private, and cheating which relies on the public goods secreted by other organisms. Given that external metabolism is very frequent in nature, we set out to study its competitiveness compared to the internal metabolism. Moreover we find how that competitiveness depends on the environmental factors such as population density or resource concentration. Next, we study how an introduction of another strain (cheat) affects the relation between external and internal metabolisers. We manage to recover and explain the recent empirical finding, which suggests that the presence of cheats may help to maintain diversity in a larger microbial community. We also extrapolate that result by studying the three strain community dynamics in a number of different scenarios.

6.1 Introduction

Earlier chapters of this thesis studied microbial public good cooperation, focusing on isolated systems of cooperators and cheats. However, in the wild, microorganisms live in diverse communities, where interactions between different populations and species may affect species distributions [143–146], and the genetic divergence [144, 146], as noted in [147]. The interspecific interactions are also known to affect the dynamics of microbial public goods systems, in which an introduction of a new competitor, significantly alters the existing social interactions [147–149]. Interestingly, the previous studies lead to contrasting conclusions: an introduction of a new competitor into a cooperative system of public goods can either stabilise [147, 149] or destabilise the cooperative communities [147, 148], depending on the studied species.

One of these studies [148] focused on a well known public good system of *Pseudomona aeruginosa*, composed of 'cooperators', who produce an iron binding agent, siderophore, and 'cheats', who benefit from that public good, without contributing to its production. An introduction of another pathogen, *Staphylococcus aureus*, to that system increased the selection for cheats, and thus destabilised their coexistence with cooperators [148].

On the other hand, the introduction of another pathogen to the same cooperative system: a strain of *Psuedomona aeruginosa*, which produces and uses a different kind of siderophore, increased the chances of cooperators to survive, and eventually led to the maintenance of biodiversity in the population [149]. Similarly the introduction of bacteria *Escherichia coli* to the cooperative system of *Saccharomyces cerevisiae* has been reported to sustain the biological diversity [147].

What are the factors that can lead to such disparate results, which point either to stabilisation or destabilisation of cooperative systems? Could both scenarios be observed depending only on environmental factors such as resource concentration?

Although both studies [147, 149] show that a new competitor can have an effect on the existing public good system, that effect is only temporary. Can a new competitor also affect the long-term dynamics of the cooperative systems? A recent experimental study [36] reported that the introduction of a new competitor

into a system of *S. cerevisiae* can result in a long-term coexistence. Motivated by this result, here we build a mathematical model describing the possible dynamics of the recent experimental system [36].

Similarly as was done in [36], we study three strains of *S. cerevisiae*: **'external metaboliser'**, **'internal metaboliser'** and a **'cheat'**, schematically presented in Fig. 6-1. The 'external metaboliser' is the wild type invertase producer, described in the previous chapters. It secretes an enzyme, invertase, which extracellularly breaks down sucrose into simpler sugars (hexose), namely glucose and fructose. This step of digestion is performed outside the cell wall, allowing the neighbouring individuals to benefit from the broken down molecules. The 'cheat', is the $\Delta suc2$ invertase mutant, described in the previous chapters. It fails to produce invertase, but reaps the simple sugars provided in the environment by the external metabolisers. The 'internal metaboliser' is the strain genetically engineered in previous studies [142, 150] and used in [36]. It privatises its invertase, by keeping it in the cytoplasm, and not allowing other cells to benefit from it. Moreover, it is supplied with a high-affinity and high-capacity sucrose transporter $SRT1$, found also in a plant pathogen *Ustilago maydis*. Thus, it can uptake sucrose before breaking it down to simple sugars inside the cell. The internal metaboliser has intact hexose transporters - identical to those in the external metaboliser and in the cheat strains. Therefore, apart from uptaking sucrose and metabolising it internally, it can also uptake the hexoses available in the environment.

Following the study presented in [36], we first ask whether secreting public goods (as done by the external metabolisers) may be advantageous compared to the strategy of keeping the goods private (as done by internal metabolisers). Although secreting public goods is prone to invasion by potential cheats, who use the public goods without contributing to its production [32, 61–64], this strategy is often deployed within fungi and microbes [70, 92], where organisms secrete costly extracellular enzymes which hydrolise the complex molecules of resources available in the environment. Why is this external digestion so abundant in nature, in spite of bringing the risk of invasion by cheats? The current literature points out several advantages of external digestion, such as greater control over substances entering the cell (and therefore lower risk of infection) and a bigger chance to match the enzyme production to particular needs (see [70] for a broader review). Can the competitiveness of external metabolism also depend on the en-

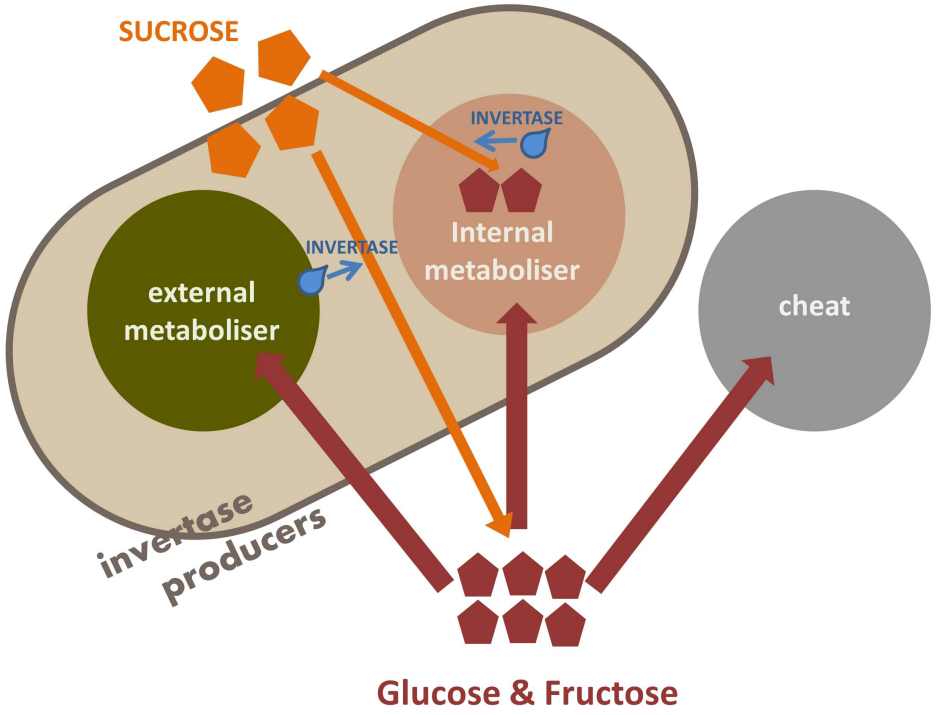

Figure 6-1: **A schematic representation of the three strains of *S. cerevisiae* we consider.**
The external and internal metabolisers produce an enzyme, invertase, which breaks down molecules of sucrose into simple sugars, namely glucose and fructose. The invertase produced and secreted by external metabolisers acts extracellularly, and therefore it may benefit the other organisms in the environment: the 'internal metabolisers' and the 'cheats' who do not produce any invertase. On the contrary, the invertase produced by the internal metabolisers is 'privatised' and it can only hydrolyse the sucrose inside the internal metaboliser cells.

vironmental factors such as resource concentration or population density?

To find when the external metabolisers have an advantage over internal metabolisers, we first consider the system composed only of these two strains. We recover and explain the recent empirical finding that the dynamics between external an internal metabolisers differs significantly depending if the strains compete at low or high initial sucrose concentration [36]. Then we test if an introduction of cheats can stabilise the biodiversity in the population of external and internal metabolisers as shown empirically in [36]. We examine the dynamics of such three strain microbial community in a number of different scenarios, and we aim to understand how that dynamics differ depending on the sucrose concentration, and population density.

6.2 Mathematical model

Following the empirical study in [36], we consider a system composed of three strains, namely: two types of invertase producers (the 'external metabolisers', and the 'internal metabolisers') and the invertase non-producer, termed 'cheat'. Our model is based on the model proposed in [14] and it tracks in time the concentrations of sucrose (S), hexose (H) and the densities external metabolisers (N_E), internal metabolisers (N_I), and cheats (N_C).

Here we briefly describe the basic assumptions of our model with more detailed description presented in Chapter 2: Methods.

In our model all the strains take up resources R and use them to generate ATP using a simple, unbranched pathway [37]. We represent microbial growth as a linear function of the rate of ATP production, as described in more detail in Chapter 2: Methods.

The external metabolisers secrete invertase, an enzyme which catalyses the extracellular hydrolysis of each molecule of sucrose into two molecules of monosaccharides, i.e. hexose (H). The rate of conversion of sucrose into hexose is represented by Inv, a saturating function of sucrose concentration.

The cost of invertase secretion is denoted by a constant c_E, estimated empirically in [14]. Moreover, in [14] the fitness of external metabolisers was calculated as the ratio of population doublings during competition on glucose with cheats, and it was found that external metabolisers suffer a fitness disadvantage. To reflect this in our model, we multiply the fitness of external metabolisers by $(1-c_E)$ as was done in [14, 33]. Following the postulation in [14], we assume the activity of the secreted invertase is immediate and it does not accumulate in time. It also does not diffuse, since it is known to stay near the cell membrane [151]. The internal metabolisers also produce invertase in order to hydrolyse sucrose. Although the invertase produced by internal metabolisers is a private good, not accessible for any other cells, we assume its production incurs some energetic cost c_I. Since the invertase produced by the internal metabolisers is kept inside the cytoplasm and not transported outside the cell membrane, we assume its production cost c_I is lower than the cost c_E which external metabolisers need to pay

for invertase production and transport to the periplasm.

Hexoses are transported into the cell by hexose transporters and the rate of the hexose pathway is denoted by J^H, where the efficiency of this pathway is denoted by a constant η_e^{Hxt}. In our model there is no hexose provided externally to the system (the initial hexose concentration is zero). Therefore, the only 'source' of hexose in the culture are the external metabolisers, which hydrolyse the sucrose available in the environment. Because the molecules of sucrose are hydrolysed in the close proximity of external metaboliser cells, these cells are assumed to have preferential access to the hexose they provide. This is because, even in a well mixed environment, the molecules of hexose will form a high local concentration around the external metaboliser cells before they diffuse away to other organisms in the culture [33]. In previous chapters this phenomenon was captured by considering the physical space, and explicit modelling of the diffusion. In this chapter we represent this phenomenon by assuming that the Michaelis-Menten constants of the hexose uptake K_m^H are different for external metabolisers and the other strains (K_{Em}^H and K_{Im}^H respectively). We set $K_{Em}^H < K_{Im}^H$, which effectively means the external metabolisers have a higher hexose uptake rate than the internal metabolisers (Supplementary Fig. 6-9a). Thus, in terms of uptaking hexose from the environment, the external metabolisers have an advantage over internal metabolisers, especially at low hexose concentrations, at which the hexose uptake rate J_E^H of external metabolisers is significantly higher than the hexose uptake rate of internal metabolisers J_I^H (Supplementary Fig. 6-9b). At the same time, we assume that the cheat has the same access to the publicly available hexose and the same uptake rate as the internal metaboliser, that is $J_I^H = J_C^H$.
For simplicity, we assume that neither external metabolisers nor the cheats can uptake sucrose directly. On the contrary, the internal metabolisers can use their novel sucrose transporter $SRT1$ to take up sucrose, before they metabolise it internally into simpler sugars and eventually into molecules of ATP. The rate of that sucrose pathway is defined by:

$$J^S = \frac{V_{max}^S S}{K_m^S + S},$$

where V_{max}^S denotes the maximal rate of the pathway while K_m^S denotes the respective Michaelis-Menten constant. The efficiency of that pathway is denoted by

a constant η_e^S. Motivated by the properties of the introduced sucrose transporter ($SRT1$) [150], we assume that $V_{max}^S << V_{max}^H$ and $K_m^S << K_{Em}^H$, and we set these parameters to the constants estimated in [150]. The parametrisation of all of the above terms can be found in Supplementary Table 6.1.

6.2.1 The system dynamics

We consider the assumptions on the microbial growth, described in the previous subsection, and we finally assume that the environment is well mixed and that the studied concentrations S, H, N_E, N_I, N_C do not depend on spatial location. Thus we arrive at the following Ordinary Differential Equation (ODE) model:

$$\frac{dS}{dt} = -InvN_E - J^S N_I \tag{6.2.1}$$

$$\frac{dH}{dt} = (2Inv - J_E^H)N_E - J_I^H N_I - J_C^H N_C \tag{6.2.2}$$

$$\frac{dN_E}{dt} = (1 - c_E)\eta_e^{Hxt} J_E^H N_E \tag{6.2.3}$$

$$\frac{dN_I}{dt} = (1 - c_I)(\eta_e^S J^S + \eta_e^{Hxt} J_I^H)N_I \tag{6.2.4}$$

$$\frac{dN_C}{dt} = \eta_e^{Hxt} J_C^H N_C, \tag{6.2.5}$$

together with the following initial conditions $S(0) = S_0$, $H(0) = 0$, $N_E(0) = N_{E0}$, $N_I(0) = N_{I0}$, $N_C(0) = N_{C0}$, where the total initial density N_0 is defined as $N_0 = N_{E0} + N_{I0} + N_{C0}$.

The model (6.2.1)-(6.2.5) describes the co-growth of the three considered strains, in a homogeneous environment initially supplemented with a given sucrose concentration S_0.

In our simulations, we set some initial conditions $S(0) = S_0, H(0) = 0$, and initial frequencies of external and internal metabolisers and cheats: f_E, f_I, f_C respectively, such that $N_{E0} = f_E N_0$, $N_{I0} = f_I N_0$, $N_{C0} = f_C N_0$ and $f_E + f_I + f_C = 1$. According to the model (6.2.1)-(6.2.5), we simulate the growth of all of the three strains in the common environment for time T (a 'season'), and we calculate the final frequencies of the studied phenotypes $f_{Eend}, f_{Iend}, f_{Cend}$ in the end of each season. Next, we initiate the next season with the following initial conditions $S(0) = S_0, H(0) = 0$, $N_E(0) = f_{Eend} N_0$, $N_I(0) = f_{Iend} N_0$, $N_C(0) = f_{Cend} N_0$. We repeat this procedure for a number of times, until the frequencies of the studied phenotypes stabilise, and

we study how the frequencies $f_{Eend}, f_{Iend}, f_{Cend}$ change over the seasons. By performing that procedure we aim to represent the experimental setup of the 'serial transfer', used in the empirical study [36], and described in more detail in the subsection 2.2.3 in Chapter 2: Methods.

6.3 Results: competition between external and internal metabolisers

Firstly, similarly as in [36], we study the competitiveness of external metabolism, by considering the competition between external and internal metabolisers in various ecological conditions such us resource concentration and population density.

6.3.1 Destabilisation through resource depletion

According to the model (6.2.1)-(6.2.5), we simulate one season of competition between two types of invertase producers, i.e.: the external and internal metabolisers, at low and high sucrose concentrations, and in the absence of cheats ($f_C = 0$). Subsequently, we calculate the relative fitness of external metabolisers to the internal metabolisers $W(f)$ for various initial frequencies of external metabolisers ($f_E = f$). As described in Chapter 2: Methods, the relative fitness measure allows to examine the outcome of a long-term competition between two strains. In particular, if for certain initial frequency of external metabolisers f, $W(f) > 1$, then that frequency will increase over a season, if $W(f) < 1$, then that frequency will decrease over a season, and if for some f^* we have $W(f^*) = 1$, then the two strains can coexist, at the frequency f^* of external metabolisers. Additionally, if $W(f)$ is locally decreasing around f^*, then the coexistence is stable. Otherwise, if $W(f)$ is locally increasing around f^*, then the coexistence is unstable.

Our results show qualitatively different system dynamics depending on the initial sucrose concentration S_0. When initial sucrose concentration is high, the relative fitness of external metabolisers may be negative frequency dependent in some frequency range (Fig. 6-2a), allowing for stable coexistence between external and internal metabolisers. Otherwise, when the initial sucrose concentration is low, the relative fitness of external metabolisers is positive frequency dependent (Fig. 6-2b), leading to extinction of either of the strains (bistability). Such a swap

from negative to positive frequency dependence in the external metabolisers relative fitness has been also reported in the experimental study on the interaction between internal and external metabolisers [36], and we include their results in Supplementary Fig. 6-10.

According to our study, at high initial sucrose concentration, the system has both: an unstable and a stable coexistence states (Fig. 6-2a), at the external metabolisers frequencies f^* and f^{**} respectively. It means that if the system is started with a very small external metaboliser frequency $f < f^*$ at which $W(f) < 1$, it will lead to fixation of the internal metabolisers (such a trajectory over a number of seasons is shown in Supplementary Fig. 6-11a). Otherwise, if $f > f^*$ the community will converge to a fixed coexistence of two types at the stable equilibrium frequency of external metabolisers f^{**} (Supplementary Fig. 6-11b).

On the contrary, at low initial sucrose concentration, the relative fitness is positively frequency dependent, and there is an unstable equilibrium frequency of external metabolisers f^*, at which external and internal metabolisers could potentially coexist (Fig. 6-2b). However, if the system is initiated at any other frequency of external metabolisers $f \neq f^*$ it will converge to a fixation of one type only. If the initial frequency of external metabolisers $f < f^*$, then the external metabolisers will go extinct and the system will converge to a fixation of internal metabolisers (Supplementary Fig. 6-11c). Otherwise, if $f > f^*$, then the system will converge to a fixation of external metabolisers (Supplementary Fig. 6-11d).

Interestingly the relative fitness of external metabolisers shown in Fig. 6-2 is nonlinear. This is because of the phenomenon known as the 'Allee Effect' [100], according to which populations grow quicker when their densities are higher. The known ecological mechanisms, which drive the Allee Effect include, amongst others: mate limitation, cooperative defense or cooperative feeding. Since our external metabolisers do feed cooperatively, they grow quicker when their population density is higher, which has been confirmed empirically in [36]. This effect is especially pronounced when the external metabolisers densities are very low, corresponding to their low frequencies in Fig. 6-2. In that case the speed of sucrose hydrolysis, and therefore the growth speed of external metabolisers increases quickly with their increasing density (Supplementary Fig. 6-12). Since an increase in external metabolisers frequency effectively means an increase in their density within the population, which in turn results in an increased growth

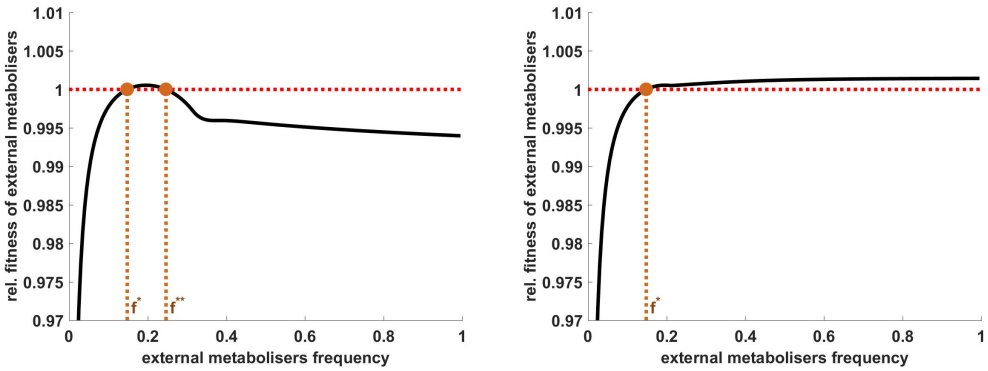

Figure 6-2: **Relative fitness of external metabolisers to internal metabolisers at high and low initial sucrose concentration.**
The relative fitness of external metabolisers, depending on their initial frequency calculated at
(6-2a): high initial sucrose concentration;
(6-2b): low initial sucrose concentration.
The stable coexistence frequencies are denoted by f^{**}, while the unstable coexistence frequencies are denoted by f^{*}. Fig. 6-2a shows that if the system is started with a very low frequency of external metabolisers ($f < f^{*} \approx 0.15$), they will go extinct ($f = 0$). Otherwise, the system will converge to a stable coexistence of the two types at the external metaboliser frequency $f = f^{**} \approx 0.25$.
Fig. 6-2b, shows that if the system is started with a very low frequency of external metabolisers ($f < f^{*} \approx 0.15$), they will go extinct ($f = 0$). Otherwise, they will outcompete the internal metabolisers ($f = 1$). This phenomenon is termed bistability, whereas two different steady states may be observed depending on the initial state of the system.

speed, the relative fitness of external metabolisers increases sharply at low frequencies in Fig. 6-2. That process, however, slows down at higher densities of external metabolisers (Supplementary Fig. 6-12), corresponding to their higher frequencies in Fig. 6-2. When the external metabolisers are sufficiently dense to reach the growth rate comparable to the growth rate of the internal metabolisers, they do not face the Allee Effect and the relative fitness of external metabolisers saturates around a constant value ≈ 1 as shown in Fig. 6-2b, or starts decreasing if the amount of hexose produced by external metabolisers is high enough to allow the internal metabolisers to benefit from it (Fig 6-2a).

6.3.2 Explanation of the change in stability depending on the resource concentration

The internal and external metabolisers can stably coexist when the resource concentration in the environment is sufficiently high, and this coexistence becomes unstable when the resource concentration is decreased. In order to understand this puzzling result, also observed in the experimental data obtained in [36], we study two toy models, in which we consider the competition of external metabolisers with the following strains:
(i) **'cheat'**, described in the section 6.2, which can uptake hexose available in the environment, but is not able to uptake sucrose ($J^S = 0, c_I = 0$)
(ii) **'perfect internal metaboliser'**, which is able to uptake and hydrolyse sucrose, but is not able to uptake hexose ($J_I^H = 0$).

The internal metaboliser described by the main model (6.2.1)-(6.2.5) can uptake both hexose and sucrose at the same time ($J_I^H > 0, J^S > 0$). Here we study how the composition of these two traits shapes the behaviour of internal metabolisers in competition with external metabolisers.

When the external metabolisers compete with the cheats (i), the system reproduces the classical system of public good producers (i.e.external metabolisers) and non-producers (i.e. cheats) who benefit from the public good but do not pay any cost for its production. Then the relative fitness of external metabolisers to cheats is negative frequency dependent (Fig. 6-3a), which can be understood as follows: a little amount of cheats can use up the resources and have a quicker growth than the external metabolisers, without affecting much the environment.

However, if the fraction of cheats is higher, there will be relatively less public goods they can exploit, and therefore their relative fitness to external metabolisers is smaller, than if they were only a small fraction of the population. If we additionally assume that the external metabolisers have preferential access to the resources they produce [33], then the relative fitness curve may cross one, which suggests a possible stable coexistence between the types (Fig. 6-3a). This is the classical scenario in a public good system described in Chapter 4, and in a number of previous studies [14, 36, 62, 64].

On the contrary, when the external metabolisers compete with the perfect internal metabolisers (ii), their relative fitness is positive frequency dependent, as illustrated in Fig. 6-3b, which means the coexistence between the two strains is unstable. This is due to the Allee Effect, described in the subsection 6.3.1. Large populations of external metabolisers secrete more invertase, which results in a quicker decomposition of sucrose into simple sugars, and a higher concentration of hexose in the environment. Thus increasing the frequency of external metabolisers gives them increasing advantage over their competitor, who is not able to take advantage of the hexose available in the environment.

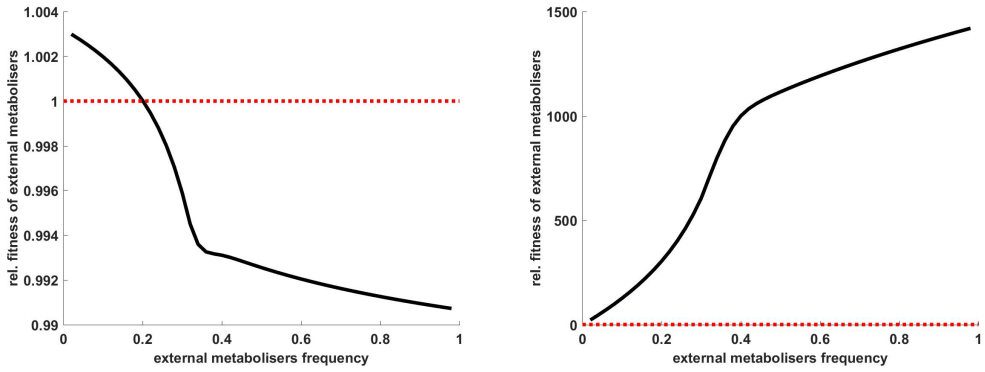

(a) *(b)*

Figure 6-3: **Relative fitness of external metabolisers to cheats/perfect internal metabolisers.**
The relative fitness of external metabolisers, depending on their initial frequency within the population, calculated at high initial sucrose concentration.
(6-3a): The competitor is the cheat, which can uptake hexose, but is not able to uptake sucrose: $J^S = 0$, $c_I = 0$;
(6-3b): The competitor is the perfect internal metaboliser, which can uptake sucrose, but is not able to uptake hexose: $J_I^H = 0$.

The internal metaboliser we describe in the main model (6.2.1)-(6.2.5) can directly uptake both resources, and thus it combines the traits of cheats and perfect internal metabolisers. In cultures abundant in hexose, the internal metabolisers

behave as cheats. This is because their maximal sucrose uptake rate V^S_{max} is very low, and therefore it does not play a major role in abundance of hexose. On the contrary, in cultures with high sucrose and low hexose concentrations, the internal metabolisers behave as perfect internal metabolisers. This is because at low hexose concentrations the sucrose uptake will be significant in comparison to the hexose uptake (see Supplementary Fig. 6-13), due to the low sucrose uptake affinity K^S_m.

Therefore, depending on the resource available in the environment, the relationship between the internal and external metabolisers may be described by the system of either external metabolisers and cheats (Fig. 6-3a), external metabolisers and perfect internal metabolisers (Fig. 6-3b), or a combination of both resulting in a possible non-monotonous relative fitness of external metabolisers (as in Fig. 6-2a). In particular, when the initial sucrose concentration is high, the external metabolisers will break it down into a large amount of hexose which will appear in the environment, and the system defaults to the dynamics of external metaboliser and cheat described in Fig. 6-3a. In such a scenario, the relative fitness of external metabolisers to internal metabolisers may be negative frequency dependent, allowing for a stable coexistence between both strains (as shown in Fig. 6-2a). On the other hand, when the initial resource concentration is sufficiently low, there will be little hexose in the environment, and the system will default to the external metaboliser and the perfect internal metaboliser dynamics described in Fig. 6-3b. In that case the relative fitness of external metabolisers to internal metabolisers is positive frequency dependent, leading to unstable coexistence between both strains (as shown in Fig. 6-2b).

6.3.3 The interplay between resource concentration and population density

The changes in the relative fitness of external metabolisers to internal metabolisers can be forced by decreasing the concentration of resources . However, they can be also controlled by a decrease in the overall population density. When the initial sucrose concentration is high, a drop in the population density destabilises the coexistence between external and internal metabolisers (Fig. 6-4), similarly to a drop in the sucrose concentration (Fig. 6-2).

The parallel between the resource concentration and population density is illustrated in Supplementary Fig. 6-14. A change in the population density results in a different environment in which the strains compete. At low density, there is little external metabolisers who could hydrolyse sucrose into the molecules of hexose. This hydrolysis happens very slowly, and thus, for the duration of the growth (a season), there is almost no hexose to compete for (Supplementary Fig. 6-14c). In that case, the strains compete only for sucrose and they behave as the toy system of external metabolisers and perfect internal metabolisers, described in Fig. 6-3b. The bigger the initial density of the population, the higher the amount of hexose available in the environment (Supplementary Fig. 6-14e) and the systems behaviour shifts towards the dynamics of the toy system of external metaboliser and cheat, described in Fig. 6-3a.

On the other hand, the higher the initial sucrose concentration, the quicker the population growth, and the bigger the effective size of the competing population. This means that, by varying initial resource concentration, one varies also the population density and the type of competition between external and internal metaboliser.

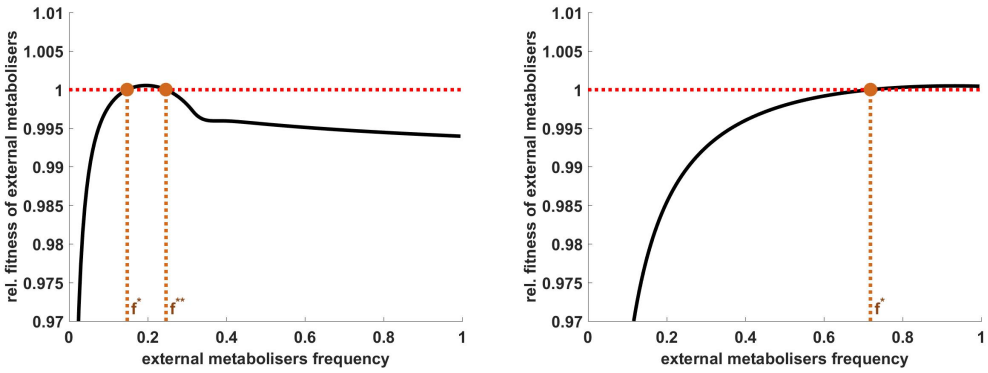

Figure 6-4: **Relative fitness of external metabolisers to internal metabolisers at high initial sucrose concentration and at high and low population densities.**
The relative fitness of external metabolisers to internal metabolisers, depending on their initial frequency, calculated at (6-4a): high initial population density $N_0 = 0.005$ [g/L], (6-4b): low initial population density $N_0 = 0.001$ [g/L].
The stable coexistence frequencies are denoted by f^{**}, while the unstable coexistence frequencies are denoted by f^{*}.

6.4 Results: Introduction of a cheat within the invertase producers

In this section we verify how an introduction of a new competitor (cheat) affects the studied pairwise competition between the internal and external metabolisers. In order to follow that pairwise interaction in a larger microbial community, we define the frequencies of external and internal metabolisers 'within invertase producers' as: $f_{Eend}/(f_{Eend} + f_{Iend})$ and $f_{Iend}/(f_{Eend} + f_{Iend})$, respectively.

We simulate the competition between external and internal metabolisers, in absence and in presence of cheats, as described by the model (6.2.1)-(6.2.5). After one season of such competition we record the final densities of both strains and we calculate the relative fitness of the external metabolisers to the internal metabolisers.

6.4.1 Competition at high initial sucrose concentration

In nature, different species and strains compete for common resources, and thus an appearance of a new competitor may result in depletion of resources available to the others. If a change in the resource concentration can shift the dynamics between external and internal metabolisers from stable coexistence (as shown in Fig. 6-2a), to bistability between the two types (as shown in Fig. 6-2b), could the introduction of a new competitor which depletes resources from the environment, lead to the same shift?

To answer that question we calculate the relative fitness of external metabolisers to internal metabolisers, in absence and in presence of cheats. The results indicate, that while in the absence of cheats, the external and internal metabolisers can stably coexist (Fig. 6-5a), an introduction of cheats may destabilise that coexistence (Fig 6-5b). Thus the outcome of the competition between external and internal metabolisers initiated at high initial sucrose concentration and in the presence of cheats (Fig. 6-5b) is qualitatively the same as the outcome of that competition initiated at low initial sucrose concentration and in the absence of cheats (Fig. 6-2b). The same phenomenon can be observed if the new competi-

tor instead of uptaking hexose, uptakes sucrose (Supplementary Fig. 6-15). Also in that case, the presence of a new competitor destabilises the coexistence of the two types of invertase producers, by leading to a positive frequency dependent relative fitness of external metabolisers to internal metabolisers.

Thus presence of new competitors results in lower resource concentration in the culture, which makes the coexistence between internal and external metabolisers switch from being stable (Fig. 6-2a and Fig. 6-5a) to being unstable (Fig. 6-2b and Fig. 6-5b) .

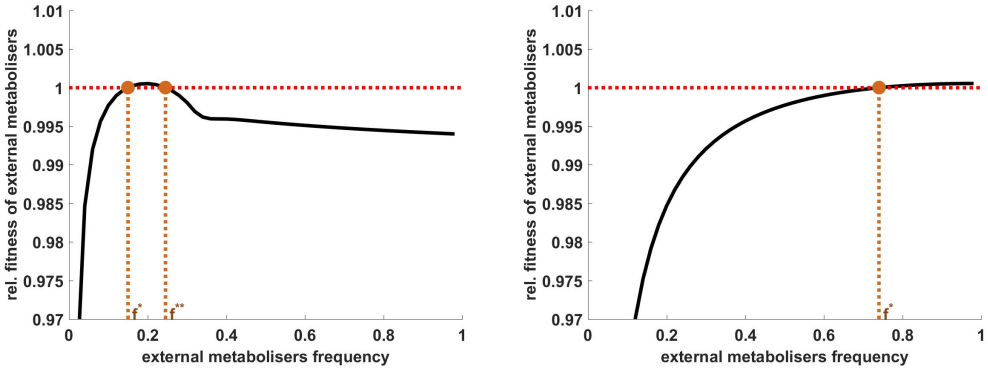

Figure 6-5: **Relative fitness of external metabolisers to internal metabolisers at high initial sucrose concentration and in the absence and presence of cheats.**
The relative fitness of external metabolisers, depending on their initial frequency within the invertase producers , calculated at high initial sucrose concentration and
(6-5a) in the absence of cheats, (6-5b) in the presence of cheats.
The initial frequency of introduced cheat is $f_C = 0.8$.
The stable coexistence frequencies are denoted by f^{**}, while the unstable coexistence frequencies are denoted by f^{*}.

6.4.2 Competition at low initial sucrose concentration

We calculate the relative fitness of external metabolisers to internal metabolisers at low initial sucrose concentration, and in absence and presence of cheats. The obtained results indicate there is no stable coexistence between the two strains, regardless of the presence of cheats (Fig. 6-6a-6-6c). This means that in the long term, regardless of the presence of cheats, either external or internal metabolisers will go extinct, depending on their initial frequencies. In the absence of cheats, the external metabolisers are expected to increase their frequency, if the culture is started with external metaboliser frequency $f > f^* \approx 0.15$ (that is when W(f)>1 as shown in Fig. 6-6a). However, in the presence of cheats, the external metabolisers frequency within invertase producers can increase, only if their starting frequency within the invertase producers population is $f > f^* \approx 0.35$ (Fig. 6-6b). On the contrary, if $f < f^* \approx 0.35$, the internal metabolisers will increase in frequency . In conclusion, the presence of cheats increases the value of the unstable coexistence frequency of external metabolisers f^*, at the same time giving an advantage to the internal metabolisers.

Moreover, the higher the frequency f_C of cheats in the population, the smaller the relative fitness of external metabolisers to internal metabolisers (Fig. 6-6c), and the higher is the minimal frequency f^* of external metabolisers within invertase producers, such that: $W(f^*) > 1$ (Fig. 6-6d).

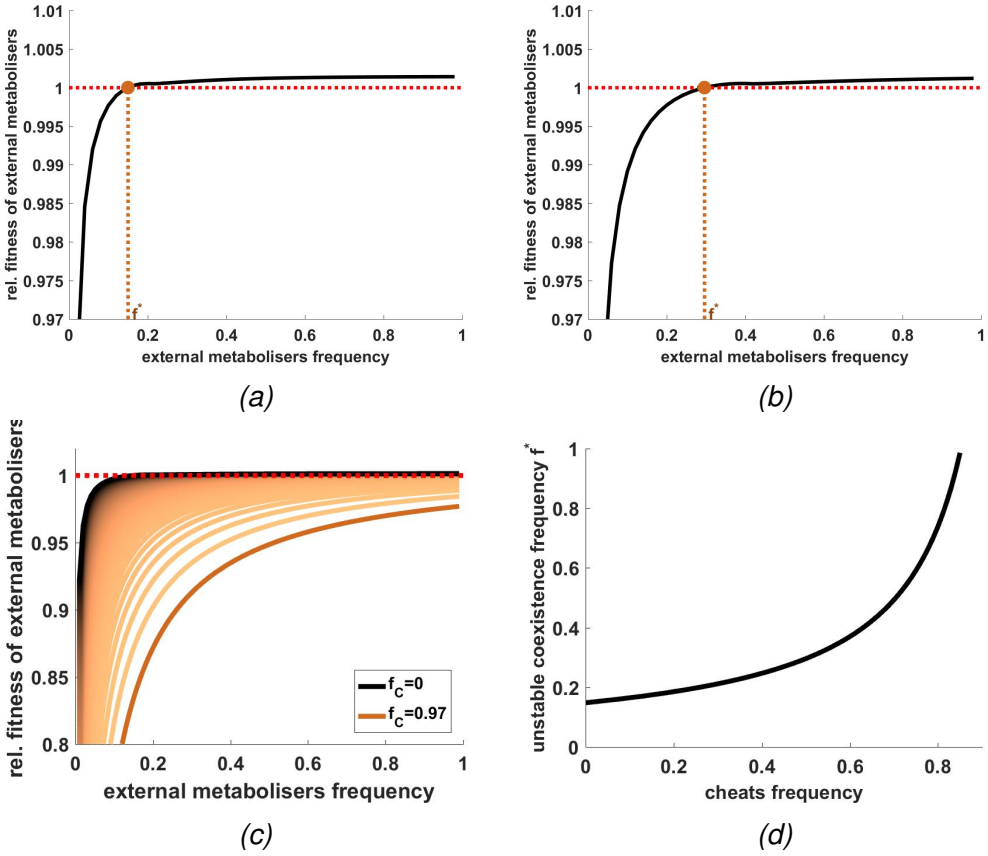

Figure 6-6: **Relative fitness of external metabolisers to internal metabolisers at low initial sucrose concentration and in the absence and presence of cheats.**
(6-6a)-(6-6b): The relative fitness of external metabolisers, depending on their initial frequency within invertase producers, calculated at low initial sucrose concentration and in (6-6a): absence of cheats ($f_C = 0$), and (6-6b): presence of cheats ($f_C = 0.5$).
The entire spectrum of results for various values of f_C is presented in Fig. 6-6c & Fig. 6-6d
(6-6c): The relative fitness of external metabolisers, for various initial frequencies f_C of cheats in the population.
(6-6d): The unstable coexistence equilibrium frequency of external metabolisers f^* (the minimum frequency of external metabolisers within invertase producers, that allows them to overtake the population of invertase producers in the long term), depending on the initial frequency of cheat f_C in the entire population.
In Fig. 6-6a and Fig. 6-6b, the unstable coexistence frequencies are denoted by f^*.

6.5 Results: competition in the three strain community

Finally, we focus on the dynamics of the whole three strains community, and we study the frequencies $f_{Eend}, f_{Iend}, f_{Cend}$ of each of the three strains. By performing the serial transfer procedure described in the section 6.2, we calculate the frequencies of external metabolisers (f_{Eend}), internal metabolisers (f_{Iend}), and cheats (f_{Cend}) in the population, over a number of seasons. We will first follow the frequencies of external and internal metabolisers within the invertase producers: $f_{Eend}/(f_{Eend} + f_{Iend}), f_{Iend}/(f_{Eend} + f_{Iend})$, and then the frequencies of all of the three strains: $f_{Eend}, f_{Iend}, f_{Cend}$

6.5.1 Competition at high initial sucrose conentration

When the initial sucrose concentration S_0 is high, the internal and external metabolisers can coexist in the absence of cheats (Fig. 6-7a), as predicted by the relative fitness in Fig. 6-2a. However, the introduction of cheats may destabilise the interaction between these two strains. Namely the population of invertase producers becomes dominated either by the external metaboliser (Fig. 6-7b) when the initial frequency of introduced cheat f_C is sufficiently low, or by the internal metaboliser (Fig. 6-7c), when the initial frequency of introduced cheat f_C is sufficiently high. Thus, two different equilibria states can be observed depending on the initial fraction of the newly introduced cheat. This result is in accordance with the result from the previous section, which predicted that an introduction of cheat would deplete the available resources and thus destabilise the interaction between the external and the internal metaboliser (Fig. 6-5).

What are the equilibria when we look at the whole three strain system? When the initial frequency of introduced cheats f_C is sufficiently low, the cheats outcompete the internal metabolisers, and in the end they coexist with the external metabolisers (Fig. 6-7d). Otherwise, when the initial frequency of introduced cheats f_C is sufficiently high, the cheats abuse the external metabolisers driving them to extinction (Fig. 6-7e). This scenario can be refereed to as 'the tragedy

of the commons' [65, 66], according to which, individuals driven by their own selfish interest, decrease the fitness of the whole group and potentially lead to its extinction. In our case cheats use the hexose provided by external metabolisers, thus decreasing the hexose concentration in the environment. This leads to a decrease in the fitness of both strains. After the external metabolisers vanish from the population, the cheats, do not have any more resources to grow on, and they also go extinct. In that scenario, the only strain that remains in the culture, is the internal metaboliser independent of hexose.

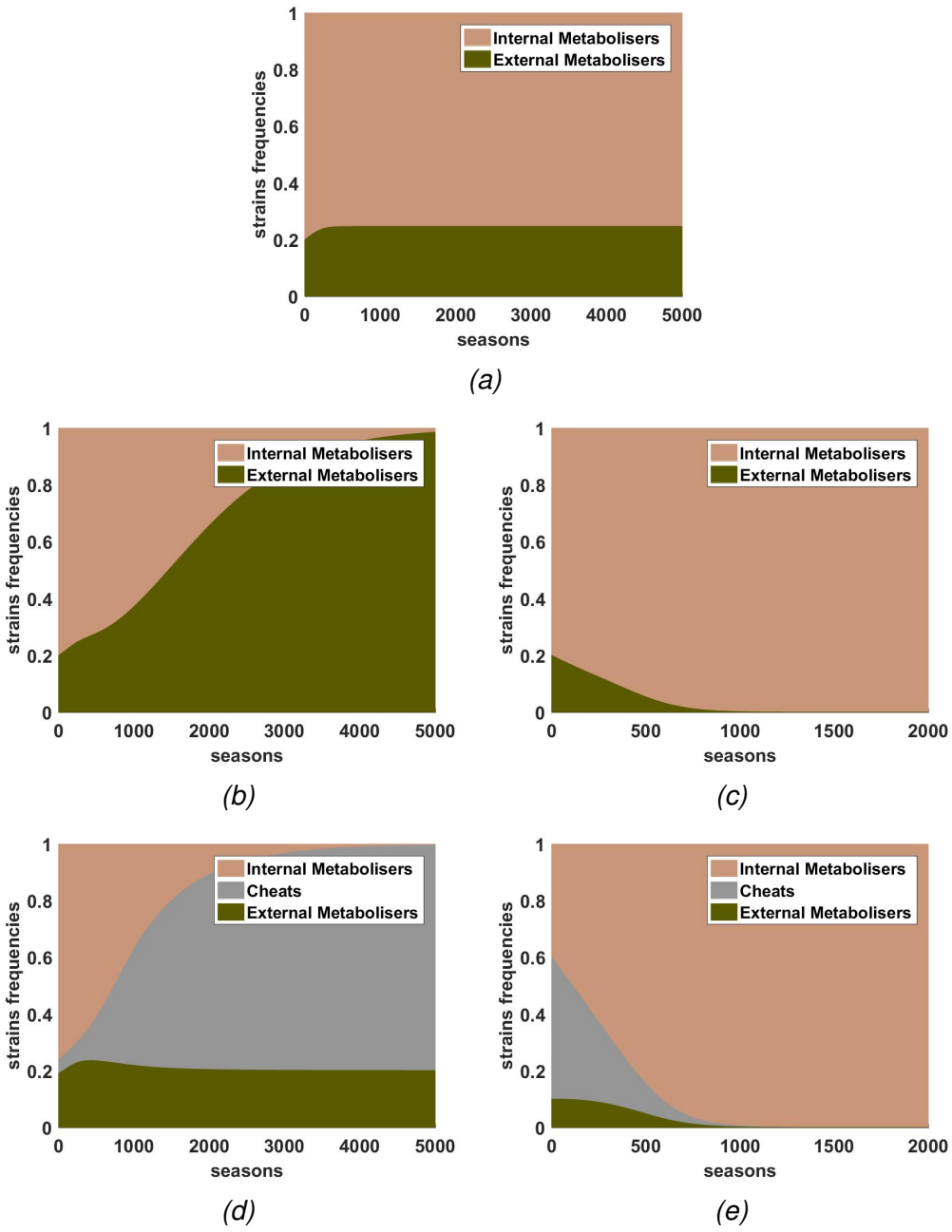

Figure 6-7: **Competition at high initial sucrose concentration. Changes in frequencies of the strains in the absence and presence of cheats.**
(6-7a): Strains frequencies in the absence of cheats. The initial frequency of the external metabolisers is 0.2.
(6-7b-6-7c): Strains frequencies within the invertase producers, in the presence of cheats. The initial frequency of the external metabolisers within the invertase producers is 0.2. The initial frequency of cheats is (6-7b): $f_C = 0.05$, (6-7c): $f_C = 0.5$.
(6-7d)-(6-7e): Strains frequencies within the entire population, in the presence of cheats. The initial frequency of cheats is (6-7b): $f_C = 0.05$, (6-7c): $f_C = 0.5$. The initial frequency of the external metabolisers within the invertase producers is 0.2.

6.5.2 Competition at low initial sucrose concentration

At low initial sucrose concentration, the system composed of internal and external metabolisers in the absence of cheats , does not allow for stable coexistence, and it tends to favour the external metabolisers leading to their fixation in the environment (Fig. 6-8a & Fig. 6-8b), if their initial frequency in the population is sufficiently high. Otherwise, when the initial frequency of external metabolisers is very low, they may go extinct, outcompeted by the internal metabolisers (Supplementary Fig. 6-11c). This agrees with our predictions based on the relative fitness of external metabolisers to internal metabolisers at low initial sucrose concentration (Fig. 6-2b and Fig. 6-6a). The coexistence is unstable, meaning that if the culture is initiated at low initial external metabolisers frequency $f < f^* \approx 0.15$, they will go extinct, otherwise if $f > f^* \approx 0.15$, they will outcompete the internal metabolisers.

Interestingly, whereas at high initial sucrose concentration, the introduction of cheats led to destabilisation of the system of internal and external metabolisers, at low initial sucrose concentration they may temporarily stabilise it by increasing their own frequency, and thus prolonging the period of coexistence of the internal and external metabolisers (Fig. 6-8c opposed to Fig. 6-8a). Otherwise, the cheats may also give privilege to internal metabolisers: the strain that loses the competition in the absence of cheats (Fig. 6-8d opposed to Fig. 6-8b), Thus even if the cheat eventually vanishes from the population (Fig. 6-8f), its introduction to the population of invertase producers may permanently affect the relationship between the other strains (Fig. 6-8d opposed to Fig. 6-8b).

In summary, although the system of invertase producers exhibits significantly different dynamics at low and high initial sucrose concentrations, an introduction of the new competitor (cheat) in both cases leads to the same possible scenarios: either to the stable coexistence of external metabolisers and cheats (Fig. 6-7d & Fig. 6-8e), or to the fixation of internal metabolisers (Fig. 6-7e & Fig. 6-8f).

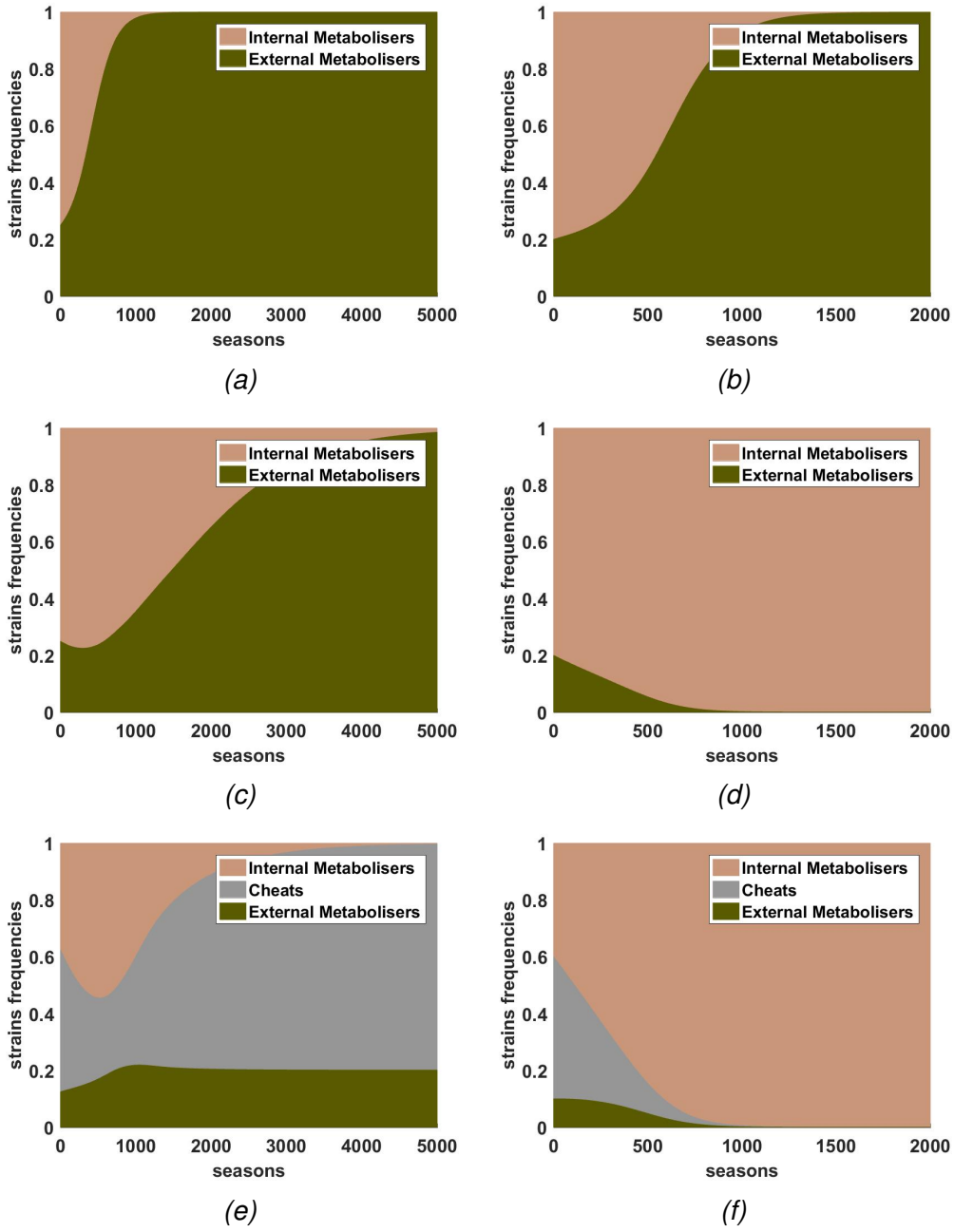

Figure 6-8: **Competition at low initial sucrose concentration. Changes in frequencies of the strains in the absence and presence of cheats.**
(6-8a)-(6-8b): Strains frequencies in the absence of cheats. The initial frequency of the external metaboliser is (6-8a): 0.25, (6-8b): 0.2.
(6-8c)-(6-8d): Strains frequencies within the invertase producers, in the presence of cheats.
The initial frequency of cheats in the entire population is $f_C = 0.5$.
The initial frequency of the external metaboliser, within the invertase producers is (6-8e): 0.25, (6-8f): 0.2.
(6-8e)-(6-8f): Strains frequencies within the entire population, in the presence of cheats.
The initial frequency of cheats in the entire population is $f_C = 0.5$.
The initial frequency of the external metaboliser, within the invertase producers is (6-8e): 0.25, (6-8f): 0.2.

6.5.3 Cheats maintain the diversity

As shown in Fig. 6-8e, the introduction of cheats into the population of invertase producers may temporarily stabilise the coexistence of the two types of invertase producers: external and internal metabolisers. This is a counter-intuitive result, based on the fact that cheats are known to exploit the public good systems they invade [32, 61–64], and in special cases, they even may lead to the collapse of entire populations [66].

In the trajectory shown in Fig 6-8e the frequency of internal metabolisers initially increases which can be explained by the increase in their relative fitness, in presence of cheats, as predicted by the Fig. 6-6b. Nonetheless, they eventually vanish from the population, leaving only the external metabolisers and cheats at play. This is because, together with the initial increase in the frequency of internal metabolisers, the frequency of cheats decreases, leading the relative frequency of external metabolisers over internal metabolisers to increase, as predicted in the Fig 6-6c.

The frequency of external metabolisers keeps increasing in the population, and eventually it is so high that the further increase in the cheats frequency is not sufficient to favour the internal metabolisers (Fig. 6-8e). Interestingly, at that phase cheats increase in frequency at the cost of internal metabolisers but not at the cost of the external metabolisers they take advantage of. This is because the introduced cheats are 'supreme cheats' to the internal metabolisers, which have the same access to the public hexose but need to pay energetic costs of their private invertase production.

Let us notice that, even if the frequency of introduced cheats decreases over seasons (Fig. 6-8f), it significantly affects the proportions of the two types of invertase producers (that is internal and external metabolisers). When the culture is initiated with a small portion of external metabolisers (Fig. 6-8f), their frequency is decreased, and (by the time the frequency of cheats drops) it is driven to such a small ratio that even without the cheats influence it will be outcompeted by internal metabolisers (as predicted by Fig 6-6a and shown in Supplementary Fig. 6-11c).

6.6 Discussion

In our study we focused on the cooperative system composed of external metabolisers, which secrete a public good (invertase), and internal metabolisers, which privatise the invertase they produce by keeping it inside the cell. We observe that the external metabolisers can stably coexist with the internal metabolisers when the initial resource concentration and population density is sufficiently high (Fig. 6-2a and Fig. 6-4a). However, when the resource concentration or population density drops that coexistence becomes unstable (Fig. 6-2b and Fig. 6-4b). At low initial sucrose concentration and high population density, the external metabolisers have a big chance to outcompete the internal metabolisers (as long as their initial frequency in the culture is sufficiently high, as shown in the Fig. 6-2b), because the speed of their metabolism is high (Supplementary Fig. 6-14a), and they have preferential access to the hexose they provide in the culture. However, at low initial density the relative fitness of external metabolisers to internal metabolisers is below one, meaning that they are unfavoured in such environmental conditions (Supplementary Fig. 6-14a). This conclusion agrees with our findings from Chapter 5, which show that low population density is a potential threat for the cooperative populations performing external metabolism.

We also examine the stability of the system composed of internal and external metabolisers in larger microbial communities. Namely we study the dynamics of the system after an introduction of a new competitor: cheat, which takes advantage of the costly public goods produced by the external metabolisers. Cheats are known to exploit the public good producers, and in extreme cases, they are expected to drive the whole populations to extinction: a scenario known as the 'tragedy of the commons' [65, 66].

Nonetheless, in our system this may not be the case. Paradoxically, instead of devastating their communities, cheats may help to maintain biodiversity (Fig. 6-8e). An introduction of a cheat into the system, in which the external metabolisers have a growth advantage over the internal metabolisers, balances the selection strengths in such a way that the internal metabolisers can be maintained in the population for longer time (Fig. 6-8c), than in the absence of cheats (Fig. 6-8a).

The frequency of external metaboliser becomes limited by the introduced cheat, but it does not decrease to zero. This agrees with other studies, which show that public good producers can coexist with cheats, because they have some preferential access to the public goods they produce [14, 33, 36, 147].

Why does an introduction of cheats slow down the extinction of the unfavoured strain? The relative fitness of external metabolisers to internal metabolisers is density and frequency dependent (Supplementary Fig. 6-14a), as also reported in [36]. Because of the Allee effect, the subpopulation of external metabolisers grows quickest at intermediate densities. Therefore, a drop in their population density may result in slower growth and, as a consequence, in being disadvantaged compared to the internal metabolising strain. Such a drop in the external metabolisers density $N_E = f_E N_0$ can be achieved either by decreasing the overall population density N_0, by decreasing the external metabolisers frequency f_E, or by decreasing the amount of available resources, which in turn will limit the population density N_0. This is what is effectively done by the introduced cheats who deplete the available resources, and thus constrain the density of external metabolisers.

Decreasing the resource concentration and introducing a new competitor which effectively depletes the resources will limit the external metabolisers density and slow their growth. This finding is in accordance with the study of [147], in which the density limitation is at the core of the mechanism promoting cooperation. Although our study agrees on the population density being the crucial factor that affects the stability of the cooperative system, the underlying mechanisms are different from the ones described in [147]. In [147], a decrease in population density favoured the cooperative external metabolisers, who naturally would be disadvantaged in comparison with their selfish competitors. Decreasing the population density was expected to limit the access of the selfish individuals to the public good, and therefore to decrease their advantage over the external metabolisers. In our system, a sufficient decrease in population density favours the internal metabolisers (Supplementary Fig. 6-14a & 6-14b) and changes the behaviour of the system: from the one described by a negative frequency dependent relative fitness, to the one with positive frequency dependent relative fitness. This result can be explained as follows. At high population density, the strains compete mostly for hexose (Supplementary Fig. 6-14e). In that case the sucrose uptake

by internal metaboliser becomes negligible and the internal metabolisers free-ride on the hexose hydrolysed in the environment by the external metabolisers. In this case, the relative fitness of external metabolisers is negative frequency dependent, as in the classical system of public good producers and non-producers (Fig. 6-3a). On the contrary, at low population density, only a very small fraction of sucrose in the environment is broken down into simple sugars (Supplementary Fig. 6-14c), and the strains effectively compete for sucrose instead of hexose. This can be described by the toy system of external metabolisers and perfect internal metabolisers, characterised by the positive frequency dependent relative fitness (Fig. 6-3b). In that case the internal metabolisers have an advantage over the external metabolisers. They uptake sucrose directly into their cells and they do not need to pay a cost of transporting the invertase outside the cell membrane. Additionally they do not need to rely on the invertase secreted by the other cells and that is why their performance is not significantly affected by low population density, in contrary to the performance of external metabolisers (see Chapter 5).

In extension to the study of [147], which perturbed a cooperative system by introducing a new competitor, and which reported short-term consequences of such perturbation, we also examine the steady states obtained in perturbed populations. We discover that the introduction of a new competitor can change the equilibrium dynamics. Even if the new competitor, cheat, eventually vanishes from the population, it can invert the outcome of a long-term competition leading to fixation of the strain which would have gone extinct if the cheats had never been introduced to the population (Fig. 6-8d compared to 6-8b). It means that even short-term invasions and coexistence with other strains or species may significantly influence the long-term dynamics of a cooperative system. Moreover, in our system, an introduction of the new strain may significantly prolong the time in which the strains coexist. This stabilisation mechanism is especially interesting, given that the strain we introduce is the classical 'cheat', which is usually believed to destroy ecological systems, or even lead to their collapse [32].

We find that, depending on the environmental factors, the system may either converge to a stable coexistence of external metabolisers and cheats, or to the fixation of internal metabolisers. If a system of stably coexisting external and internal metabolisers at high initial sucrose concentration is perturbed with an introduction of a small fraction of cheats, these cheats act as a 'superior cheats' to the intenal

metabolisers. They have the same access to the hexose available in the environment but, contrary to the internal metabolisers, they do not pay any energetic cost of producing invertase. Thus cheats start to be favoured over the internal metabolisers and the system converges to elimination of internal metabolisers and to the stable coexistence of the external metabolisers and cheats (Fig. 6-7d).

If a larger fraction of cheats is introduced, they exploit the external metabolisers and drive the external metabolisers and themselves to extinction, which can be described as the tragedy of the commons within the population of external metabolisers and cheats. In such a case, although the presence of cheats in the culture is only temporary, it can affect the long-term outcome of the competition between internal and external metabolisers (Fig. 6-7e). What is noticeable is that, at high initial sucrose concentration, the tragedy of the commons can be forced in a culture that in the absence of cheats would stably coexist (Fig. 6-7a). At low initial sucrose concentration, the tragedy of the commons and the extinction of external metabolisers can be forced in a population of invertase producers, which in the absence of cheats would end up being composed of the external metabolisers only (Fig. Fig. 6-8f).

As we have shown, the effect of cheats introduced to our cooperative system of external and internal metabolisers varies depending on several factors. The conflicting results obtained previously in the literature, according to which a new competitor could either stabilise [147, 149] or destabilise [147, 148] the cooperative systems, may have been observed not only because the studied strains and species were different. Such disparate results can be also observed in a single system in which the only varied parameter is the resource concentration, or the initial strains frequencies. In our system an addition of a new competitor may result in a number of scenarios: it may prolong the three strains coexistence, leading eventually to stable coexistence of external metabolisers and cheats (Fig. 6-8e), it may destabilise the stable coexistence of external and internal metabolisers leading to stable coexistence of external metabolisers and cheats (Fig. 6-7d), or it may lead to the scenario of tragedy of the commons (Fig. 6-7e & 6-8f).

Although the experimental system we base our study on is genetically engineered, we believe the model is general enough to be applicable to a wider class of intra- and interspecific microbial systems, which compete for a common resource pool. In general, our strains represent three different feeding strategies:

external metabolism, internal metabolism, and cheating: the strategy relying on the resources provided by the others. Our results present a mechanistic understanding of the interactions between individuals or species adopting each of these three strategies.

Finally, we highlight that the relative fitness in our model could be nonlinear and non-monotonous, which we explained with our toy models. Although, a possibility of obtaining nonlinear relative fitness has been recently discussed [152], to our knowledge, this is the first case of non-monotonous relative fitness reported in the literature. An observation that the relative fitness may be a non-monotonous function of competitors frequency has significant consequences for many empirical results. In particular, the relative fitness is often measured only for the extreme frequencies (very low fraction of either of the competitors), and it is assumed to be linear between such obtained points [62]. If this was done in our case, for example in Fig 6-2a, we would conclude that the entire line lies below one, and therefore, regardless of the initial frequencies of the two considered strains, the external metabolisers would always go extinct. This is however not true. As pointed out in the subsection 6.3.1, the strains can stably coexist at external metaboliser frequency $f^{**} \approx 0.25$.

So why is our relative fitness non-monotonous? As shown in [36], whilst the external metabolisers face a strong Allee effect, the internal metabolisers do not show a significant change in their growth rate depending on their population density. Thus, the external metabolisers growth rate is the highest at intermediate population density, and so is its relative fitness to the internal metabolisers (Supplementary Fig. 6-14a). Since varying the external metabolisers frequency will also vary their density in the population of external and internal metabolisers, the relative fitness of external metabolisers may be non-monotonous at the densities at which both increase and decrease in the relative fitness can be observed (Supplementary Fig. 6-14b). For instance, depending on the considered density (or resource concentration resulting in that density), the observed relative fitness may be positive frequency dependent (for small densities, as denoted by grey line in Supplementary Fig. 6-14a), negative frequency dependent (for large densities, as denoted by black line in Supplementary Fig. 6-14a), or non-monotonous (at intermediate densities, as plotted in Supplementary Fig. 6-14b).

6.7 Supplementary Material

6.7.1 Supplementary figures

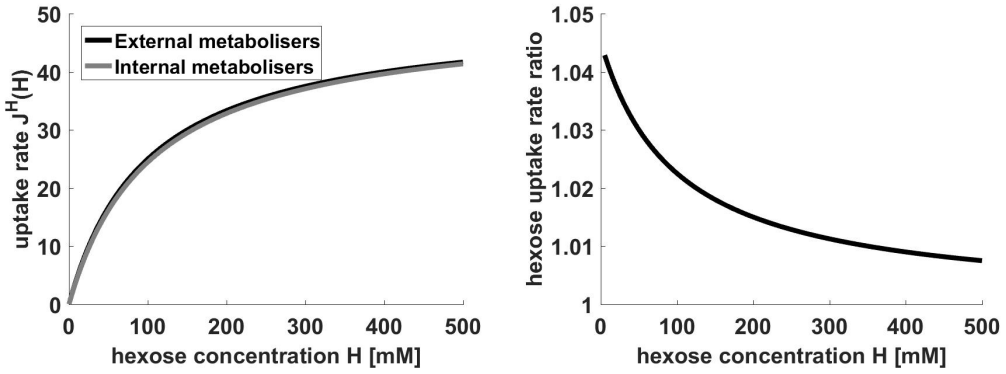

(a) *(b)*

Supplementary Figure 6-9: **Hexose uptake rates for external and internal metabolisers.**
(6-9a): the uptake rates of both strains, (6-9b): the ratio of the uptake rate of external metaboliser to the uptake rate of internal metaboliser $\frac{J_E^H(H)}{J_I^H(H)}$, depending on the hexose concentration H in the environment.

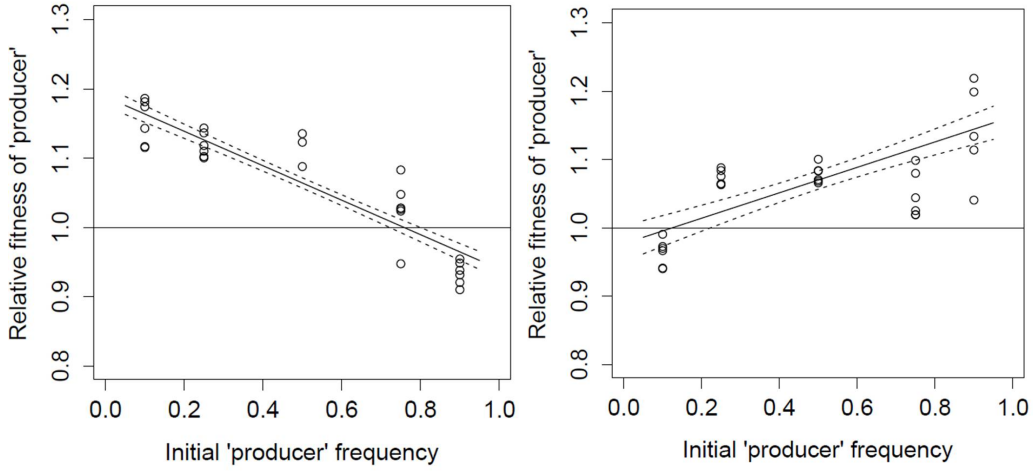

(a) *(b)*

Supplementary Figure 6-10: **Experimental data obtained by Richard Lindsay.**
The plots have been shown in [36]. (6-10a)-(6-10b): The relative fitness of external metabolisers (termed 'producers' in [36]) to the interal metabolisers (termed 'transporters' in [36]), in the competition in: (6-10a) high (25mM) and (6-10b) low (10mM) sucrose concentrations.

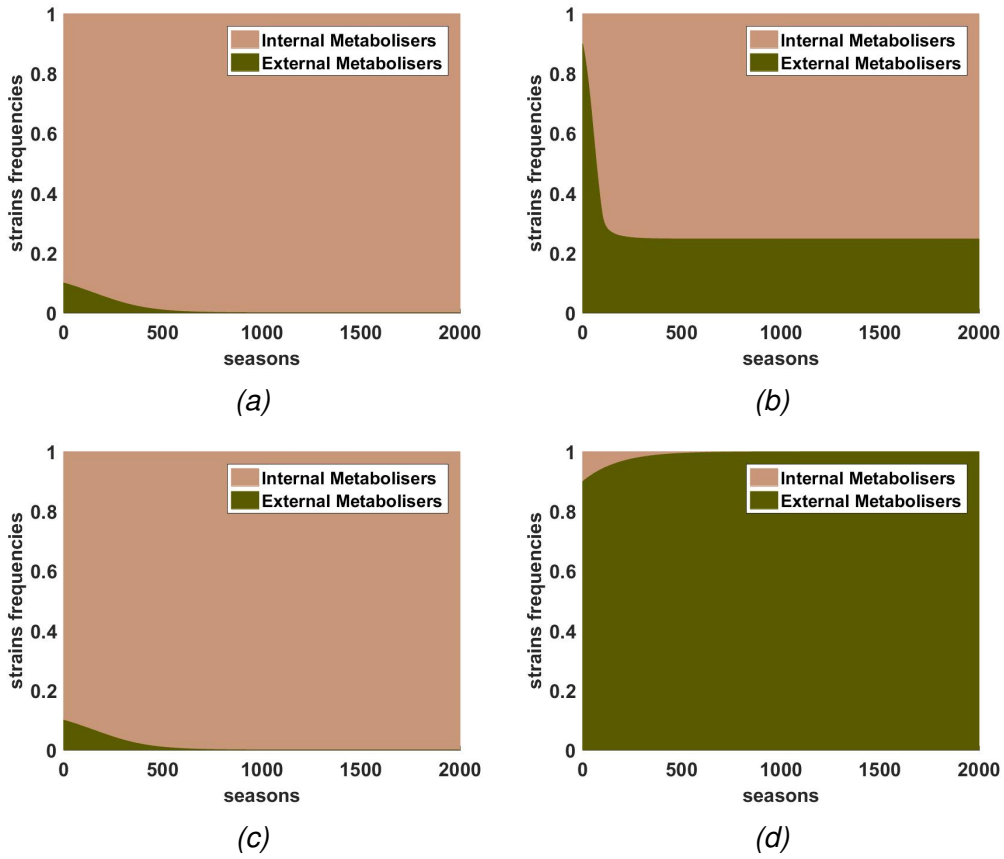

Supplementary Figure 6-11: **Changes in frequencies within the invertase producers.** (6-11a)-(6-11b): Strains frequencies in the competition between external and internal metabolisers, at high initial sucrose concentration. The initial frequency of the external metaboliser is: (6-11a) 0.1 (6-11b) 0.9. These two scenarios represent the bistability resulting from the presence of a stable and an unstable coexistence equilibria f^{**}, and f^{*} as studied in Fig. 6-2a.
(6-11c)-(6-11d): Strains frequencies in the competition between external and internal metabolisers, at low initial sucrose concentration. The initial frequency of the external metaboliser is: (6-11c) 0.1 (6-11d) 0.9. These two scenarios represent the bistability resulting the from presence of an unstable coexistence equilibrium f^{*} as studied in Fig. 6-2b.

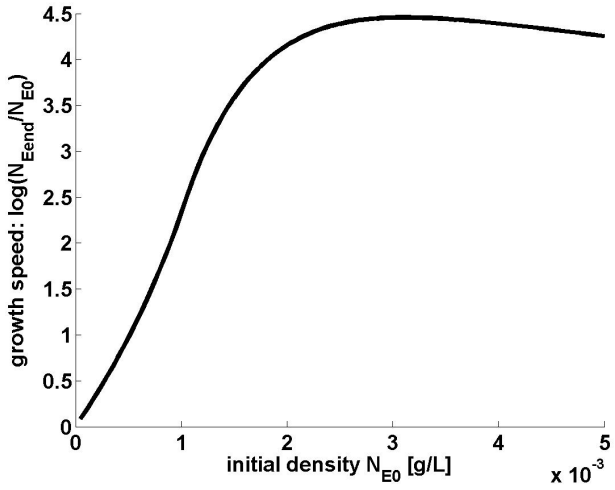

Supplementary Figure 6-12: **Allee Effect for the homogeneous population of external metabolisers.**
The growth speed, calculated here as $\ln(N_{Eend}/N_{E0})$. At low initial densities N_{E0}, the growth speed is an increasing function of the initial population density N_{E0}, whereas at higher initial densities N_{E0}, it starts decreasing.

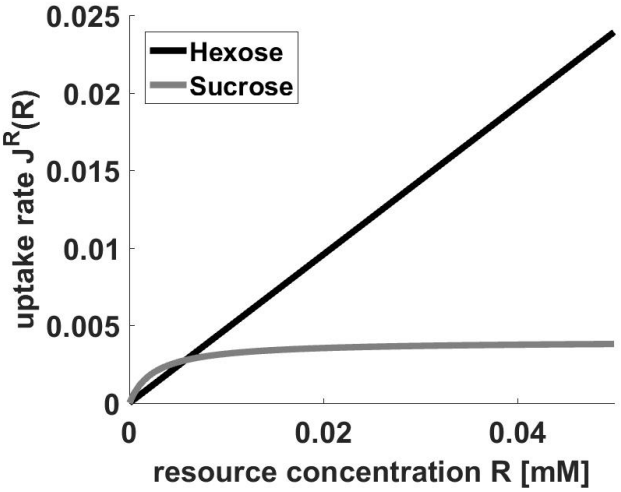

Supplementary Figure 6-13: **Uptake rates of hexose and sucrose for the internal metaboliser, depending on the resource (hexose/sucrose) concentration R.**

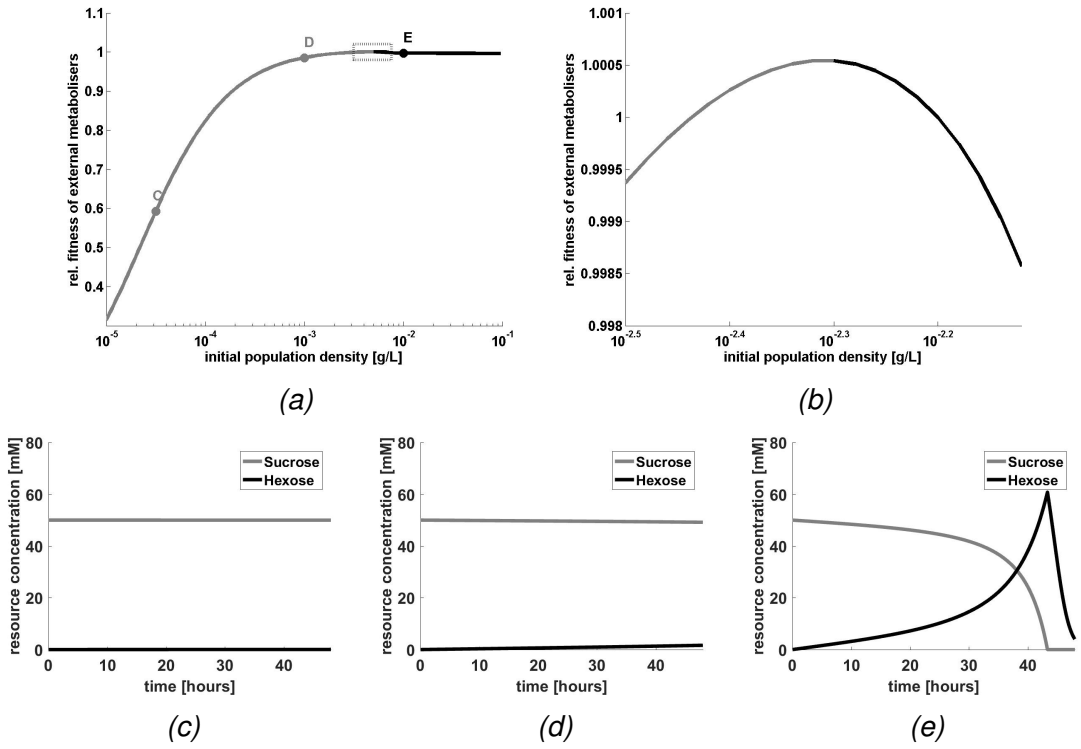

Supplementary Figure 6-14: **Relative fitness of external metabolisers depending on the initial total density of the population.**
(6-14a)-(6-14b): The relative fitness of external metabolisers to the internal metabolisers in the competition in high initial sucrose concentration, at initial frequency of external metabolisers $f = 0.5$.
(6-14b): Zoom into the area in the rectangle plotted in (6-14a). The grey lines denote relative fitness increasing with the population density, and the black lines denote relative fitness decreasing with the population density.
(6-14c)-(6-14e): The concentrations of sucrose and hexose in the culture during one season of growth, starting at high sucrose concentration and at (6-14c): low (6-14d): medium (6-14e): high population density, as denoted in Fig. 6-14a. Here the grey lines denote the sucrose concentration (S), and the black lines denote the hexose concentration (H) in time.

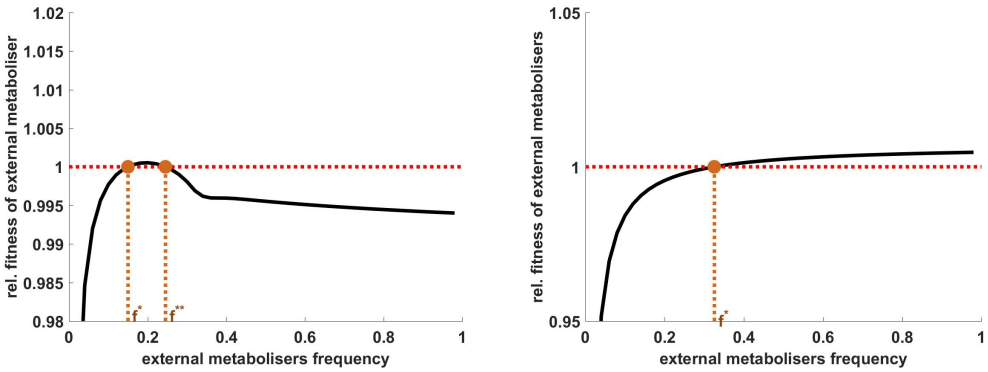

(a) *(b)*

Supplementary Figure 6-15: **Relative fitness of external metabolisers to internal metabolisers in the absence and presence of the new competitor uptaking sucrose.** The relative fitness of external metabolisers, depending on their initial frequency within the invertase producers, calculated at high initial sucrose concentration and in
(6-15a): absence of the new competitor,
(6-15b): presence of the new competitor.
The frequency of introduced competitor is $f_n = 0.8$.
The stable coexistence frequencies are denoted by f^{**}, while the unstable coexistence frequencies are denoted by f^{*}.

6.7.2 Parameter values

The Michaelis-Menten forms of the hexose uptake, and the form of invertase activity have been estimated in [14], and their simplified forms have been described in Chapter 2: Methods. Here we take the parameter values for $V^H_{max}, K^H_{Pm}, r_{in}, k_{in}, c_E$ directly from Chapter 4. The hexose and sucrose pathway efficiencies η^{Hxt}_e, η^S_e are assumed to be constant for the sake of simplicity. Moreover, because the internal metabolism involves the same process (sucrose hydrolisis) as the external metabolism, we assume both pathways yield the same amount of energy per gram of sucrose, which can be denoted by $\eta^S_e = 2\eta^{Hxt}_e$. For simplicity, we assume there is no direct sucrose uptake for the external metabolisers and cheats. The parameter values V^S_{max}, K^S_m for sucrose uptake via the novel sucrose transporter are taken from [150], where they have been estimated, based on the growth of *S. cerevisiae* supplemented with the novel sucrose transporter $SRT1$. Because the secretion of invertase to the cell periplasm involves sophisticated molecular processes [153], we assume it implies some energetic cost for the external metabolisers, and therefore $c_E > c_I$. The parameter values of K^H_{Im} and c_I have been chosen such that $c_E > c_I$ and $K^H_{Im} > K^H_{Em}$, and their exact values (which have not been estimated elsewhere) are chosen in such a way that the resulting system behaviour matches the observations in the experimental system. Namely, they allow: the external metabolisers to stably coexist with cheats, internal an external metabolisers to stably coexist when the initial sucrose concentration is high, and coexist unstably when the initial sucrose concenration is low.

Supplementary Table 6.1: Parameters values for the mathematical model (6.2.1)-(6.2.5)

V_{max}^{H}	50 [mmol hexose / (g protein · hour)]
K_{Em}^{H}	100 [mM hexose]
K_{Im}^{H}	104.5 [mM hexose]
V_{max}^{S}	0.004 [mmol sucrose / (g protein · hour)]
K_{m}^{S}	0.0026 [mM sucrose]
η_{e}^{S}	0.04 [g protein/mmol sucrose]
η_{e}^{Hxt}	0.02 [g protein/mmol hexose]
r_{in}	77 [mmol/ (g protein · hour)]
k_{in}	$5 \cdot 10^{-3}$ [mM sucrose]
c_E	0.04
c_I	0.004
S_0	10 [mM] for 'low concentration' and 50 [mM] for 'high concentration'
N_0	0.005 [g/L], or 0.001 [g/L] for 'low population density'
T	48 [hours]

Chapter 7

Evolution of internal and external metabolism

Abstract

Why have certain species developed the external metabolism, which involves secretion of costly enzymes (public goods) and brings the risk of being exploited by other organisms, while other species stay 'selfish' and perform internal metabolism? Here we consider a population composed of a number of phenotypes which deploy various feeding strategies, and we study how that population evolves depending on the environmental conditions. We examine populations under the mutation-selection balance in a chemostat setting, and we discover that the evolution towards the internal or external metabolism is determined by the chemostat dilution rate. The low dilution rates (meaning low mortality) select for external metabolism, whereas high dilution rates (meaning high mortality) select for internal metabolism. Moreover, for some range of dilution rates, a population may evolve either towards the cooperative external or towards the selfish internal metabolism, depending on its initial density and composition.

7.1 Introduction

The rice pathogen *Magnaporthe oryzae* has been reported to display a cooperative behaviour, in which a public good is created collectively by a number of cells [36]. The considered public good is an enzyme invertase, which allows for a more efficient metabolism. It extracellularly breaks down sucrose into simpler sugars

(hexose) which can be then easily transported into the cells and metabolised. On the contrary, another plant pathogen *Ustilago maydis* behaves in a 'selfish way'. It is able to transport the whole sucrose molecules into the cell, and thus it does not need to digest it extracellularly with the help of other surrounding individuals [92]. Thus it avoids the risk of being exploited by other organisms, who potentially do not contribute to the collective public good production, but still reap the rewards.

Why have certain microorganisms, such as *M. oryzae* [36] or *Saccharomyces cerevisiae* [32], developed external metabolism involving the cooperative secretion of public good, while some others, such as *U.maydis*, stay 'selfish'? Is there any crucial point in the course of evolution that leads to the shift towards the selfish or cooperative behaviour? How does that shift happen and what ecological events can trigger it?

The ecological setup, in which evolution leads towards intensification of cooperative behaviour, has been observed experimentally in a system of *S.cerevisiae* [141]. This species is not able to persist in liquid cultures at low population density, because the simple sugars that have been broken down by invertase diffuse away from the cells and become hard to capture. This phenomenon has been found in various setups: batch cultures [1], serial dilutions [93] and chemostats (Chapter 5). *S.cerevisiae* populations evolved in such harsh conditions have been reported to increase the invertase production rate, and thus to intensify the cooperation [141]. Out of 12 studied clonal populations, almost all increased the invertase production. However, this evolutionary change was not the only one. At the same time, the studied populations also increased their hexose uptake by both: clumping together (which facilitates the hexose uptake from the environment [1]), and by increasing the number of hexose transporters [141].

Before performing the evolutionary experiments, the authors of [141] hypothesised that, in order to overcome the problem of capturing simple sugars, the cells could also evolve towards the improvement of the direct sucrose uptake. Interestingly, this did not happen in any of 12 studied populations. Are there any environmental conditions in which the evolution could lead to development of the 'selfish' sucrose uptake and disappearance of the cooperative external digestion? Finally if a change in some environmental conditions could lead a cooperative population to become selfish, would that transition between cooperative and selfish states be smooth allowing for evolution of stable intermediate states between full coopera-

tion and full selfishness, or would it be sharp, switching directly between entirely cooperative and entirely selfish cultures?

A recent theoretical study [154] found that when public good production and multicellularity evolve jointly, a small change in the genetic relatedness between the cells ('whole group' relatedness) may lead to a sharp transition between the evolutionary outcomes: from a multicellular and cooperative to a sparse and 'selfish' population which does not secrete any public goods. In general, sharp transitions between different states of ecological systems are ubiquitous in nature [93, 155–157] and they are of particular interest to biologists because they may lead to irreversible events, such as species extinction or even the whole ecosystem degradation [155]. For instance, such irreversible shifts have been reported in microbial communities, for example in cyanobacterial mats [157, 158], or in gut microbial system [159, 160], in which the composition of the population changed drastically after certain ecological perturbations, such as a hurricane in the case of cyanobacterial mat, or antibiotic treatments in the case of gut microbiota. Apart from the antibiotics, there are other environmental factors that may disturb microbial ecosystems, such as the temperature or CO_2 increase [161].

Here we study the evolution of various feeding strategies in a chemostat (for a detailed description of chemostat systems see the subsection 2.2.1 in Chapter 2: Methods) and we show how perturbations in the dilution rate, and population density can disturb the system. As pointed out in Chapter 2, the chemostat culture is a laboratory setup which represents certain ecological conditions. Namely it imitates environments in which microorganisms face a constant inflow of fresh resources and a constant outflow of the waste products and cells [42]. Thus, it may be relevant to any microbial communities residing in liquid environments, such as oceans, or certain human organs [43–48]. There are known microbial species that live in such environments and perform extracellular digestion similarly as the microorganisms studied in this chapter [162]. An example of bacteria that lives in liquid environments and uses external digestion is the human pathogen *Vibrio cholerae*, which secretes extracellular enzymes in order to digest its most common resource: chitin [31, 163]. Could that feeding strategy change in the course of evolution?

Motivated by previous studies [53, 54], we construct a mutation-selection model subject to competition for resources. This allows us to combine evolutionary dy-

namics with ecological interactions. In this framework, we show that the dilution rate and population density are the factors that determine the evolution towards selfish or cooperative behaviour. A perturbation in these environmental factors may disturb the ecosystem leading to a sharp transition between cooperative and a selfish states.

Moreover, we report a non-monotonous relationship between the total population density and the biodiversity in our system. Although a switch from cooperative to selfish behaviour results in a drop in the total population density (i.e. in population size in a given space unit), it is followed by an increase in the diversity. This means that the biological diversity may not be correlated with the population size, as previously thought [164, 165] and the methods of predicting the diversity based on the population size [166, 167] may not always give the correct estimates.

7.2 Mathematical model

To study the possible evolutionary outcomes of a public good system, in which the resources may be digested either externally or internally, we built an N-type chemostat, mutation-selection model, such as the one studied in [54]. Our model is based on the ecological principle of competition for resources in a continuous culture, and it describes the growth and evolution of a population, composed of phenotypes having diverse feeding strategies.

We assume that during the course of evolution, mutations may occur and they give rise to cells of different phenotypes $i \in \{1, 2, ..., N\}$, where N denotes a positive integer. Throughout time, these phenotypes compete for resources and, depending on selection strengths, their frequencies in the population change until they stablise at a steady state (termed also an 'equilibrium'). Here we study these steady state frequencies of different phenotypes in the population.

Although we base the assumptions of our model on the metabolism in *S. cerevisiae* (described in more detail in Chapter 2: Methods), which is known to perform external digestion, here we consider a whole range of different feeding strategies: varying from perfectly external to perfectly internal digestion.

7.2.1 Microbial growth

In our model all the strains take up resources R and use them to generate ATP using a simple, unbranched pathway [37]. We represent microbial growth as a linear function of the rate of ATP production, as described in more detail in Chapter 2: Methods.

Some of the considered phenotypes are able to secrete invertase, which catalyses the extracellular hydrolysis of each molecule of sucrose into two molecules of monosaccharides, i.e. hexose (H). The rate of conversion of sucrose into hexose is represented by Inv, a saturating function of sucrose concentration and, as described in Chapter 2: Methods, it takes the following form:

$$Inv = \frac{r_{in} S}{k_{in} + S},$$

where k_{in} is the saturation constant, and r_{in} is a constant invertase activity, specific to each of the considered phenotypes. The cells we consider can uptake both: sucrose (S) and hexose (H), with the following uptake rates:

$$J^S = \frac{V^S_{max} S}{K^S_m + S},$$

$$J^H = \frac{V^H_{max} H}{K^H_m + H},$$

for sucrose and hexose respectively .

For simplicity we assume there is no rate-efficiency trade-off, meaning that the quantity of ATP produced per resource unit does not depend on the uptake rate of that resource. We also assume that both: invertase secretion and the sucrose metabolism incur some energetic costs for the cells: c_1 and c_2 respectively. Based on the study in [14], we reflect these costs by multiplying the efficiencies of sucrose metabolic pathway (η^S_e) and of hexose metabolic pathway (η^{Hxt}_e) by $(1-c_2)$ and $(1-c_1)$, respectively. Hence, in the model we will use the net efficiencies of the metabolic pathways, i.e. $n^S_e = (1-c_2)\eta^S_e$ for the pathway utilising sucrose, and $n^{Hxt}_e = (1-c_1)\eta^{Hxt}_e$ for the pathway utilising hexose.

Hexose-sucrose uptake trade-off. Although throughout the evolution, different cell lines may improve their metabolism, we assume that there are restrictions on

the energy allocated to the improvement of resource uptake. Namely, evolving cells cannot increase hexose and sucrose uptakes at the same time. Instead, because of energetic constraints, we assume that during the evolution, an increase in the maximal uptake rate of hexose V^H_{max} will lead to a decrease in the maximal uptake rate of sucrose V^S_{max}. Thus we assume the for each phenotype, its maximal sucrose uptake rate V^S_{max} depends on its maximal hexose uptake rate V^H_{max}, and can be defined as:

$$V^S_{max} = h(V^H_{max}),$$

where h is a decreasing function, and it denotes the trade-off between the sucrose and hexose uptake. The assumption of a trade-off between uptakes of two different resources is classical within the resource allocation problem and it is widely used throughout the literature [51, 53, 130, 168]. Because the shape of ecological trade-offs is known to play a key role in ecological models [51, 52, 168], we will consider a range of functions h, described as linear, concave, convex, sigmoidal or cubic.

In the recent empirical study, hexose uptake was reported to evolve in parallel with the invertase production [141]. Therefore, we assume that extracellular invertase production evolves jointly with the improvement of the hexose uptake. Namely, the phenotypes characterised by high hexose uptake rates, have also high invertase activity, which can be written as:

$$r_{in} = g(V^H_{max}),$$

where g is an increasing function.

Phenotypic mutations. We consider mutations that change the maximal uptake rates of hexose (V^H_{max}) and sucrose (V^S_{max}), and they happen at a specific mutation rate ϵ. Similarly as in [54], in our model mutations can happen even if no reproduction occurs (i.e. when the microbial growth rate $G = 0$), and that is why the mutation rates are expressed as values per time. Thus the term 'mutation' is not necessarily restricted to the changes in DNA, but it generally describes the transitions between heritable traits (which may be for example due to heritable epigenetic changes, as noticed in [54]).

The mutations give rise to the cells with different maximal uptake rates V^H_{max}

and $V^S_{max} = h(V^H_{max})$. To represent the mutations between various phenotypes, we consider N values of V^H_{max}: $V^H_{max}(1) < V^H_{max}(2) < .... < V^H_{max}(N) \in [0, B]$, where

$$V^H_{max}(1) = 0,\ V^S_{max}(1) = h(V^H_{max}(1)) = B,$$

and

$$V^H_{max}(N) = B,\ V^S_{max}(N) = h(V^H_{max}(N)) = 0.$$

If a mutation affects a cell characterised by the maximal hexose uptake rate $V^H_{max}(i)$, the mutant will have the maximal hexose uptake rate $V^H_{max}(i-1)$ (with probability 0.5), or $V^H_{max}(i+1)$ (with probability 0.5). The phenotypes with the boundary maximal uptake rates: $V^H_{max}(1)$ and $V^H_{max}(N)$ represent a special case (boundary conditions), in which they can mutate to $V^H_{max}(2)$ or $V^H_{max}(N-1)$ respectively, with probability 0.5, or they can stay unchanged, with the probability 0.5. This effectively means that they can mutate only into one other phenotype, and their mutation rate is twice lower than the mutation rate of all the other phenotypes, i.e. $\epsilon/2$.

To describe mathematically the above assumptions, we define a matrix of transition probabilities M, such that m_{ij} is the probability of mutation from the phenotype i to the phenotype j, assuming that a mutation occurs. M is of size NxN and it can be written as follows:

$$M = \begin{pmatrix} 0 & 1 & 0 & 0 & 0 & \dots & 0 & 0 & 0 & 0 \\ 0.5 & 0 & 0.5 & 0 & 0 & \dots & 0 & 0 & 0 & 0 \\ 0 & 0.5 & 0 & 0.5 & 0 & \dots & 0 & 0 & 0 & 0 \\ \vdots & \vdots & \vdots & \vdots & \ddots & \vdots & \vdots & \vdots & \vdots & \vdots \\ \vdots & \vdots & \vdots & \vdots & \ddots & \vdots & \vdots & \vdots & \vdots & \vdots \\ \vdots & \vdots & \vdots & \vdots & \ddots & \vdots & \vdots & \vdots & \vdots & \vdots \\ 0 & 0 & 0 & 0 & 0 & \dots & 0.5 & 0 & 0.5 & 0 \\ 0 & 0 & 0 & 0 & 0 & \dots & 0 & 0.5 & 0 & 0.5 \\ 0 & 0 & 0 & 0 & 0 & \dots & 0 & 0 & 1 & 0 \end{pmatrix}$$

The mutation probabilities ε_i for each phenotype i, are defined as:

$$\varepsilon_i = \begin{cases} \epsilon/2, & \text{if } i = 1 \text{ or } i = N \\ \epsilon & \text{if } i \in \{2, 3, .., N-1\}, \end{cases}$$

for a fixed parameter value ϵ. Here we assume that the mutations have only small effect on phenotype, which translates to $m_{jk} = 0$ for $|j-k| > 1$. Taking into account the mutation probabilities ε_i, and the matrix of transition probabilities M we can associate our mutations with a continuous time Markov chain, with the following transition rate matrix:

$$K = \begin{pmatrix} -\epsilon/2 & \epsilon/2 & 0 & 0 & 0 & \dots & 0 & 0 & 0 & 0 \\ \epsilon/2 & -\epsilon & \epsilon/2 & 0 & 0 & \dots & 0 & 0 & 0 & 0 \\ 0 & \epsilon/2 & -\epsilon & \epsilon/2 & 0 & \dots & 0 & 0 & 0 & 0 \\ \vdots & \vdots & \vdots & \vdots & \ddots & \vdots & \vdots & \vdots & \vdots & \vdots \\ \vdots & \vdots & \vdots & \vdots & \ddots & \vdots & \vdots & \vdots & \vdots & \vdots \\ \vdots & \vdots & \vdots & \vdots & \ddots & \vdots & \vdots & \vdots & \vdots & \vdots \\ 0 & 0 & 0 & 0 & 0 & \dots & \epsilon/2 & -\epsilon & \epsilon/2 & 0 \\ 0 & 0 & 0 & 0 & 0 & \dots & 0 & \epsilon/2 & -\epsilon & \epsilon/2 \\ 0 & 0 & 0 & 0 & 0 & \dots & 0 & 0 & \epsilon/2 & -\epsilon/2 \end{pmatrix}$$

Competition in the chemostat. Our model allows us to track in time the concentrations of the primary resource: sucrose (S), the secondary resource: hexose (H), the total population density (P), and the frequencies of each of the considered phenotypes at a given time t ($\mathbf{f}(t) = [f_1(t), f_2(t), ..., f_N(t)]$).

An individual within the phenotype i will have the following resource uptake rates:

$$J_i^H = \frac{V_{max}^H(i)H}{K_m^H + H}, \text{ for hexose,}$$

$$J_i^S = \frac{h(V_{max}^H(i))S}{K_m^S + S}, \text{ for sucrose,}$$

and the following invertase activity:

$$r_{in_i} = g(V_{max}^H(i)).$$

7.2.2 The system dynamics

Putting all of our assumptions together, we propose the following mutation-selection model

$$\frac{d}{dt}S = - < \mathbf{Inv} + \mathbf{J^S}, \mathbf{f} > P - D(S - S^0) \tag{7.2.1}$$

$$\frac{d}{dt}H = < 2\mathbf{Inv} - \mathbf{J^H}, \mathbf{f} > P - DH \tag{7.2.2}$$

$$\frac{d}{dt}P = < \mathbf{G}, \mathbf{f} > P - DP \tag{7.2.3}$$

$$\frac{d}{dt}\mathbf{f} = \mathbf{Gf} - < \mathbf{G}(S, H), \mathbf{f} > \mathbf{f} + \mathbf{f}K, \tag{7.2.4}$$

where G is the vector of growth rates for each phenotype: $\mathbf{G} = n_e^{Hxt}\mathbf{J^H} + n_e^S\mathbf{J^S}$. The bold symbols account for the vector notation, and $< \mathbf{x}, \mathbf{y} >$ denotes the Euclidean inner product: $\sum_{i=1}^{N} x_i y_i$, whenever $\mathbf{x} = [x_1, x_2, ..., x_N]$, and $\mathbf{y} = [y_1, y_2, ..., y_N]$.are vectors of the same length N. The term $\mathbf{Gf}$ denotes the element-wise multiplication of the growth rate vector G and the vector of phenotype frequencies f. The process of mutation is described by the term: K which is the matrix of transition rates, as described in the previous paragraph. The parameter D is the chemostat dilution rate, which describes the rate of influx of the resource into the culture, and the rate of washout of the content of the culture. The inflowing resource concentration is described by the parameter S^0.

7.3 Results

We consider various phenotypes: ranging from the ones that have high hexose uptake rates and secrete large quantities of invertase (termed **'external metabolisers'**), to the ones with high sucrose uptake, and low invertase activity. These individuals, termed **'internal metabolisers'**, have low hexose uptake rates, and therefore, in contrary to the 'non-producers' or 'cheats' considered in Chapters 3,4,6, they do not benefit from the simple sugars publicly available in the environment. Instead, they simply behave in a non-cooperative way, uptaking the sucrose directly and independently of each other. This is why, throughout this study, we will term their metabolism **'selfish'**. Our internal metabolisers relate to the internal metaboliser strain of *S. cerevisiae* introduced in Chapter 6, and studied empirically in [36]. That strain had an improved sucrose uptake compared to

the wild type invertase producer, but it suffered a disadvantage in terms of uptaking hexose. Here we extrapolate that concept, allowing the internal metabolisers to evolve and to increase further their sucrose uptake, for the cost of decreased hexose uptake rates.

Our 'boundary' phenotypes 1 and N represent the special cases. The phenotype 1, termed **'perfect internal metaboliser'**, represents the strain which is not able to secrete invertase ($r_{in_1} = 0$) nor to uptake any hexose ($V^H_{max}(1) = 0$). On the contrary, the phenotype N, termed **'perfect external metaboliser'**, is not able to uptake any sucrose directly from the environment ($V^S_{max}(N) = h(V^H_{max}(N) = 0)$.

7.3.1 Linear hexose-sucrose uptake trade-off.

In order to study the evolution of a population composed of a number of phenotypes, possesing various feeding strategies, we first assume that the trade-off h between sucrose and hexose uptake rates is linear taking the form: $h(V^H_{max}) = B - V^H_{max}$, and we study the stable steady states of the chemostat system defined in (7.2.1)-(7.2.4). In particular, we follow the equilibria total population densities P^*, and the distributions of the population density into different phenotypes: $P^*\mathbf{f}^*$, where $\mathbf{f}^* = [f^*_1, f^*_2, ..., f^*_N]$ denotes the vector of equilibria frequencies of the phenotypes $\{1, 2, ..., N\}$, and $\sum_{i=1}^{N} f^*_i = 1$.

Because of the mutation-selection balance, the stable populations in our system are composed of phenotypes distributed around the fittest phenotypes i, which have locally the highest population densities: $P^* f^*_i$, and will be termed **'the dominant types'**. The populations, in which the dominant types i can be described as external metabolisers ($V^H_{max}(i) > B/2$) are termed **'cooperative'**, and those in which the dominant types i can be described as internal metabolisers ($V^H_{max}(i) < B/2$) are termed **'selfish'**. We will also refer to the total population density P. Populations with high total population density P will be termed **'dense'**, while those with low total population density will be termed **'sparse'**.

The selection for or against cooperative behaviour highly depends on the dilution rate. For low dilution rates, the dominant phenotype is the perfect external metaboliser, i.e. the type that feeds only extracellularly (Fig. 7-1a & 7-1b). On the contrary, when the dilution rate is high, the dominant phenotype becomes the perfect internal metaboliser, which relies only on the intracellular sucrose metabolism

(Fig. 7-1a & 7-1d). There is also a wide range of intermediate dilution rates, at which the bistability occurs (Fig. 7-1a). These rates, depending on the initial conditions, can sustain either a cooperative population of external metabolisers at high total population density (brown line in Fig. 7-1a and brown distribution in Fig. 7-1c), or a selfish population of internal metabolisers at low total population density (blue line in Fig. 7-1a and blue distribution in Fig. 7-1c). It means that, depending on the initial conditions, the population may either become dense and cooperative or sparse and selfish, as reported in [154]. The range of dilution rates, at which such bistability can be observed depends on the mutation rate ϵ, and it is larger for lower mutation rates ϵ (Supplementary Fig. 7-14).

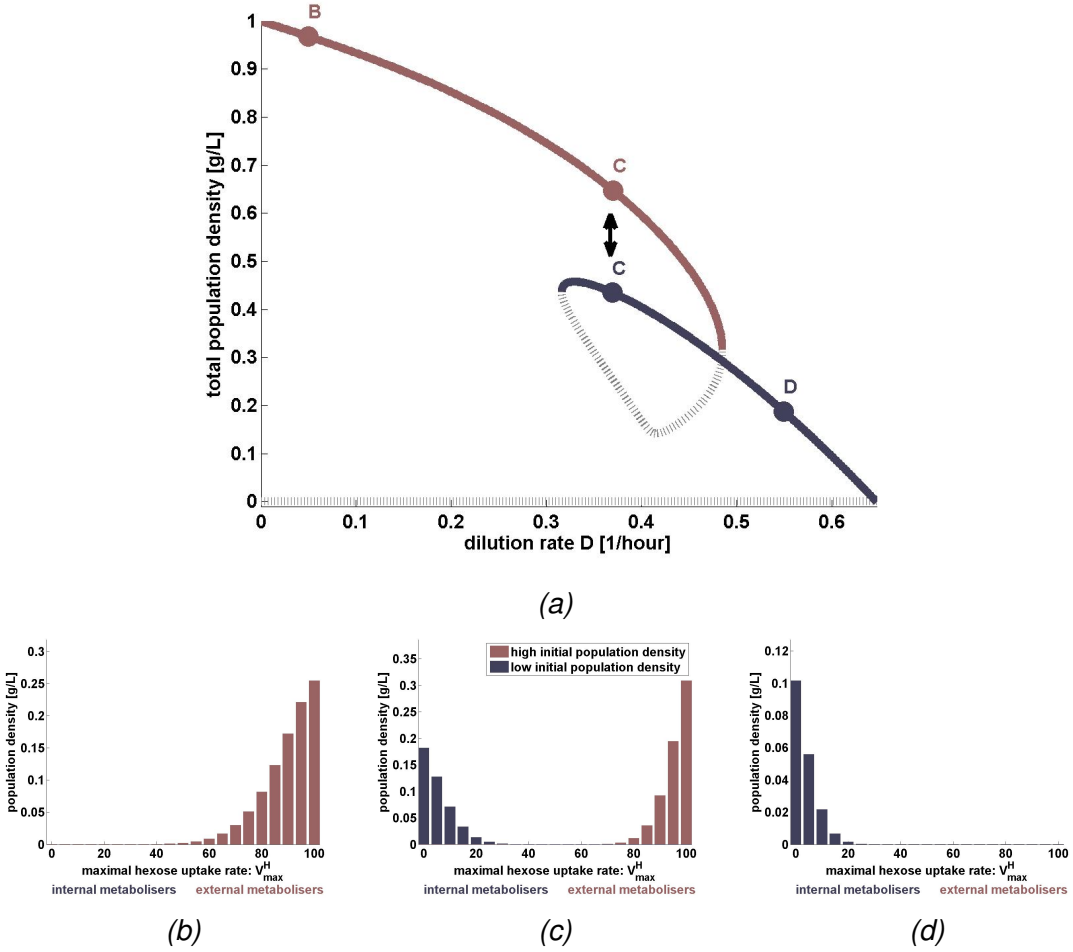

Figure 7-1: **Positive steady states of a population under mutation-selection balance.** The brown lines and plots indicate populations dominated by external metabolisers, whereas the blue lines and plots indicate populations dominated by internal metabolisers. The individuals with maximal hexose uptake rate $V^H_{max} = 0$ are the perfect internal metabolisers, while the individuals with maximal hexose uptake rate $V^H_{max} = 100$ are the perfect external metabolisers.
(7-1a): Total population density P^* depending on the dilution rate D; The stable steady states are denoted by solid lines, while the unstable steady states are denoted by dashed lines.
(7-1b) & (7-1d): Distribution of population density into phenotypes ($P^*\mathbf{f}^*$) in the population for (7-1b) low and (7-1d) high dilution rates, denoted in Fig. 7-1a by 'B' and 'D', respectively. Each bar represents the density of one particular phenotype: $P^* f_i$.
(7-1c): Possible stable distributions of population density into phenotypes ($P^*\mathbf{f}^*$) at an intermediate dilution rate, denoted in Fig. 7-1a by 'C'. The resulting distributions depend on the initial distribution and total density of the population.

In particular, in the range of dilution rates which support bistability, a population started with density homogeneously distributed over all the phenotypes ($f_1 = f_2 = ... = f_N$) and with sufficiently high total population density will become cooperative and dense (Fig. 7-2b and brown line in Fig. 7-2a), and the one started with sufficiently low population density, will become sparse and selfish (Fig. 7-2c and blue line in Fig. 7-2a). Similarly, the populations started with the same total densities, but different distributions of population density into the phenotypes, may diverge into either cooperative or selfish (Fig. 7-3). Figure 7-3 also shows that our ecological system is highly conservative. Namely, at intermediate dilution rates, a population once dominated by external or internal metabolisers, will converge to the dominance of the perfect external metaboliser or the perfect internal metaboliser, respectively, and it will not allow for the coexistence of both.

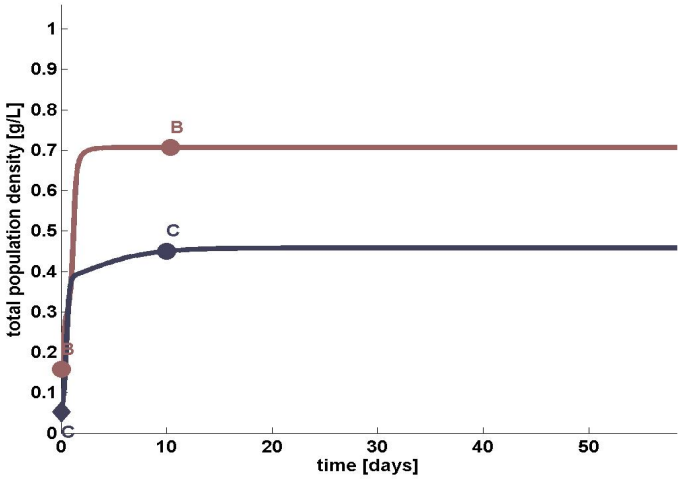
total population density [g/L]
time [days]
B
C
B
C

(a)

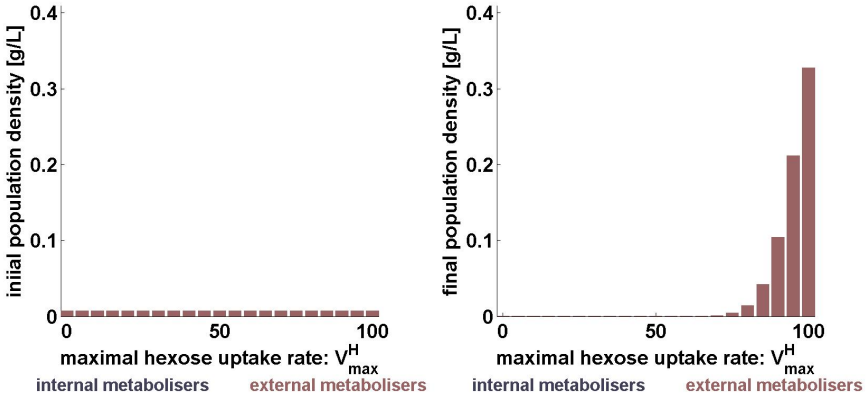
iniial population density [g/L]
final population density [g/L]
maximal hexose uptake rate: V^H_{max}
internal metabolisers
external metabolisers

(b)

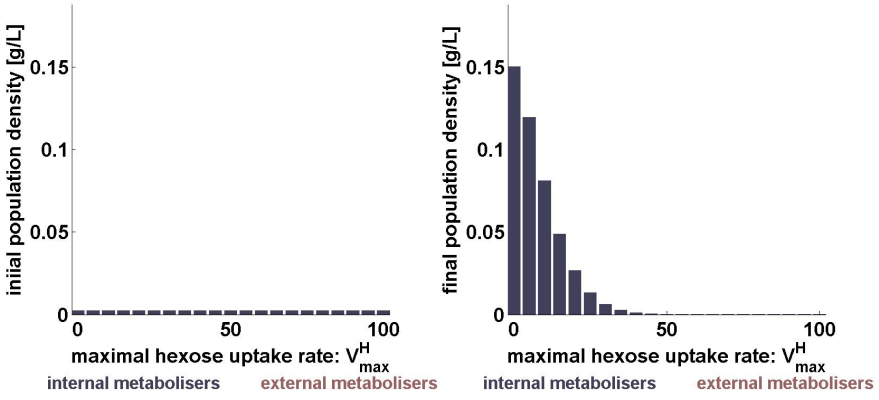
iniial population density [g/L]
final population density [g/L]
maximal hexose uptake rate: V^H_{max}
internal metabolisers
external metabolisers

(c)

Figure 7-2: **The system behaviour depending on the initial total population density.** Two populations, started with slightly different total population densities P, may diverge into completely different stable steady states: either a dense population of external metabolisers (with the population density distribution $P^*\mathbf{f}^*$ shown in Fig. 7-2b, *right*), or a sparse population of internal metabolisers (with the population density distribution $P^*\mathbf{f}^*$ shown in Fig. 7-2c, *right*).
The brown lines and plots indicate populations which become dominated by external metabolisers, whereas the blue lines and plots indicate populations which become dominated by internal metabolisers. The individuals with maximal hexose uptake rate $V^H_{max} = 0$ are the perfect internal metabolisers, while the individuals with maximal hexose uptake rate $V^H_{max} = 100$ are the perfect external metabolisers.
(7-2a): The trajectories of total population density P depending on the initial conditions. (7-2b)-(7-2c): the initial (*left*), and the final (*right*) population density distributions for two populations, whose total densities are plotted in Fig. 7-2a. The initial total population density in (7-2b) is slightly higher than the one in (7-2c). Each bar represents the density of one particular phenotype: $P^* f_i$.
The simulations were performed at dilution rate $D = 0.33$ [1/hour].

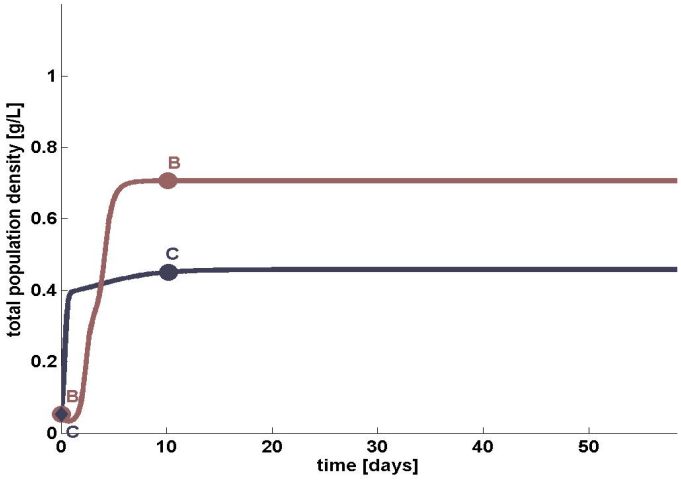
total population density [g/L]
time [days]
B
C
B
C

(a)

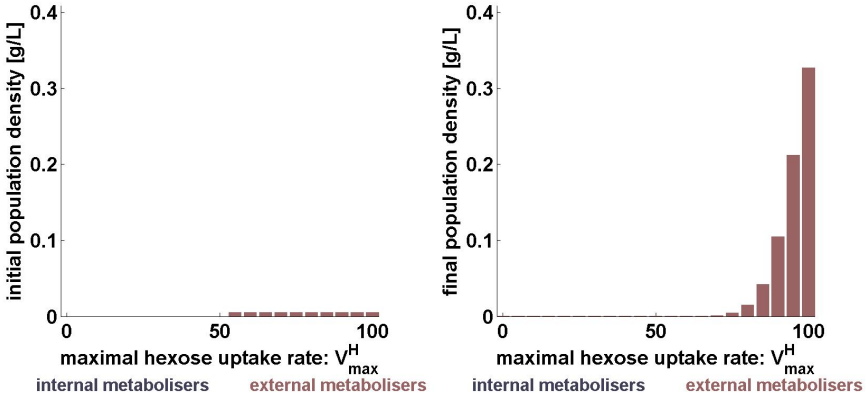
initial population density [g/L]
final population density [g/L]
maximal hexose uptake rate: V^H_{max}
internal metabolisers
external metabolisers

(b)

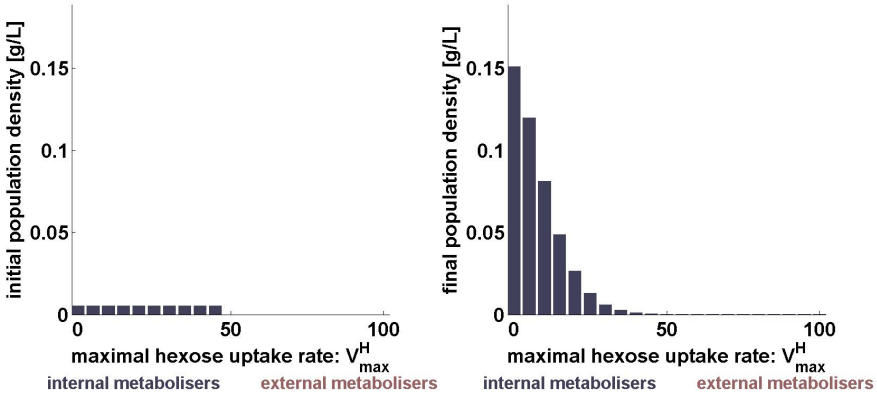
initial population density [g/L]
final population density [g/L]
maximal hexose uptake rate: V^H_{max}
internal metabolisers
external metabolisers

(c)

Figure 7-3: **The system behaviour depending on the initial population density distribution.**
Two populations, started with the same total population densities, but different distributions over the considered phenotypes, may diverge into completely different stable steady states: either a dense population of external metabolisers (with the population density distribution $P^*\mathbf{f}^*$ shown in Fig. 7-3b, *right*), or a sparse population of internal metabolisers (with the population density distribution $P^*\mathbf{f}^*$ shown in Fig. 7-3c, *right*).
The brown lines and plots indicate populations which become dominated by external metabolisers, whereas the blue lines and plots indicate populations which become dominated by internal metabolisers. The individuals with maximal hexose uptake rate $V^H_{max} = 0$ are the perfect internal metabolisers, while the individuals with maximal hexose uptake rate $V^H_{max} = 100$ are the perfect external metabolisers.
(7-3a): The trajectories of total population density P depending on the initial conditions.
(7-3b)-(7-3c): the initial (*left*) and the final (*right*) population density distributions for the populations, whose total densities are plotted in Fig. 7-3a and started with a cooperative (7-3b) and selfish (7-3c) populations. Each bar represents the density of one particular phenotype: $P^* f_i$.
The simulations were performed at dilution rate $D = 0.33$ [1/hour].

However, a stable selfish population, may shift into a cooperative one if a perturbation in the population density or distribution occurs. Such a scenario is presented in Fig. 7-4, in which the density of external metabolisers is suddenly increased (as denoted by the red vertical arrow in Fig. 7-4 and shown in Fig. 7-4c). After such a perturbation in population density of external metabolisers, the selfish population shifts towards being cooperative (Fig. 7-4b & Fig. 7-4d). Similar shift between the two types of population may occur if to perturb the dilution rate D (Fig. 7-5). A selfish population of internal metabolisers exposed to a small decrease in the dilution rate D, may become cooperative (Fig. 7-5a - Fig. 7-5c). Alternatively an initially cooperative population of external metabolisers subject to a small increase in the dilution rate D may switch into a selfish one (Fig. 7-5d - Fig. 7-5f). Although in our simulation, the perturbed population eventually stabilises as a population of internal metabolisers, in undergoes a critical decrease in the total population density (Fig. 7-5f). In nature, such a decrease of population density means an extreme risk of extinction of the whole microbial community.

Are there any dilution rates which would select for the phenotypes which are able to uptake both sucrose and hexose? We study the optimal phenotypes for a range of dilution rates and interestingly it turns out that, regardless of the dilution rate, the population can be only dominated by the perfect external or perfect internal metabolisers. (Fig. 7-6). As discussed previously, there is a range of dilution rates, which select either for external or internal metabolisers depending on the initial conditions. However, a change in dilution rate may also result in a shift between the population dominated by the perfect external metaboliser and a population dominated by the perfect internal metaboliser. Moreover, the shift between these two types of population is sharp: the distribution of the population density into the phenotypes switches directly between the one dominated by internal and the one dominated by external metabolisers (as shown by the red vertical arrows in Fig. 7-6). In other words, the dominance of intermediate phenotypes, which would be able to digest sucrose internally and externally at the same time (having intermediate values of V^H_{max}), is not possible at any range of dilution rates D. This observation seems to be consistent with the natural systems in which, according to our knowledge, species specialise either in the external (as *S. cerevisiae* or *M. oryzae*) or internal (such as *U. maydis*) sucrose digestion.

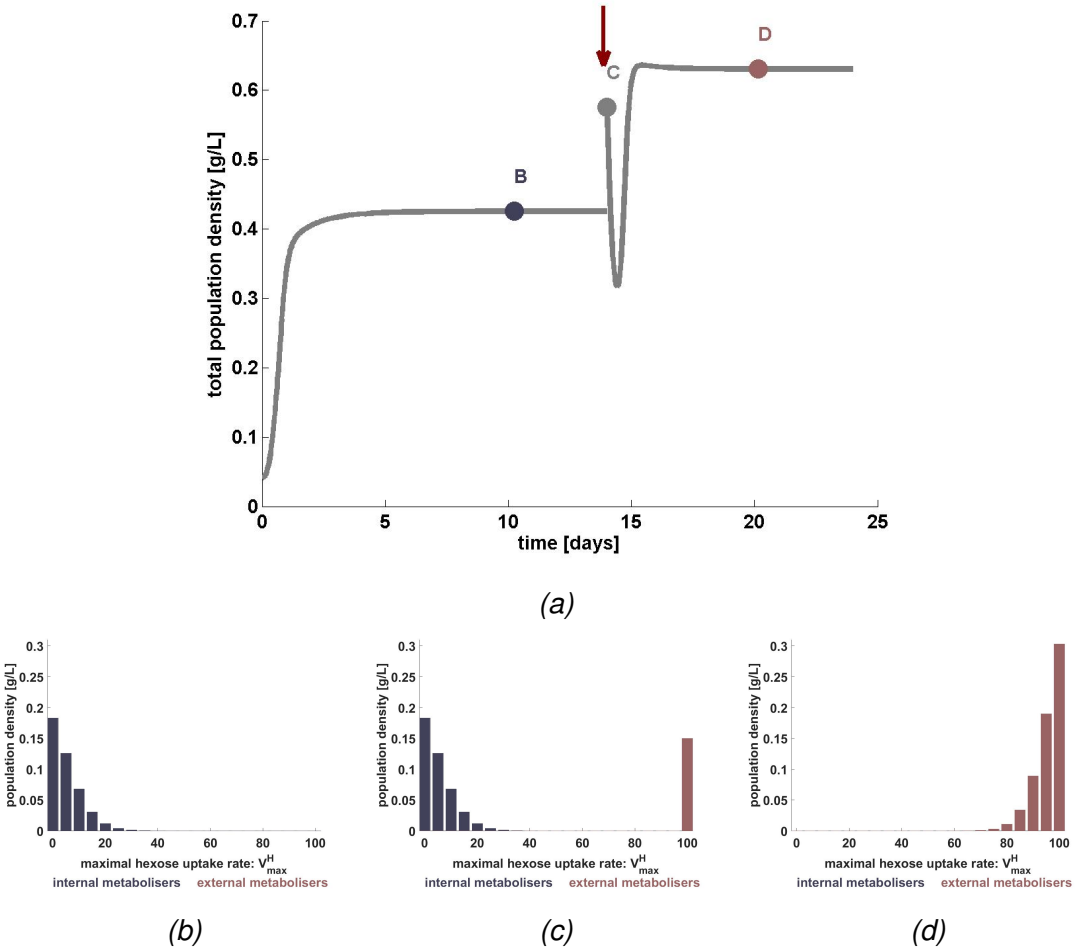

Figure 7-4: **Critical shift after a perturbation in the population density of external metabolisers.**
The perturbation (a sudden increase in the density of external metabolisers) is indicted with the red vertical arrow in Fig 7-4a.
The brown lines and plots indicate populations dominated by external metabolisers, whereas the blue lines and plots indicate populations dominated by internal metabolisers. The individuals with maximal hexose uptake rate $V^H_{max} = 0$ are the perfect internal metabolisers, while the individuals with maximal hexose uptake rate $V^H_{max} = 100$ are the perfect external metabolisers.
(7-4a): total population density before and after the perturbation respectively;
(7-4b) - (7-4d): distributions of population density $P^*\mathbf{f}^*$ into the phenotypes, at the time points denoted in the Fig. 7-4a by: (7-4b): B; (7-4c): C, (7-4d): D, i.e. before and after the perturbation. In particular, Fig. (7-4c) shows the population density distribution just after the perturbation. Each bar represents the density of one particular phenotype: $P^* f_i$.
The simulations were performed at dilution rate $D = 0.38$ [1/hour].

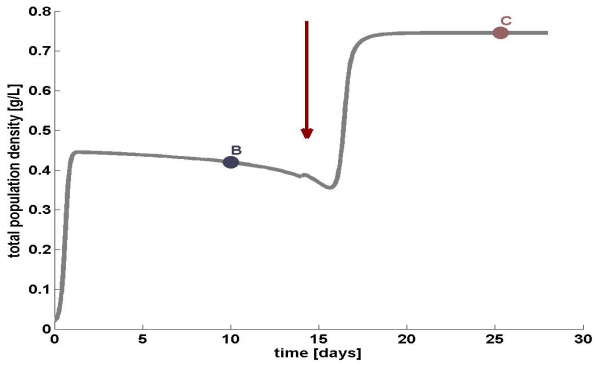
total population density [g/L]
time [days]
B
C

(a)

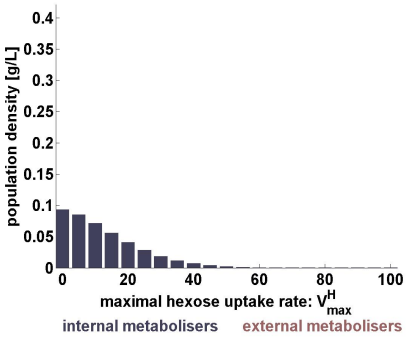
population density [g/L]
maximal hexose uptake rate: V^H_{max}
internal metabolisers
external metabolisers

(b)

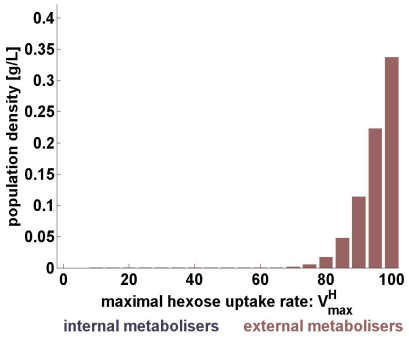
population density [g/L]
maximal hexose uptake rate: V^H_{max}
internal metabolisers
external metabolisers

(c)

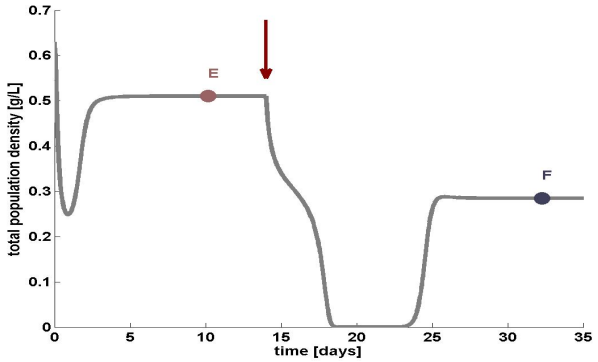
total population density [g/L]
time [days]
E
F

(d)

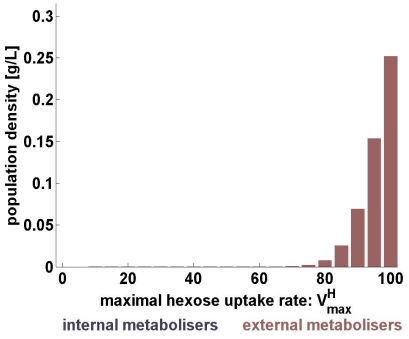
population density [g/L]
maximal hexose uptake rate: V^H_{max}
internal metabolisers
external metabolisers

(e)

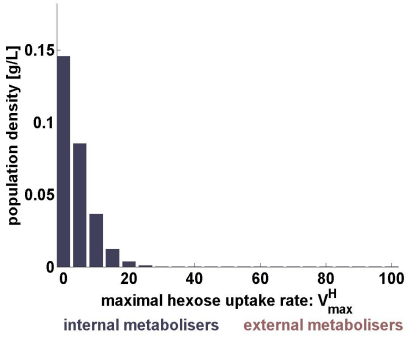
population density [g/L]
maximal hexose uptake rate: V^H_{max}
internal metabolisers
external metabolisers

(f)

Figure 7-5: **Critical shifts after perturbations in the dilution rate.**
The brown lines and plots indicate populations dominated by external metabolisers, whereas the blue lines and plots indicate populations dominated by internal metabolisers. The individuals with maximal hexose uptake rate $V_{max}^H = 0$ are the perfect internal metabolisers, while the individuals with maximal hexose uptake rate $V_{max}^H = 100$ are the perfect external metabolisers.
Perturbations are indicted with the red vertical arrow in Fig. 7-5a and Fig. 7-5d.
(7-5a): total population density before and after perturbation in dilution rate from $D = 0.31$ [1/hour] to $D = 0.30$ [1/hour];
(7-5b) - (7-5d): distribution of the population density $P^*\mathbf{f}^*$ into phenotypes, at the time points denoted in the Fig. 7-5a by: (7-5b): B; (7-5c): C, i.e. before and after the perturbation, respectively. Each bar represents the density of one particular phenotype: $P^* f_i$.
(7-5e): total population density before and after perturbation in dilution rate from $D = 0.44$ [1/hour] to $D = 0.445$ [1/hour];
(7-5e) - (7-5f): distribution of the population density $P^*\mathbf{f}^*$ into phenotypes, at the time points denoted in the Fig. 7-5d by: (7-5e): E; (7-5f): F, i.e. before and after the perturbation, respectively. Each bar represents the density of one particular phenotype: $P^* f_i$.

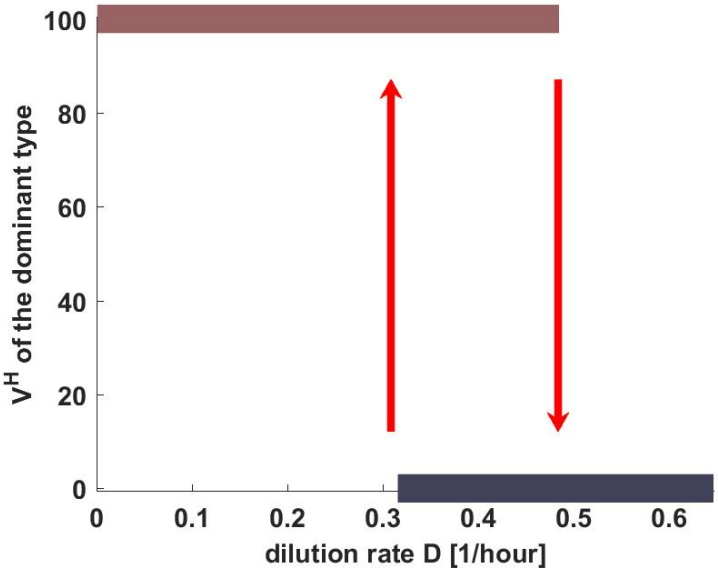

Figure 7-6: **The dominant phenotype in the population under mutation-selection balance depending on the chemostat dilution rate D.**
The maximal hexose uptake rate V_{max}^H of the dominant phenotype in the stable populations whose total densities are shown in the Fig. 7-1a. For intermediate dilution rates, there may be two optimal values of V_{max}^H: depending on the initial conditions (brown corresponding to the cooperative equilibria branch plotted in Fig. 7-1a, and blue corresponding to the selfish equilibria branch plotted in Fig. 7-1a). The transition between the dominant types, depending on the dilution rates, is sharp, which means that a small change in dilution rate may result in a significant shift between the dominant type in the population, as shown by the red vertical arrows.

Another interesting trait of our system, is the non-monotonous relation between the biodiversity and the total population density (Fig. 7-7a). Although, a decrease in the dilution rate results in higher total population density (Fig. 7-7b), it may also result in a decrease in the biological diversity. ('F' to 'E' in Fig. 7-7c). Let us consider a sparse population of internal metabolisers at the edge of its equilibria branch, that is at the dilution rate around $D = 0.31$ [1/hour] (denoted by the point 'F' in Fig 7-7b, and with the population density distribution shown in Fig. 7-7f). In such a case. a small decrease in the dilution rate may result in a dilution rate D that supports only one stable equilibrium: a cooperative population of external metabolisers (brown line in Fig. 7-7b). Then our selfish population (with the population density distribution shown in Fig. 7-7f) will turn into dense and a ccoperative one (denoted by the point 'E' in Fig 7-7b, and with the population density distribution shown in Fig. 7-7e), with a much narrower population density distribution $P^*\mathbf{f}^*$, that is, less diverse. Thus, a shift from one equilibria branch to another (internal to external metabolisers), may result in a shift in the diversity.

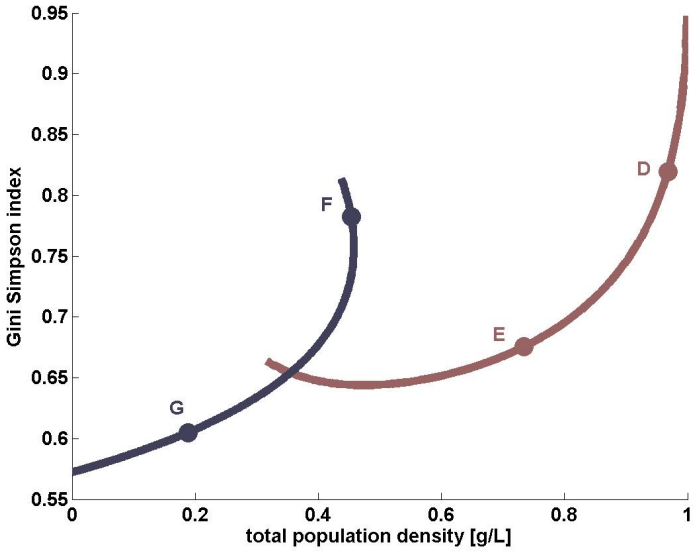
Gini Simpson index
total population density [g/L]
D
E
F
G

(a)

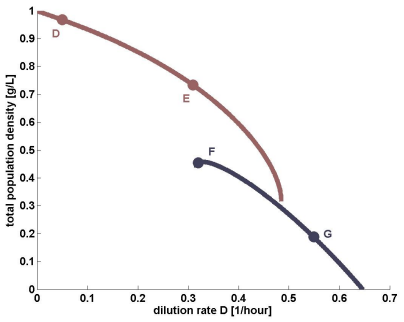
total population density [g/L]
dilution rate D [1/hour]
D
E
F
G

(b)

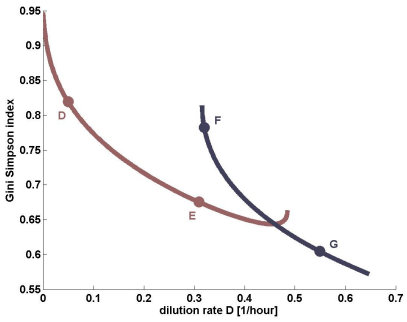
Gini Simpson index
dilution rate D [1/hour]
D
E
F
G

(c)

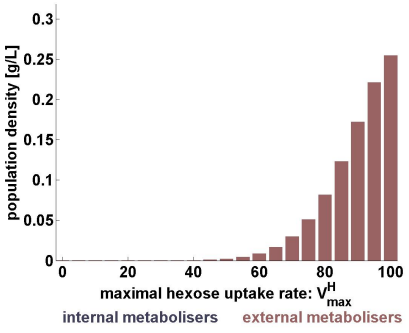
population density [g/L]
maximal hexose uptake rate: V^H_{max}
internal metabolisers
external metabolisers

(d)

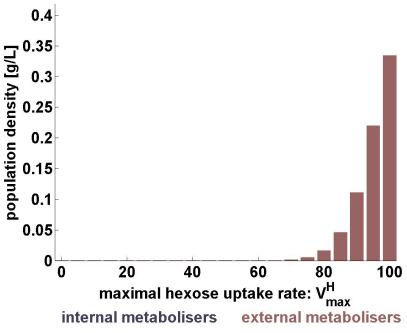
population density [g/L]
maximal hexose uptake rate: V^H_{max}
internal metabolisers
external metabolisers

(e)

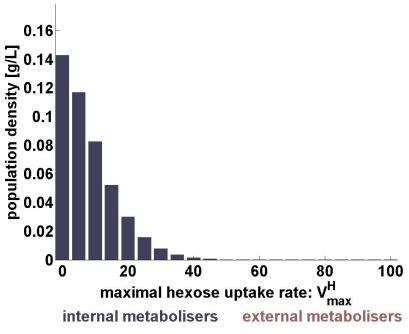
population density [g/L]
maximal hexose uptake rate: V^H_{max}
internal metabolisers
external metabolisers

(f)

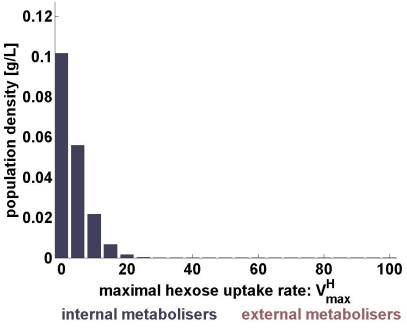
population density [g/L]
maximal hexose uptake rate: V^H_{max}
internal metabolisers
external metabolisers

(g)

Figure 7-7: **Biological diversity depending on the dilution rate D.**
The biodiversity in a population may not be a monotonous function of population density. This phenomenological result can be explained by looking at the influence of dilution rate D on the resulting total population density and on the biodiversity measure: Gini-Simpson index, defined as $GS = 1 - \sum_{i=1}^{N} f_i^2$.
The brown lines and plots indicate populations dominated by external metabolisers, whereas the blue lines and plots indicate populations dominated by internal metabolisers. The individuals with maximal hexose uptake rate $V_{max}^H = 0$ are the perfect internal metabolisers, while the individuals with maximal hexose uptake rate $V_{max}^H = 100$ are the perfect external metabolisers.
(7-7a): Gini-Simpson index for the population at stable equilibrium, depending on total population density.
(7-7b): total population density of the population at stable equilibrium, depending on the dilution rate D.
(7-7c): Gini-Simpson index for the population at stable equilibrium, depending on the dilution rate D.
(7-7d)-(7-7g): distributions of the population density $P^*\mathbf{f}^*$ into phenotypes, at various dilution rates D, denoted in the Fig. 7-7a by: (7-7d: D; (7-7e: E; (7-7f: F; (7-7g: G. Each bar represents the density of one particular phenotype: $P^* f_i$.

7.3.2 Simplified models

We verify if our results are specific to the number of considered phenotypes N. Here we compute all the steady states for the simplified system, with $N = 3$. This means we assume there are only three possible phenotypes, that are significantly different from each other: $V^H_{max}(1) = 0$, $V^H_{max}(2) = B/2$, $V^H_{max}(3) = B$, and the mutations cause switches between these three phenotypes with probabilities $\epsilon/2$ for the phenotypes 1 and 3, and ϵ for the phenotype 2. We keep the linear hexose-sucrose uptake trade-off assumption $h(V^H_{max}) = B - V^H_{max}$, and therefore $V^S_{max}(1) = h(V^H_{max}(1)) = B$, $V^S_{max}(2) = h(V^H_{max}(2)) = B/2$, $V^S_{max}(3) = h(V^H_{max}(3)) = 0$.

The positive steady states of such simplified system are presented in Fig. 7-8a. These results preserve our main conclusion. Namely, low dilution rates select for dense and cooperative populations, i.e. the populations composed of the external metabolisers (Fig. 7-8b and brown line in Fig. 7-8a), the large dilution rates select for sparse and selfish populations composed of internal metabolisers (Fig. 7-8e and blue line in Fig. 7-8a), and there is a range of intermediate dilution rates that result in bistability (7-8a). In that case the population may be either dense and cooperative or sparse and selfish (7-8c-7-8d), depending on the initial conditions. Moreover, similarly as in the main model, we observe that the dominance of phenotypes that would be able to uptake hexose and sucrose at the same time is not allowed (Fig. 7-9). Instead, a perturbation in dilution rate may lead to a shift between the population dominated by the perfect external metaboliser and the one dominated by the perfect internal metaboliser (as shown by the red vertical arrows in Fig. 7-9),

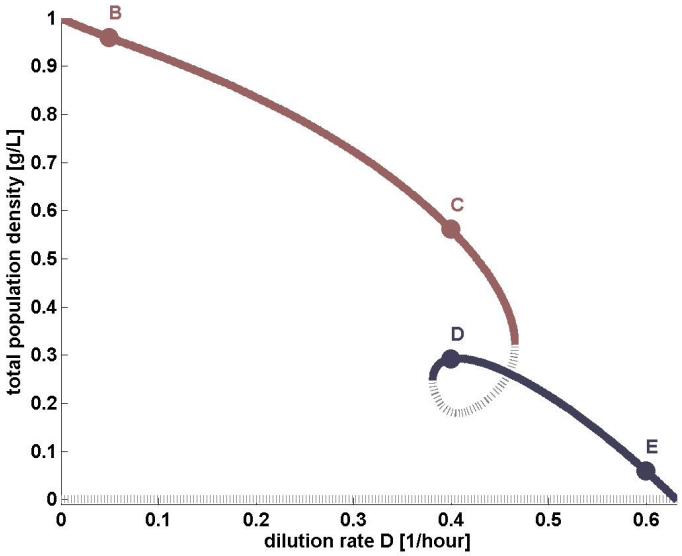
B
C
D
E
total population density [g/L]
dilution rate D [1/hour]
0
0.1
0.2
0.3
0.4
0.5
0.6
0.7
0.8
0.9
1

(a)

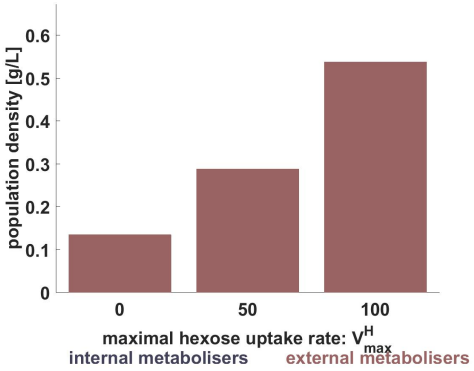
population density [g/L]
0
0.1
0.2
0.3
0.4
0.5
0.6
0
50
100
maximal hexose uptake rate: V^H_{max}
internal metabolisers
external metabolisers

(b)

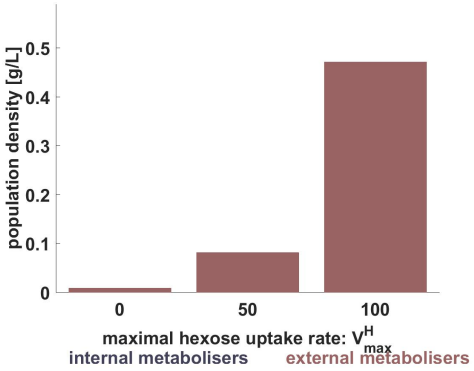
population density [g/L]
0
0.1
0.2
0.3
0.4
0.5
0
50
100
maximal hexose uptake rate: V^H_{max}
internal metabolisers
external metabolisers

(c)

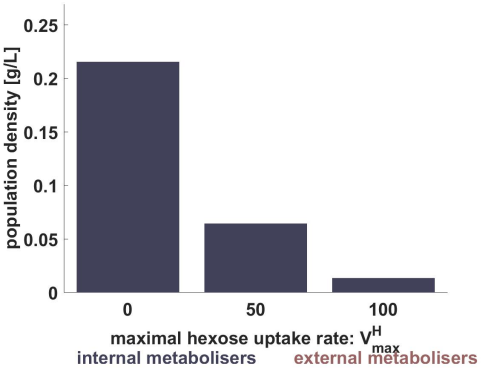
population density [g/L]
0
0.05
0.1
0.15
0.2
0.25
0
50
100
maximal hexose uptake rate: V^H_{max}
internal metabolisers
external metabolisers

(d)

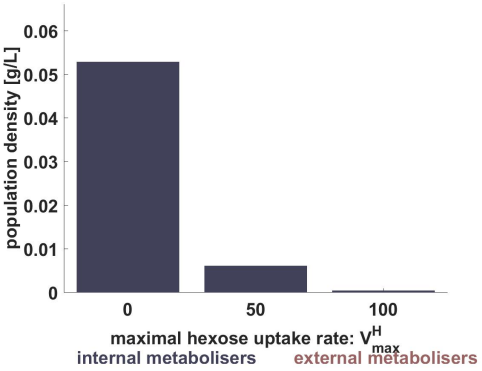
population density [g/L]
0
0.01
0.02
0.03
0.04
0.05
0.06
0
50
100
maximal hexose uptake rate: V^H_{max}
internal metabolisers
external metabolisers

(e)

Figure 7-8: **Positive steady states in the mutation-selection model with only three phenotypes ($N = 3$).**
The brown lines and plots indicate populations dominated by external metabolisers, whereas the blue lines and plots indicate populations dominated by internal metabolisers. The individuals with maximal hexose uptake rate $V_{max}^H = 0$ are the perfect internal metabolisers, while the individuals with maximal hexose uptake rate $V_{max}^H = 100$ are the perfect external metabolisers.
(7-8a) The total population density P^*, depending on the dilution rate D. The stable steady states are denoted by solid lines, while the unstable steady states are denoted by dashed lines. (7-8b)-(7-8e): distributions of the population density ($P^*\mathbf{f}^*$) into phenotypes, for (7-8b) low and (7-8e) high dilution rates, denoted in Fig. 7-8a by 'B' and 'E', respectively.
The figures (7-8c)-(7-8d) show the population density distribution at the same intermediate dilution rate, but two distinct equilibria branches, denoted in Fig. 7-8a by 'C' and 'D', respectively. Each bar represents the density of one particular phenotype: $P^* f_i$.

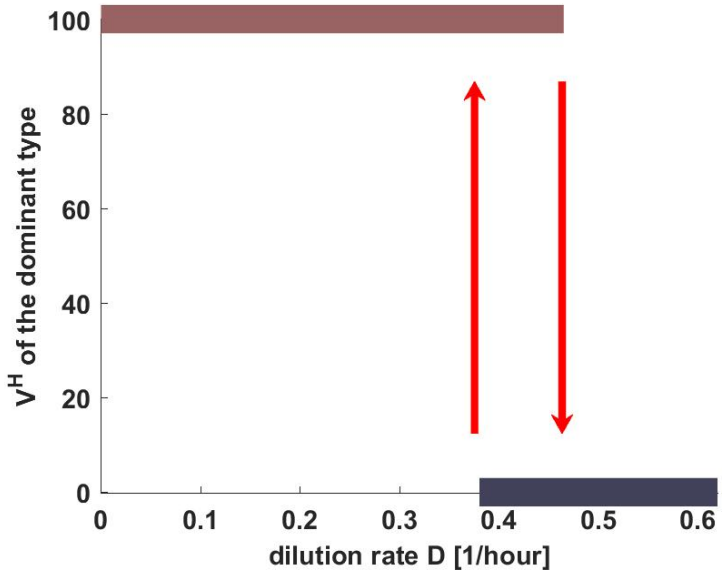

Figure 7-9: **The dominant phenotype in the population under mutation-selection balance depending on the chemostat dilution rate D, model with only three phenotypes ($N = 3$).**
The maximal hexose uptake rate V_{max}^H of the dominant phenotype in the stable populations whose total densities are shown in the Fig. 7-8a. For intermediate dilution rates, there may be two optimal values of V_{max}^H: depending on the initial conditions (brown corresponding to the cooperative equilibria branch plotted in Fig. 7-8a, and blue corresponding to the selfish equilibria branch plotted in Fig. 7-8a). The transitions between the dominant types, depending on the dilution rates, is sharp, which means that a small change in dilution rate may result in a significant shift between the dominant type in the population, as shown by the red vertical arrows.

We have also analysed a simplified and purely ecological model, in which there is no mutation ($\epsilon = 0$), and only two phenotypes are considered ($N = 2$): perfect internal metabolisers ($V^H_{max}(1) = 0$ and $V^S_{max}(1) = B$) and perfect external metabolisers ($V^H_{max}(2) = B$ and $V^S_{max}(2) = 0$). According to this model, the external metabolisers are not able to persist at high dilution rates (Fig. 7-10). Moreover, if started with sufficiently low population density, they will go extinct (as predicted previously for the externally digesting *S. cerevisiae* in [1, 93] and in Chapter 5). Nonetheless, at low dilution rates their stable population density is higher than the stable population density of the selfish internal metabolisers (Fig. 7-10). There is also a big range of bistability (Fig. 7-10), where the population composed of both types may converge to be entirely selfish or cooperative depending on the initial conditions. While, both of the populations types are locally stable, the coexistence between these two types is unstable (Fig. 7-10).

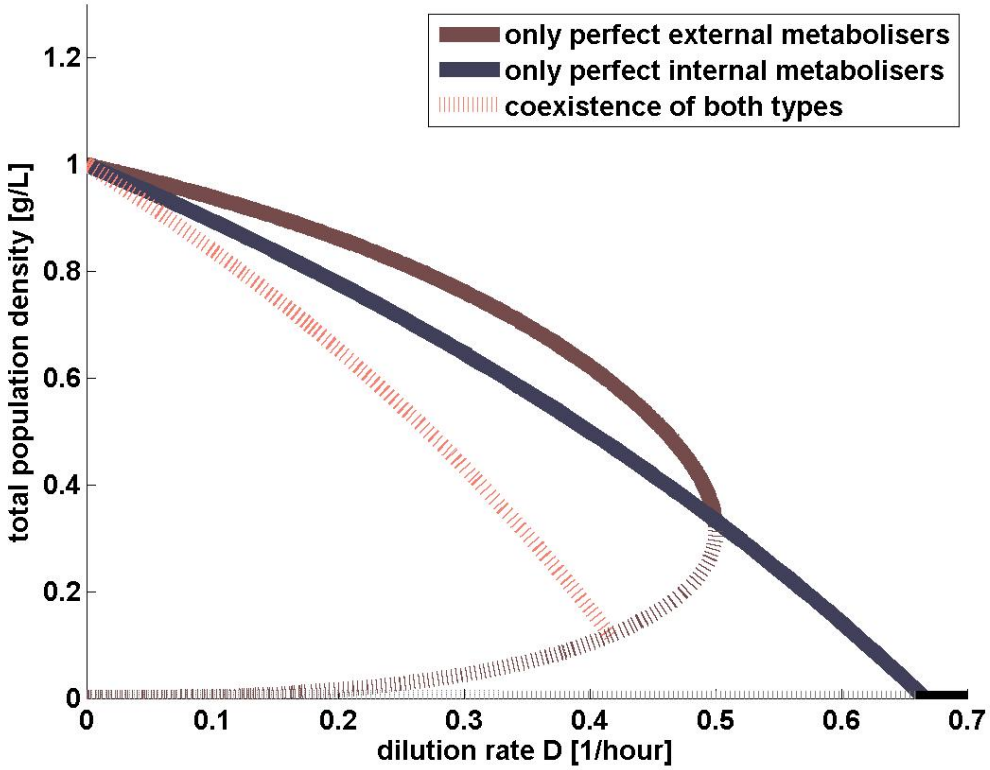

Figure 7-10: **Positive steady states in the simplified system with no mutations ($N = 2$, $\epsilon = 0$).** The stable steady states are denoted by solid lines, while the unstable steady states are denoted by dashed lines.

7.3.3 Other shapes of the hexose-sucrose uptake trade-off

The shapes of trade-offs are well known to play a crucial role in biological systems, especially in those, where the ecology and evolution could be considered in the same timescale, and therefore the ecological interactions are crucial for the direction of evolution [51, 53, 168].

To test the robustness of our results, which so far have been computed for a linear trade-off $h(V^H_{max}) = B - V^H_{max}$, here we recalculate the positive steady states of the model (7.2.1)-(7.2.4) assuming various nonlinear shapes of the hexose - sucrose uptake trade-off h, that is: concave (Fig. 7-11b), convex (Fig. 7-11c), sigmoidal (Fig. 7-11e), and cubic (Fig. 7-11e). Although the rage of bistability differs depending on the trade-off shape (Fig. 7-12), qualitatively the results represent the same phenomenon: whereas at low dilution rates, the population is cooperative and composed of external metabolisers, for sufficiently high dilution rates, the population is 'selfish' and composed of internal metabolisers (Fig. 7-12). Moreover, there may be a range of dilution rates, at which both equilibria branches are stable, meaning that either external or internal metabolisers can dominate (Fig. 7-12a, Fig. 7-12c - 7-12e), depending on history of the system. The dominance of one or another type depends on the initial conditions, and it may change with a perturbation in population density or composition.

Are there any dilution rates that allow for dominance of the phenotypes which uptake hexose and sucrose at the same time? $(0 < V^H_{max} < B)$ For some of the trade-off shapes there is a narrow range of dilution rates at which such phenotypes can stably dominate in the population (Fig. 7-13b & Fig. 7-13d). However, even in those cases, a small change in the dilution rate may result in a sudden shift between the population dominated by intermediate phenotype and the one dominated by the perfect internal (Fig. 7-13b) or perfect external metaboliser (Fig. 7-13d). For the other considered shapes of trade-off, the dominant phenotypes shift directly between the perfect internal and the prefect external metabolisers, not allowing for the dominance of any phenotype with intermediate hexose and sucrose uptakes (Fig. 7-13a, Fig. 7-13c & Fig. 7-13e). Thus, regardless of the trade-off shape, the transition between the cooperative and selfish populations is sharp, meaning that a small change in dilution rate may result in a large change

in the dominant phenotype. This means that the dilution rate can be treated as a disturbance factor, because its perturbations may lead to major ecological shifts (the shift between the two different types of populations: selfish and cooperative).

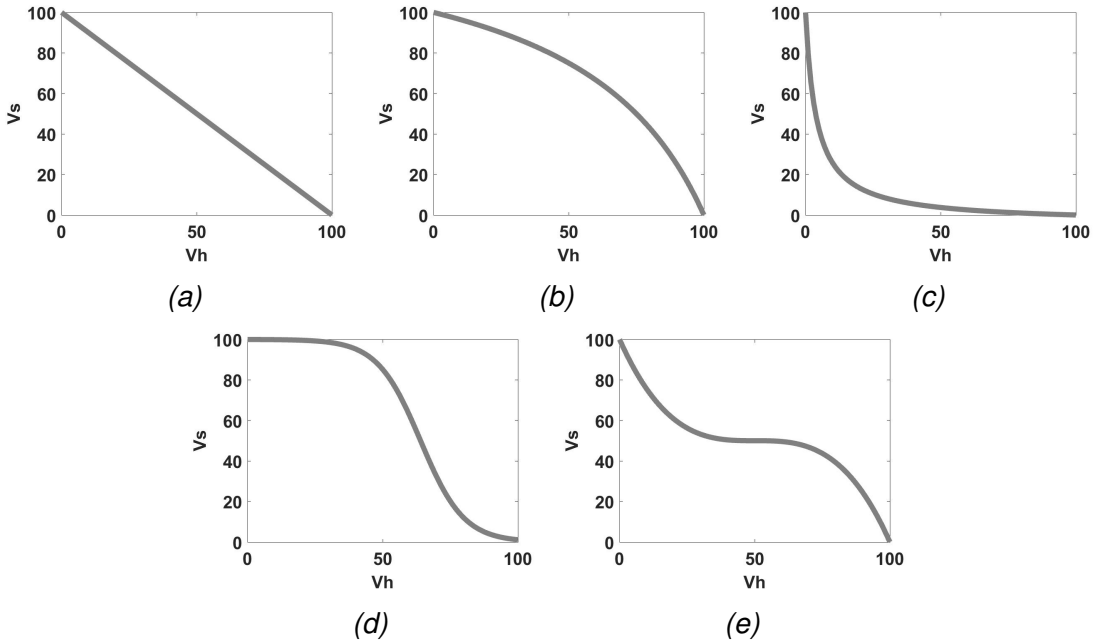

Figure 7-11: **Considered shapes of the hexose-sucrose uptake trade-off.**
(7-11a) linear trade-off: $V^S_{max} = f(V^H_{max}) = B - V^H_{max}$
(7-11b) concave trade-off: $V^S_{max} = f(V^H_{max}) = 1.5((V^H_{max} - 100)/(V^H_{max} - 150))$
(7-11c) convex trade-off: $V^S_{max} = f(V^H_{max}) = -4(V^H_{max} - 100)/(V^H_{max} + 4)$
(7-11d) sigmoidal trade-off: $V^S_{max} = f(V^H_{max}) = 100/(1 + \exp(-8(1 - V^H_{max}/64)))$
(7-11e) cubic trade-off: $V^S_{max} = f(V^H_{max}) = -4 \cdot 10^{-4}((V^H_{max} - 50)^3) + 50$

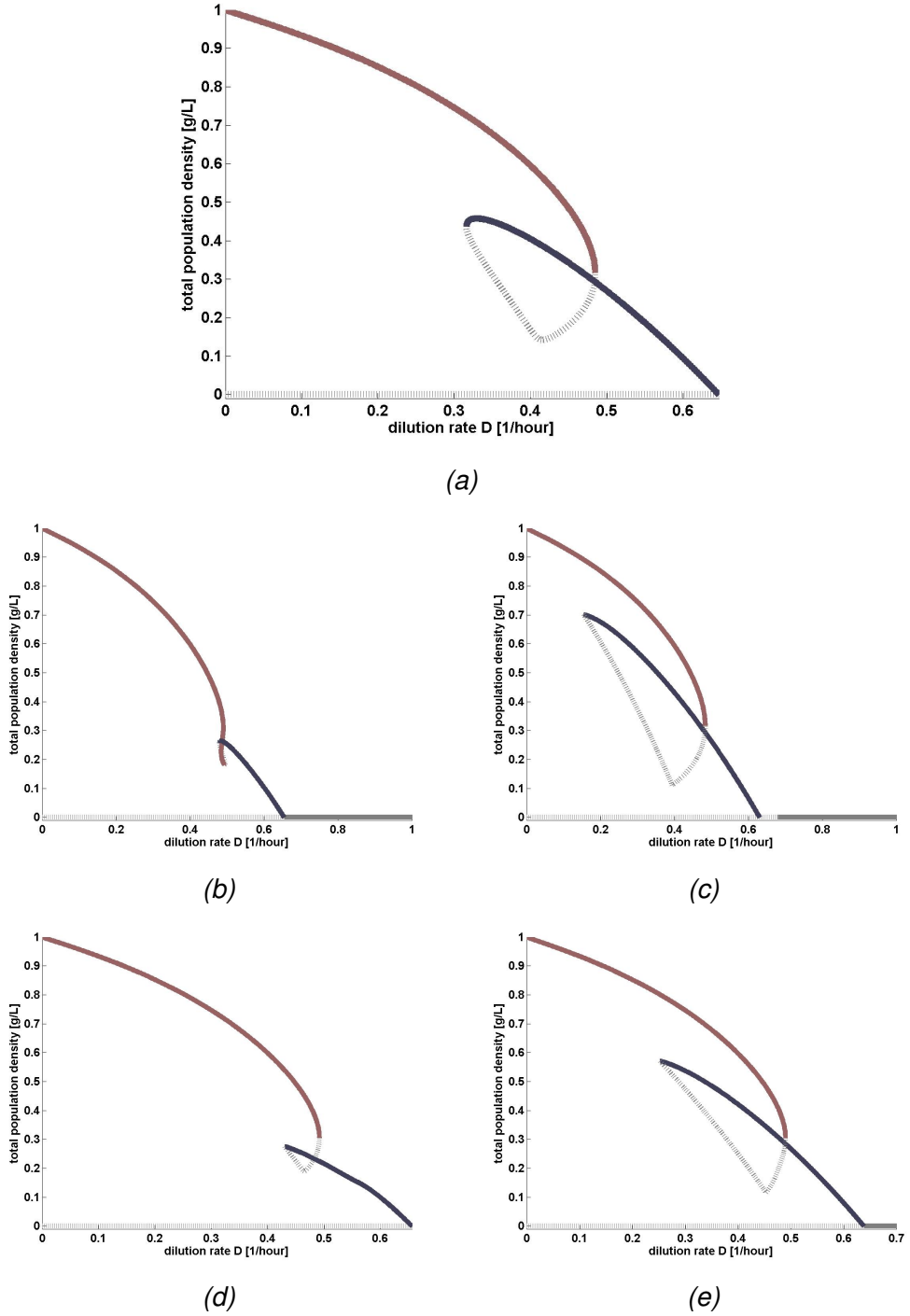

Figure 7-12: **Positive steady states of a population under mutation-selection balance, for various shapes of trade-off.**
The brown lines indicate populations dominated by external metabolisers, whereas the blue lines indicate populations dominated by internal metabolisers. The steady states have been calculated, for: (7-12a) linear trade-off (the default, used to generate Fig. 7-1 - 7-10), (7-12b) concave trade-off, (7-12c) convex trade-off, (7-12d) sigmoidal trade-off, (7-12e) cubic trade-off. The stable steady states are denoted by solid lines, while the unstable steady states are denoted by dashed lines.

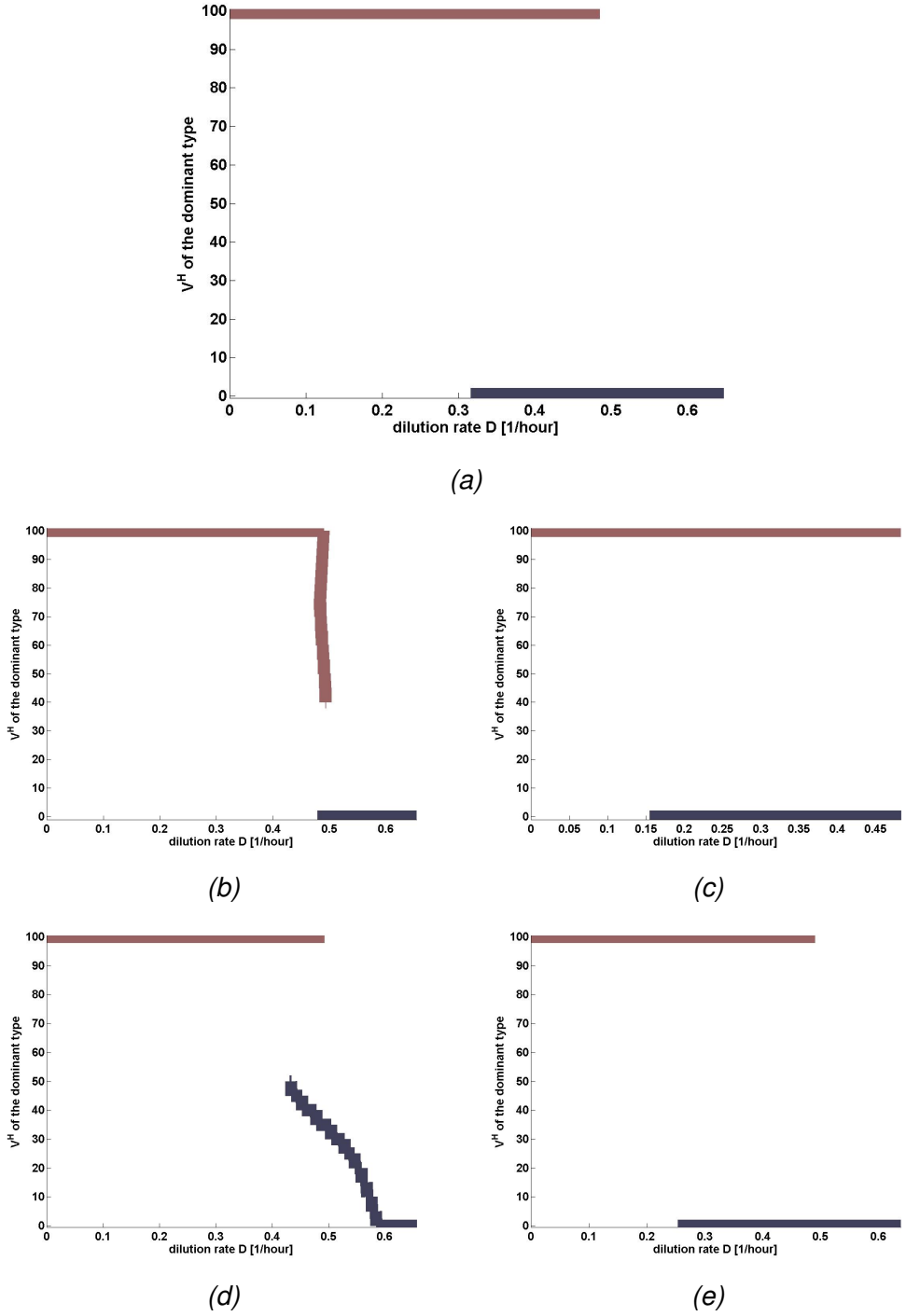

Figure 7-13: **The dominant phenotype in the population under mutation-selection balance depending on the chemostat dilution rate D, for various shapes of trade-off.**

The figures (7-13a)-(7-13e) represent the maximal hexose uptake rate V_{max}^H of the dominant phenotype in the stable populations whose total densities are shown in the Fig. 7-12. For intermediate dilution rates, there may be two optimal values of V_{max}^H: depending on the initial conditions (brown corresponding to the cooperative equilibria branch plotted in Fig. 7-12, and blue corresponding to the selfish equilibria branch plotted in Fig. 7-12). The transitions between the dominant types, depending on the dilution rates, is sharp, which means that a small change in dilution rate may result in a large shift between the dominant type in the population. The dominant types have been obtained for: (7-13a) linear trade-off (the default, used to generate Figures 7-1 - 7-10), (7-13b) concave trade-off, (7-13c) convex trade-off, (7-13d) sigmoidal trade-off, (7-13e) cubic trade-off.

7.4 Discussion

We studied some ecological factors that determine the evolution of our microbial system towards external and cooperative or internal and selfish digestion. In order to do that we deployed a mutation-selection model set in the ecological context of resource competition in a continuous culture (chemostat).

Although we based our model on the system of *S. cerevisiae* (described in more detail in Chapter 2: Methods), which is known to perform external digestion, here we considered a whole range of different feeding strategies: varying from perfectly external to perfectly internal digestion. Thus we generalise our model to an abstract population which in course of evolution may develop either external or internal metabolism, and we aim to study how different ecological factors affect that evolution. In other words, we are trying to understand what may be the ecological factors that led some species to evolve towards external metabolism (for example: *S. cerevisiae*, *M. oryzae*, or *V. cholerae*), and some others to evolve towards internal metabolism (for example: *U. maydis*).

Although external digestion is prone to being exploited by other organisms in their neighborhood [32, 61–64], and to loss of resources due to diffusion [1], it also has a number of advantages. For example, as discussed in [70], it allows for a greater control over substances entering the cell (and therefore it decreases the risk of infection), and it gives a bigger chance to match the enzyme production to particular needs. From the point of view of the resource acquisition only, is one of the feeding strategies more likely to be selected for in the course of evolution? Does the competitiveness of external and internal feeding depend on th environmental conditions? In Chapter 6 we considered two distinct strains: one performing perfectly external digestion, and one with an ability to digest internally. We showed that resource concentration and population density determine the competitiveness of the external metabolisers to the other strain. Here we consider a wider range of different feeding strategies, and we study which of these strategies is selected for in the course of evolution, depending on yet another environmental factor: chemostat dilution rate. This parameter, specific for continuous cultures, describes the rate of influx of the resource into the chemostat culture, and the rate

of washout of the content of the culture. The dilution rate may be also treated as a continuous counterpart of the dilution factor applied to the experimental set-up of serial dilutions. In such a case, it is sometimes understood as the mortality rate [93].

The results show that the chemostat dilution rate is the crucial factor for the evolution of cooperative or selfish systems. While low dilution rates favour the cooperative organisms relying on the external metabolism, high dilution rates favour the individuals that metabolise internally.

We have simulated the population behaviour assuming various shapes of the trade-off between the sucrose and hexose uptake. Interestingly, for any of the studied trade-off shapes, the internal metaboliser could not stably coexist with the external metaboliser (meaning the presence of two local maxima in the population density distribution $P^*\mathbf{f}^*$). On one hand it is possible that more trade-offs are needed to extend the parameter ranges allowing for such coexistence [54]. On the other hand, the sigmoidal and cubic trade-offs we consider do allow for multiple local maxima in the growth rate, which was sufficient for biodiversity in [53, 54]. Why in our study cannot we observe coexistence of internal and external metabolisers? The specific feature of our system is that the environmental conditions are remarkably dependent on the composition of population. If the external metabolisers dominate in the culture, they will convert sucrose into hexose, and thus they will not allow for an invasion of the internal metaboliser types who feed on sucrose. Contrarily, if an internal metaboliser type dominates in the culture, it will deplete the sucrose in the environment before the potential external metabolisers are able to digest it extracellularly. Thus the relative fitness of external metabolisers is positively correlated with their frequency, which is known as 'positive frequency dependence', and it leads to bistability (as studied in more detail in Chapter 6). Notably, in our system we do not consider any form of cheating, as in the previous chapters. In this case various phenotypes compete for sucrose in order to metabolise it, using either internal or external metabolic pathways. Moreover, these pathways affect the environment: the external digestion of sucrose, converts sucrose into hexose, making the growth only on sucrose impossible, and the internal digestion depletes sucrose quickly, making the slow invertase production unprofitable. We believe that this environmental feedback can explain the fact that stable coexistence of the external and internal metabolisers

is much more difficult to observe in our systems than in the classical cooperator-cheat systems (as eg [14, 32]).

We also believe that our results represent what happens in natural systems, where according to our knowledge, the organisms within the same species either develop internal or external digestion, not allowing for coexistence of subpopulations with two significantly different feeding strategies.

For a range of dilution rates, our system instead of leading to coexistence, turns out to be bistable. At these dilution rates the population may become either selfish (with the dominant type being the perfect internal metaboliser, which does not secrete public goods and it uptakes sucrose directly) or cooperative (with the dominant type being the perfect external metaboliser, which secretes the public good and digests sucrose only extracellularly) depending on the initial conditions. This result holds for various shapes of trade-off between the resource uptakes (Fig. 7-12).

Varying the dilution rate D may lead to a shift in the dominant phenotype in the population. Interestingly, that shift is sharp, meaning that a small change in the dilution rate results in a a significant shift between the dominant phenotypes in the population (Fig. 7-13). Such sharp transition between selfish and cooperative cultures, is in line with the study [154] which reported that, when public good production and multicellularity evolve jointly, a small change in the genetic relatedness between the cells may lead to a sharp transition between the evolutionary outcomes: from multicellular and cooperative to sparse and 'selfish' populations which do not secrete any public goods. Although we do not model multicellularity explicitly, motivated by [1], we argue that multicellularity may be one of the strategies to increase the hexose uptake. Thus we generalise the result obtained in [154], by not only considering multicellularity, but any possible mechanism by which the hexose uptake changes. Apart from forming multicellular groups it could be also other mechanisms such as hexose transporter multiplication. Thus our result holds for the joint evolution of public good production and any strategy of improved hexose uptake.

We showed that for any of the considered shapes of the hexose-sucrose uptake trade-off, dilution rate can be treated as a disturbance factor, because its perturbation may lead to an abrupt shift between two types of population: cooperative and selfish. The disturbance in the population composition may be of special

relevance to natural systems of pathogens that potentially form cooperative structures. In these systems the dilution rate naturally varies (for example an increase in the water flow in aquatic environments, the natural habitat of *V. cholerae*, may be understood as an increase in the dilution rate). In such a case, an increase in the dilution rate may result in a shift between the cooperative and selfish populations. Moreover, at a range of dilution rates, there is a risk of swapping between these two states, due to random events. For example, a small increase in the population density may result in a shift towards the cooperative population (Fig. 7-4), which is able to grow to much higher total densities than the selfish one (see Fig. 7-10 illustrating the dynamics of each of the types, in a short time-scale, that in absence of mutation $\epsilon = 0$).

Similarly, a small change in the dilution rate may lead to a switch between the cooperative and selfish population types (Fig. 7-5). Moreover, even when the dilution rate comes back to its previous value, this process may not revert. This is because of the hysteresis phenomenon (see eg. [50]): there are multiple possible stable equilibria for a given dilution rate (as shown in Fig. 7-1a), and the equilibrium at which the system will stabilise, depends on the history of the system. For instance if a population started as selfish (point 'C' on the blue line in Fig. 7-1a) is affected by a decrease in the dilution rate, it will be taken into the region, in which only one stable equilibrium is allowed: the dense and cooperative population (brown line in Fig. 7-1a). Thus the total population density and its structure will 'jump' towards the new equilibrium. However, if the dilution rate will be increased again, the equilibrium state will not jump back towards the previous one, but it will move along the brown curve in Fig. 7-1a.

We also show that the switch between cooperative and selfish culture implies a change in the biodiversity. It is believed that the small populations show lower levels of biodiversity, because of the genetic drift [169]. This phenomenon has also been reported in natural systems, in which small populations have smaller diversity and therefore are prone to extinction (review in [170]). Contrary to this, in our system, a shift from cooperative to selfish behaviour results in a drop in the total population density, and therefore population size, which counter-intuitively is followed by an increase in the diversity. This means that the biological diversity may not be correlated with the population size, as tends to be believed [164, 165]. In population genetics it is known that there are factors that may invert the

relationship between population density and diversity: such as migration or the loss of heterozygosity in diploid populations. However, in our system the only reason for a shift in biodiversity is the change of the environment: from the one created by external metabolisers which digest sucrose externally and therefore supply the environment with large quantities of simple sugars, to the one created by the internal metabolisers, which uptake sucrose directly, and therefore do not lead to appearance of any other resources in the environment. This highlights that the ecological features may be determinative of the diversity and that estimating the population size based on genetic diversity as in [166, 167] may not always be accurate.

7.5 Supplementary Material

7.5.1 Dependence on the mutation rate ϵ

The stable states of the system (7.2.1)-(7.2.4) depend on the mutation rate parameter ϵ. The lower the mutation rates, the larger the bistability region, and the larger the range of dilution rates D, at which internal metabolisers can dominate the population (Fig 7-14).

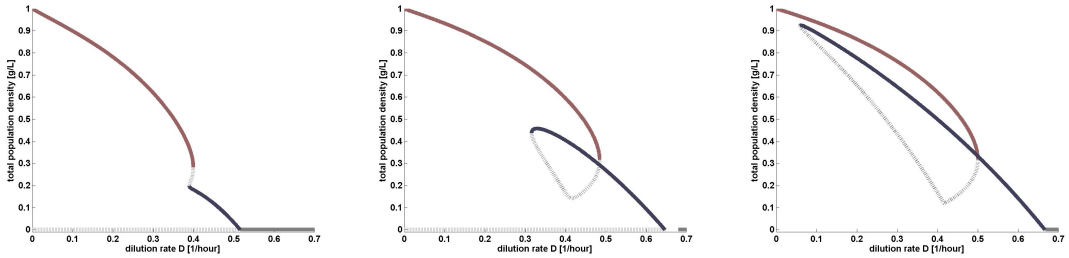

(a) *(b)* *(c)*

Supplementary Figure 7-14: **Positive steady states of a population under mutation-selection balance, for various mutation rates ϵ.**
The brown lines indicate populations dominated by external metabolisers, whereas the blue lines indicate populations dominated by internal metabolisers.
7-14a: $\epsilon = 8$ [1/hour], 7-14b: $\epsilon = 8 \cdot 10^{-2}$ [1/hour], 7-14c: $\epsilon = 8 \cdot 10^{-5}$ [1/hour].
Here we assume the linear shape of the hexose-sucrose uptake trade-off. The stable steady states are denoted by solid lines, while the unstable steady states are denoted by dashed lines.

7.5.2 Dependence on the inflowing resource concentration S^0.

The stable states of the system (7.2.1)-(7.2.4) also depend on the resource concentration in the chemostat reservoir S^0. At larger resource concentrations, the populations are able to grow at higher dilution rates and they reach higher total population sizes (Fig. 7-15). Nonetheless, regardless of S^0 our main conclusions hold. Namely low dilution rates select for perfect internal metabolisers, high dilution rates select for perfect external metabolisers, and there is a range of dilution rates which lead to bistability between these two population types.

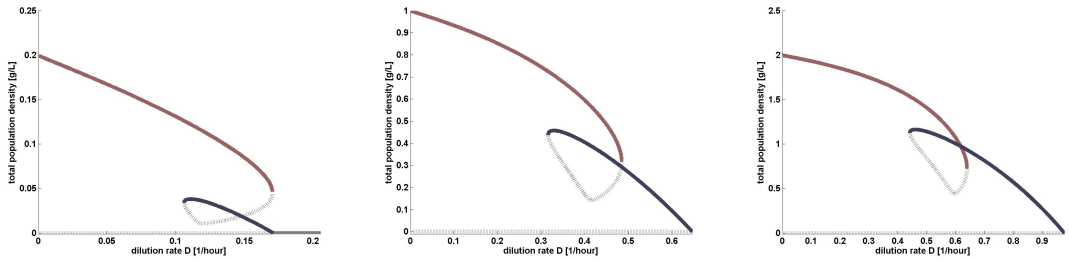

(a) *(b)* *(c)*

Supplementary Figure 7-15: **Positive steady states of a population under mutation-selection balance, for various resource concentrations S^0.**
The brown lines indicate populations dominated by external metabolisers, whereas the blue lines indicate populations dominated by internal metabolisers.
7-15a: $S^0 = 10$ [mM], 7-15b: $S^0 = 50$ [mM], 7-15c: $S^0 = 100$ [mM].
Here we assume the linear shape of the hexose-sucrose uptake trade-off. The stable steady states are denoted by solid lines, while the unstable steady states are denoted by dashed lines.

7.5.3 Methods and Parameter values

In order to study the steady states of the system (7.2.1)-(7.2.4), we used the model parameters gathered in the Table 7.1. Although, we base our system on the system of the public good production in *S. cerevisiae*, we deliberately decide not to use the exact parameters values describing that system. This is because, our mutation-selection model is a certain abstraction from the reality, and is not supposed to describe fully the system of yeast, but instead it aims to give an intuitive understanding on the evolution of external and internal metabolism in general. The wild type strain of *S. cerevisiae* has a very slow and inefficient direct sucrose uptake, and thus it may represent the case of the perfect external

metaboliser. Instead, here we study a hypothetical system which can perform both types of digestion (external and internal), and we study the potential directions of its evolution.

We obtain the positive equilibria distributions $P^*\mathbf{f}^*$ and the equilibria total population densities P^*, using the continuation software MAT-CONT.

The results of the simplified models were calculated for:

- $N = 3$, $V^H = \{0, 50, 100\}$ and $\epsilon = 8 \cdot 10^{-2}$ for the simplified model (Fig. 7-8).

- $N = 2$, $V^H = \{0, 100\}$ and $\epsilon = 0$ for the purely ecological model with no mutations (Fig. 7-10).

Supplementary Table 7.1: Parameters values for the mathematical model (7.2.1)-(7.2.4).

N	21
K_m^H	50 [mM hexose]
K_m^S	100 [mM sucrose]
k_{in}	5 [mM sucrose]
$Inv(S)$	$r_{in}S/(k_{in}+S)$
n_e^{Hxt}	0.01 [g protein/mmol hexose]
n_e^S	0.02 [g protein/mmol sucrose]
ϵ	$8 \cdot 10^{-2}$ [1/hour]
B	100
$h(V_{max}^H)$	$B - V_{max}^H$ [mmol sucrose / (g protein $\cdot$ hour)]
$g(V_{max}^H)$	V_{max}^H

Chapter 8

General Discussion

Our study aimed to address a number of questions concerning the ecology and evolution of the microbial public good systems. Based on the known biological details of *S. cerevisiae*, widely studied in the context of public good cooperation [1, 14, 32–34], and motivated by the previous study [14], we built a mathematical model describing the common growth of organisms which produce the public good (termed 'producers'), and those who don't (termed 'non-producers'). Throughout this thesis, we extrapolated our model to various contexts, in order to answer a number of questions concerning the evolution of public good systems, such as: What happens if a fraction of cheats is introduced to the population of cooperators? How can a population of cooperators survive an invasion of cheats who do not pay any cost of invertase production, but reap the rewards? What are the advantages and disadvantages of extracellular digestion, which involves producing costly public goods? Is this cooperative form of digestion competitive in comparison to the 'selfish metabolism' in which none of the steps of digestion is shared with the other cells? In order to make empirically testable predictions, and to gain mechanistic understanding of the empirically observed phenomena, we aimed to cut the natural complexity of the microbial systems and we sought to build models as simple as possible, but being capable of generating qualitatively testable results.

We first sought to obtain the mechanistic understanding of the recent empirical result [36], which tested and invalidated the virulence reduction strategy, termed 'Hamiltonian medicine', based on the competitive exclusion principle [113, 114] within the public good systems. This study revealed that, contrary to the previous claims [27, 56, 57, 67, 68], a mixture of virulent public good producers and

non-virulent non-producers, may exhibit enhanced virulence in comparison to the cultures composed only of the virulent strain. Our mathematical model, which was able to track in space and time the concentrations of available resources, and the population densities of the two considered strains, not only reproduced that empirical result [36], but it also unraveled the factors sufficient to explain it, namely: the interplay between spatial structure and two cooperative traits (public good an self-restraint as discussed in Chapter 3). Taking into account how wide spread are cooperative traits amongst microbes [16–18], our results indicate that the Hamiltonian medicine, instead of cure is likely to render the desease more severe.

After studying the consequences of mixing the public good producers with non-producers, on the whole microbial population, we examined how a mixture of these two strains affects the fitness of each of them separately. It is known that the environmental factors such as resource supply [171] or population density [32, 34, 63, 76] affect the outcome of the competition between public good producers and non-producers. However, the existing literature does not agree on the effect of population density on public good cooperation [32, 63, 76]. In Chapter 4 we deployed a mathematical model to verify if the way the experiments were performed in the previous experimental studies could be the reason of the inconsistency between the previous findings. We discovered that the way the spatial structure is represented in the beginning of the experiment significantly alters the competition results and the evolutionary predictions. Therefore, we defined a measure of the degree of spatial structure and, for a number of these degrees, we verified if high population density favours cooperation. We showed that high population density favours the cooperative public good producers when the space is highly structured and the available resources are scarce. On the contrary, it tends to favour non-producers in abundance of resources, or when the space is not sufficiently structured. Thus, not only we discovered a consistent answer to the question 'Does high population density favour cooperation?', but also we highlighted that the experimental results may not be consistent with each other because of their unquantitative approach to spatial structure.

Having studied the competition between public good producers and non-producers throughout Chapters 3 & 4, in Chapter 5 we set out to discover if there are any other environmental factors that may be a potential threat for the survival of public

good producers, apart from invasion of non-producers. We found that a homogeneous and cooperative population of *S. cerevisiae* is prone to extinction when cultured at low population densities. This phenomenon could not be observed in the absence of the cooperative external metabolism (that is when *S. cerevisiae* was grown on hexose which does not require the extracellular digestion). Although the vulnerability of *S. cerevisiae* at low population densities had been reported before [1, 93], here we extended that result to chemostat cultures, where small populations turn out to extinct while the large populations grown at the same conditions are able to survive. This result contradicts the classical chemostat theory [49], which states that at a given chemostat setting, a culture grown on a single resource shall converge to a unique globally attractive stable steady state. In contrary to this, we observed two possible stable states at a single chemostat setting.

After identifying potential threats for the public good systems, in which the organisms perform cooperative and extracellular digestion, in Chapter 6 we decided to verify why the external digestion feeding strategy is so abundant within fungi and other microbes [70, 92], in spite of its weaknesses. In order to do that, we built a mathematical model describing the co-growth of externally feeding public good producers (termed 'external metabolisers') and a genetically engineered strain, termed 'internal metaboliser', which 'privatises' its goods, and performs the digestion internally [36]. We not only aimed to understand the pairwise dynamics of the two strain competition, as in earlier chapters, but also to understand how an introduction of a new competitor influences that pair of interacting strains. We first modelled the competition of external and internal metabolisers, and then we studied the dynamics of a larger, three-strain community composed of external and internal metabolisers, and the invertase non-producers (termed 'cheats') also studied in earlier chapters. We found, in agreement with the recent empirical study [36], that the coexistence of external and internal metabolisers is highly affected by the resource availability. At sufficiently high resource concentration the strains can stably coexist, however, at lower resource concentration, or in the presence of another competitor, that coexistence becomes unstable. On the other hand, when the resources are scarce and the new competitor ('cheat') is introduced to the mixture of external and internal metabolisers, it prolongs the period of coexistence between these two strains, which has been also observed

experimentally [36]. Our model not only was able to recover the empirical results [36], but also it extrapolated these results to a number of different scenarios and discovered a whole range of three strain community dynamics. Moreover, by testing a number of scenarios, it provided a mechanistic understanding of these complex results.

Having observed that the coexistence between the two feeding strategies (internal and external metabolism) may be unstable, we extended our study to evolutionary timescale and we sought to find the evolutionary stable populations under a mutation - selection balance. In Chapter 7, we found how the cooperative external metabolism can evolve, and when the evolution would lead to appearance of internal and selfish metabolism instead. Similarly as in Chapter 6, we found out that there may be bistability between these two types of population. This means that depending on the initial density and composition of a population, it may either become cooperative (performing external digestion) or selfish (performing internal digestion). Since our model described the growth and evolution in a chemostat, we also linked different feeding strategies to different chemostat dilution rates.

In conclusion, our thesis sought to understand the behaviour and evolutionary dynamics of public good systems, which involve external metabolism. We started by looking at the effects on the whole population of an introduction of public good non-producers to the population of producers. Then we studied how the relative fitness of public good producers to non-producers is affected by a range of environmental conditions, and when the producers can survive the invasion of non-producers. We found possible disadvantages of performing the cooperative external digestion (i.e. the feeding strategy deployed by public good producers), and then we verified how competitive that feeding strategy is compared to the internal metabolism. We also verified how these two strategies can appear in the course of evolution.

In order to address all of these questions we used a bottom-up approach. We built mathematical models, based on biologically relevant assumptions, which are able capture the observed biological phenomena, with as little complexity as possible. This allowed us to test a number of biologically relevant scenarios, and to gain a mechanistic understanding of the described systems. Thanks to the dynamical approach, in which none of the fitness effects is predefined ad-hoc, but they appear based on the models assumptions, we captured the whole dynamics

of the considered systems and we could track how the experimental complexity arises in time.

References

[1] J. H. Koschwanez, K. R. Foster, and A. W. Murray, “Sucrose utilization in budding yeast as a model for the origin of undifferentiated multicellularity,” *PLoS biology*, vol. 9, p. e1001122, Aug. 2011.

[2] W. D. Hamilton, “The genetical evolution of social behaviour. I,” *Journal of theoretical biology*, vol. 7, pp. 1–16, July 1964.

[3] W. D. Hamilton, “Selfish and spiteful behaviour in an evolutionary model,” *Nature*, vol. 228, pp. 1218–1220, Dec. 1970.

[4] J. L. Sachs, U. G. Mueller, T. P. Wilcox, and J. J. Bull, “The evolution of cooperation,” *The Quarterly Review of Biology*, vol. 79, pp. 135–160, June 2004.

[5] S. A. West, A. S. Griffin, and A. Gardner, “Social semantics: altruism, cooperation, mutualism, strong reciprocity and group selection,” *Journal of evolutionary biology*, vol. 20, no. 2, pp. 415–432, 2007.

[6] C. R. Darwin, “On the origin of species by means of natural selection, or the preservation of favoured races in the struggle for life,” *Murray, London*, 1859.

[7] L. A. Dugatkin, *Cooperation among animals: an evolutionary perspective*. New York: Oxford University Press, 1997.

[8] R. L. Trivers, “The Evolution of Reciprocal Altruism,” *Quarterly review of biology*, vol. 46, pp. 35–57, Mar. 1971.

[9] R. Axelrod, *Axelrod’s" The Evolution of Cooperation"*. New York: Basic Books, 1984.

[10] M. A. Nowak and K. Sigmund, “Tit for tat in heterogeneous populations,” *Nature*, vol. 355, pp. 250–253, Jan. 1992.

[11] M. A. Nowak and K. Sigmund, “Evolution of indirect reciprocity by image scoring,” *Nature*, vol. 393, pp. 573–577, June 1998.

[12] M. A. Nowak and R. M. May, “Evolutionary games and spatial chaos,” *Nature*, vol. 359, pp. 826–829, Oct. 1992.

[13] V. C. Wynne-Edwards, *Animal Dispersion in relation to social behaviour*. Edinburgh: Oliver & Boyd, 1972.

[14] R. C. MacLean, A. Fuentes-Hernandez, D. Greig, L. D. Hurst, and I. Gudelj, “A mixture of "cheats" and "co-operators" can enable maximal group benefit,” *PLoS biology*, vol. 8, p. e1000486, Jan. 2010.

[15] C. D. Nadell, K. R. Foster, and J. a. B. Xavier, “Emergence of spatial structure in cell groups and the evolution of cooperation,” *PLoS computational biology*, vol. 6, p. e1000716, Mar. 2010.

[16] B. J. Crespi, “The evolution of social behavior in microorganisms,” *Trends in ecology & evolution*, vol. 16, pp. 178–183, Apr. 2001.

[17] G. J. Velicer, “Social strife in the microbial world,” *Trends in microbiology*, vol. 11, pp. 330–337, July 2003.

[18] S. a. West, S. P. Diggle, A. Buckling, A. Gardner, and A. S. Griffin, “The Social Lives of Microbes,” *Annual Review of Ecology, Evolution, and Systematics*, vol. 38, pp. 53–77, Dec. 2007.

[19] R. E. Lenski, M. R. Rose, S. C. Simpson, and S. C. Tadler, “Long-term experimental evolution in escherichia coli. i. adaptation and divergence during 2,000 generations,” *The American Naturalist*, vol. 138, pp. 1315–1341, Dec. 1991.

[20] F. Vasi, M. Travisano, and R. E. Lenski, “Long-term experimental evolution in escherichia coli. ii. changes in life-history traits during adaptation to a seasonal environment,” *American Naturalist*, vol. 144, pp. 432–456, Sept. 1994.

[21] M. Travisano, F. Vasi, and R. E. Lenski, “Long-term experimental evolution in escherichia coli. iii. variation among replicate populations in correlated responses to novel environments,” *Evolution*, vol. 49, pp. 189–200, Feb. 1995.

[22] M. Travisano and R. E. Lenski, “Long-term experimental evolution in escherichia coli. iv. targets of selection and the specificity of adaptation,” *Genetics*, vol. 143, pp. 15–26, May 1996.

[23] F. Harrison, L. E. Browning, M. Vos, and A. Buckling, “Cooperation and virulence in acute Pseudomonas aeruginosa infections,” *BMC biology*, vol. 4, no. 1, 2006.

[24] K. P. Rumbaugh, S. P. Diggle, C. M. Watters, A. Ross-Gillespie, A. S. Griffin, and S. A. West, “Quorum Sensing and the Social Evolution of Bacterial Virulence,” *Current Biology*, vol. 19, pp. 341–345, Feb. 2009.

[25] E. J. G. Pollitt, S. A. West, S. A. Crusz, M. N. Burton-Chellew, and S. P. Diggle, “Cooperation, quorum sensing, and evolution of virulence in Staphylococcus aureus,” *Infection and Immunity*, vol. 82, pp. 1045–1051, Mar. 2014.

[26] B. Raymond, S. a. West, a. S. Griffin, and M. B. Bonsall, “The Dynamics of Cooperative Bacterial Virulence in the Field,” *Science*, vol. 337, pp. 85–88, July 2012.

[27] S. A. West and A. Buckling, “Cooperation, virulence and siderophore production in bacterial parasites,” *Proceedings. Biological sciences / The Royal Society*, vol. 270, pp. 37–44, Jan. 2003.

[28] A. Buckling, F. Harrison, M. Vos, M. A. Brockhurst, A. Gardner, S. A. West, and A. Griffin, “Siderophore-mediated cooperation and virulence in pseudomonas aeruginosa,” *FEMS microbiology ecology*, vol. 62, pp. 135–141, Nov. 2007.

[29] T. Köhler, A. Buckling, and C. van Delden, “Cooperation and virulence of clinical Pseudomonas aeruginosa populations,” *Proceedings of the National Academy of Sciences of the United States of America*, vol. 106, pp. 6339–6344, Feb. 2009.

[30] G. W. Gooday, “The ecology of chitin degradation,” in *Advances in microbial ecology*, pp. 387–430, Springer, 1990.

[31] K. Drescher, C. D. Nadell, H. a. Stone, N. S. Wingreen, and B. L. Bassler,

"Solutions to the public goods dilemma in bacterial biofilms," *Current biology : CB*, vol. 24, pp. 50–5, Jan. 2014.

[32] D. Greig and M. Travisano, "The prisoner's dilemma and polymorphism in yeast suc genes," *Proceedings of the Royal Society of London B: Biological Sciences*, vol. 271, pp. S25–S26, Feb. 2004.

[33] "Snowdrift game dynamics and facultative cheating in yeast," *Nature*, vol. 459, pp. 253–6, May 2009.

[34] A. Chen, A. Sanchez, L. Dai, and J. Gore, "Dynamics of a producer-freeloader ecosystem on the brink of collapse," *Nature communications*, vol. 5, p. 3713, Jan. 2014.

[35] B. U. Stambuk, a. S. Batista, and P. S. De Araujo, "Kinetics of active sucrose transport in Saccharomyces cerevisiae," *Journal of bioscience and bioengineering*, vol. 89, pp. 212–214, Jan. 2000.

[36] R. J. Lindsay, *Polymorphic metabolism and the eco-evolutionary influence of social feeding strategies*. PhD thesis, University of Exeter, April 2016.

[37] T. Pfeiffer, S. Schuster, and S. Bonhoeffer, "Cooperation and competition in the evolution of ATP-producing pathways," *Science (New York, N.Y.)*, vol. 292, pp. 504–507, Apr. 2001.

[38] T. Bauchop and S. R. Elsden, "The growth of micro-organisms in relation to their energy supply," *Journal of general microbiology*, vol. 23, pp. 457–469, Dec. 1960.

[39] J. R. Dickinson and M. Schweizer, *The metabolism and molecular physiology of Saccharomyces cerevisiae*. CRC. Press, 2004.

[40] E. Postma, C. Verduyn, W. A. Scheffers, and J. P. Van Dijken, "Enzymic Analysis of the Crabtree Effect in Glucose-Limited Chemostat Cultures of Saccharomyces cerevisiae," *Applied and environmental microbiology*, vol. 55, pp. 468–477, Feb. 1989.

[41] R. a. Weusthuis, J. T. Pronk, P. J. van den Broek, and J. P. van Dijken, "Chemostat cultivation as a tool for studies on sugar transport in yeasts," *Microbiological reviews*, vol. 58, pp. 616–630, Dec. 1994.

[42] A. Novick and L. Szilard, “Description of the chemostat,” *Science*, vol. 112, pp. 715–716, Dec. 1950.

[43] R. J. Carman and M. A. Woodburn, “Effects of low levels of ciprofloxacin on a chemostat model of the human colonic microflora,” *Regulatory Toxicology and Pharmacology*, vol. 33, pp. 276–284, June 2001.

[44] R. J. Carman, M. A. Simon, H. E. Petzold, R. F. Wimmer, M. R. Batra, A. H. Fernández, M. A. Miller, and M. Bartholomew, “Antibiotics in the human food chain: Establishing no effect levels of tetracycline, neomycin, and erythromycin using a chemostat model of the human colonic microflora,” *Regulatory Toxicology and Pharmacology*, vol. 43, no. 2, pp. 168–180, 2005.

[45] E. Allen-vercoe, “Bringing the gut microbiota info focus through microbial culture : Recent Progress and Future Perspective,” *Current opinion in microbiology*, vol. 16, pp. 625–629, Oct. 2013.

[46] G. S. Crowther, C. H. Chilton, S. L. Todhunter, S. Nicholson, J. Freeman, S. D. Baines, and M. H. Wilcox, “Development and validation of a chemostat gut model to study both planktonic and biofilm modes of growth of Clostridium difficile and human microbiota,” *PLoS ONE*, vol. 9, p. e88396, Feb. 2014.

[47] P. A. Hoskisson and G. Hobbs, “Continuous culture - Making a comeback?,” *Microbiology*, vol. 151, pp. 3153–3159, Oct. 2005.

[48] F. O’Grady, I. P. Mackintosh, D. Greenwood, and B. W. Watson, “Treatment of "bacterial cystitis" in fully automatic machanical models simulating conditions of bacterial growth in the urinary bladder,” *British journal of experimental pathology*, vol. 54, pp. 283–90, jun 1973.

[49] H. L. Smith and P. Waltman, *The theory of the chemostat: dynamics of microbial competition*, vol. 13. New York: Cambridge university press, 1995.

[50] J. D. Murray, *Mathematical biology. I. , An introduction*. Interdisciplinary applied mathematics, New York: Springer, 2002.

[51] I. Gudelj, F. van den Bosch, and C. a. Gilligan, “Transmission rates and adaptive evolution of pathogens in sympatric heterogeneous plant popu-

lations," *Proceedings. Biological sciences / The Royal Society*, vol. 271, pp. 2187–2194, Oct. 2004.

[52] I. Gudelj, C. D. Coman, and R. E. Beardmore, "Classifying the role of trade-offs in the evolutionary diversity of pathogens," *Proceedings of the Royal Society A: Mathematical, Physical and Engineering Sciences*, vol. 462, pp. 97–116, Jan. 2006.

[53] I. Gudelj, R. E. Beardmore, S. S. Arkin, and R. C. MacLean, "Constraints on microbial metabolism drive evolutionary diversification in homogeneous environments," *Journal of evolutionary biology*, vol. 20, pp. 1882–1889, Sept. 2007.

[54] R. E. Beardmore, I. Gudelj, D. a. Lipson, and L. D. Hurst, "Metabolic trade-offs and the maintenance of the fittest and the flattest," *Nature*, vol. 472, pp. 342–346, Apr. 2011.

[55] P. F. Verhulst, "Recherches mathématiques sur la loi d'accroissement de la population," *Nouveaux Mémoires de l'Académie Royale des Sciences et Belles-Lettres de Bruxelles*, vol. 18, pp. 14–54, 1845.

[56] S. P. Brown, M. E. Hochberg, and B. T. Grenfell, "Does multiple infection select for raised virulence?," *Trends in Microbiology*, vol. 10, no. 9, pp. 401–405, 2002.

[57] A. Buckling and M. A. Brockhurst, "Kin selection and the evolution of virulence," *Heredity*, vol. 100, pp. 484–488, Jan. 2008.

[58] H. H. Lee, M. N. Molla, C. R. Cantor, and J. J. Collins, "Bacterial charity work leads to population-wide resistance," *Nature*, vol. 467, pp. 82–85, Sept. 2010.

[59] S. Brown, "Cooperation and conflict in host–manipulating parasites," *Proceedings of the Royal Society of London B: Biological Sciences*, vol. 266, pp. 1899–1904, Sept. 1999.

[60] H. C. Leggett, S. P. Brown, and S. E. Reece, "War and peace: social interactions in infections," *Philosophical transactions of the Royal Society of*

London. Series B, Biological sciences, vol. 369, no. 1642, p. 20130365, 2014.

[61] A. S. Griffin, S. A. West, and A. Buckling, "Cooperation and competition in pathogenic bacteria," *Nature*, vol. 430, pp. 1024–1027, Aug. 2004.

[62] A. Ross-Gillespie, A. Gardner, S. a. West, and A. S. Griffin, "Frequency dependence and cooperation: theory and a test with bacteria," *The American naturalist*, vol. 170, pp. 331–342, Sept. 2007.

[63] A. Ross-Gillespie, A. Gardner, A. Buckling, S. a. West, and A. S. Griffin, "Density dependence and cooperation: theory and a test with bacteria," *Evolution; international journal of organic evolution*, vol. 63, pp. 2315–2325, Sept. 2009.

[64] R. Kümmerli, A. S. Griffin, S. a. West, A. Buckling, and F. Harrison, "Viscous medium promotes cooperation in the pathogenic bacterium Pseudomonas aeruginosa," *Proceedings. Biological sciences / The Royal Society*, vol. 276, pp. 3531–3538, Oct. 2009.

[65] G. Hardin, "The tragedy of the commons," *Science*, vol. 162, no. 3859, pp. 1243–1248, 1968.

[66] D. J. Rankin, K. Bargum, and H. Kokko, "The tragedy of the commons in evolutionary biology," *Trends in ecology & evolution*, vol. 22, pp. 643–651, Dec. 2007.

[67] S. P. Brown, S. a. West, S. P. Diggle, and A. S. Griffin, "Social evolution in micro-organisms and a Trojan horse approach to medical intervention strategies," *Philosophical transactions of the Royal Society of London. Series B, Biological sciences*, vol. 364, pp. 3157–3168, Oct. 2009.

[68] B. Crespi, K. Foster, and F. Úbeda, "First principles of Hamiltonian medicine," *Philosophical transactions of the Royal Society of London. Series B, Biological sciences*, vol. 369, no. 1642, p. 20130366, 2014.

[69] R. a. Wilson and N. J. Talbot, "Under pressure: investigating the biology of plant infection by Magnaporthe oryzae," *Nature reviews. Microbiology*, vol. 7, no. 3, pp. 185–195, 2009.

[70] T. a. Richards and N. J. Talbot, “Horizontal gene transfer in osmotrophs: playing with public goods,” *Nature reviews. Microbiology*, vol. 11, pp. 720–727, Oct. 2013.

[71] J. L. Parrent, T. Y. James, R. Vasaitis, and A. F. Taylor, “Friend or foe? Evolutionary history of glycoside hydrolase family 32 genes encoding for sucrolytic activity in fungi and its implications for plant-fungal symbioses,” *BMC evolutionary biology*, vol. 9, June 2009.

[72] J. Fernandez, J. D. Wright, D. Hartline, C. F. Quispe, N. Madayiputhiya, and R. A. Wilson, “Principles of Carbon Catabolite repression in the rice blast fungus: Tps1, Nmr1-3, and a MATE-family pump regulate glucose metabolism during infection,” *PLoS Genetics*, vol. 8, May 2012.

[73] H. Weber and T. Roitsch, “Invertases and life beyond sucrose cleavage,” *Trends in Plant Science*, vol. 5, no. 2, pp. 47–48, 2000.

[74] L. Dai, K. S. Korolev, and J. Gore, “Slower recovery in space before collapse of connected populations,” *Nature*, vol. 496, pp. 355–358, Apr. 2013.

[75] R. C. MacLean and I. Gudelj, “Resource competition and social conflict in experimental populations of yeast,” *Nature*, vol. 441, pp. 498–501, May 2006.

[76] a. Dobay, H. C. Bagheri, a. Messina, R. Kümmerli, and D. J. Rankin, “Interaction effects of cell diffusion, cell density and public goods properties on the evolution of cooperation in digital microbes,” *Journal of evolutionary biology*, vol. 27, pp. 1869–1877, Sept. 2014.

[77] S. P. Brown and P. D. Taylor, “Joint evolution of multiple social traits: a kin selection analysis,” *Proceedings. Biological sciences / The Royal Society*, vol. 277, pp. 415–422, Feb. 2010.

[78] C. D. Nadell, J. B. Xavier, and K. R. Foster, “The sociobiology of biofilms,” *FEMS microbiology reviews*, vol. 33, pp. 206–224, Jan. 2009.

[79] E. Verbruggen, C. El Mouden, J. Jansa, G. Akkermans, H. Bücking, S. a. West, and E. T. Kiers, “Spatial structure and interspecific cooperation: the-

ory and an empirical test using the mycorrhizal mutualism," *The American naturalist*, vol. 179, pp. E133–46, May 2012.

[80] O. X. Cordero, L.-A. Ventouras, E. F. DeLong, and M. F. Polz, "Public good dynamics drive evolution of iron acquisition strategies in natural bacterioplankton populations," *Proceedings of the National Academy of Sciences of the United States of America*, vol. 109, pp. 20059–20064, Dec. 2012.

[81] D. C. Queller, "Does population viscosity promote kin selection?," *Trends in ecology & evolution (Personal edition)*, vol. 7, no. 10, pp. 322–324, 1992.

[82] J. Mitteldorf and D. S. Wilson, "Population viscosity and the evolution of altruism," *Journal of theoretical biology*, vol. 204, no. 4, pp. 481–96, 2000.

[83] L. Lehmann, V. Ravigné, and L. Keller, "Population viscosity can promote the evolution of altruistic sterile helpers and eusociality," *Proceedings. Biological sciences / The Royal Society*, vol. 275, pp. 1887–1895, May 2008.

[84] S. Lion and M. V. Baalen, "Self-structuring in spatial evolutionary ecology," *Ecology letters*, vol. 11, pp. 277–95, Mar. 2008.

[85] M. Le Gac and M. Doebeli, "Environmental viscosity does not affect the evolution of cooperation during experimental evolution of colicigenic bacteria," *Evolution; international journal of organic evolution*, vol. 64, pp. 522–33, Mar. 2010.

[86] G. B. Pollock, "Population viscosity and kin selection," *American Naturalist*, vol. 122, pp. 817–829, Dec. 1983.

[87] M. Boots and M. Mealor, "Local interactions select for lower pathogen infectivity," *Science*, vol. 315, no. 5816, pp. 1284–1286, 2007.

[88] T. W. Berngruber, S. Lion, and S. Gandon, "Evolution of suicide as a defence strategy against pathogens in a spatially structured environment," *Ecology letters*, vol. 16, no. 4, pp. 446–453, 2013.

[89] M. S. Datta, K. S. Korolev, I. Cvijovic, C. Dudley, and J. Gore, "Range expansion promotes cooperation in an experimental microbial metapopulation," *Proceedings of the National Academy of Sciences of the United States of America*, vol. 110, pp. 7354–7359, Apr. 2013.

[90] B. Kerr, C. Neuhauser, B. J. M. Bohannan, and A. M. Dean, "Local migration promotes competitive restraint in a host - pathogen 'tragedy of the commons'," *Nature*, vol. 442, pp. 75–78, July 2006.

[91] P. B. Rainey and M. Travisano, "Adaptive radiation in a heterogeneous environment," *Nature*, vol. 394, pp. 69–72, July 1998.

[92] N. J. Talbot, "Living the sweet life: how does a plant pathogenic fungus acquire sugar from plants?," *PLoS biology*, vol. 8, p. e1000308, Feb. 2010.

[93] L. Dai, D. Vorselen, K. S. Korolev, and J. Gore, "Generic indicators for loss of resilience before a tipping point leading to population collapse," *Science*, vol. 336, pp. 1175–7, June 2012.

[94] M. van Baalen and D. A. Rand, "The unit of selection in viscous populations and the evolution of altruism," *Journal of Theoretical Biology*, vol. 193, pp. 631–648, Aug. 1998.

[95] S. Lion and M. van Baalen, "From infanticide to parental care: Why spatial structure can help adults be good parents," *The American Naturalist*, vol. 170, pp. E26–E46, Aug. 2007.

[96] S. Lion and S. Gandon, "Habitat saturation and the spatial evolutionary ecology of altruism," *Journal of evolutionary biology*, vol. 22, pp. 1487–1502, June 2009.

[97] S. Lion, "Relatedness in spatially structured populations with empty sites: An approach based on spatial moment equations," *Journal of Theoretical Biology*, vol. 260, pp. 121–131, Sept. 2009.

[98] S. Lion, "Evolution of reproductive effort in viscous populations: The importance of population dynamics," *Journal of Evolutionary Biology*, vol. 23, pp. 866–874, Mar. 2010.

[99] D. S. Wilson, G. Pollock, and L. A. Dugatkin, "Can altruism evolve in purely viscous populations?," *Evolutionary ecology*, vol. 6, pp. 331–341, July 1992.

[100] W. C. Allee, O. Park, A. E. Emerson, T. Park, K. P. Schmidt, *et al.*, "Principles of animal ecology," no. Edn 1, 1949.

[101] S. Alizon and P. Taylor, “Empty sites can promote altruistic behavior,” *Evolution*, vol. 62, pp. 1335–1344, Mar. 2008.

[102] G. Wang and D. Or, “Hydration dynamics promote bacterial coexistence on rough surfaces,” *The ISME journal*, vol. 7, no. 2, pp. 395–404, 2013.

[103] J. W. Olejarz and M. A. Nowak, “Evolution of staying together in the context of diffusible public goods,” *Journal of theoretical biology*, vol. 360, pp. 1–12, Nov. 2014.

[104] E. E. Holmes, M. A. Lewis, J. Banks, and R. Veit, “Partial differential equations in ecology: spatial interactions and population dynamics,” *Ecology*, vol. 75, pp. 17–29, Jan. 1994.

[105] J. van Gestel, F. J. Weissing, O. P. Kuipers, and A. T. Kovács, “Density of founder cells affects spatial pattern formation and cooperation in Bacillus subtilis biofilms,” *The ISME journal*, vol. 8, pp. 2069–79, Oct. 2014.

[106] J. Barford, P. Phillips, and J. Orlowski, “A new model of uptake of multiple sugars by s. cerevisiae,” *Bioprocess Engineering*, vol. 7, pp. 303–307, Jan. 1992.

[107] K. Elbing, A. Ståhlberg, S. Hohmann, and L. Gustafsson, “Transcriptional responses to glucose at different glycolytic rates in Saccharomyces cerevisiae,” *European journal of biochemistry / FEBS*, vol. 271, pp. 4855–4864, Dec. 2004.

[108] G. Kudla, A. W. Murray, D. Tollervey, and J. B. Plotkin, “Coding-sequence determinants of gene expression in escherichia coli,” *Science*, vol. 324, pp. 255–258, Apr. 2009.

[109] H. Dong, L. Nilsson, and C. G. Kurland, “Gratuitous overexpression of genes in escherichia coli leads to growth inhibition and ribosome destruction,” *Journal of bacteriology*, vol. 177, pp. 1497–1504, Mar. 1995.

[110] L. A. Robertson, E. W. Van Niel, R. A. Torremans, and J. G. Kuenen, “Simultaneous nitrification and denitrification in aerobic chemostat cultures of thiosphaera pantotropha,” *Applied and Environmental Microbiology*, vol. 54, pp. 2812–2818, Nov. 1988.

[111] Y. Ueno, S. Otsuka, and M. Morimoto, “Hydrogen production from industrial wastewater by anaerobic microflora in chemostat culture,” *Journal of fermentation and bioengineering*, vol. 82, no. 2, pp. 194–197, 1996.

[112] C. Verduyn, E. Postma, W. A. Scheffers, and J. P. van Dijken, “Physiology of saccharomyces cerevisiae in anaerobic glucose-limited chemostat culturesx,” *Microbiology*, vol. 136, pp. 395–403, Mar. 1990.

[113] G. F. Gause, *The struggle for existence*. Baltmore, MD, USA: Williams and Wilkins, 1934.

[114] G. Hardin *et al.*, “The competitive exclusion principle,” *Science*, vol. 131, pp. 1292–1297, Apr. 1960.

[115] M. Droop, “The nutrient status of algal cells in continuous culture,” *Journal of the Marine Biological Association of the United Kingdom*, vol. 54, pp. 825–855, Nov. 1974.

[116] R. M. Sykes, “Theory of multiple limiting nutrients,” *Journal (Water Pollution Control Federation)*, no. 10, pp. 2387–2392, 1974.

[117] P. De Leenheer, S. A. Levin, E. D. Sontag, and C. A. Klausmeier, “Global stability in a chemostat with multiple nutrients,” *Journal of mathematical biology*, vol. 52, pp. 419–438, Apr. 2006.

[118] J. F. von Liebig, L. P. B. Playfair, and J. W. Webster, *Organic chemistry in its applications to agriculture and physiology*. J. Owen, 1841.

[119] G.-Y. Rhee *et al.*, “Effects of N: P atomic ratios and nitrate limitation on algal growth, cell composition, and nitrate uptake,” *Limnol. Oceanogr*, vol. 23, no. 1, pp. 10–25, 1978.

[120] L. Perego, J. C. d. S. Dias, L. Koshimizu, M. de Melo Cruz, W. Borzani, and M. Vairo, “Influence of temperature, dilution rate and sugar concentration on the establishment of steady-state in continuous ethanol fermentation of molasses,” *Biomass*, vol. 6, no. 3, pp. 247–256, 1985.

[121] L. Bruce, D. Axford, B. Ciszek, and A. Daugulis, “Extractive fermentation by zymomonas mobilis and the control of oscillatory behavior,” *Biotechnology Letters*, vol. 13, pp. 291–296, Apr. 1991.

[122] a. Q. Zamamiri, G. Birol, and M. a. Hjortsø, "Multiple stable states and hysteresis in continuous, oscillating cultures of budding yeast," *Biotechnology and bioengineering*, vol. 75, pp. 305–12, Nov. 2001.

[123] R. Maharjan, S. Seeto, L. Notley-McRobb, and T. Ferenci, "Clonal adaptive radiation in a constant environment," *Science*, vol. 313, pp. 514–517, July 2006.

[124] J. Wu, H. Nie, and G. S. Wolkowicz, "A mathematical model of competition for two essential resources in the unstirred chemostat," *SIAM Journal on Applied Mathematics*, vol. 65, no. 1, pp. 209–229, 2004.

[125] G. Stephanopoulos, A. G. Frederickson, and R. Aris, "The growth of competing microbial populations in a CSTR with periodically varying inputs," *AIChE Journal*, vol. 25, pp. 863–872, Sept. 1979.

[126] G. Butler, S. Hsu, and P. Waltman, "A mathematical model of the chemostat with periodic washout rate," *SIAM Journal on Applied Mathematics*, vol. 45, no. 3, pp. 435–449, 1985.

[127] R. E. Lenski and S. E. Hattingh, "Coexistence of two competitors on one resource and one inhibitor: a chemostat model based on bacteria and antibiotics," *Journal of Theoretical Biology*, vol. 122, pp. 83–93, Sept. 1986.

[128] S.-B. Hsu and P. Waltman, "Analysis of a model of two competitors in a chemostat with an external inhibitor," *SIAM journal on applied mathematics*, vol. 52, no. 2, pp. 528–540, 1992.

[129] T. Pfeiffer and S. Bonhoeffer, "Evolution of cross-feeding in microbial populations," *The American naturalist*, vol. 163, pp. E126–E135, June 2004.

[130] M. Doebeli, "A model for the evolutionary dynamics of cross-feeding polymorphisms in microorganisms," *Population Ecology*, vol. 44, pp. 59–70, Aug. 2002.

[131] A. B. Jarzebski, "Modelling of oscillatory behaviour in continuous ethanol fermentation," *Biotechnology Letters*, vol. 14, pp. 137–142, Feb. 1992.

[132] A. J. Daugulis, P. J. McLellan, and J. Li, “Experimental investigation and modeling of oscillatory behavior in the continuous culture of Zymomonas mobilis,” *Biotechnology and Bioengineering*, vol. 56, pp. 99–105, Oct. 1997.

[133] P. J. McLellan, A. J. Daugulis, and J. Li, “The incidence of oscillatory behavior in the continuous fermentation of Zymomonas mobilis,” *Biotechnology Progress*, vol. 15, no. 4, pp. 667–680, 1999.

[134] P. Garhyan, S. S. E. H. Elnashaie, S. M. Al-Haddad, G. Ibrahim, and S. S. Elshishini, “Exploration and exploitation of bifurcation/chaotic behavior of a continuous fermentor for the production of ethanol,” *Chemical Engineering Science*, vol. 58, pp. 1479–1496, Apr. 2003.

[135] S. S. Pilyugin and P. Waltman, “Multiple limit cycles in the chemostat with variable yield,” *Mathematical biosciences*, vol. 182, pp. 151–66, Apr. 2003.

[136] A. S. Batista, L. C. Miletti, and B. U. Stambuk, “Sucrose fermentation by saccharomyces cerevisiae lacking hexose transport,” *Journal of molecular microbiology and biotechnology*, vol. 8, pp. 26–33, Feb. 2005.

[137] W. L. Marques, V. Raghavendran, B. U. Stambuk, and A. K. Gombert, “Sucrose and Saccharomyces cerevisiae: a relationship most sweet,” *FEMS yeast research*, vol. 16, pp. 1–16, Dec. 2015.

[138] T. O. Basso, M. G. Dario, A. Tonso, B. U. Stambuk, and A. K. Gombert, “Insufficient uracil supply in fully aerobic chemostat cultures of Saccharomyces cerevisiae leads to respiro-fermentative metabolism and double nutrient-limitation,” *Biotechnology letters*, vol. 32, pp. 973–977, July 2010.

[139] T. O. Basso, S. de Kok, M. Dario, J. C. a. do Espirito-Santo, G. Müller, P. S. Schlölg, C. P. Silva, A. Tonso, J.-M. Daran, A. K. Gombert, A. J. a. van Maris, J. T. Pronk, and B. U. Stambuk, “Engineering topology and kinetics of sucrose metabolism in Saccharomyces cerevisiae for improved ethanol yield,” *Metabolic engineering*, vol. 13, pp. 694–703, Nov. 2011.

[140] P. Beteta and S. Gascon, “Localization of invertase in yeast vacuoles,” *FEBS Letters*, vol. 13, pp. 297–300, Mar. 1971.

[141] J. H. Koschwanez, K. R. Foster, and A. W. Murray, “Improved use of a public good selects for the evolution of undifferentiated multicellularity,” *eLife*, vol. 2, p. e00367, Jan. 2013.

[142] C. A. Kaiser and D. Botstein, “Secretion-defective mutations in the signal sequence for saccharomyces cerevisiae invertase,” *Molecular and cellular biology*, vol. 6, pp. 2382–2391, July 1986.

[143] J. H. Connell, “The influence of interspecific competition and other factors on the distribution of the barnacle chthamalus stellatus,” *Ecology*, vol. 42, pp. 710–723, Oct. 1961.

[144] D. Schluter, “Experimental evidence that competition promotes divergence in adaptive radiation,” *PNAS*, vol. 266, pp. 798–801, Nov. 1994.

[145] T. W. Schoener, “Field Experiments on Interspecific Competition,” *The American Naturalist*, vol. 122, pp. 240–285, Aug. 1983.

[146] P. R. Grant and B. R. Grant, “Evolution of character displacement in darwin’s finches,” *Science*, vol. 313, pp. 224–226, July 2006.

[147] H. Celiker and J. Gore, “Competition between species can stabilize public-goods cooperation within a species,” *Molecular systems biology*, vol. 8, p. 621, Jan. 2012.

[148] F. Harrison, J. Paul, R. C. Massey, and A. Buckling, “Interspecific competition and siderophore-mediated cooperation in Pseudomonas aeruginosa,” *The ISME journal*, vol. 2, no. 1, pp. 49–55, 2008.

[149] R. F. Inglis, J. M. Biernaskie, A. Gardner, and R. Kümmerli, “Presence of a loner strain maintains cooperation and diversity in well-mixed bacterial communities,” *Proceedings of the Royal Society B: Biological Sciences*, vol. 283, p. 20152682, Jan. 2016.

[150] R. Wahl, K. Wippel, S. Goos, J. Kämper, and N. Sauer, “A novel high-affinity sucrose transporter is required for virulence of the plant pathogen Ustilago maydis,” *PLoS Biology*, vol. 8, p. e1000303, Feb. 2010.

[151] T. Tanino, T. Matsumoto, H. Fukuda, and A. Kondo, “Construction of system for localization of target protein in yeast periplasm using invertase,” vol. 28, pp. 259–264, 2004.

[152] N. Ribeck and R. E. Lenski, “Modeling and quantifying frequency-dependent fitness in microbial populations with cross-feeding interactions,” *Evolution*, vol. 69, pp. 1313–1320, Apr. 2015.

[153] L. Neigeborn and M. Carlson, “Genes affecting the regulation of SUC2 gene expression by glucose repression in Saccharomyces cerevisiae,” *Genetics*, vol. 108, no. 4, pp. 845–858, 1984.

[154] J. M. Biernaskie and S. A. West, “Cooperation, clumping and the evolution of multicellularity,” *Proceedings of the Royal Society B: Biological Sciences*, vol. 282, p. 20151075, Aug. 2015.

[155] J. a. Hutchings and J. D. Reynolds, “Marine Fish Population Collapses: Consequences for Recovery and Extinction Risk,” *BioScience*, vol. 54, pp. 297–309, Apr. 2004.

[156] C. Folke, S. R. Carpenter, B. Walker, M. Scheffer, T. Elmqvist, L. Gunderson, and C. S. Holling, “Regime Shifts, Resilience, and Biodiversity in Ecosystem Management,” *Annual Review of Ecology, Evolution, and Systematics*, vol. 35, no. 2004, pp. 557–581, 2004.

[157] A. C. Yannarell, T. F. Steppe, and H. W. Paerl, “Disturbance and recovery of microbial community structure and function following Hurricane Frances,” *Environmental Microbiology*, vol. 9, pp. 576–583, Nov. 2007.

[158] M. Ferris, S. Nold, N. Revsbech, and D. Ward, “Population structure and physiological changes within a hot spring microbial mat community following disturbance,” *Applied and environmental microbiology*, vol. 63, pp. 1367–1374, Apr. 1997.

[159] D. A. Antonopoulos, S. M. Huse, H. G. Morrison, T. M. Schmidt, M. L. Sogin, and V. B. Young, “Reproducible community dynamics of the gastrointestinal microbiota following antibiotic perturbation,” *Infection and Immunity*, vol. 77, pp. 2367–2375, June 2009.

[160] A. E. Pérez-Cobas, M. J. Gosalbes, A. Friedrichs, H. Knecht, A. Artacho, K. Eismann, W. Otto, D. Rojo, R. Bargiela, M. von Bergen, *et al.*, "Gut microbiota disturbance during antibiotic therapy: a multi-omic approach," *Gut*, vol. 62, no. 11, pp. 1591–1601, 2013.

[161] S. D. Allison and J. B. H. Martiny, "Colloquium paper: resistance, resilience, and redundancy in microbial communities," *Proceedings of the National Academy of Sciences of the United States of America*, vol. 105, pp. 11512–11519, Aug. 2008.

[162] C. Arnosti, "Microbial extracellular enzymes and the marine carbon cycle," *Annual review of marine science*, vol. 3, pp. 401–425, Jan. 2011.

[163] K. L. Meibom, X. B. Li, A. T. Nielsen, C.-Y. Wu, S. Roseman, and G. K. Schoolnik, "The vibrio cholerae chitin utilization program," *Proceedings of the National Academy of Sciences of the United States of America*, vol. 101, pp. 2524–2529, Feb. 2004.

[164] A. Lammi, P. Siikamäki, and K. Mustajärvi, "Genetic diversity, population size, and fitness in central and peripheral populations of a rare plant Lychnis viscaria," *Conservation Biology*, vol. 13, pp. 1069–1078, Oct. 1999.

[165] G. Knaepkens, L. Bervoets, E. Verheyen, and M. Eens, "Relationship between population size and genetic diversity in endangered populations of the European bullhead (Cottus gobio): Implications for conservation," *Biological Conservation*, vol. 115, pp. 403–410, Feb. 2004.

[166] N. C. Ellstrand and D. R. Elam, "Population genetic consequences of small population size: implications for plant conservation," *Annual review of Ecology and Systematics*, pp. 217–242, 1993.

[167] J. C. Garza and E. G. Williamson, "Detection of reduction in population size using data from microsatellite loci," *Molecular Ecology*, vol. 10, pp. 305–318, Feb.

[168] S. E. Forde, R. E. Beardmore, I. Gudelj, S. S. Arkin, J. N. Thompson, and L. D. Hurst, "Understanding the limits to generalizability of experimental evolutionary models," *Nature*, vol. 455, pp. 220–3, Sept. 2008.

[169] M. Groom, G. Meffe, and C. Carroll, *Principles of Conservation Biology*. Mass., 2006.

[170] R. Frankham, “Society for conservation biology relationship of genetic variation to population size in wildlife,” *Conservation Biology*, vol. 10, pp. 1500–1508, Dec. 1995.

[171] M. A. Brockhurst, A. Buckling, D. Racey, and A. Gardner, “Resource supply and the evolution of public-goods cooperation in bacteria,” *BMC biology*, vol. 6, p. 20, May 2008.